universität wien

MASTERARBEIT

Titel der Masterarbeit

"New constraints on the timing of the Mae Ping fault zone, NW-Thailand"

Verfasser

Jürgen Österle B.Sc.

angestrebter akademischer Grad

Master of Science (M.Sc.)

Wien, 2014

Studienkennzahl lt. Studienblatt:	A 066 815
Studienrichtung lt. Studienblatt:	Masterstudium Erdwissenschaften
Betreuerin / Betreuer:	Ao. Univ. Prof. Mag. Dr. Urs Klötzli

Contents

1 Acknowledgement

This master thesis is based on a collaboration between the University of Vienna and the Chulalongkorn University, Bangkok, and was proposed to me by Urs Klötzli. Therefore, I owe a first big thank you to Urs Klötzli who supported me at any time and from whom I could learn so much during my time as a student. I also want to say thank you to Markus Palzer, who worked on the same topic, for being a good colleague and who's enthusiasm and data were vital for this study. Moreover, I owe a debt of gratitude to the University of Vienna, to the ASEA Uninet, to Pitsanupong Kanjanapayont and the Chulalongkorn University for their organizational and financial support. I want to say thank you to Eva Klötzli, Franz Biedermann, Elizaveta Kovaleva, Claudia Beybel and Sigrid Hrabe for helping me with the sample preparation and to Hugh Rice and Constantin Petrakakis for their technical support with the SEM and optical microscope. And last but not least I want to say thank you to my parents Walter and Ruth Österle who have always supported me all my life long.

2 Introduction

The Mae Ping fault zone (MPFZ) is one of the four major strike-slip shear zones in Thailand. It is considered by some authors to contribute to the lateral extrusion of SE-Asia. Within this fault zone, a core complex of ductile deformed amphibolite-facies rocks, the so-called Lan Sang gneisses, occurs. Despite several former investigations, some aspects concerning the timing, regime and cause of exhumation remain controversial. New detailed structural, petrological, geochemical and geochronological investigations of the Lan Sang gneisses were undertaken to establish a PTt-path in order to constrain the evolutionary history of these rocks. Concerning the timing of the MPFZ, an undeformed discordant subvolcanic dyke has been found within the strongly deformed Lan Sang gneisses. In-situ U-Th-Pb LA-ICP-MS dating of soccer ball zircons, which are formed during anatexis from this dyke yield an age of 42 ± 2 Ma and suggest a deformation of the MPFZ prior to this time. However, the zircon ages of the subvolcanic dyke clearly conflict with $^{40}Ar/^{39}Ar$ dating on biotites by Lacassin et al. (1997) who interpreted the cooling ages of c. 30 Ma to reflect the last increments of ductile sinistral deformation. Furthermore, these results question the MPFZ to be one of the shear zones contributing to the lateral extrusion of SE-Asia as a consequence of the Himalayan orogeny. Thus, the deformation should be older and could potentially be of Indosinian (Triassic) origin as a result of the collision between Indochina and Sibumasu.

This work is a joint study of the author and Markus Palzer, who focused on the structural part and petrology of the Lan Sang gneisses. His part of the work is summarized in Palzer (2013).

3 Geological setting

3.1 Sundaland

SE-Asia, as noted by Mickein (1997), is a mosaic of Gondwana-derived terranes which were accreted to SE-Asia in the uppermost Paleozoic to lower Mesozoic. The continental core of SE-Asia (Figure 3.1), widely referred to as Sundaland, consists of the South China block, the Indochina block, the Sibumasu terrane, the West Burma block and the SW Borneo block (Metcalfe, 2013a,b). Thailand, which lies within this geological entity, comprises Indochina in the East, and Sibumasu in the West. Both have their origin in Gondwana, but they show a different evolution until they collided during the Indosinian orogeny in the Mesozoic to form the core of Sundaland (Ridd et al., 2011). Located between Sibumasu and Indochina is the Sukhothai fold belt (Linchang, Sukhothai, Chanthaburi terranes and the Central and Eastern belts of the Malay Peninsula) and the Inthanon zone (Changning-Menglian suture, Chiang Mai-Inthanon suture, Bentong-Raub suture zone). Both are assumed to be related to the subduction of the Paleo-Tethys.
As mentioned by Palzer (2013), the exact location of the suture zones between Indochina, Sukhothai and Sibumasu, especially in the South, and therefore the exact differentiation between these terranes, as well as the origin and interpretation of the Sukhothai fold belt are still under debate, mainly due to a lack of clear suture-related rocks and the presence of N-S trending basins obscuring any evidence for these features. However, Sundaland, which is defined after Searle and Morley (2011) to the SE by the limit of continental crust and to the NW by major Cenozoic strike-slip faults, namely the Ailao Shan-Red River fault zone (ASRRFZ) and the Sagaing fault, is nowadays moving eastwards with respect to Eurasia, while being rotated clockwise (Figure 3.2). Whether these Cenozoic strike-slip faults coincide neatly with older terrane boundaries is a matter of debate (Searle and Morley, 2011). However, it seems to be commonly accepted that the ASRRFZ and the Sagaing fault accommodate the relative motion between Sundaland and its surrounding terranes, whatever the true amount of accommodation might be (Morley et al., 2011; Searle and Morley, 2011).

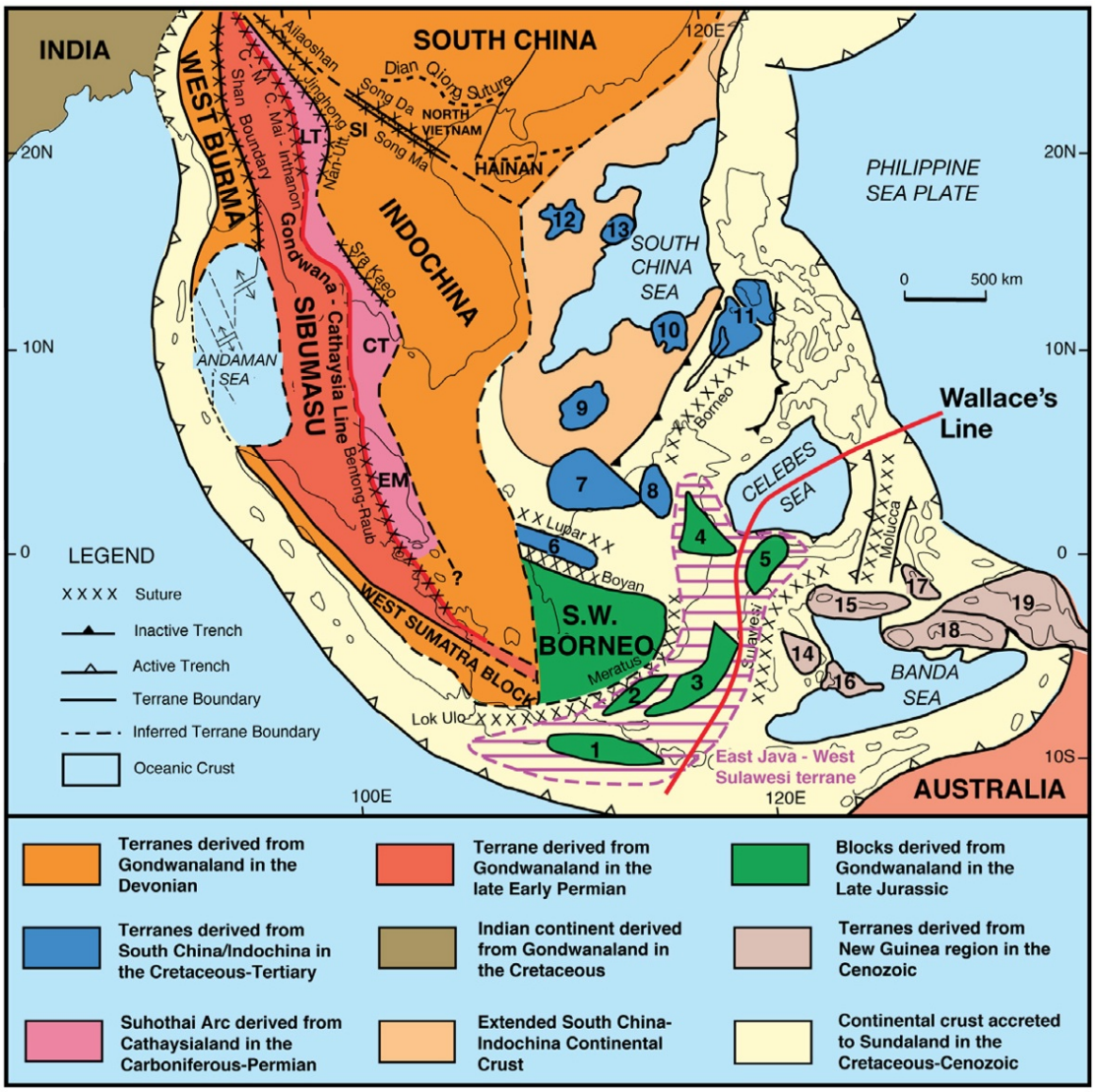

Figure 3.1: Distribution of continental blocks, terranes, and principal sutures of SE-Asia. Numbered micro-continental blocks: 1. East Java; 2. Bawean; 3. Paternoster; 4. Mangkalihat; 5. West Sulawesi; 6. Semitau; 7. Luconia; 8. Kelabit–Longbowan; 9. Spratly Islands–Dangerous Ground; 10. Reed Bank; 11. North Palawan; 12. Paracel Islands; 13. Macclesfield Bank; 14. East Sulawesi; 15. Bangai–Sula; 16. Buton; 17. Obi–Bacan; 18. Buru–Seram; 19. West Irian Jaya. LT = Lincang terrane, ST = Sukhothai terrane and CT = Chanthaburi terrane, EM = East Malaya. C–M = Changning–Menglian suture, C.-Mai = Chiang Mai suture and Nan–Utt. = Nan–Uttaradit suture. From Metcalfe (2013a).

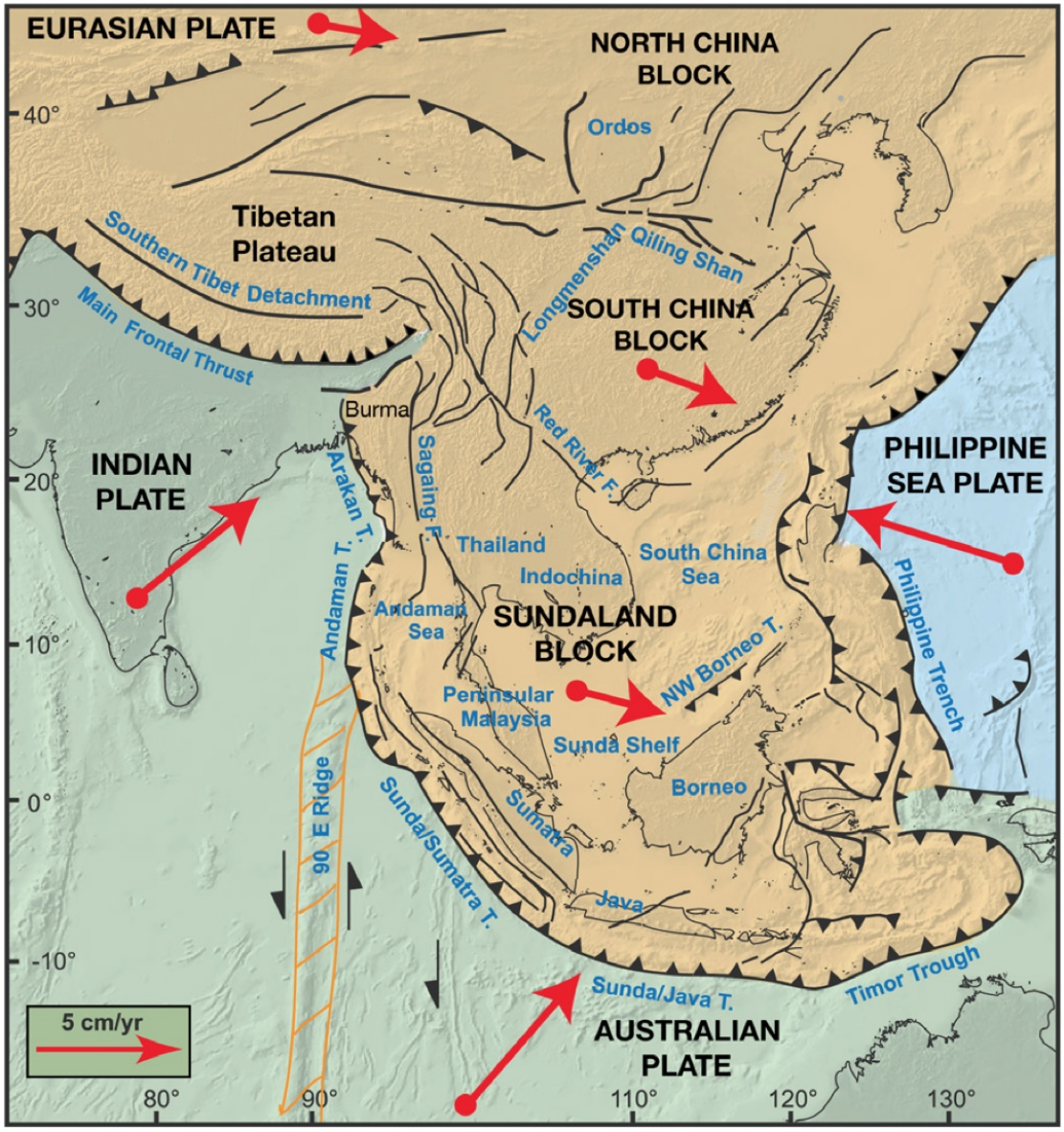

Figure 3.2: Topography and main active faults in SE-Asia at the zone of convergence of the Eurasian (pale orange), Philippine (pale blue) and Inidan-Australian plates (pale green). Large arrows indicate absolute motions of plates. From Metcalfe (2013a).

3.1.1 Paleozoic evolution

The Paleozoic evolution of Sundaland, as noted by Metcalfe (2013a,b), is marked by the collision of a number of Gondwana-derived terranes in three episodes of rifting, separation and northwards drift as three successive ocean basins, the Paleo-Tethys (Devonian-Triassic), the Meso-Tethys (late Early Permian-Late Cretaceous) and the Ceno-Tethys (Late Jurassic-Late Cretaceous) opened and subsequently closed. The closure of the Paleo-Tethys, which resulted in the Indosinian orogeny, lead to the collision of Sibumasu, which is considered to be the eastern part of the Cimmerian continent, and Indochina during Late Triassic/Early Jurassic (Figure 3.4). Both, though Gondwana-derived terranes, show a different evolution. While Indochina exhibits a more diversified, warm-water fauna, Sibumasu seems to have a cooler-water fauna during Carboniferous to Permian times. Moreover, paleomagnetic results and the presence of Late Carboniferous-Early Permian glacial marine diamictites suggest that Sibumasu may have been situated higher in the latitudes of the southern hemisphere compared to Indochina (Figure 3.3) (Assavapatchara et al., 2006; Metcalfe, 2013a).
However, during the latest Carboniferous-Early Permian a back-arc was constructed on the margin of Indochina by northwards subduction of the Paleo-Tethys. This back-arc, which is embodied by volcanic rocks of the Sukhothai fold belt, was probably separated from Indochina by the opening of a narrow back-arc basin. Spreading commenced during Early-Middle Permian and the ocean subsequently closed in the Late Permian-Triassic (Metcalfe, 2013a; Ridd et al., 2011; Searle and Morley, 2011). This short-lived back-arc basin ocean is nowadays present as the Nan-Uttaradit suture (Assavapatchara et al., 2006; Ridd et al., 2011; Metcalfe, 2013a,b). The suture presumed to mark the Paleo-Tethys ocean separating Indochina and Sibumasu, is believed to be embodied by the Inthanon zone. Geologic evidence is thought to be recorded in oceanic rocks that were thrusted westwards over Sibumasu in an accretionary complex (Metcalfe, 2013a,b; Ridd et al., 2011).

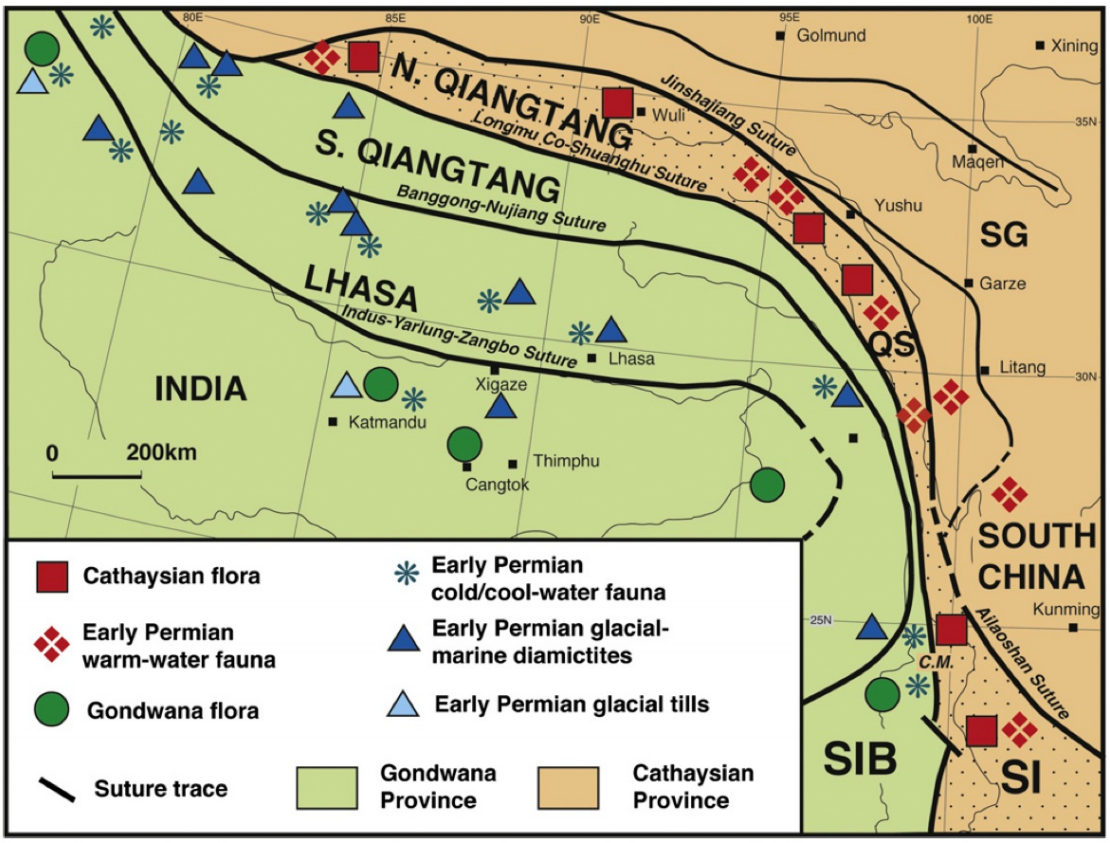

Figure 3.3: Distribution of Lower Permian Gondwana and Cathaysian province faunas and floras, showing the highly contrasting cool- and warm-climate on either side of the main Paleo-Tethyan divide which is represented by the Longmu Co-Shuanghu and Changning-Menglian (C.M.) suture zones. QS = Qamdo-Simao block, SIB = Sibumasu terrane, SI = Simao terrane (northern Indochina), SG = Songpan Ganzi accretionary complex. From Metcalfe (2013a).

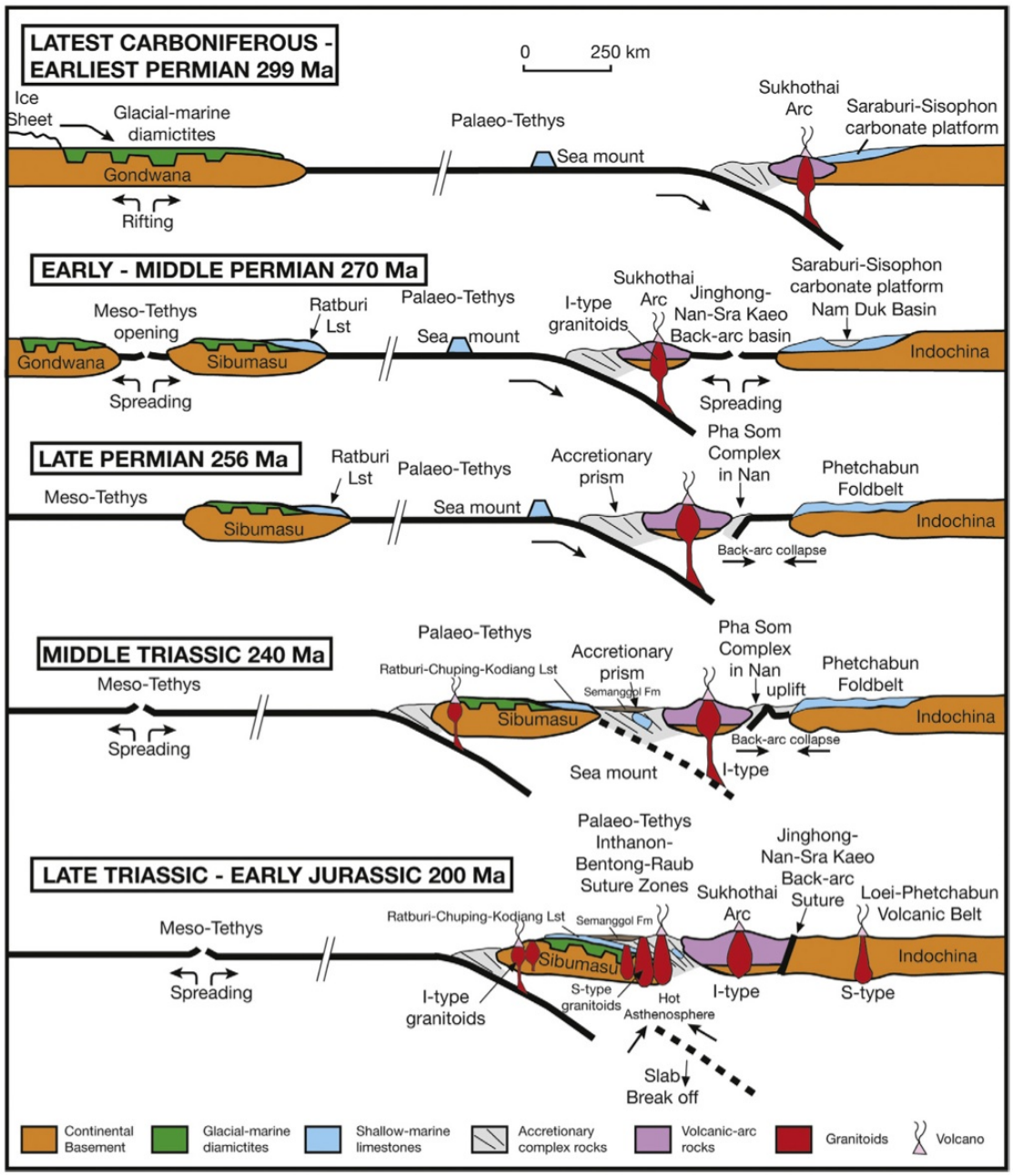

Figure 3.4: Cartoon showing the tectonic evolution of Sundaland during Late Cretaceous-Early Jurassic times. From Metcalfe (2013a).

3.1.2 Mesozoic evolution

By the late Early Jurassic Thailand was a single tectonic entity, according to Ridd et al. (2011). The post-collisional development of Sundaland was governed by tectonic quiescence until the Cretaceous. In the western part of the country, shallow-marine sedimentation occurred, while in the eastern part the collision was followed by continental sedimentation which commenced in the Late Triassic. These non-marine sedimentation is nowadays represented by the Khorat plateau in the NE of Thailand. The regression, which commenced in the Late Triassic reached its maximum extent in the Cretaceous, with extensive red-beds cropping out in the Khorat plateau (Ridd et al., 2011). The tectonic quiescence ended with the subduction of the Meso-Tethys reaching its maximum during the Late Cretaceous (Metcalfe, 2013a). The subduction beneath Sundaland during the Early Cretaceous resulted in granite emplacement and intensifying deformation (Morley et al., 2011; Searle and Morley, 2011). A second phase of igneous activity commenced in the Late Cretaceous-Paleogene and has been proposed to have happened due to collision of the West Burma block with the Shan plateau. Searle and Morley (2011) question this assumption and rather suggest a Triassic age. They concluded that, due to recent data from the Jade Mines belt and the Mogok metamorphic belt in Myanmar, subduction and initiation of Andean margin activity during the Late Cretaceous-Paleogene in Thailand and Myanmar appears to be a reasonable explanation for the observed tectonic events.

3.1.3 Cenozoic evolution

The Cenozoic evolution of Sundaland is markedly influenced by the collision of India and Eurasia, resulting in the Himalayan orogeny. The timing of this collision, as mentioned by Metcalfe (2013a) is hotly debated, with an early collision of around 60 Ma being favored by some authors, and a much younger Eocene-Oligocene collision being proposed by others, who suggest that the collision at c. 60-55 Ma was between India and an intra-oceanic island arc. Recent U-Pb/Hf/Nd zircon data support this contention of an intra-ocean island arc. A Middle Eocene age (45 Ma) for the initial collision of India (with accreted island arc) with Eurasia, temporally coinciding with large-scale regional and global plate reorganizations at this time, is proposed by Metcalfe (2013a). However, the timing of the ultimate „hard“ collision between India and Eurasia is still a matter of debate (Metcalfe, 2013a).
The collision is believed to have initiated strike-slip faulting accommodating the strain and relative motion of India with respect to Sundaland and simultaneously leading to the lateral extrusion of this geologic entity along these fault zones (Lacassin et al., 1997). It is however still controversial which of the strike-slip faults have contributed to the lateral extrusion and to which extent, if at all. In Thailand the four major strike-slip faults are the NW-SE trending Mae Ping fault zone (MPFZ) and Three Pagodas fault zone (TPFZ) and their, as assumed by some authors, conjugated NE-SW trending Ranong fault zone and Khlong Marui fault

zone (Figure 3.5). Models concerning the lateral extrusion linking motion along strike-slip faults and basin formation were proposed by some authors. Predominantly based on their plasticine experiments and satellite images, Peltzer and Tapponnier (1988) and Tapponnier et al. (1986) proposed the continental extrusion model involving the horizontal motion of rigid ‚blocks' bounded by strike-slip faults. The two major strike-slip faults contributing to the continental extrusions are the left-lateral ASRRFZ and the right-lateral Sagaing fault, but also the NW-SE trending left-lateral MPFZ and TPFZ in Thailand play an important role in their model. So far only the Sagaing fault is documented to be a major crustal-scale strike-slip fault taking up most of the differential motion of indenting India (Searle and Morley, 2011).
Polachan and Sattayarak (1989) considered the mainly N-S trending basins in Thailand to be formed by right-lateral motion along the MPFZ and TPFZ and in doing so contradicted Peltzer and Tapponnier (1988) and Tapponnier et al. (1986). Their interpretation, primarily based on the clockwise rotation of Sundaland and geometrical relationships of strike-slip and extensional faults, suggests that progressive rotation of SE-Asia resulted in an increasingly oblique plate convergence which enabled the movement along major strike-slip faults with the associated development of pull apart basins in Thailand. Morley (2001) on the other hand, introduced the idea of subduction-rollback to be responsible for basin formation and that strike-slip faulting was only of minor importance. He also mentioned the possibility of subduction-rollback being related to the metamorphic core complex formation (e.g. Doi Inthanon) by non-uniform lithospheric stretching resulting in lower lithospheric thinning, heating of the crust and subsequent isostatic uplift triggering low-angle detachment faults. However, as long as the timing of the Himalayan orogeny and the timing as well as the nature of the major strike-slip faults are not well constrained, these models can't be accepted at face value.

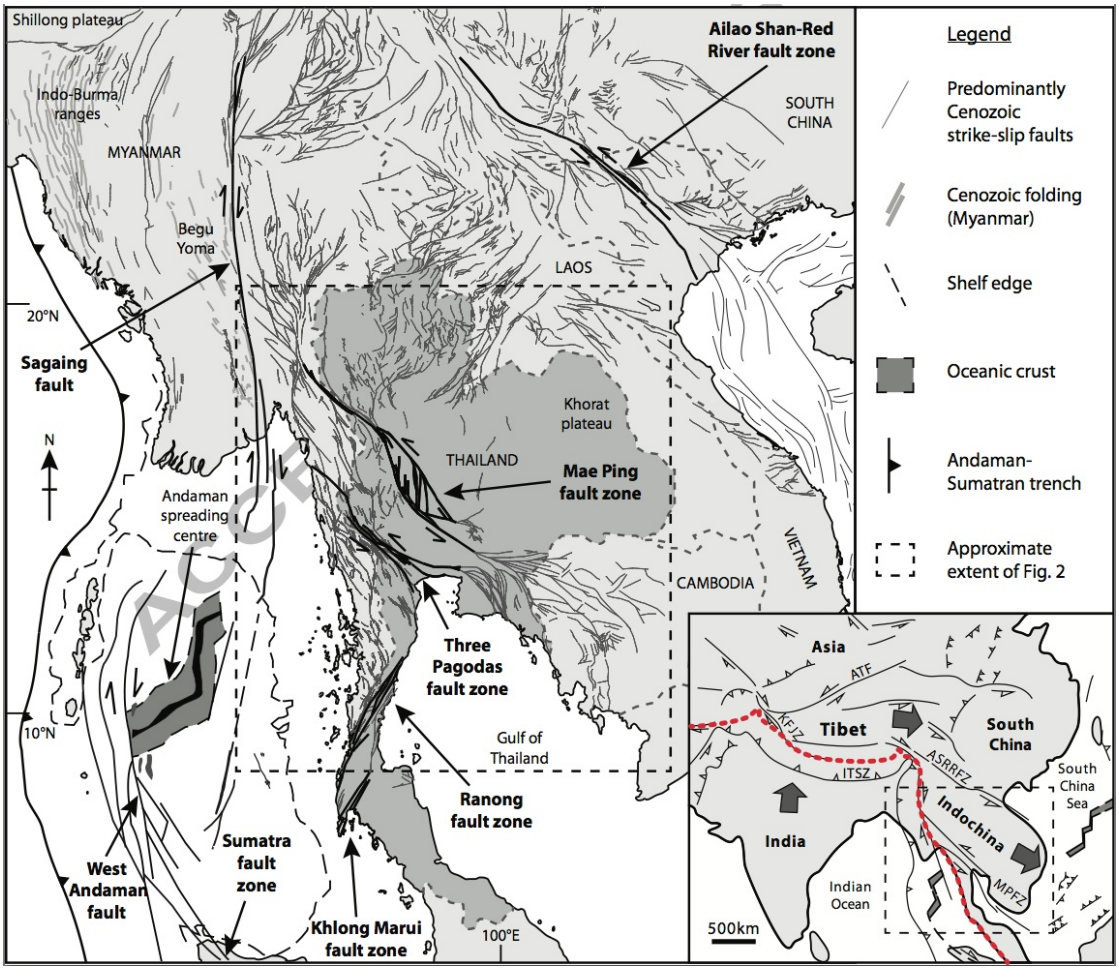

Figure 3.5: Simplified tectonic map of SE-Asia showing regional fault patterns. ITSZ, Indus–Tsangpo suture zone (approximate position marked by red dashed line); ATF, Altyn Tagh fault; KFJZ, Karakoram-Jiale fault zone; ASRRFZ, Ailao Shan-Red River fault zone; MPFZ, Mae Ping fault zone. From Palin et al. (2013).

3.2 The Lan Sang gneisses

The first detailed petrographical description of the gneisses cropping out in the Lan Sang National Park (Figure 3.6), the so-called Lan Sang gneisses, stem from Campbell (1975), who identified a predominantly metasedimentary origin of the rocks, mainly consisting of quartz-feldspar-biotite gneiss, calc-silicate rocks, marble and non-schistose quartz-feldspar rich rocks. He further noted the presence of subordinate orthogneiss components, primarily granite gneiss, pegmatite and granodiorite with a varying intensity of foliation, which are intimately mixed with and restricted to the quartz-feldspar-biotite gneisses. The steeply dipping gneisses are bordered to the NE by metasediments, separated from the gneisses by a high-angle NE-dipping normal fault, and to the SW by low-grade metamorphic rocks. Lacassin et al. (1997) also described the Lan Sang gneisses to be strongly deformed metasediments, orthogneisses and veins of pegmatite, quartz and microgranite steeply dipping towards the NE and having foliations more or less parallel to the outlines of the fault zone. Moreover, they mentioned results estimating the high-grade metamorphism to have experienced temperatures of 800 $\pm$ 50°C within the calc-silicate rocks. The presence of widespread mylonitic fabrics with foliations, stretching lineations, and left-lateral shear criteria lead them to the conclusion that the MPFZ is a major ductile shear zone, without any clear evidence of earlier shear increments under high-temperature conditions.
However, what brought the Lan Sang gneisses to the surface is still controversially debated. Lacassin et al. (1997) suggest that the gneisses have been exhumed by late normal faulting. Their assumption is supported by foliation planes having chlorite-bearing down-dip slickenside due to normal-, down to the NE-, slip. Others support the idea of a restraining bend being the reason for the exhumation of the gneisses, e.g. Morley et al. (2007). For the northern part of the Chiang Mai-Lincang belt (CM-L belt), which is bisected and offset by the MPFZ, other exhumation models exist. The N-S trending CM-L belt consists predominantly of high-grade metamorphic rocks and granites (Doi Inthanon and Doi Suthep massifs, Umphang, Lan Sang and Khlong Lan gneisses), which are by some authors interpreted as the crystalline basement of Sibumasu (Searle and Morley, 2011). However, the Doi Inthanon and Doi Suthep are considered to be exhumed either by normal faulting (Dunning et al., 1995) or by nappe tectonics and subsequent normal faulting (Mickein, 1997; Hansen and Wemmer, 2011). Palzer (2013) tried to adapt the core complex model of Dunning et al. (1995) to the Lan Sang gneisses and argued that the model proposed by Mickein (1997) and Hansen and Wemmer (2011) requires E-W compression during the Miocene, which conflicts with the E-W extension coupled with N-S trending basin formation starting around the same time.

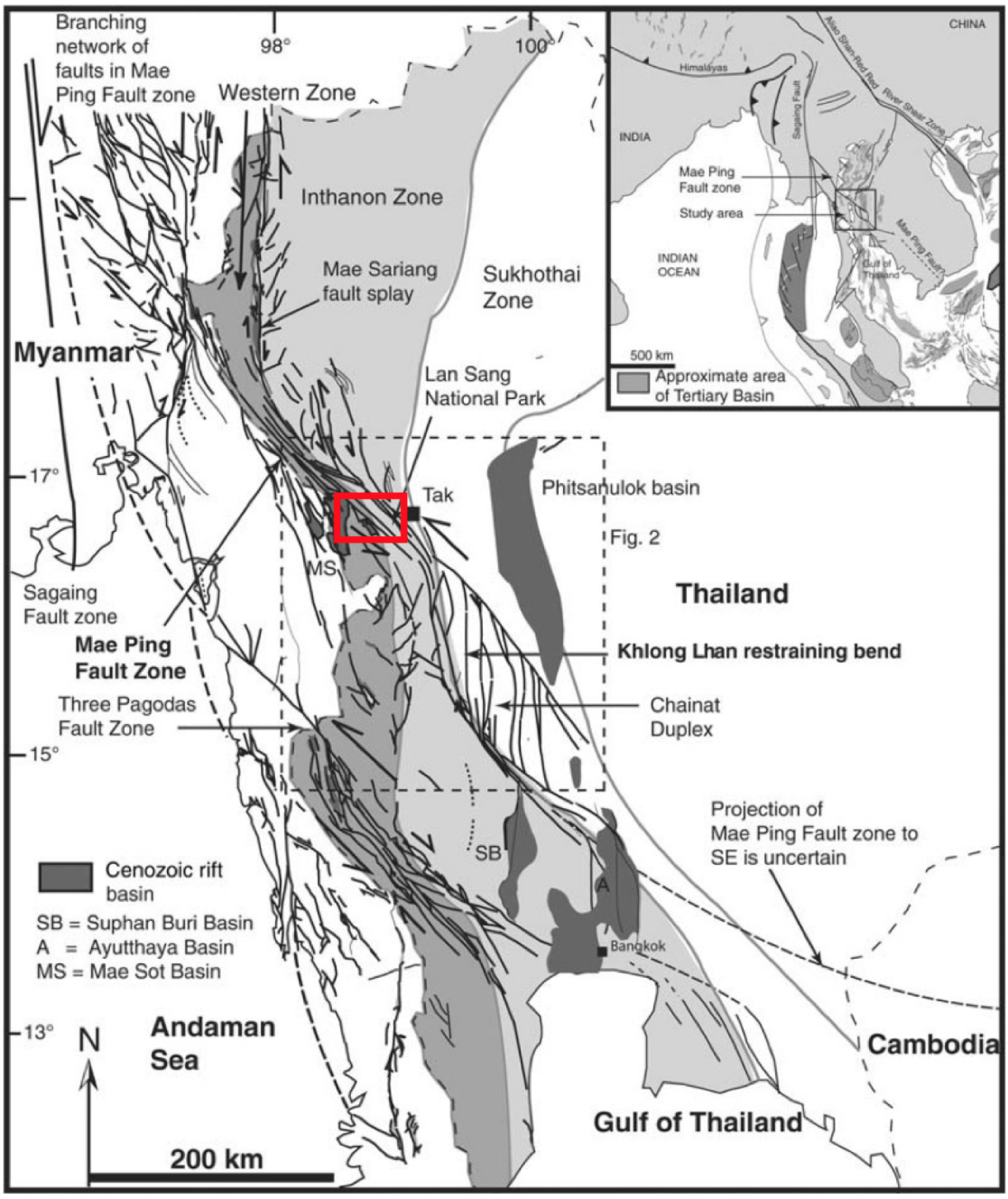

Figure 3.6: The MFPZ with the main study area indicated by the small red box. After Morley et al. (2007).

3.3 Previous geochronological investigations

The timing of the MPFZ represents the focus of this work. So far, radiometric data concerning the timing of the MPFZ are available from investigations undertaken by Ahrendt et al. (1991, 1993), Mickein (1997), Lacassin et al. (1997) and Palin et al. (2013). However, the first to propose an age for the gneisses cropping out in Western Thailand were Brown et al. (1951) and Buravas (1952) who assigned a Precambrian age to all gneisses and weakly metamorphosed rocks. Campbell (1975) who studied the metamorphic and structural evolution of the gneisses exposed in the Lan Sang National Park was the first to show that the paragneisses have suffered an amphibolite-facies metamorphism and that granitic material was conformably injected into the gneisses at the climax of metamorphism (Hansen and Wemmer, 2011). He also assumed a Precambrian age of the gneisses.
The first radiometric data come from Ahrendt et al. (1991, 1993). They obtained an U/Pb zircon age of 197 +2/-3 Ma for the gneisses along the road from Tak to Mae Sot. They suggest that these rocks reflect the timing of the amphibolite-facies metamorphism at the Triassic-Jurassic boundary. Dunning et al. (1995) proposed that the Triassic-Jurassic age represents the timing of the intrusion of the protolith of the orthogneiss of the Doi Inthanon complex, which they assumed to be the of the same origin as the Mae Cham pluton (205 +3/-4 Ma) to the west of the Doi Inthanon. In other words, they suggested the intrusion of the protolith of the orthogneiss to take place simultaneously with the emplacement of the Mae Cham pluton. Furthermore, based on monazite U/Pb ages, they proposed the amphibolite-facies metamorphism to occur during Cretaceous times.
However, concordant U/Pb zircon ages of 190 +3/-3 Ma by Mickein (1997) confirmed the results of Ahrendt et al. (1991, 1993). ϵ_TCHUR(Nd)-values of -10.64 to -13.69, clearly classifying the gneiss protoliths to be of sedimentary origin, led Mickein (1997) to the conclusion that the Late Triassic to Early Jurassic U/Pb zircon ages reflect the last amphibolite-facies peak metamorphism and thus excluded the possibility of an intrusion related age of the zircons. Both, Ahrendt et al. (1991, 1993) and Mickein (1997) undertook U/Pb dating on zircons of paragneisses and thus U/Pb data from orthogneisses were still lacking.
Lacassin et al. (1997), who carried out detailed structural investigations of the Lan Sang gneisses, also produced $^{40}Ar/^{39}Ar$ ages on biotites. They interpreted their results to document the last increments of left-lateral ductile shear along the MPFZ. They assumed that rapid cooling of the gneisses accompanied the late stages of left-lateral motion from 32.5 to 30.5 Ma. By 30.5 Ma temperature had dropped below 185°C not allowing for the continuation of ductile shear. Moreover, a second cooling phase was proposed to have taken place around 23.5 Ma. This latter cooling phase was inferred to be related to the reversal from left- to right-lateral shear which may have been coeval with the onset of E-W extension (Lacassin et al., 1997). Thus, they were the first authors to propose an age for the deformation along the MPFZ. Also they attributed their results to the continental extrusion model of Peltzer and Tapponnier (1988) and Tapponnier et al. (1986)

and at the same time supported the idea of northward diachronism in the onset and cessation of strike-slip movements leading to the lateral extrusion of SE-Asia (Figure 3.7).
The first U/Pb ages of an orthogneiss come from Palin et al. (2013). They obtained U/Pb and Th/U ages from monazites within the Lan Sang National Park. Because they ascribed $^{238}U/^{206}Pb$ ages to be incorrectly older due to excess ^{206}Pb, they used both U/Pb and Th/Pb isotope systems to provide geochronological constraints but favored Th/Pb ages for their interpretations, although they usually carry significantly larger associated uncertainties than U/Pb ages. However, their analyses from two monazite cores yield U/Pb lower intercept ages of 135.2 ± 3.4 and 134.1 ± 5.1 Ma while Th/Pb analyses yield 113.5 ± 9.0 Ma and 123.1 ± 12.6 Ma. U/Pb analyses ranging from c. 53 Ma and c. 38 Ma and Th/Pb analyses of c. 45 Ma and c. 37 Ma from the remainder of grains indicate significantly younger ages that may be related to partial recrystallization of older grains. The Cretaceous monazite ages were interpreted to represent initial magmatic protolith emplacement of the orthogneiss sample. Furthermore, Palin et al. (2013) suggest that Th/Pb monazite ages between c. 45 and c. 37 Ma represent a period of prograde metamorphic heating and monazite growth. Young grains parallel to (or in) the mylonitic foliation lead them to the conclusion that the mylonitic fabric was superimposed on the orthogneiss after metamorphism whilst the rock was still at high temperature. This interpretation was the first proposal of a maximum age of left-lateral motion and initiation of the MPFZ (Palin et al., 2013).

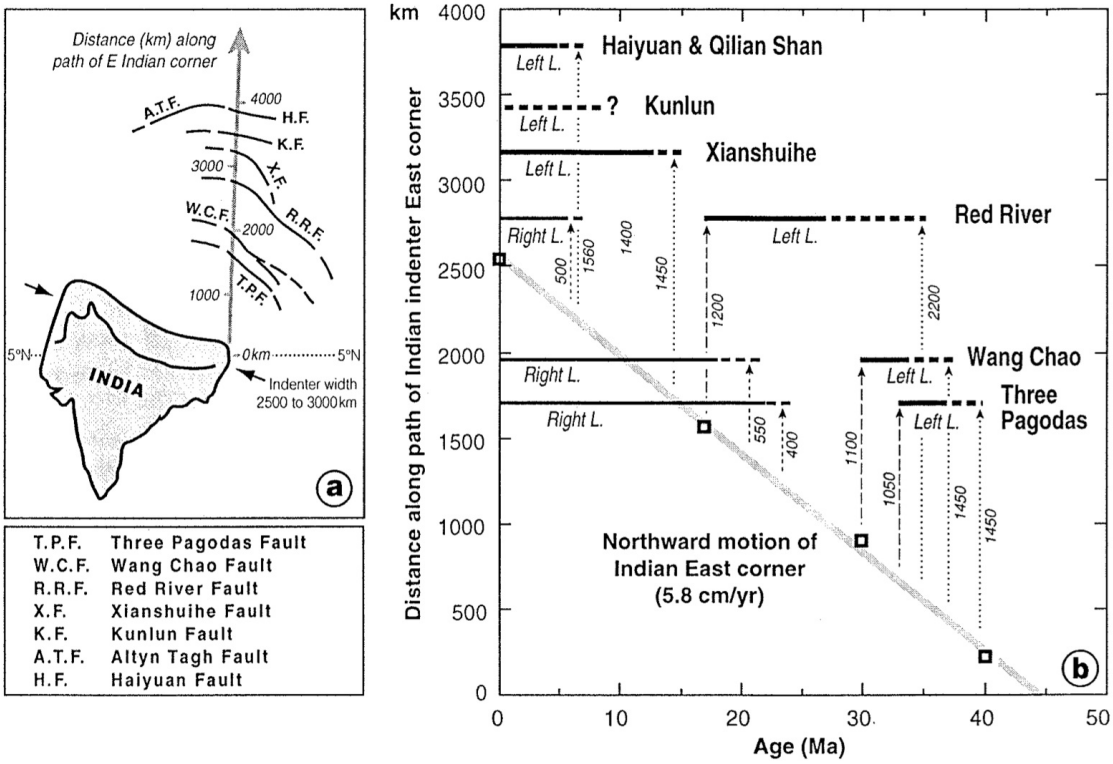

Figure 3.7: (a) Map showing indentation path of India (grey arrow) and present-day approximate distances between fault traces and Indian indenter (44 Ma). (b) Location, in N-S geographical frame, of major strike-slip faults of eastern and southeastern Asia plotted as a function of the ages of motion. Horizontal bars show periods of activity along each strike-slip fault. From Lacassin et al. (1997).

4 Methods

In a joint study with other investigators several methods have been combined in order to establish a time-dependent PT-history of the rocks cropping out in the Lan Sang National Park. Methods include field investigations, optical microscopy, geochemistry, thermometry, pseudsections and geochronology. Therefore, only the methods applied by the author will be discussed.

4.1 Field investigations

Field investigations were executed in February and March 2012 and 2013 in various locations in NW-Thailand. The main study area was near the city of Tak in the Lan Sang National Park. Further investigations were undertaken on the road from Tak to Mae-Sot (Lan Sang gneisses), the road from Mae-Ramat to Ban-Tak (Lan Sang gneisses), in the Khlong Lan National Park, at the Khlong Nam Lai waterfall and at the road from Hot to Omkoi („Omkoi Klippe“). Samples were taken for petrographical, petrological, geochemical and geochronological purposes. Pictures, GPS and compass measurements were made to document, localize and characterize outcrops.

4.2 Optical microscopy

More than 100 mostly oriented thin sections were made and studied to reveal mineral content, texture, micro-structures, shear sense indicators, etc. to get a rough idea of the temperature and pressure conditions and the deformation history. Moreover, thin sections were used in order to reveal zircon and monazite locations.

4.3 Geochemistry

For geochemical analyses the crushed, unsieved fraction of three samples taken for dating purposes was used (see 4.4.1). In order to obtain a representative sample, the fraction was quartered and half of it was retained while the other half was put aside. The halved fraction again was quartered. This process was repeated until the required sample amount (c. 20 g) was obtained. The sample then was ground by an agate mill containing Isopropanol for three to six hours. Afterwards the slurry was put into an oven, the dry whole rock powder was weighed and sent to Acme Analytical Laboratories (Vancouver) Ltd. for analysis. Six samples were sent to Vancouver in total. Sample 06/01 II and 13/01 IV stem from the subvolcanic

dyke and 01/01 IV and 12/02 II belong to the biotite-gneiss. Sample 12/02 III come from the augen-gneiss and 12/02 V from a leucocratic dyke. The main purposes of geochemical analyses were the classification of the samples after the Streckeisen scheme (QAPF) and the differentiation between ortho- and paragneiss. Furthermore, rare earth elements (REE) analysis was carried out and results were compared to data from the literature..

4.4 In-situ U-Th-Pb LA-ICP-MS Geochronology

For geochronological purposes three samples were taken and processed using standard grain size and gravity separation techniques: an augen-gneiss, a biotite-gneiss and a subvolcanic dyke. In order to avoid contamination of the isotopic system only fresh samples were used. The samples stem from river beds within the Lan Sang National Park. The sample quantity was about 30 kg each. The main goal of the sample preparation was to obtain zircons and monazites for in-situ U-Th-Pb LA-ICP-MS.

4.4.1 Sample preparation

The samples, after removing any possible source of contamination (lichen, dirt, weathered crust), were smashed using a hammer and crushed by a jaw breaker until the maximum grain size of c. 1 cm. They were then sieved resulting in three fractions: $>$ 1 mm, 1 - 0.3 mm, $>$ 0.3 mm. After sieving the finest sub-fraction ($<$ 0.3 mm) was separated using a Wilfley shaking table. Again three fractions were the result and the coarsest was taken for the subsequent heavy liquid separation, for which 2-Iod-Methane was used. The outcome of the separation procedure was a heavy mineral culmination. The final compartmentation was carried out by mounting zircons and monazites onto a sticky tape adhered to an object plate using a binocular microscope.

4.4.2 External morphology and internal texture

Zircons and monazites both were handpicked based on their appearance and their size. BSE and CL images also revealed their internal texture. Based on their external and internal appearance, an attempt was undertaken to classify them and ascribe either igneous or metamorphic characteristics.

4.4.3 Epoxy mount casting

For casting mounts a two-component adhesive was used. In the case of monazites Araldit was taken while for zircons it was Körapox. Körapox has turned out to be thermally more resistant than Araldit (see Figure 4.1). The heat generated by the laser during in-situ analyses seems to soften the resin and thus makes the grains ‚floating'. Furthermore, more resin is deposited within the mass spectrometer.

The zircon mounts of the subvolcanite sample were put into an oven for 48 hours at 800°C to get rid of possible Pb contaminants in grooves and cracks of the zircon surfaces and interior.

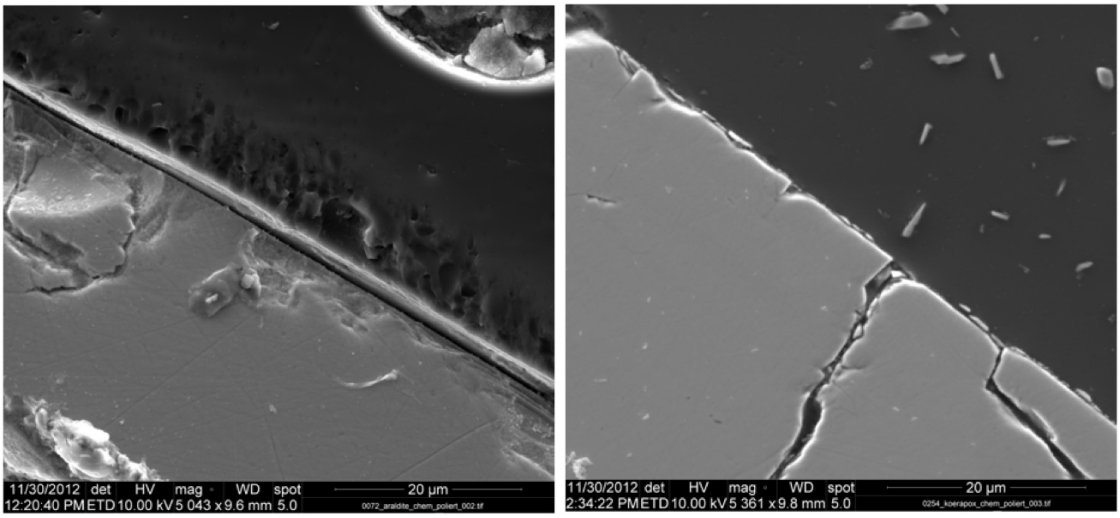

Figure 4.1: Left: Well-preserved grain-resin interface (Körapox). Right: Ablation effects caused by the released heat of the laser during in-situ analyses (Araldit).

4.4.4 Grinding and polishing

Grinding and polishing was undertaken manually for monazites, as they have to be treated with more caution due to their lower grinding hardness, and mechanically using a Buehler Minimet Polisher for zircons until crystals were ground to approximately mid-sections. Grinding was done using a silicon carbide powder (600, 1000) and polishing using diamond paste (3 μm, 1 μm and $\frac{1}{4}$ μm).

4.4.5 Scanning electron microscopy

Scanning electron microscopy using a FEI INSPECT S was applied to zircons and monazites to obtain images of the crystal surface. Different techniques were used to determine the chemical composition as well as to reveal the chemical zoning of both zircons and monazites.

Energy dispersive X-ray spectroscopy, EDX

EDX was applied on the mounted crystals in order to determine the approximate chemical composition. Based on the EDX analysis an explicit assignment and therefore determination of the minerals could be conducted. The voltage of the current was set to 15 kV and the spot size to 5.

Backscatter electrons, BSE

As monazites do not fluoresce, BSE were used to resolve the chemical zoning. The voltage of the current was set to 10 kV and the spot size to 5.

Cathodoluminescence, CL

CL was used to reveal the chemical zoning of zircons. The voltage of the current was set to 15 kV and the spot size to 5.

4.4.6 In-situ LA-ICP-MS

In-situ laser ablation inductively coupled plasma mass-spectrometry was undertaken on zircons and monazites at the Department of Lithospheric Research at the University of Vienna. U/Pb ages were determined using a 193 nm solid state Nd-YAG laser (NewWave UP193-SS) coupled to a multi-collector ICP-MS (Nu Instruments HR). For detailed information, see Klötzli et al. (2009). 237 measurements were carried out on zircons and monazites of the three samples, 46 on monazites and 191 on zircons. The isotopic measurements where analyzed with Isoplot 4.15. Replicate analyses of 0293 Plešovice gelb (mount 285, 286, 287, 288, 289, 290) and 0292/1255 Plešovice rot (mount 301, 302, 303, 305) standard zircon and 0198/1240 Dobragneis (mount 283, 284) standard monazite were used to determine the isotope ratios of the unknown material. CL and BSE images were used in order to select appropriate spots to place the laser beam. Mean ages are given at 95 % confidence level.

5 Remarks on zircons and monazites

5.1 Zircon

Zircon is a tetragonal orthosilicate mineral ($ZrSiO_4$) in which isolated SiO_4 tetrahedra are linked through sharing their edges and corners with intervening ZrO_8 dodecahedra. Its widespread applications make it of singular importance in Earth science (Harley and Kelly, 2007). Following Corfu et al. (2003) the mineral zircon is extremely variable both in terms of external morphology and internal textures reflecting the geologic history of the mineral (episode(s) of magmatic or metamorphic crystallization/recrystallization, strain imposed both by external forces and by internal volume expansion and chemical alteration).

External morphology

Zircon most commonly grows as doubly-terminated prismatic crystals with elongated (length-to-width) ratios. This ratio is commonly believed to reflect crystallization velocity. While needle-shaped acicular zircons are common in rapidly crystallized, porphyritic, subvolcanic intrusions, stubby and equant forms are more common in deep-seated, slowly cooled intrusions. Other factors affecting the shape of the zircon crystals are the composition and possibly the temperature of the crystallization medium (Corfu et al., 2003). The Pupin diagram classifies zircons based on the relative development of the 100 vs. 110 prismatic forms and the 211 vs. 101 pyramidal crystal forms. Dry alkalic and tholeiitic igneous rocks tend to be dominated by 100 vs. 101 forms, whereas those from aluminous to calc-alkaline rocks exhibit various combinations of forms with a prominent presence of 211, and those from water-rich granites and pegmatites tend to have 110 vs. 101 as their dominant forms. Skeletal zircons, which are characterized by the development of crystal-beams and walls surrounding empty space, are the most extreme form of rapid growth. On the other hand, metamorphically grown or modified zircons generally exhibit subrounded and highly resorbed shapes, but euhedral shapes are also possible. In the case of granulite-facies rocks, zircons sometimes also display multifaceted exteriors and considering metamorphosed rocks, irregular zircon shapes such as the cauliflower are possible (Corfu et al., 2003).

Zoning pattern

Zoning patterns in zircons reflect compositional variations of Zr and Si and more importantly, variations in Hf, P, Y, REEs, U and Th, where the composition of

the zones tends to vary between two end-members, one low in trace elements and one highly enriched in trace elements (Corfu et al., 2003). Various zoning patterns are known, such as oscillatory zoning, sector zoning, fir-tree zoning, patchy zoning, all representing different growth conditions, trace element concentration and variations in diffusion rates (Schaltegger et al., 1999; Corfu et al., 2003). It is in some cases, however, still a matter of debate which mechanism causes which zoning pattern. For example, sector zoning is believed by some authors to reflect kinetic factors and rapid changes in the growth environment during crystal development, while others propose the relation between growth rates and lattice diffusivity to be the reason and again others attribute sector zoning to rapidly fluctuating and unequal growth rates related to roughness of the growth surface and degree of saturation of the growth medium. Irregular and patchy textures are proposed to have experienced strain during final magmatic emplacement or to indicate local recrystallization along longitudinal micro fractures. Fir-tree zoning, on the other hand, reflects strong fluctuations of growth rates. And sometimes zircons suffer multiple episodes of resorbtion, recrystallization and/or growth of new zircons leading to a complex zoning pattern (Corfu et al., 2003).

Soccer ball zircons

Soccer ball zircons are described as being equant and with a ‚soccer ball' or ‚multi-faceted' habit and display little or no oscillatory zoning but show planar banding or sector zoning (Harley and Kelly, 2007). Vavra et al. (1996) cited, that they grow during prograde high-temperature anatexis, at different times in different rock compositions depending on the melting reactions intersected. On the other hand, sector-zoned soccer ball zircons are attributed by Schaltegger et al. (1999) to high-temperature subsolidus growth, whereas planar-zoned overgrowth and acicular grains form during melt crystallization. Klötzli-Chowanetz et al. (1997) states that soccer ball zircons grow during highest metamorphic, granulite-facies conditions. Concluding these statements, a consensus on the high-temperature growth conditions is given (Figure 5.1). However, these zircons might be interpreted to mark a state of partial melting or crystallization eventually leading to an intrusion (oral communication by Urs Klötzli).

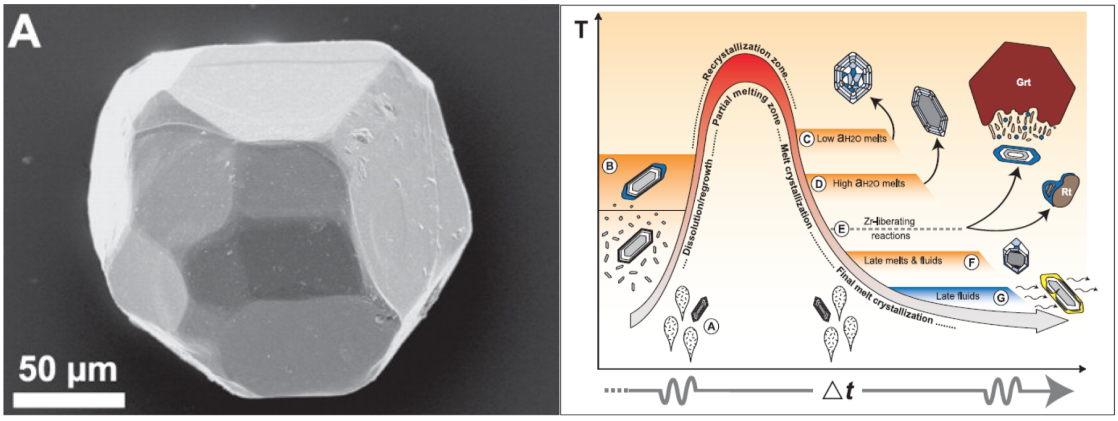

Figure 5.1: Left: Soccer ball zircon SEM image exhibiting multi-faceted outlines. Right: Schematic temperature (T) – time (Δt) path for a hypothetical high-T terrain formed in the deeper parts of a hot orogen. After Harley et al. (2007).

5.2 Monazite

Monazite is a monocline phosphate mineral ([LREE, Th]PO_4) and increasingly recognized as a powerful mineral for age dating in a wide variety of igneous and metamorphic rocks (Scherrer et al., 2000). Moreover, it is generally less affected by Pb loss compared to zircons, presumably because of the greater resistance of monazite to radiation damage effects (Kohn and Malloy, 2004). Still, relatively little is known about monazite forming reactions according to Scherrer et al. (2000) but the fact, that monazites are found in rocks of nearly every metamorphic grade, ranging from greenshist to granulite-facies (Spear and Pyle, 2002; Kohn and Malloy, 2004). However, one potential monazite forming reaction might be due to the prograde breakdown of allanite (Kohn and Malloy, 2004). Apparently, Al^{3+} and Ca^{2+} contents are controlling factors for either monazite or allanite growth (Spear and Pyle, 2002).

Concerning the external morphology, the size tends to depend on the temperature, i.e. the higher the temperature the coarser-grained the monazites (Spear and Pyle, 2002). Referring to the zoning patterns of monazite, three distinct types of are known so far (Spear and Pyle, 2002): concentric, patchy and "intergrowth-like" zoning patterns. Euhedral and prismatic outlines and a compositional zoning pattern are features indicative of a magmatic origin, while subrounded monazites containing patchy internal zoning patterns with brighter and darker domains seem to be typical for a metamorphic origin (Ayers et al., 1999). Episodic growth, dissolution and/or precipitation and the fact that Pb diffusion in monazite is very slow (in the order of 10^{-20} to 10^{-21}; after Cherniak et al. (2004)) result in domains of different chemistries and ages and therefore might be an explanation why metamorphic monazite crystals frequently exhibit complex internal zoning (Kohn and Malloy, 2004).

6 Results

The results of the field investigations, microprobe analyses, thermometry and pseudosections are extensively described in the accompanying work of Palzer (2013).

6.1 Field investigations

Palzer (2013) described all lithologies, in terms of mineral content, texture and microstructures, cropping out in the Lan Sang National Park and compared them with investigations undertaken on the road from Tak to Mae-Sot, the road from Mae-Ramat to Ban-Tak, in the Khlong Lan National Park, at the Khlong Nam Lai waterfall and at the road from Hot to Omkoi („Omkoi Klippe“). In doing so, he tried to find similarities between the lithologies, all being part of the CM-L belt. Our findings match more or less with the ones of Campbell (1975) and Lacassin et al. (1997). While in the NE of the cross section different kinds of orthogneisses can be identified, towards the SW orthogneisses become less abundant and calc-silicates, marbles and quartzite increase in quantity, indicating a probable sedimentary origin of the rocks. In addition, two discordant, clearly undeformed subvolcanic dykes (UTM N1854567/E500276, 367 m; N1855040/E499822, 438 m) situated within the highly deformed gneisses could be identified. One is located at the main river and another one within a dry riverbed more to the N. They are isolated small bodies occupying only a few square meters. For the purpose of in-situ U-Th-Pb LA-ICP-MS dating three samples have been taken. These samples stem from the augen- and biotite-gneiss (N1855299 E501748, 260 m) and from the subvolcanic dyke (UTM N1854567/E500276, 367 m) and are described in the following.

Augen-gneiss (01/01 II)
A porphyric gneiss showing a well-developed foliation of alternating dark (mainly biotite) and light (predominantly quartz and plagioclase) bands. Centimeter-scale K-feldspar augen are floating in a fine-grained groundmass of biotite. The augen-gneiss exhibits a mylonitic texture indicating a strong deformation (Figure 6.1).

Figure 6.1: Image of the augen-gneiss showing cm-scale feldspar augen within a finer-grained groundmass.

Biotite-gneiss (01/01 IV)

The more massive biotite-gneiss mainly consists of biotite, quartz and feldspar. Its appearance is much darker and finer-grained. Within the biotite-gneiss a dyke, having reaction rims towards the host rock and a lower biotite content, occurs. The reaction rims limit sharply to the adjacent host rock and consist of feldspar and quartz and are enriched in garnets, which probably grew in favor of biotite (Figure 6.2).

Subvolcanic dyke (06/01 II)

A relatively homogenous lithology having a granitic mineral composition and a reaction rim at the boundary of the surrounding calc-silicate rocks. Biotite and tabular feldspars are situated within a fine-grained groundmass revealing a porphyric texture (Figure 6.3).

Figure 6.2: Image of the darker, finer-grained biotite-gneiss, which intruded into the augen-gneiss.

Figure 6.3: Image of the undeformed, discordant subvolcanic dyke (lower part) in contact to the concordant, strongly deformed calc-silicate rocks (upper part).

6.2 Optical microscopy

6.2.1 Augen-gneiss (01/01 II)

The augen-gneiss has a porphyric texture and consists predominantly of K-feldspar (c. 50-60 %), quartz (c. 20-30 %), plagioclase (c. 5-10 %) and bitotite (c. 5-10 %). Accessory minerals are zircon, monazite and apatite. Big K-feldspar and plagioclase augen (a few cm in size) are situated within a fine-grained groundmass of biotite, quartz and plagioclase (a few mm in size). K-feldspar often shows perthitic exsolutions, symplectitic decomposition, relictic magmatic zoning and Karlsbad twins. Feldspars are generally well preserved and only slightly affected by kaolinitization. Plagioclase is characterized by polysynthetic twins and sometimes kink bands and undulatory extinction are visible. Quartz is characterized by undulatory extinction, grain boundary migration and bulging and sometimes has inclusions of biotite. Brownish biotites exhibit strong pleochroism and are formed by dynamic recrystallization representing greenshist- to amphibolite-facies conditions. Some of the biotites are affected by chloritization. In general, grains exhibit rather anhedral crystal outlines, only biotite also has euhedral crystals. Commonly minerals are well preserved. Veins filled with calcite and/or white mica follow decomposition structures within feldspars. Monazites were found in K-feldspar and biotite grains. Zircons were also located in K-feldspar and biotite grains, and additionally in quartz.

6.2.2 Biotite-gneiss (01/01 IV)

The main constituents are K-feldspar (c. 30-40 %), quartz (c. 20-30 %), plagioclase (c. 10-20 %), biotite (c. 10-15 %), calcite (c. 2-3 %) and chlorite (c. 1-2 %). The texture is generally rather mylonitic but in some parts relics of a porphyric texture are visible. Throughout the thin section a greenshit-facies overprint is visible. Biotites are marked by strong pleochroism and are affected by chloritization. K-feldspar is also strongly affected by fluid activity and sometimes shows relic magmatic zoning. K-feldspar is commonly larger than other minerals (up to cm-scale). Quartz shows undulatory extinction, relic grain boundary migration and bulging. Plagioclase is marked by polysynthetic twins. Mineral grains only seldom exhibit euhedral outlines and are rather anhedral. Quartz and plagioclase grains are usually a few millimeters in scale, while biotite is mostly smaller. Zircons could be found within quartz and plagioclase grains. Biotite- and augen-gneiss have a similar composition, although the latter is richer in feldspar and less affected by fluid activity. Moreover, the deformation recorded in the biotite-gneiss is much higher.

6.2.3 Subvolcanic dyke (06/01 II)

The subvolcanic dyke has a porphyric texture and consists of a fine-grained quartz-feldspar-chlorite groundmass and sometimes zoned and/or twinned, euhedral feldspar

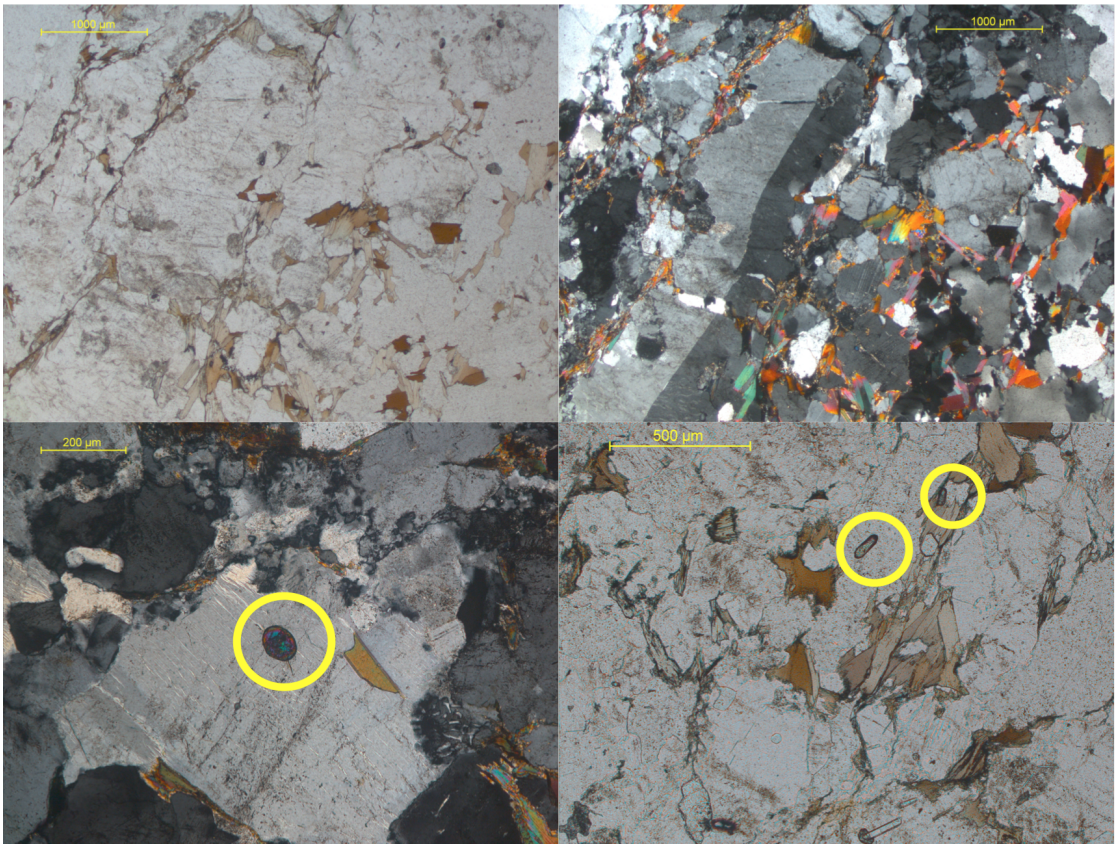

Figure 6.4: Top left: Image exhibiting the texture of the augen-gneiss (scale bar: 1000 μm). Top right: Same picture in cross-polarized view showing big, twinned K-feldspar augen within a finer grained matrix of plagioclase, quartz and biotite (scale bar: 1000 μm). Bottom left: Cross-polarized image of a monazite situated within a feldspar grain (scale bar: 200 μm). Bottom right: Image showing zircons within quartz and biotite (scale bar: 500 μm).

phenocrysts (up to 3-4 mm in size). The groundmass makes up roughly 60-70 %, plagioclase (c. 20 %), quartz (c. 5 %) and chlorite (c. 5 %) phenocrysts approximately 30 %. Quartz is anhedral and does not show undulatory extinction. Chlorite in most cases shows bladed crystal forms, but sometimes it is anhedral. It is green in color and exhibits a weak pleochroism. No obvious orientation is visible, neither shape nor crystal preferred orientation. Towards the border of the subvolcanic dyke the groundmass is glassy, while it is crypto-crystalline in the center of the dyke. Furthermore, the amount of calcite increases dramatically towards the rim. Also phenocrysts like pyroxene, hornblende and garnet, which are, despite some exceptions, not present in the central part of the dyke, occur. They were probably assimilated. Zircons could be found within quartz grains and also within the groundmass.

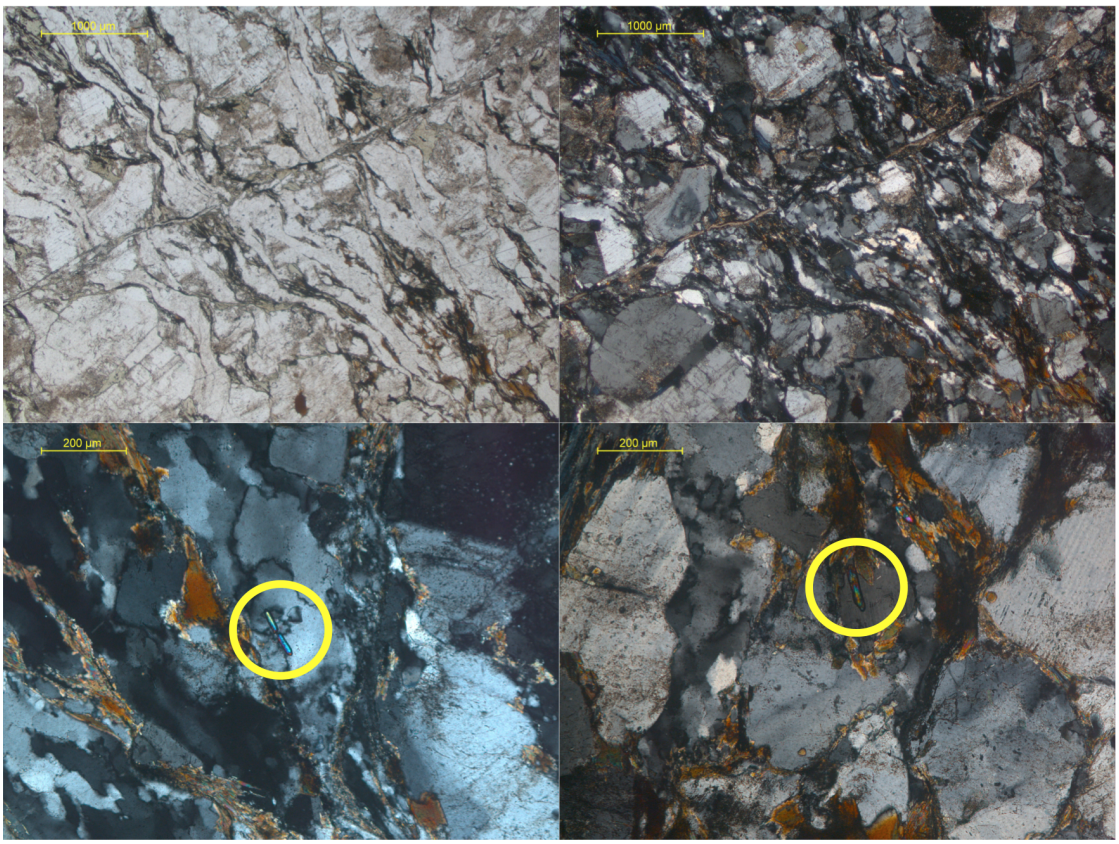

Figure 6.5: Top left and right: Images showing the texture of the biotite-gneiss and the strong fluid activity, e.g. chloritization and calcite veins (scale bar: 1000 μm). Bottom left and right: Cross-polarized images exhibiting locations of zircons within quartz and feldspar, respectively (scale bar: 200 μm).

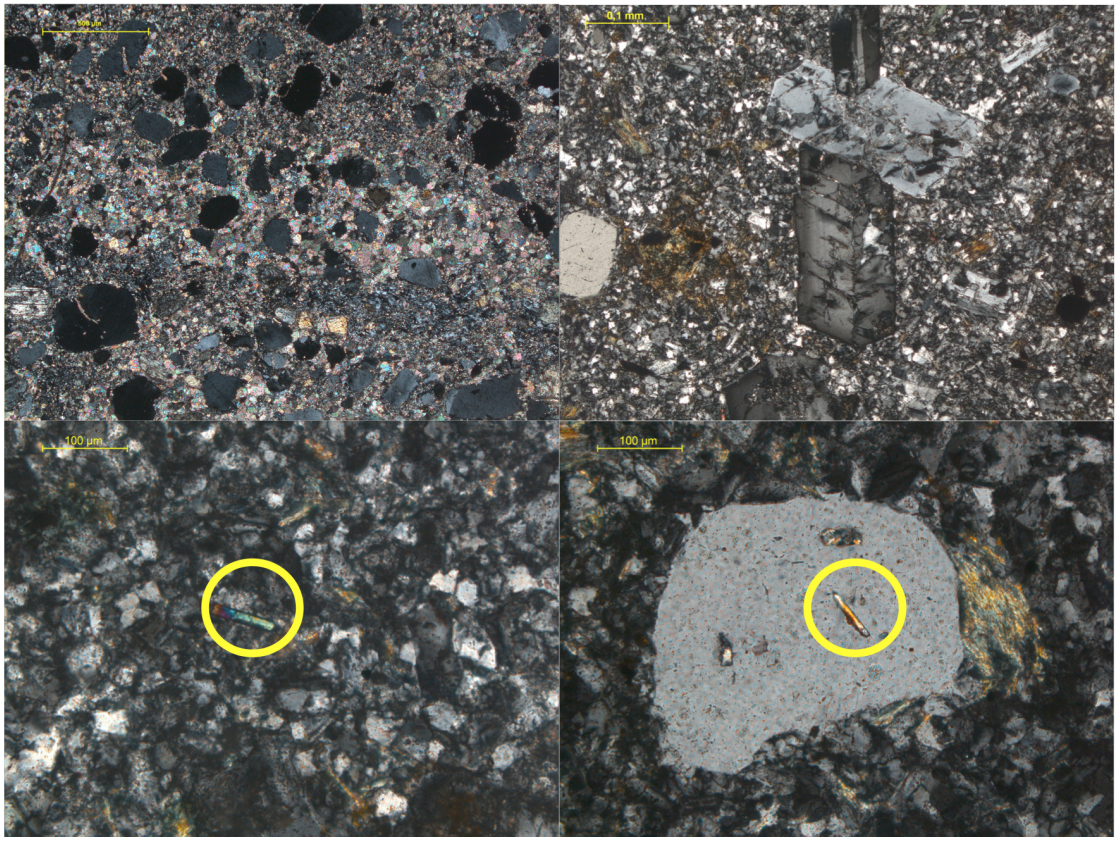

Figure 6.6: Top left: Cross-polarized image exhibiting the increased amount of calcite within the glassy matrix (scale bar: 500 μm). Top right: Cross-polarized pictures showing a magmatically zoned feldspar-twin within the porphyric texture of the subvolcanic dyke (scale bar: 0.1 mm). Bottom left and right: Cross-polarized images indicating zircon locations within the groundmass and within quartz grains, respectively (scale bar: 100 μm).

6.3 Geochemistry

Classification after Streckeisen (QAPF) scheme

In total six samples were plotted using the Excel spread sheet 'Ternplot', containing the minerals quartz, plagioclase and alkali-feldspar. Samples 06/01 II, 13/01 IV, 01/01 IV and 12/02 II plot within the granodioritic domain. The first two samples (06/01 II and 13/01 IV) come from the subvolcanic dyke, the third and fourth (01/01 IV and 12/02 II) are from the biotite-gneiss. Sample (12/02 V) from the leucocratic dyke is also located within the granodiorite domain (close to the granodiorite/tonalite boundary), while sample 12/02 III (augen-gneiss) lies within the granitic domain. Quartz, plagioclase and alkali-feldspar values are listed in the appendix (III. 4.2. Ternplot data (06/01 II, 13/01 IV, 12/02 V) and III. 4.3. Ternplot data (01/01 IV, 12/02 II, 12/02 III)).

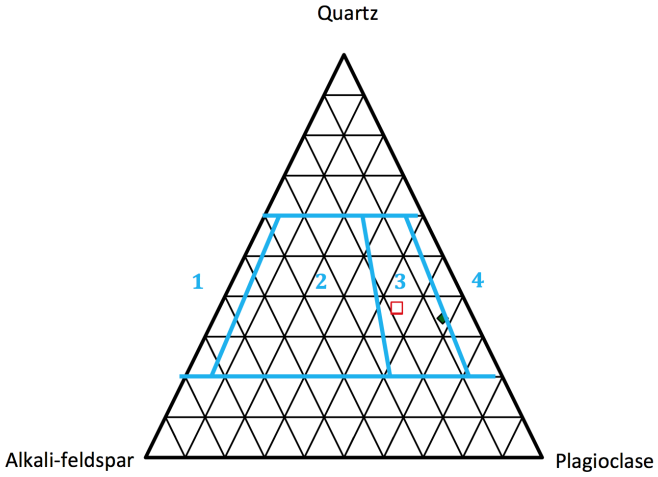

Figure 6.7: Ternplot of the subvolcanic dyke (06/01 II and 13/01 IV; red squares) and leucocratic dyke (12/02 V; green diamond) samples. Both subvolcanic dyke samples exhibit nearly identical composition, thus only one red square is visible. Numbers 1 to 4 represent: 1. Alkali-feldspar granite; 2. Granite; 3. Granodiorite; 4. Tonalite.

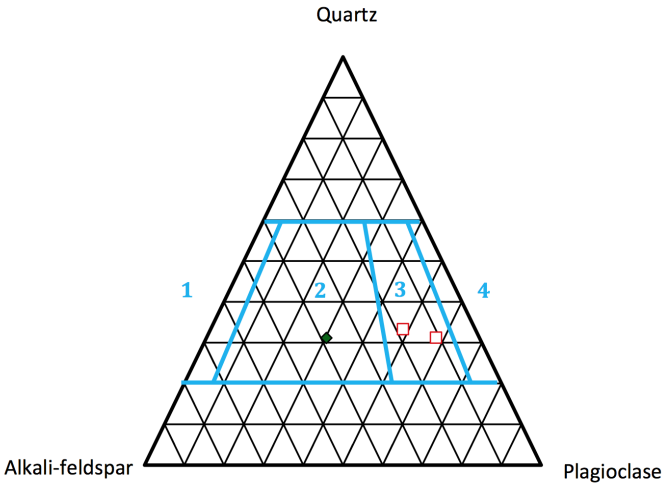

Figure 6.8: Ternplot of the biotite-gneiss (01/01 IV and 12/02 II; red squares) and augen-gneiss. Numbers 1 to 4 represent: 1. Alkali-feldspar granite; 2. Granite; 3. Granodiorite; 4. Tonalite.

REE patterns

The REEs show a distinctive behavior. All samples are enriched in LREEs (light rare earth elements) compared to HREEs (heavy rare earth elements). Starting with La, first and lightest of the REEs, the amount diminishes towards Lu, last and heaviest of the REEs (Figure 6.9, Figure 6.10, Figure 6.11). Lu usually is the least abundant. Passing from higher towards lower values, a change in the trend is marked by the elements Sm and Nd. From La to Sm and Nd, numbers have dropped dramatically from 250 and 150, respectively, marking a steep negative trend, and reaching Lu they are more or less equal, between approximately 20 and 5, reflecting a rather horizontal trend. REEs were normalized using chondrite values from McDonough and Sun (1995). Data can be found in the appendix (III. 4.4. REE diagram data).

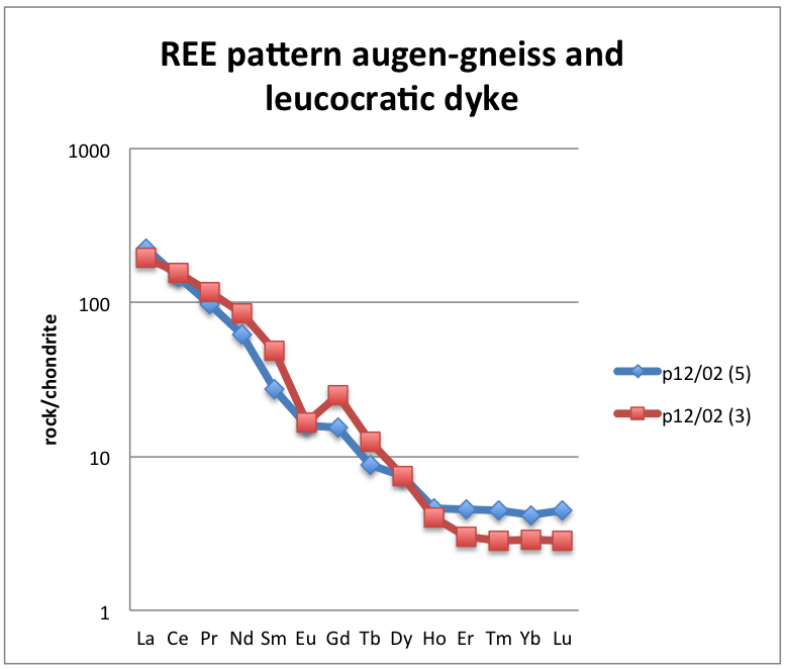

Figure 6.9: REE pattern of sample 12/02 V (leucocratic dyke) and 12/02 III (augen-gneiss) with a small Eu anomaly in the case of the augen-gneiss.

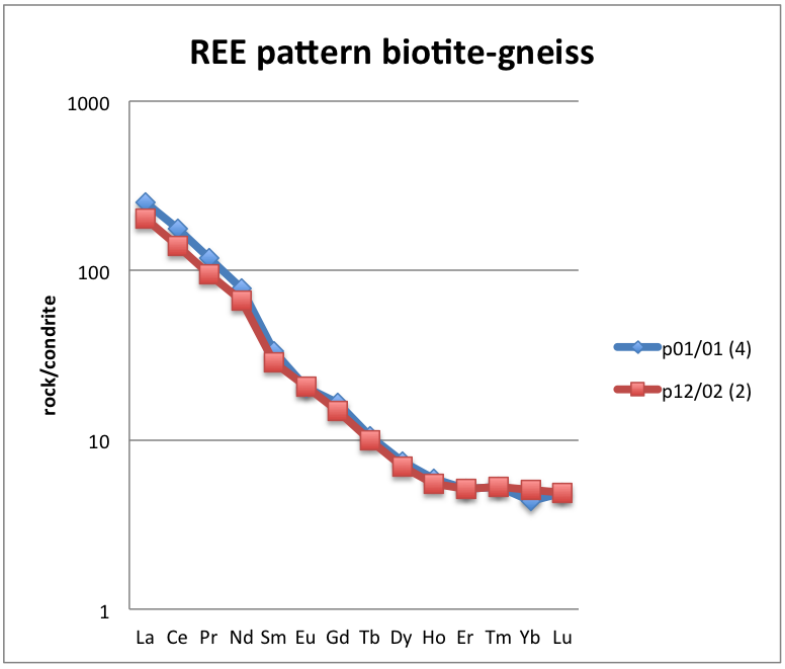

Figure 6.10: REE pattern of sample 01/01 IV and 12/02 II (biotite-gneiss).

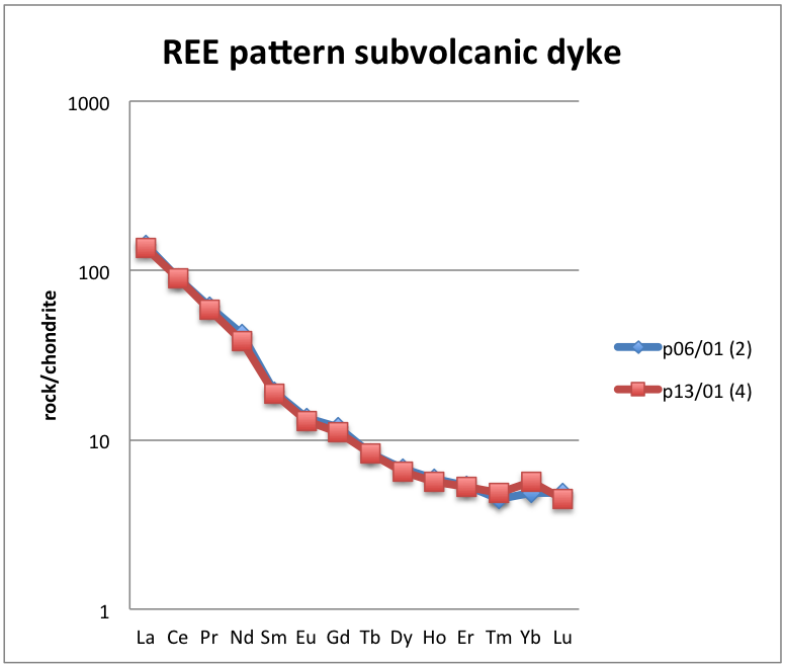

Figure 6.11: REE pattern of sample 06/01 II and 13/01 IV (subvolcanic dyke).

6.4 External morphology and internal texture

CL and BSE images of zircons and monazites, respectively, are attached in the appendix. Moreover, for each mount and the corresponding zircons and monazites, a reference is given in the subsections of the section 6.5 In-situ U-Th-Pb LA-ICP-MS Geochronology.

Augen-gneiss (01/01 II)

Both zircons and monazites are abundant. Zircons occur in different kind of shapes, reaching from prismatic to subrounded, and most of them are euhedral. Conversely, monazites do not vary in shape but in size, maybe indicating different growth conditions and/or different generations. Monazites usually exhibit subrounded shapes. No monazites displaying euhedral and prismatic outlines, indicative of a magmatic origin (Ayers et al., 1999) could be found. While zircons are usually colorless, with some exceptions being reddish or brownish, monazites tend to be yellowish in color. Both, zircons and monazites are transparent.

Biotite-gneiss (01/01 IV)

Zircons and especially monazites are both rare within the biotite-gneiss sample. Most zircons exhibit an elongated ratio and they are smaller compared to the zircons of the other two samples. It seems somehow counterintuitive, as the biotite-gneiss has probably experienced more strain than the augen-gneiss, and therefore big crystals should be more resistant to deformation than smaller, fragile ones. Basically, only prismatic zircons with low length-to-width ratios could be identi-

fied. Monazites again are subrounded in shape. Both, zircons and monazites are transparent and zircons are colorless whereas monazites are yellowish in color.

Subvolcanic dyke (06/01 II)

In this sample only zircons, but no monazites, could be found. The variety of zircons is exceeding the diversity of zircons in the augen-gneiss and biotite-gneiss by having also soccer ball zircons. Some of the crystals, however, are characterized by anhedral shapes, which is due to dissolution rather than to mechanical rounding related to detrital processes, while others exhibit perfectly euhedral shapes. Prismatic crystals also show differences in their elongated (length-to-width) ratios. The mean length (c-axis) of prismatic zircons in this sample is about 200 μm. Zircons are transparent and colorless.

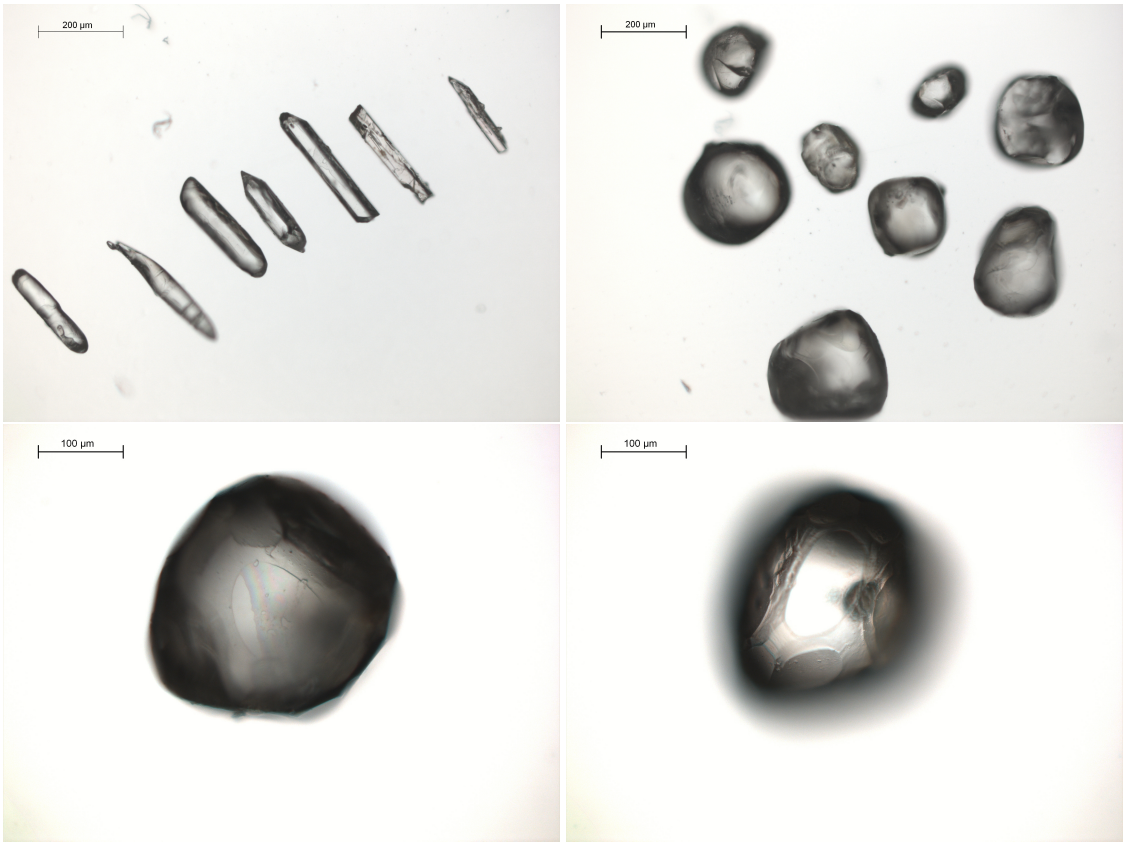

Figure 6.12: Optical microscopy photographs of zircons of the subvolcanic dyke, showing different morphologies (scale bar: 200 μm). Top left: Elongated euhedral and anhedral zircons (scale bar: 200 μm). Top right: Spherical and subrounded soccer ball zircons. Bottom left and right: Faceted outlines (crystal faces) of soccer ball zircons (scale bar: 100 μm).

6.5 In-situ U-Th-Pb LA-ICP-MS Geochronology

In total 237 age measurements could be obtained from zircons and monazites. About 12 % of the measurements are scattered between 40 and 50 Ma indicating an Eocene event, while roughly 23 % yield ages between 190 and 220 Ma, inferred to be related to the Indosinian orogeny. Approximately 29 % of the ages are distributed between these two geologic events. The remainder of measurements is either younger than 40 Ma or older than 220 Ma. A list of all mass-spectrometry data is available in the appendix (III. 1. Mass-spectrometry data zircon and III. 2. Mass-spectrometry data monazite).

6.5.1 Augen-gneiss (01/01 II)

283 monazite (small subrounded grains)

Monazites are generally subrounded in shape ranging from c. 50 to 150 μm exhibiting a predominantly patchy and only in a few cases concentric zoning pattern (see Appendix, III. 3.1.1. 283 Monazite (small subrounded grains)). The length-to-width ratio is between 1:1 and 2:1. Th/U ratios vary between 3.2 and 23.5. In total nine monazite ages range between c. 50 and c. 230 Ma comprising two Concordia ages of 78 ± 24 Ma and 215 ± 35 Ma (Figure 6.13 and Figure 6.14).

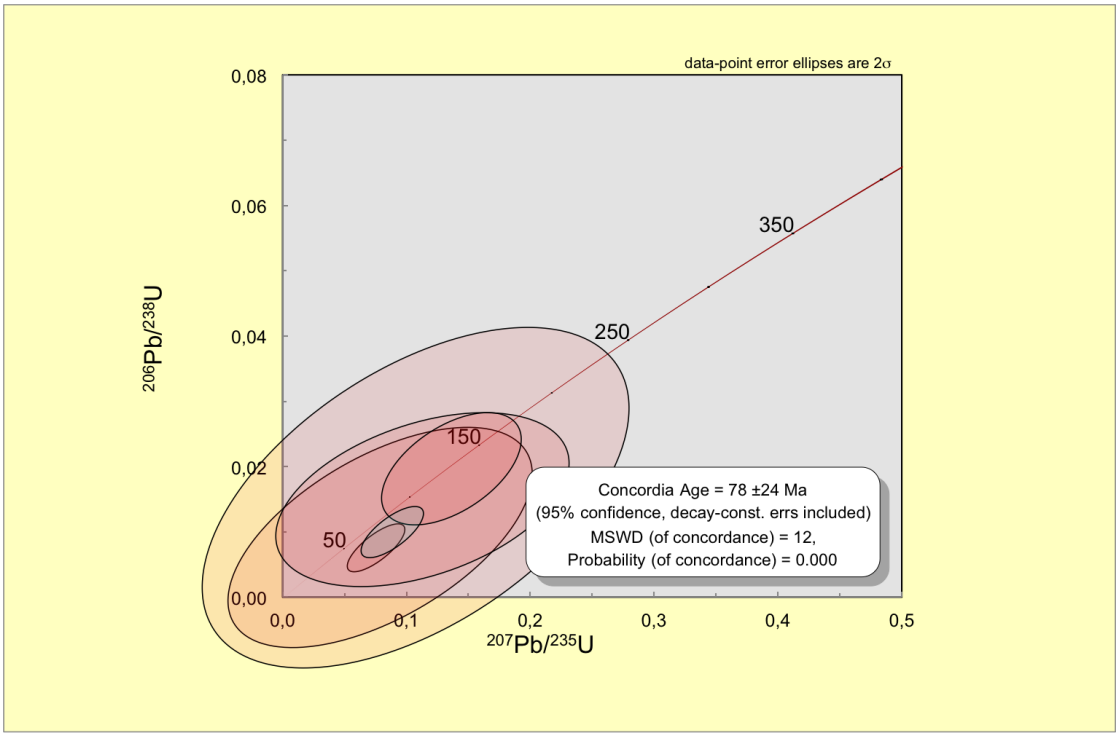

Figure 6.13: Concordia plot of mount 283. Concordia age of 78 ± 24 Ma.

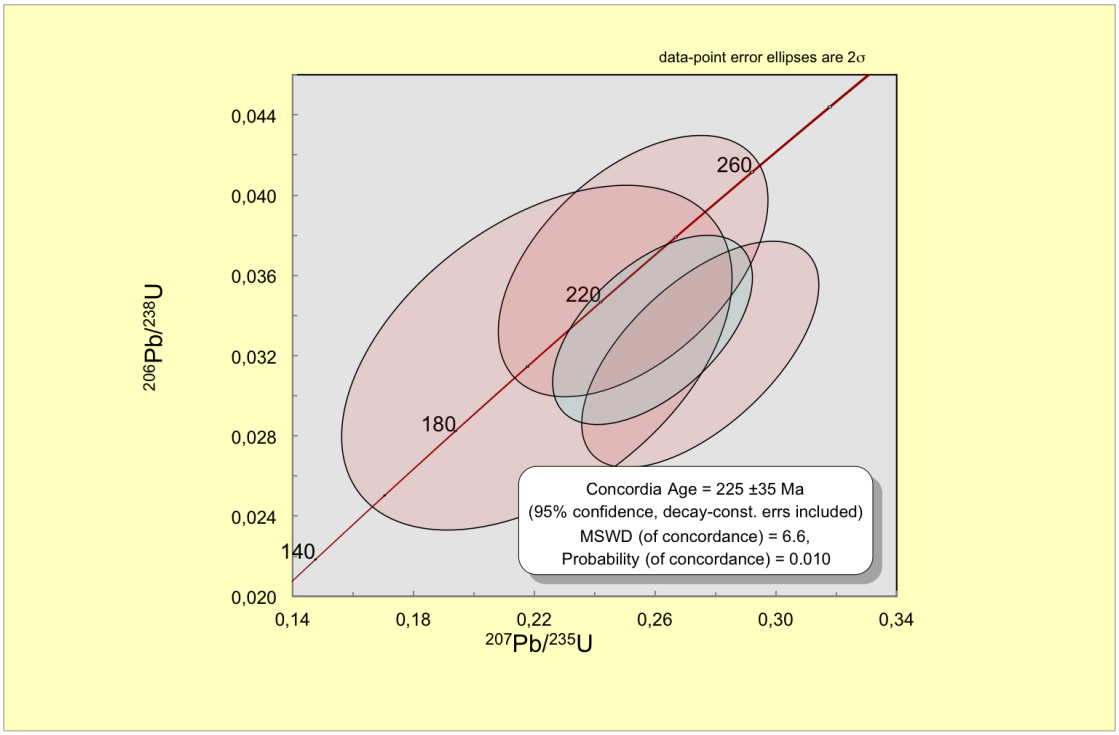

Figure 6.14: Concordia plot of mount 283. Concordia age of 225 ± 35 Ma.

284 monazite (large subrounded grains)

Monazites are generally subrounded in shape ranging from c. 100 to 400 μm exhibiting a predominantly patchy zoning pattern (see Appendix, III. 3.1.2 284 Monazite (large subrounded grains)). The length-to-width ratio is between 1:1 and 2:1, with most of the monazite having ratios of 1:1. Th/U ratios vary between 0.4 and 74.1, with most of the values between 27.1 and 74.1 and only two values below 27.0. In total 31 monazite ages range between c. 40 and c. 230 Ma. The majority of monazite ages clusters roughly between 45 Ma and 55 Ma exhibiting a Tera-Wasserburg age of 48.6 ± 0.9 Ma (Figure 6.15). Only 3 monazite ages are not part of this Eocene cluster forming a Concordia age of 219 ± 8 Ma.

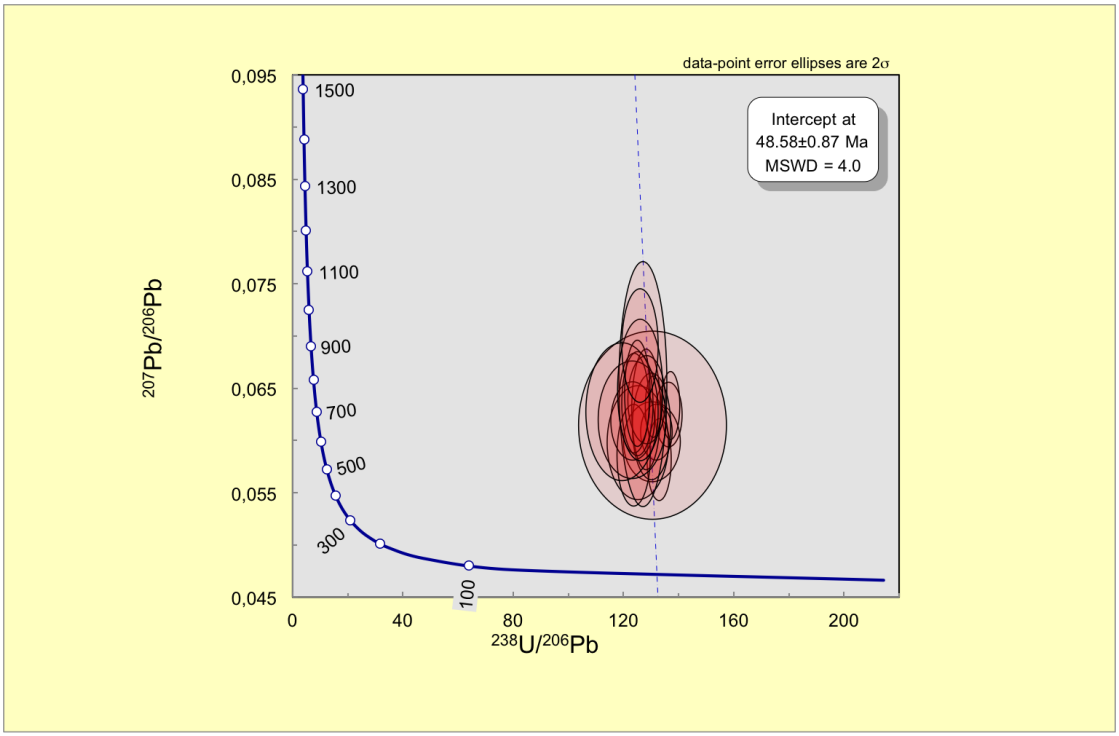

Figure 6.15: Concordia plot of mount 284. Tera-Wasserburg age of 48.6 ± 0.9 Ma.

301 zircon (small prismatic grains)

Zircons are prismatic in shape ranging from c. 150 to 250 μm and the length-to-width ratio is between 3:1 and 5:1. Zircons mainly exhibit oscillatory and patchy zoning patterns (see Appendix, III. 3.1.3. 301 Zircon (small prismatic grains)). Th/U ratios vary between 0.01 and 0.49. Roughly 60 % of the values are scattered between 0.01 and 0.09, the rest consists of values higher than 0.10. In total 30 zircon ages range between c. 120 and c. 230 Ma, while the majority of ages lies between 190 and 230 Ma (Figure 6.16) and only two ages are located closer towards the origin of the plot. Unfortunately, no Concordia age could be obtained. Moreover, some of the ages are above Concordia.

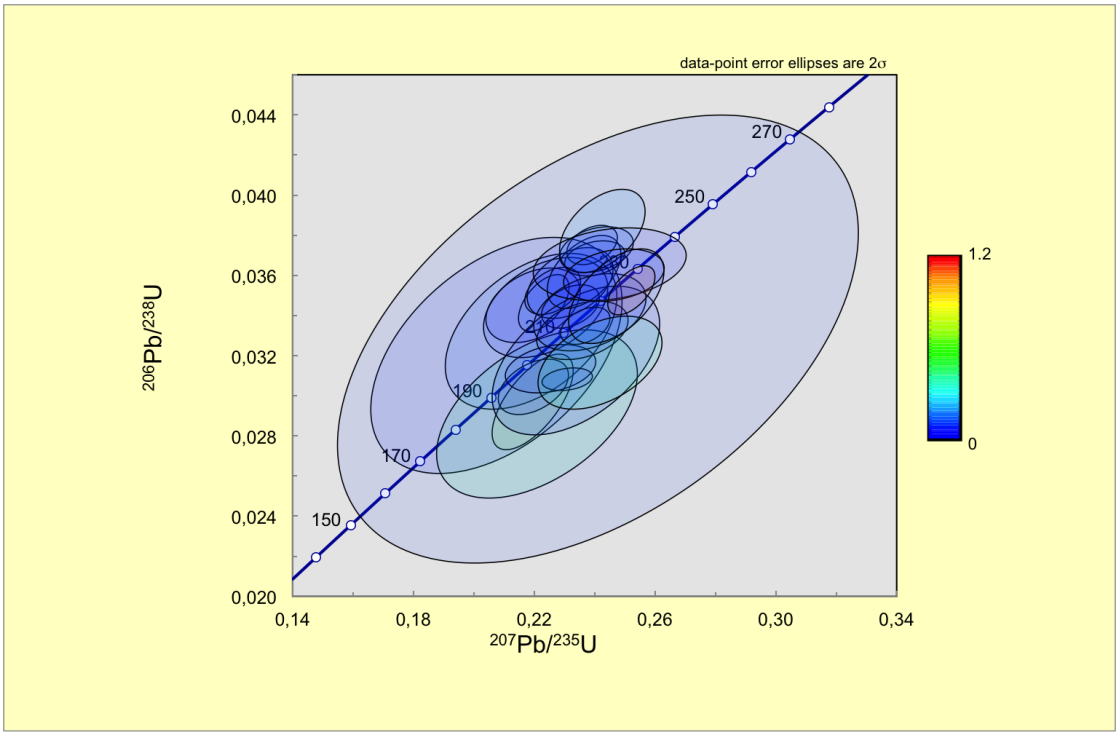

Figure 6.16: Concordia plot of mount 301. Age cluster between c. 190 and c. 230 Ma.

302 zircon (medium-length prismatic grains)

Zircons exhibit in general prismatic shapes with some exceptions and range between c. 100 and c. 300 μm. The zoning pattern is mainly oscillatory or complex (see Appendix, III. 3.1.4. 302 zircon (medium-length prismatic grains)). Length-to-width ratios are between 1.5:1 and 5:1, but for most of the zircons it is 3:1. Th/U ratios vary between 0.01 and 0.42. Roughly 65 % of the values are scattered between 0.01 and 0.07, the rest consists of values higher than 0.10. In total 20 zircon ages range between c. 50 and c. 1800 Ma. Most zircon ages plot roughly between 200 and 225 Ma (Figure 6.17). Two zircon ages plot around 50 Ma, four zircon ages between 160 and 180 Ma and two other zircon ages exhibit Precambrian ages. Again, no Concordia age could be obtained.

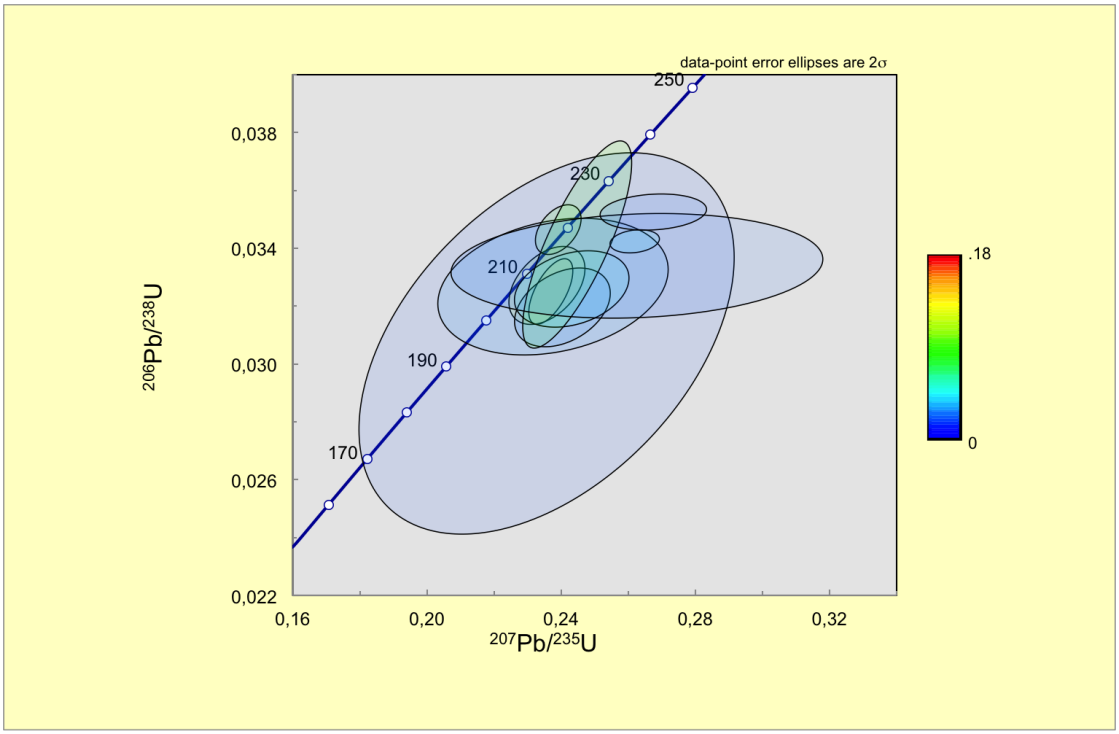

Figure 6.17: Concordia plot of mount 302. Age population between approximately 200 and 225 Ma.

303 zircon (large prismatic grains)

Zircons are prismatic to subrounded in shape and c. 150 to 250 μm in size exhibiting length-to-width ratios of 1:1 to 2.5:1. Zoning patterns are complex and only a few zircons show oscillatory zoning (see Appendix, III. 3.1.5. 303 zircon (large prismatic grains)). Th/U ratios vary between 0.01 and 0.76. Roughly 60 % of the values are scattered between 0.01 and 0.09, the rest consists of values higher than 0.15. In total 22 zircon ages range between c. 50 and c. 700 Ma but lie predominantly between 210 and 230 Ma (Figure 6.18). Three zircon ages are located approximately at 60 Ma and three zircon ages are scattered between 300 and 700 Ma. No Concordia age could be obtained from this mount.

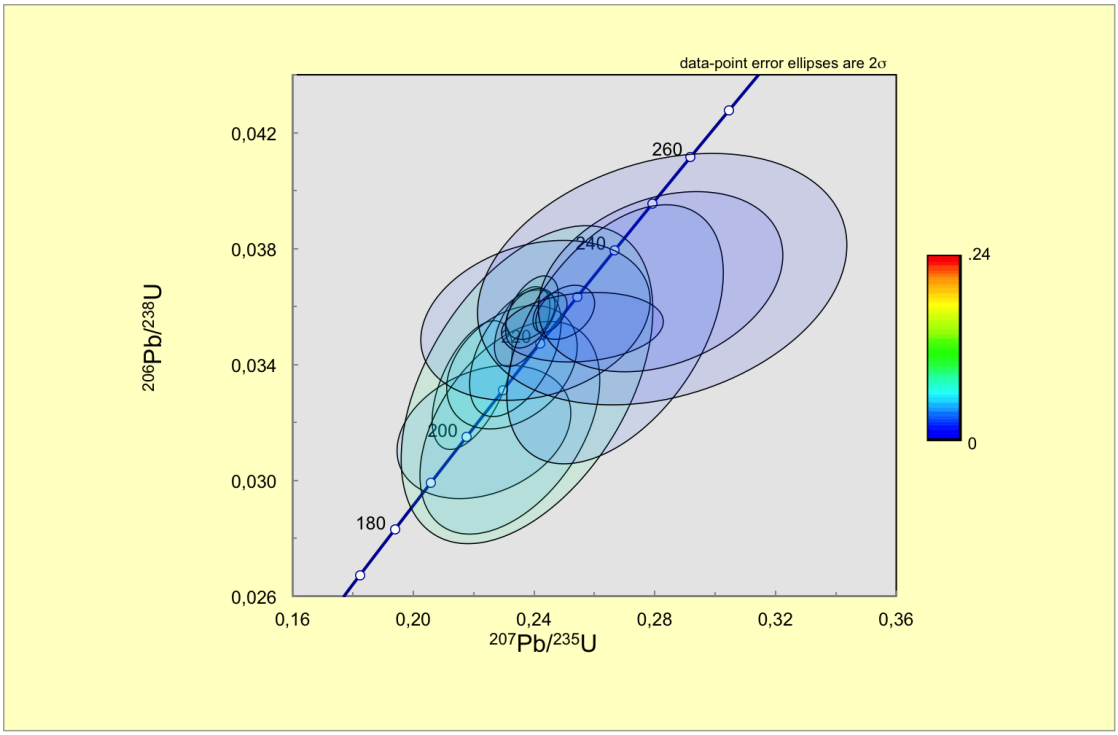

Figure 6.18: Concordia plot of mount 303. Age cluster spanning between c. 210 and c. 230 Ma.

6.5.2 Biotite-gneiss (01/01 IV)

Zircon and monazite ages in the biotite-gneiss reach from around 30 Ma to almost 2600 Ma. A Concordia age of 40 ± 2 Ma could be derived from monazites. Zircons on the other hand yield mainly ages between 180 and 280 Ma, but also older ages could be identified. A Concordia age of 276 ± 16 Ma could be conducted from zircons.

283 monazite (small subrounded grains)

Monazites are 150 to 250 μm in size exhibiting length-to-width ratios of 1:1 or 1.5:1. They are subrounded in shape and have a patchy zoning pattern (see Appendix, III. 3.2.1. 283 monazite (small subrounded grains)). Th/U ratios vary between 40.4 and 132.9, with nearly 80 % being scattered between 40.4 and 50.1. In total six ages could be obtained from monazites of this mount. All of them form a cluster around 40 Ma, which is represented by a Concordia age of 40 ± 2 Ma (Figure 6.19).

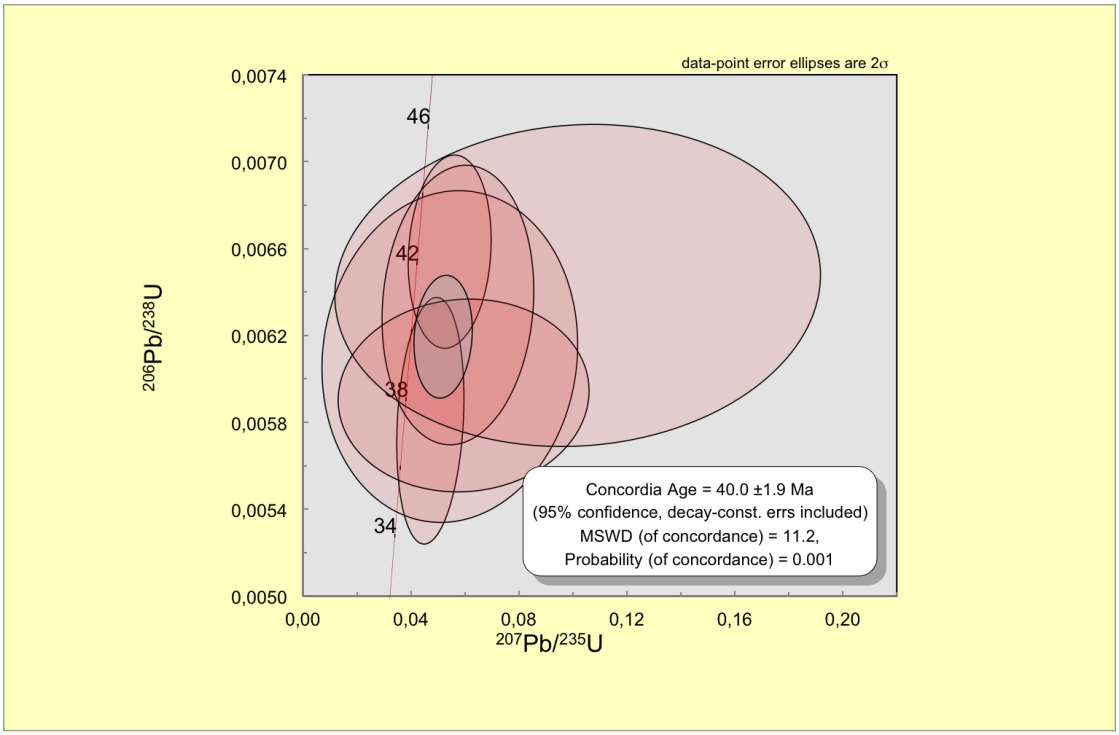

Figure 6.19: Concordia plot of mount 283. Concordia age of 40 ± 2 Ma.

305 zircon (prismatic grains)

Zircons are predominantly prismatic but some are also subrounded in shape and typically 100 to 200 μm in size. The length-to-width ratio varies between 1.5:1 and 4:1, with most of them having a ratio of 3:1. Zircons often exhibit oscillatory and sometimes complex or patchy zoning patterns (see Appendix, III. 3.2.2. 305 zircon (prismatic grains)). Th/U ratios vary between 0.03 and 0.61. Roughly 20 % of the values are scattered between 0.03 and 0.16 and roughly 75 % of the values lie between 0.19 and 0.61. In total 22 zircon ages range between c. 40 and c. 2600 Ma. Most of the zircon ages lie between 180 and 280 Ma with two clusters, one approximately at 200 Ma and the other approximately at 280 Ma. Fife zircon ages form an age accumulation between 40 and 55 Ma (Figure 6.20) and three zircon ages exhibit Precambrian ages.

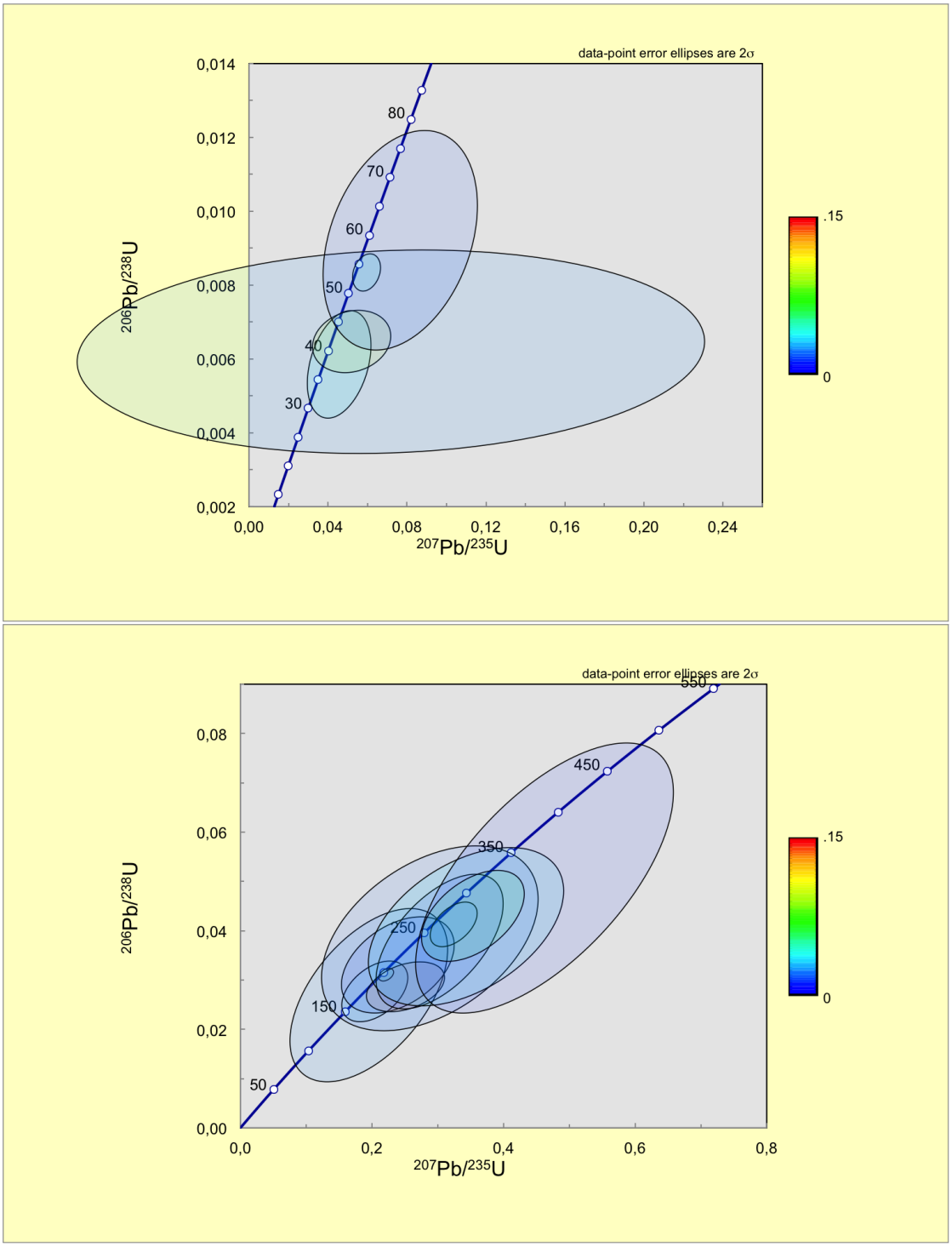

Figure 6.20: Concordia plots of mount 305. Top: Age cluster between 40 and 55 Ma. Bottom: Age populations at c. 200 Ma and c. 280 Ma.

6.5.3 Subvolcanic dyke (06/01 II)

Zircon ages of the subvolcanic dyke show a wide distribution from approximately 30 Ma to nearly 900 Ma. The youngest Concordia age found in this sample is 29 ± 3 Ma, being the youngest age found in all of the samples. An age cluster, containing zircon ages between 40 Ma and 50 Ma with Concordia ages of 42 ± 2 Ma and 51 ± 2 Ma, could be found. The mentioned Concordia ages are made up by soccer ball zircons. Moreover, a cluster yielding zircon ages between 180 Ma and 240 Ma could be identified as well as a few older zircon ages including a Concordia age of 430 ± 56 Ma.

285 zircon (small soccer ball grains)

Zircons are roughly between 80 and 200 μm in size. Most of the zircons are sub-rounded to elongated in shape exhibiting length-to-width ratios between 1:1 and 2.5:1. Zircons show primarily patchy and complex zoning patterns (see Appendix, III. 3.3.1. 285 zircon (small soccer ball grains)). Th/U ratios vary between 0.1 and 0.7, where only two values are below 0.2. In total 13 zircon ages range between c. 40 and c. 200 Ma. All of the ages are scattered within these limits and no real age population is present. Four ages tend to form a cluster at 80 Ma and five ages seem to accumulate approximately at 140 Ma giving upper and lower Cretaceous ages, respectively (Figure 6.21). Some of the zircon ages of the older cluster are located above Concordia.

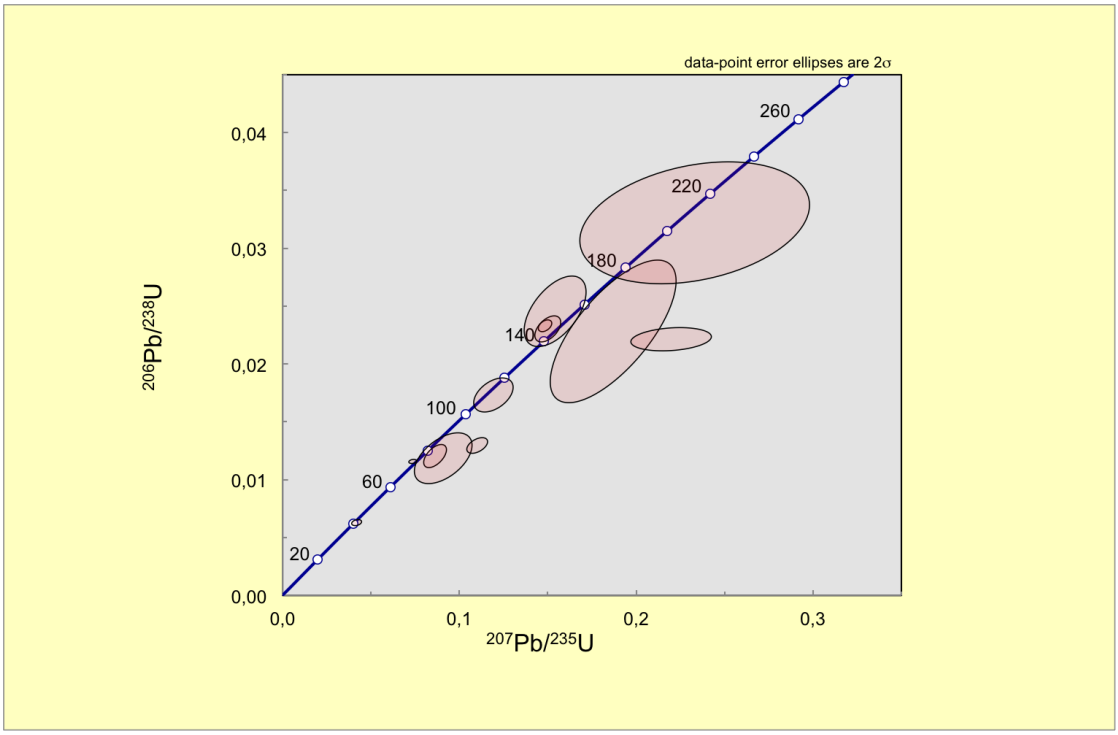

Figure 6.21: Concordia plot of mount 285. Cretaceous age populations (?) approximately at 80 and 140 Ma.

286 zircon (large soccer ball grains)

Zircons are mostly spherical in shape but some are rather elliptically resulting in length-to-width ratios of 1:1 and 1:1.5. The size varies between 150 and 300 μm. Zircons show sector, oscillatory and patchy zoning patterns (see Appendix, III. 3.3.2. 286 zircon (large soccer ball grains)). Th/U ratios vary between 0.1 and 0.4, where only two values are below 0.2. In total 16 zircon ages range between c. 40 and c. 650 Ma. Apart from three zircon ages, two of them around 180 Ma and one around 650 Ma, all zircon ages form a cluster between 40 and 50 Ma. Two Concordia ages could be obtained (42 ± 2 Ma (Figure 6.22) and 51 ± 2 Ma (Figure 6.23)) from this cluster.

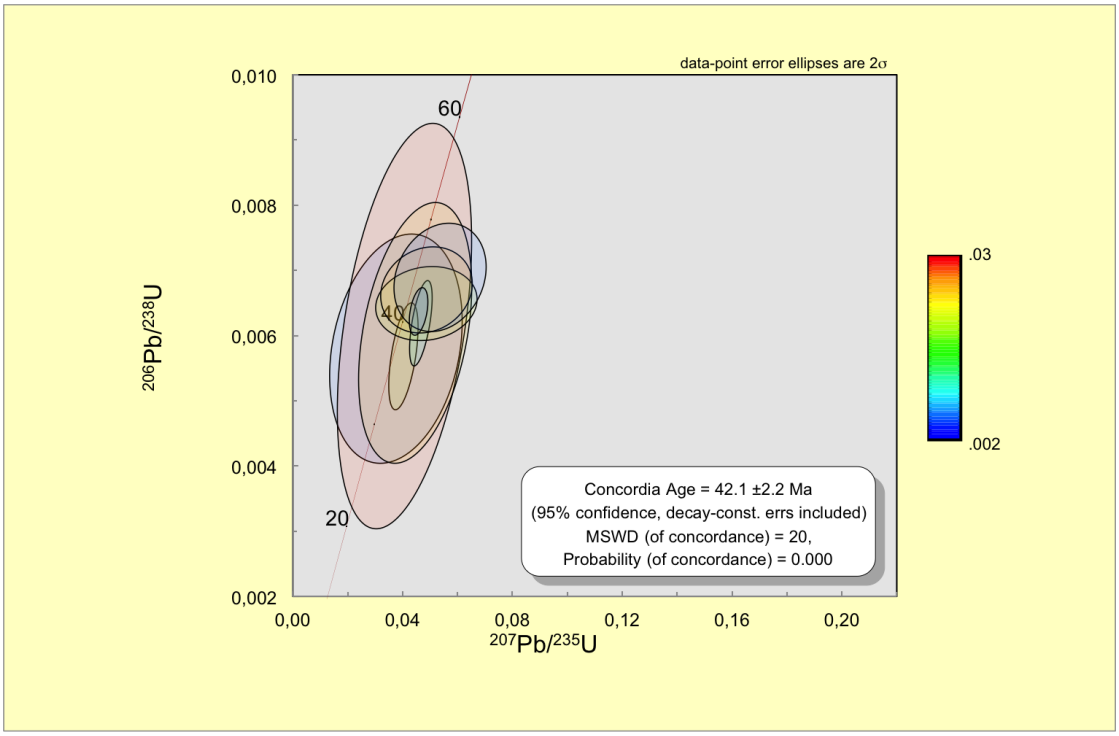

Figure 6.22: Concordia plot of mount 286. Concordia age of 42 ± 2 Ma.

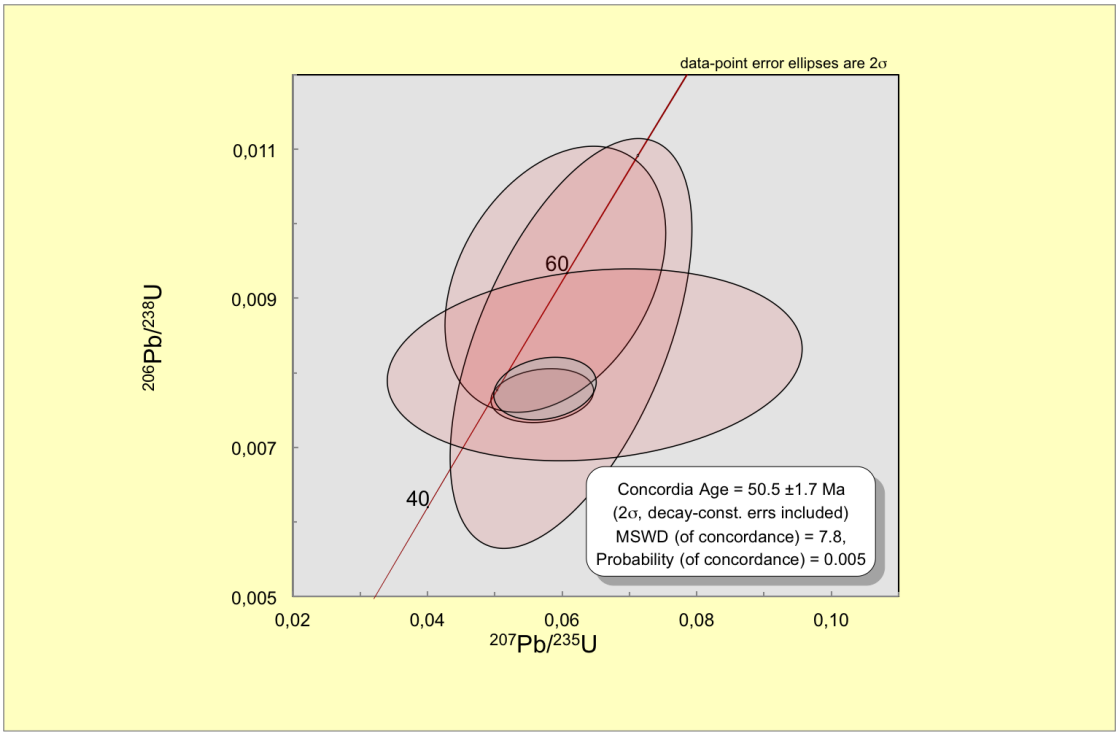

Figure 6.23: Concordia plot of mount 286. Concordia age of 51 ± 2 Ma.

287 zircon (small euhedral and spherical grains)

The four spherical zircons added to this mount, due to their small size, exhibit mainly subrounded outlines, while the remainder of grains has an elongated prismatic shape. Zircons are roughly between 100 and 200 μm in size. Length-to-width ratios vary between 1:1 and 11:1, while spherical zircons exhibit ratios of 1:1 or 2:1 and the majority of elongated prismatic zircons reveal ratios ranging between 4:1 and 6:1. Zircons generally have oscillatory or patchy zoning patterns (see Appendix, III. 3.3.3. 287 zircon (small euhedral and spherical grains)). Th/U ratios vary between 0.07 and 0.48, where most of the values are scattered between 0.19 and 0.48 and roughly a third of them ranging from 0.07 to 0.14. As the predominantly oscillatory zoning is very narrow it was impossible to measure single zones. Hence, most of the measurements undertaken represent mixing ages. In total 21 zircon ages range between c. 20 and c. 550 Ma (Figure 6.24). The biggest cluster with roughly 30 % of zircon ages is located near the origin of the Concordia of c. 30 Ma. Moreover, a Concordia age of 224 ± 17 Ma and one at 458 ± 88 Ma could be obtained.

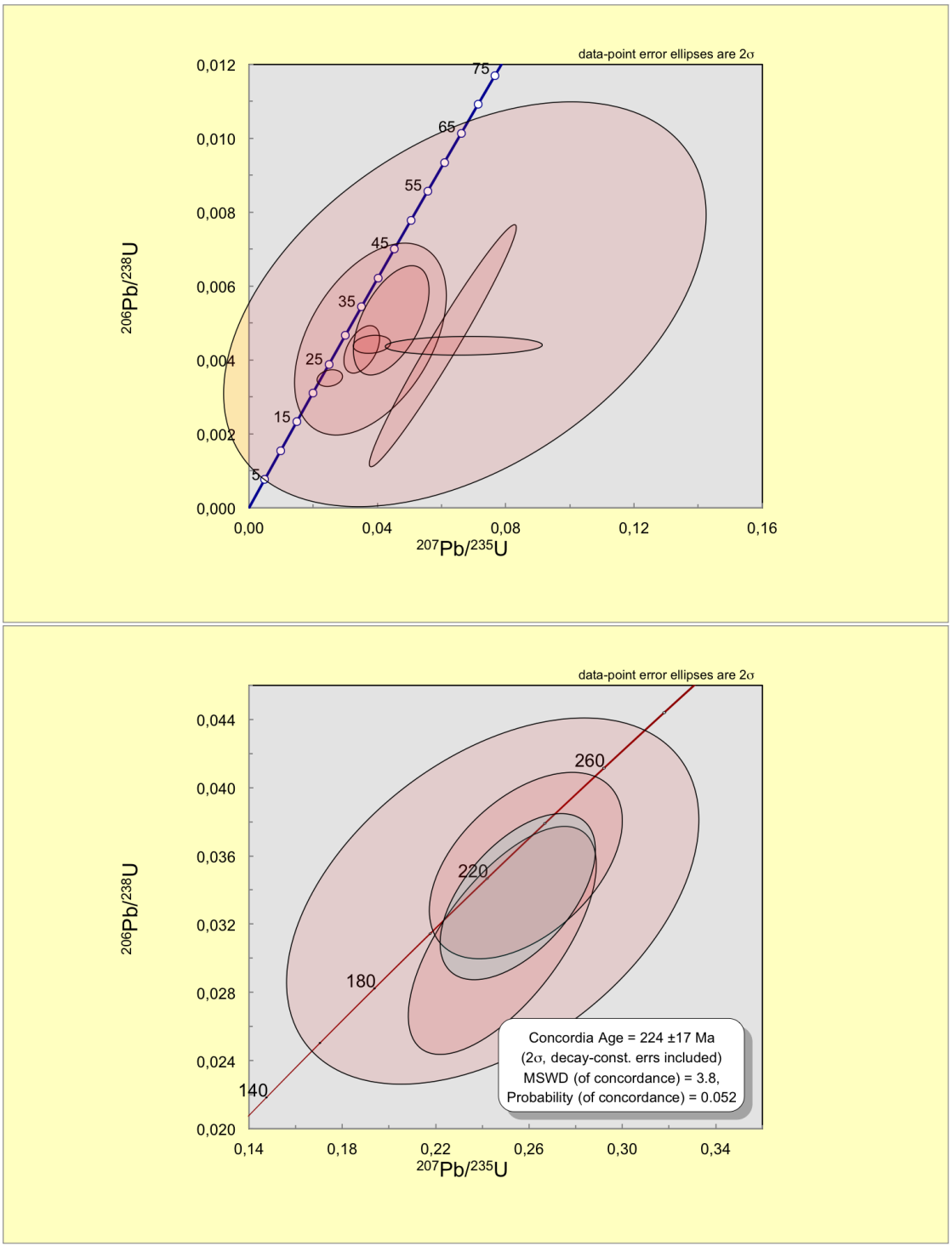

Figure 6.24: Concordia plots of mount 287. Top: The majority of ages is located towards the origin of the Concordia plot, at approximately 30-40 Ma. Bottom: Concordia age of 224 ± 17 Ma.

288 zircon (large euhedral grains)

Most of the zircons are about 120 to 200 μm in size with length-to-width ratios ranging between 1.5:1 and 5:1, but predominantly being 1.5:1 or 2:1. Generally, zircons are prismatic to subrounded in shape. Zoning patterns are oscillatory and predominantly patchy and complex (see Appendix, III. 3.3.4. 288 zircon (large euhedral grains)). Th/U ratios vary between 0.1 and 0.7. Roughly 25 % of the values are below, the remainder above 0.2. In total eleven zircon ages range between c. 80 and c. 450 Ma, with most of them between 180 and 230 Ma (Figure 6.25). No Concordia age could be derived.

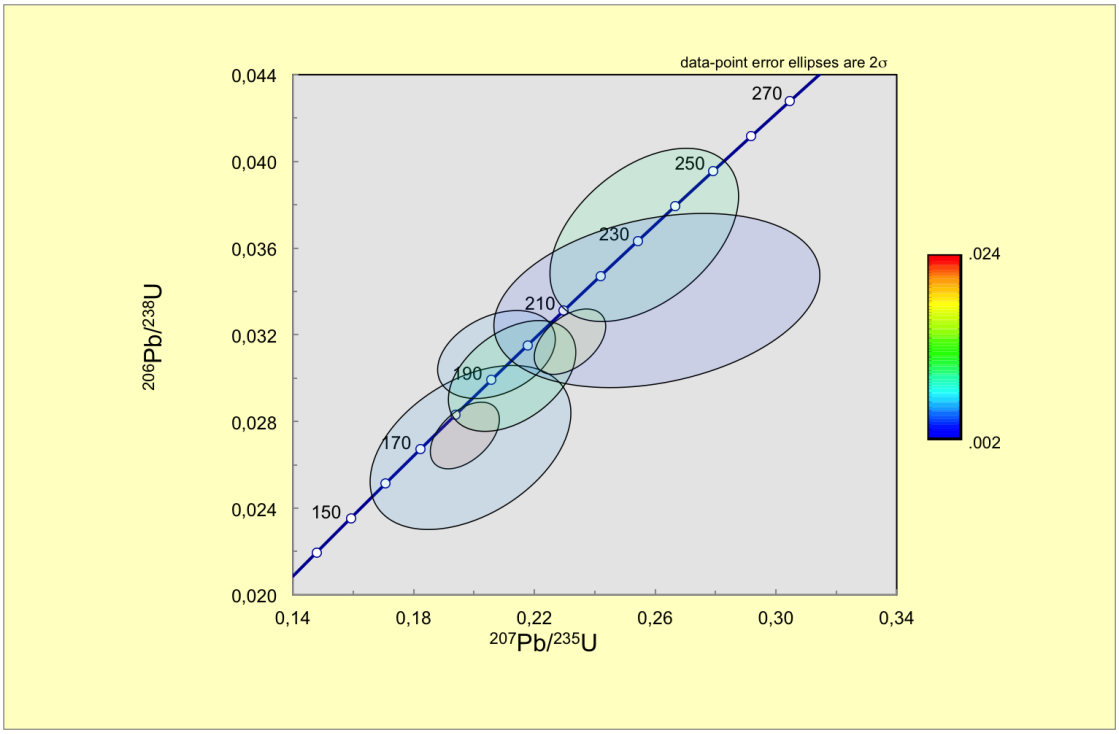

Figure 6.25: Concordia plot of mount 288. The majority of zircon ages scattered between c. 180 Ma and c. 230 Ma

289 zircon (small anhedral grains)

Zircons range in size between c. 100 and c. 250 μm. The length-to-width ratios vary between 1:5:1 and 4.5:1 but in most of the cases it is either 2:1 or 3:1. The shapes of the zircons are prismatic or subrounded. Zoning patterns are oscillatory and predominantly patchy or complex (see Appendix, III. 3.3.5. 289 zircon (small anhedral grains)). Th/U ratios vary between 0.18 and 1.82. Roughly 15 % of the values are scattered beween 0.18 to 0.24, more than 50 % range from 0.31 to 0.84 and more than 25 % from 1.01 to 1.82. In total 21 zircon ages range between c. 40 and c. 900 Ma. The majority lies within 180 to 220 Ma and a Concordia age of 203 $\pm$ 4 Ma could be obtained. Approximately a third of the ages is scattered between 40 and 130 Ma (Figure 6.26).

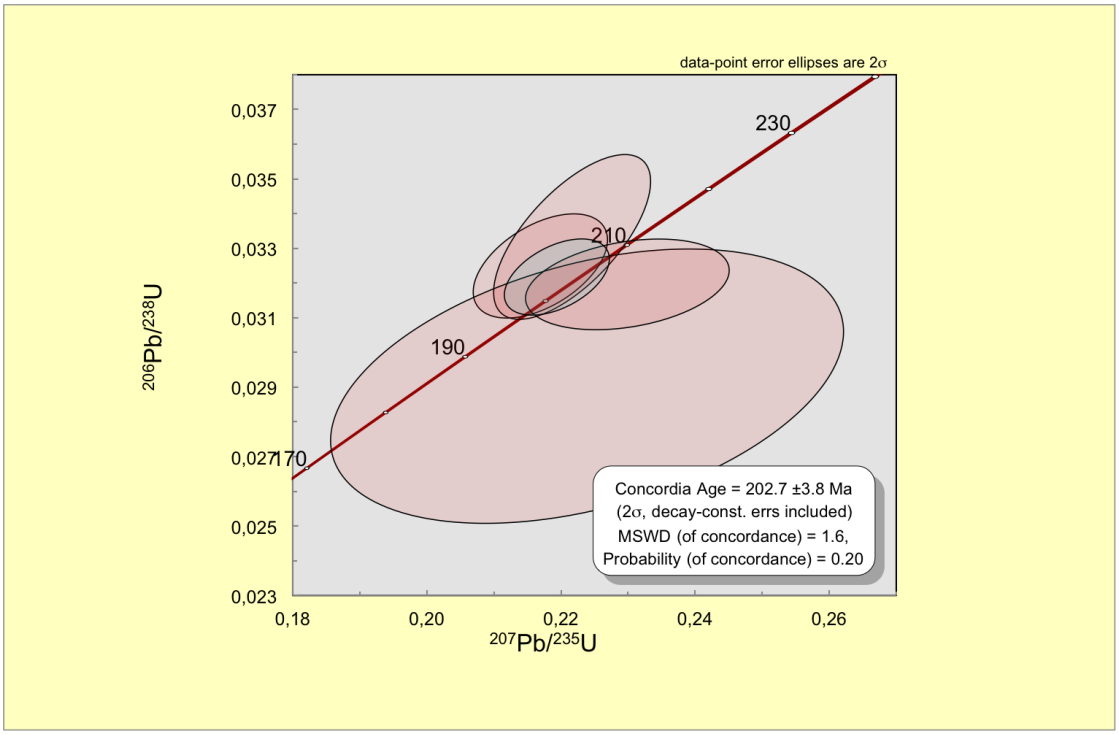

Figure 6.26: Concordia plot of mount 289. Concordia age of 203 ± 4 Ma.

290 zircon (large anhedral grains)

Zircons are 200 to 400 μm in size with length-to-width ratios between 1.5:1 and 4:1. Zoning patterns are predominantly patchy (see Appendix, III. 3.3.6. 290 zircon (large anhedral grains)). Th/U ratios vary between 0.1 and 0.9, where most of the values are scattered between 0.3 and 0.9. In total 15 zircon ages range between c. 20 and c. 250 Ma (Figure 6.27). Like in mount 285 no clear age population is visible. Zircon ages are scattered below and above Concordia and all of them are having small errors.

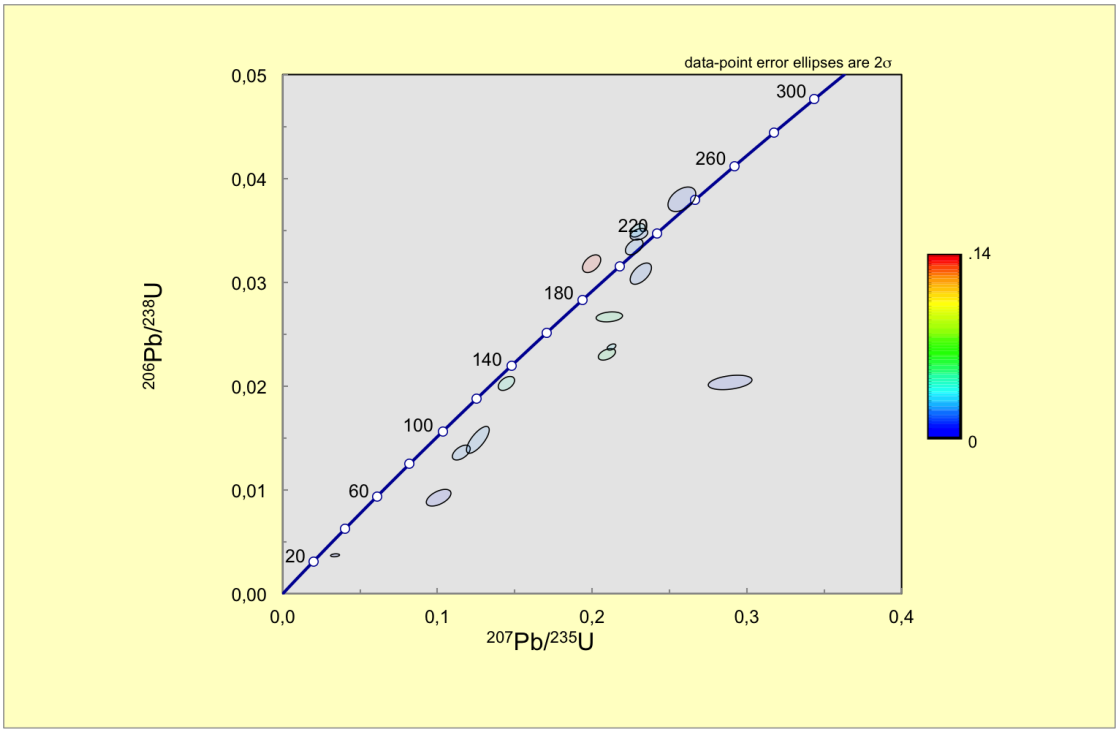

Figure 6.27: Concordia plot of mount 290. All ages are strongly scattered between 20 and 260 Ma.

7 Discussion

7.1 Results of this work

7.1.1 Augen-gneiss (01/01 II)

Approximately 50 % of the U/Pb measurements (190 to 220 Ma) yield ages related to the Indosinian orogeny and roughly 30 % (40 to 50 Ma) yield Eocene ages. The remainder of ages is scattered in between or is even older. The Triassic-Jurassic age is predominantly made up by zircon ages while the Eocene age is mainly based on monazite ages. Monazites yield noticeable age populations with no monazite ages in between. The majority of ages is accumulated between 45 and 55 Ma. In total three Concordia ages could be obtained (78 ± 24 Ma, 215 ± 35 Ma and 219 ± 8 Ma). Interestingly, smaller monazites yield rather older ages while larger monazites yield younger ages.
The Eocene monazites, which are assumed to reflect a metamorphic event, are probably affected by the same metamorphic event as the zircons of the subvolcanic dyke, at least the close age relation indicates so. Furthermore, a Tera-Wasserburg age of 48.6 ± 0.9 Ma could be derived. Interestingly, the augen-gneiss yields a Cretaceous Concordia age (78 ± 24 Ma). The Cretaceous metamorphism is poorly constrained within our samples, despite this Concordia age and several non-coherent measurements. The 215 ± 35 Ma and 219 ± 8 Ma Concordia ages are peculiar. These Indosinian ages suggest a metamorphism taking place in the Triassic and therefore are in agreement with the findings of Ahrendt et al. (1991, 1993) and Mickein (1997), as the monazites clearly exhibit metamorphic features. Simultaneously, this age is in contradiction with our opinion, that the augen-gneiss represents a granitic intrusion formed at this time. However, zircons primarily yield Triassic ages. A few zircon ages are scattered between 50 Ma and 180 Ma years, but no real age population has formed in between. Unfortunately, no zircon Concordia age could be acquired.
Therefore, inherited zircon ages of the augen-gneiss reflect the Indosinian orogeny while Eocene monazite ages of the same sample prove a further metamamorphic event. Only little evidence of a Cretaceous metamorphic event could be found.

7.1.2 Biotite-gneiss (01/01 IV)

Zircons and monazites do ‚behave' very similar as those from the augen-gneiss. Monazites yield younger Eocene ages while zircons predominantly yield Triassic or Permian ages. Two Concordia ages could be derived, a monazite age of 40 ±

2 Ma and a zircon age of 276 ± 16 Ma. The monazite Concordia age, however, is much younger than the Tera-Wasserburg age of 48.6 ± 0.9 Ma. The question has to be posed whether these monazites are affected by Pb loss or by fluid activity. In general monazites of both samples exhibit a fractured and perforated appearance allowing fluids to migrate and react easily with the grains. Therefore, the possibility of fluid-affected monazites is given. The youngest zircons yield ages accumulating between 40 and 55 Ma. The majority of zircons, however, yield Triassic and Permian ages. The younger cluster lies at roughly 200 Ma and reflects the Indosinian orogeny whereas the older cluster is located at approximately 280 Ma.
Summarizing these results, again, as in the case of the augen-gneiss, inherited zircon ages represent the Indosinian orogeny whereas monazite ages of the same sample prove an Eocene metamorphic event.

7.1.3 Subvolcanic dyke (06/01 II)

The U/Pb results obtained from zircons are surprising and conceivable at the same time. Approximately 20 % of the ages obtained are representative for the Indosinian orogeny, which took place during the Triassic-Early Jurassic. Roughly 40 % of the ages are scattered between c. 60 Ma and c. 190 Ma. These inherited ages stem from zircons, which were not affected by partial melting or were assimilated at a later stage. Zircon ages spanning this period may be related to the Cretaceous metamorphism which is widespread in igneous and metamorphic rocks all over Thailand. Striking are, however, the Eocene ages of 42 ± 8 Ma and 51 ± 2 Ma. These ages are purely deduced from soccer ball zircons of mount 285 and 286 and therefore considered to represent a state of partial melting or crystallization. The age difference of more than eight million years could either reflect two phases of anatexis or be due to isotopic perturbations of the system. Soccer ball zircons are believed to form under highest-grade metamorphic conditions or anatexis, respectively (Vavra et al., 1996; Schaltegger et al., 1999; Klötzli-Chowanetz et al., 1997). So far, there is no highest-grade metamorphic event mentioned in the literature.
Moreover, results from the augen- and biotite-gneiss do not support a strong regional metamorphism, though little evidence of an Eocene event is given by zircon ages. Furthermore, results obtained from Palzer (2013) indicate greenshist-facies conditions. Thus, the intrusion of the subvolcanic dyke is a rather small-scale feature. This is also evident from the scale of the intrusion, which covers only a few square meters in size. Prismatic zircons (mount 287) with length-to-width ratios predominantly between 4:1 and 6:1, with one exception of 2:1, yield an age population clustering at about 30 Ma, though a Concordia age purely consisting of these zircons could not be extracted. These mainly elongated, pseudo-volcanic zircons are considered to have crystallized from melts and therefore represent magmatic conditions. Hence, it is curious that a time gap of more than ten million years exists between anatectic soccer ball and magmatically grown zircons, if assumed

that this intrusion represents a rather small scale feature, which the author lacks evidence to prove so. Therefore, it seems likely that the isotopic system of these fragile elongated zircons has been affected, rather than the isotopic system of the robust soccer ball zircons, by the strong fluid taking place at that time (Palzer, 2013), which is also obvious from affected feldspars and biotite of the same sample. The remainder of ages is scattered between c. 300 and c. 900 Ma and a Concordia age of 430 ± 56 Ma could be derived. This age is interestingly made up by the smallest zircons found (c. 50 to 120 μm) with small length-to-width ratios of 1:1 or 2:1. Maybe these are soccer ball zircons too. Unfortunately, these zircons are so small that superficial features like facets cannot be seen under the binocular microscope.
However, based on these results and mainly due to the proposed Eocene intrusion age (42 ± 2 Ma) of the subvolcanic dyke, the ductile deformation along the MPFZ is suggested to have stopped prior to this time, assuming that the fault zone has acted more or less simultaneously. The subvolcanic dyke is totally undeformed and clearly of intrusive nature. Furthermore, these results conflict with the $^{40}Ar/^{39}Ar$ biotite ages of Lacassin et al. (1997) who suggested the last increments of left-lateral ductile shearing at 30.5 Ma. These results also contradict the stepwise northward shift of strike-slip activity leading to the lateral extrusion of SE-Asia proposed by Lacassin et al. (1997). They assumed ductile shearing to end along the TPFZ between c. 36-33 Ma, along the MPFZ between c. 33-30 Ma and along the ASRRFZ between c. 26-17 Ma. Assuming the correctness of our data, these interpretations cannot be supported.
However, integrating the above, zircon ages prove the Indosinian and Eocene metamorphic events. In contrast to the augen- and biotite-gneiss, inherited zircon ages also seem to reflect the Cretaceous metamorphism recorded in many locations all over SE-Asia.

In all samples inherited Precambrian ages could be found. These ages are neglected for the interpretations as they do not contribute to unravel the post-Indosinian history.

7.1.4 Th/U ratios, external morphology and internal texture

An attempt to unambiguously distinguish between metamorphic and magmatic growth was undertaken. Th/U ratios, external morphology and internal texture allow assumptions on the history of both zircons and monazites. It seems that low Th/U, anhedral, subrounded morphologies and a patchy compositional zoning pattern reflect metamorphic growth conditions whereas high Th/U, euhedral, prismatic outlines with concentric compositional zoning indicate a magmatic origin.

Zircons of the subvolcanic dyke yield Th/U ratios between 0.1 and 1.8. Roughly 40 % of Th/U ratios are below 0.3 and at least 20 % of Th/U ratios are above 0.5. Zircons of the augen-gneiss yield Th/U ratios between 0.01 and 0.76. More

than 80 % of the values are below 0.30 and predominantly between 0.01 and 0.09. Monazites of the same sample yield Th/U ratios between 0.4 to 74.1, whereby the value of 0.4 is an exception and all other values are at least higher than 1.0 and predominantly higher than 30.0. Zircons of the biotite-gneiss yield Th/U ratios between 0.03 and 0.61. More than 60 % of the values are below 0.30 and only 5 % of Th/U ratios are above 0.50. Monazites on the other hand yield Th/U rates between 40.4 and 132.9. These results suggest a metamorphic tendency for the augen- and biotite-gneiss whereas zircons of the subvolcanite tend to be of magmatic origin. While low Th/U ratios seem to reflect metamorphic conditions, high Th/U ratios seem to be representing magmatic conditions. This is, however, not always the case and sometimes it is the reverse. Therefore, considering Th/U ratios only, interpretations might be misleading (Ayers et al., 1999).

The zoning pattern of monazites of the augen- and biotite-gneiss is predominantly patchy, with only some monazites exhibiting a rather concentric compositional zoning. The zoning pattern of zircons of the same samples, on the other hand, appears to vary between oscillatory, complex and patchy. Zircons of the subvolcanic dyke have, however, rather oscillatory or patchy zoning and in some cases also complex zoning patterns. Unfortunately, zoning patterns do not appear to be a discriminating factor. However, sector zoning can be ascribed to soccer ball zircons in some cases and the majority of elongated prismatic zircons seem to exhibit oscillatory zoning, both being typical features.

Length-to-width ratios are also considered to be in some cases indicative for either magmatic or metamorphic growth conditions (Ayers et al., 1999). Monazites of the augen-gneiss yield ratios between 1:1 and 2.5:1 with most of them having ratios of 1:1 (almost 70 %) and 1.5:1 (c. 20 %). Zircons of the same sample yield ratios mainly scattered between 2:1 and 4:1 (c. 70 %). Roughly 10 % of the zircons have ratios of either 1:1 or 1.5:1 and the remainder (c. 20 %) exhibits ratios between 4.5:1 and 7:1. Thus, monazites, apart from their internal texture in some cases, show no evidence for magmatic growth, while zircons exhibit both magmatic and metamorphic ratios.
Monazites of the biotite-gneiss yield ratios of either 1:1 or 1.5:1. Zircons show ratios between 1.5:1 and 4:1 with the majority (more than 50 %) having a 3:1 ratio and almost 40 % have ratios between 1.5:1 and 2.5:1. The remainder 10 % yields the highest ratio with 4:1. Zircons and monazites of the biotite-gneiss are in good agreement with those from the augen-gneiss, despite zircons having a less elongated appearance.
Interestingly, zircons of the subvolcanic dyke, thought to represent a small-scale intrusion with mainly anatectic and magmatic zircons, yield length-to-width ratios of predominantly (c. 65 %) ranging between 1:1 and 2.5:1. Roughly 35 %, with ratios of 1:1 and 1.5:1, of these 65 % can be ascribed to soccer ball zircons. Another c. 20 % of the zircons exhibit ratios between 4:1 and 6:1. The highest ratio found, though being exceptional, was 11:1. With approximately 55 %

(35 % soccer ball zircons and 20 % elongated zircons) more than half of the zircons exhibits an either anatectic or magmatic character proving the nature of this rock.

Summarizing these results, monazites, considering Th/U ratios, length-to-with ratios and zoning patterns seem to be predominantly of metamorphic origin, while the interpretation concerning the zircons is sometimes ambiguous and both igneous and metamorphic origin can be ascribed to them.

7.1.5 Geochemistry

The biotite-gneiss, subvolcanic dyke and leucocratic dyke samples yield a granodioritic composition, while the augen-gneiss has a granitic composition. Campbell (1975) already mentioned two suites of igneous rocks within the quartz-feldspar-biotite gneisses of the Lan Sang National Park, one of granitic and a second of granodioritic composition. Due to the concordant relation to the paragneisses, the same author stated that the granitic gneiss shared the same metamorphic overprint as the quartz-feldspar-biotite gneisses. He interprets the granitic material to have originated by partial melting of the host paragneisses. On the other hand, granodioritic rocks reflect the youngest igneous phase, with some layers being concordant and some granodioritic bodies being directionless and discordant. Hence, these rocks represent a very late igneous phase during decreasing regional stress (Campbell, 1975).
As already mentioned by Palzer (2013), the augen-gneiss seems to be intruded by the biotite-gneiss, based on field evidence. This is confirmed by the geochemical results and the interpretation of Campbell (1975), respectively. The biotite-gneiss which is of granodioritic composition and thus part of the latest magmatic activity, intrudes the granitic syn-metamorphic augen-gneiss. However, comparing the results to the Tak batholith more to the NE of the Lan Sang National Park, a genetic relation is questionable. According to Cobbing (2011) the Tak batholith is a large I-type granite (sensu lato) comprising four plutons: the Eastern pluton, the Western pluton, the Mae Salit and Tak plutons. While the Eastern pluton has an overall granodioritic composition, the Western, Mae Salit and Tak plutons are rather monzo-granitic in composition. Unfortunately, with exception of the Tak pluton, none of these rocks are dated. Rb/Sr whole rock isochron ages obtained from the Tak pluton yield Triassic ages (microgranite: 213 ± 10 Ma; monzogranite: 219 ± 12 Ma; after Mahawat et al. (1990)). Geometric relations indicate a crudely defined westerly younging trend with the Eastern pluton being the oldest and the Tak pluton the youngest. Simultaneously, the compositions became more monzonitic and compositionally restricted with time (Mahawat et al., 1990). Thus, if assumed that the granodioritic rocks of the Lan Sang National Park intruded at the climax (or even later) of the Indosinian orogeny at c. 200 Ma (Campbell, 1975), an age-related correlation is arguable too.

The REE patterns obtained in this study yield a more or less common picture (Figure 7.1). All samples are enriched in LREEs while having comparatively low HREE values. In the subvolcanic dyke this pattern is not as prominent as in the samples of the augen- and biotite-gneiss, but it is definitely similar. This configuration of REEs is indicative of a crustal influence (oral communication by Urs Klötzli). Interestingly, as plagioclase forms a substantial part of the phenocrysts, an Eu anomaly is not visible in the REE pattern of the subvolcanic dyke. The REE patterns are in some cases similar to those of Mahawat et al. (1990) of the Tak batholith (Figure 7.2). As no reference for chondrite values were given, it is not completely sure if results are appropriately comparable. However, their REE patterns are usually marked by a much more prominent bend. Furthermore, this bend is located more towards lighter REEs (between Sm and Gd) compared to logarithmic REE patterns of this study (rather between Dy and Er). Additionally, HREE values obtained by Mahawat et al. (1990) tend to be higher, and in most cases are higher than 10, whereas in this work HREE values are always below 10. Hence, it is difficult to say, but rather unlikely, that the Tak batholith and the Lan Sang gneisses are genetically related. The original purpose of the REE patterns was, to see if the subvolcanic dyke can be related to the igneous rocks of the Tak batholith or if it reflected an independent magmatic phase. Only one REE pattern of the Western pluton seems to be comparable (Figure 7.2, middle left). However, both LREEs and HREEs are much more abundant, although showing the same gradual decline towards heavier REEs. Thus, the subvolcanic dyke does not seem to be genetically directly related to the same igneous activity as the plutons of the Tak batholith. The monzogranite sample of the Tak pluton and the microgranite and monzogranite of the Western pluton, on the other hand, seem to exhibit similarities to the augen-gneiss sample, including the Eu anomaly. But again, the bend is more towards lighter REEs. Moreover, both monzogranite samples have higher HREE values.

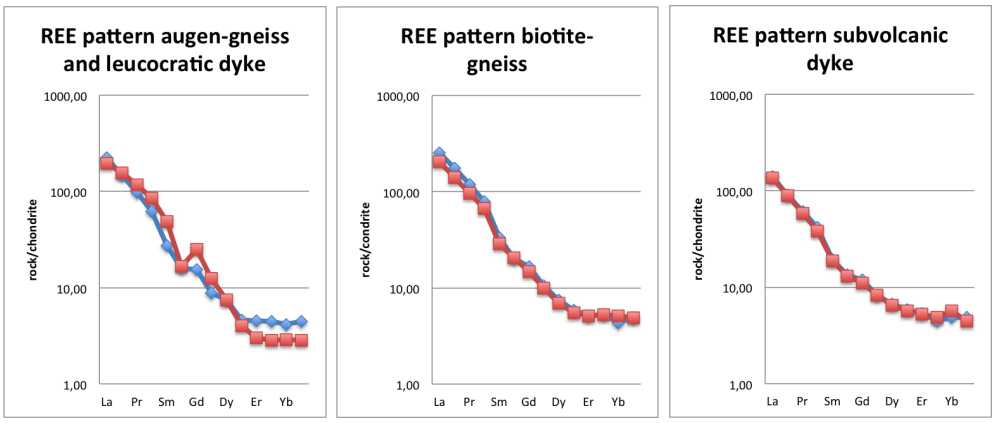

Figure 7.1: Left: REE pattern of the augen-gneiss (12/02 III, red line) and leucocratic dyke (12/02 V, blue line). Middle: REE pattern of the biotite-gneiss samples (01/01 IV, blue line; 12/02 II, red line). Right: REE pattern of the subvolcanic dyke samples (06/01 II, blue line; 13/01 IV, red line).

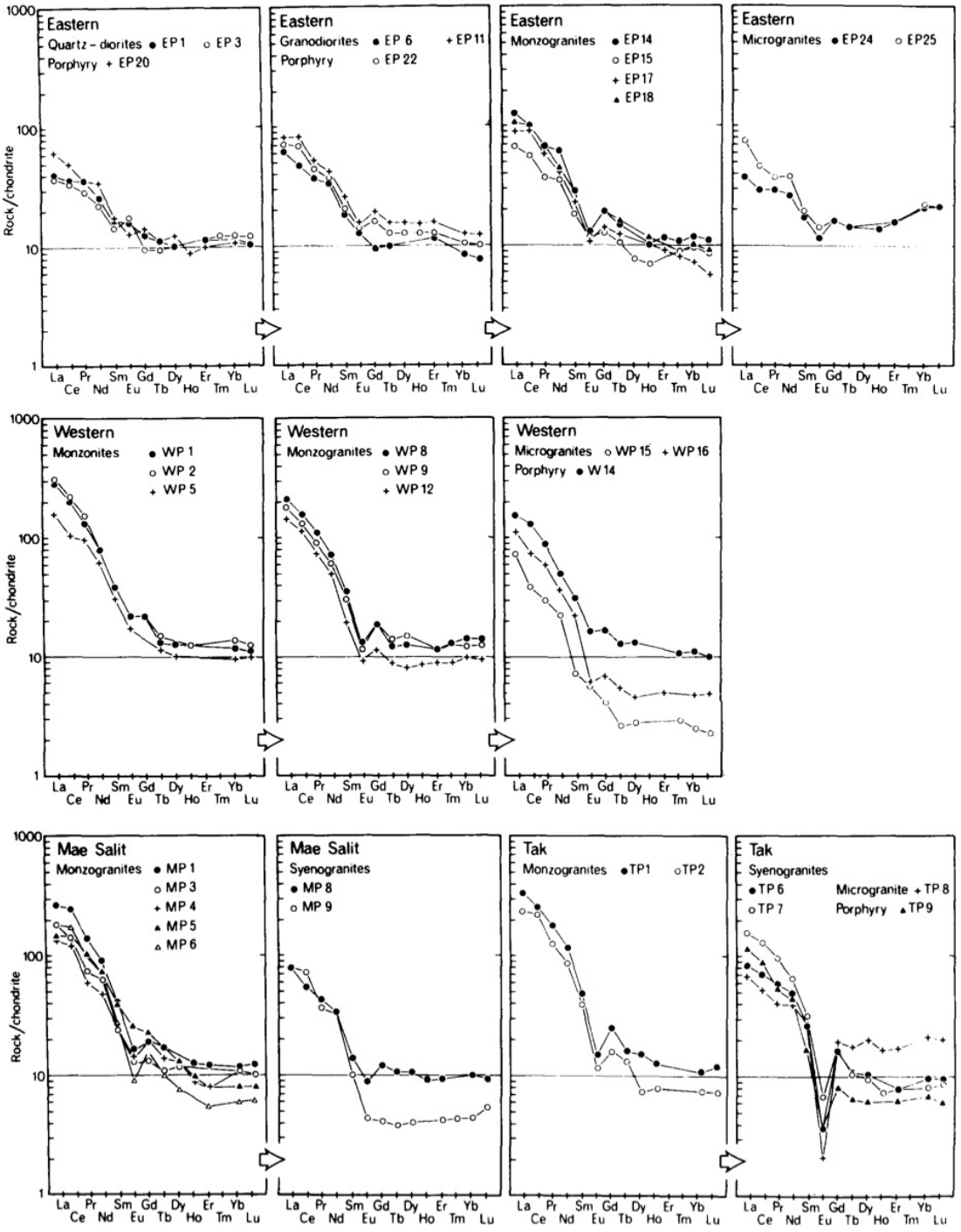

Figure 7.2: Chondrite-normalized REE diagrams for the rocks of the Tak batholith. Arrows indicate direction of increasing acidity. After Mahawat et al. (1990).

7.2 Results of the accompanying work

Based on results from field investigations, thin sections, microprobe analyses, thermometry and pseudo sections Palzer (2013) proposed six stages for the formation and evolution of the Lan Sang gneisses:

- Stage 1: Xenolithic calc-silicates exhibit two different kinds of original paragenses, a garnet-omphacite and an omphacite-anorthite paragenesis reflecting granulite-facies conditions. Field evidence indicates that both lithologies were brought together by the intrusion of the orthogneiss protolith.
- Stage 2: Intrusion of the augen-gneiss and biotite-gneiss protolith(s) during Indosinian times accompanied by deformation and folding during the late stages of these intrusions.
- Stage 3: Metamorphic overprinting under amphibolite-facies conditions including simultaneous fluid activity and growth of allanite.
- Stage 4: High-grade metamorphic overprinting affecting the gneisses in the SW, which seem to be related to the marbles.
- Stage 5: Rapid, nearly isothermal uplift of the gneisses in the NE, uplift and cooling of the marbles and the gneisses in the SW as well as subsequent greenshist-facies overprinting and deformation of the entire assemblage. Moreover, allanite decay is considered to take place at this stage, which might be related to the growth of monazite.
- Stage 6: Intensive deformation of the marbles under lower greenshist-facies conditions.

By putting all results together, Palzer (2013) obtained a potential PT-history reconstructing temperature and pressure conditions of the Lan Sang gneisses. In combination with results obtained from this work, a PTt-path could be derived, also taking the temporal evolution into account (Figure 7.3).

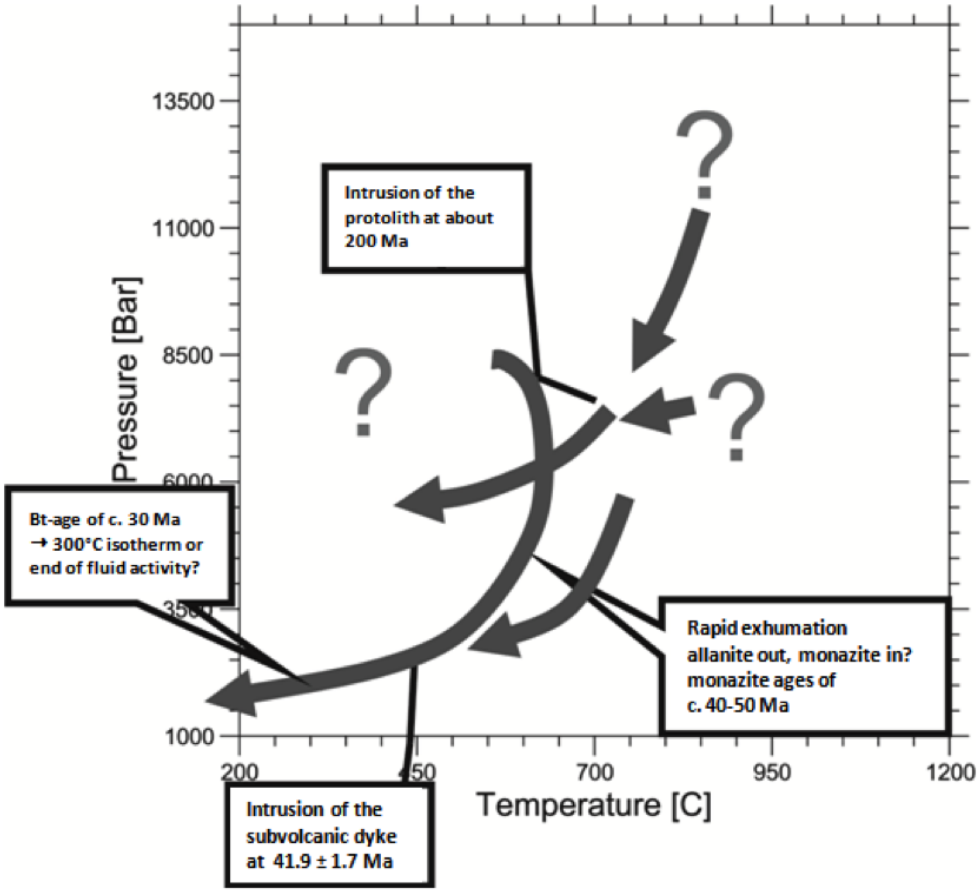

Figure 7.3: PTt-path summarizing the geochronological results obtained in this work and thermo-barometric results of Palzer (2013). After Palzer (2013).

In all samples the Indosinian metamorphism is documented by inherited zircon ages, with most of them being scattered between c. 200 and c. 220 Ma. Elongated zircons with ratios of 4:1 or 5:1 of the augen-gneiss (c. 30 %) and subvolcanic dyke (c. 20 %) indicate a rather igneous origin. Also thin section analyses with magmatically zoned feldspars and other findings of Palzer (2013) suggest an igneous activity at this time. What happened between Triassic and Eocene times is ambiguous, but at some point the amphibolite-facies overprint has to have taken place. The high-temperature metamorphism documented in the literature and believed to be the result of the coupling of West Burma with Sundaland (by some authors) is not evident from zircon and monazite ages.
Palzer (2013) related the amphibolite-facies metamorphism to the earliest stages of the Himalayan collision. Unfortunately, from a geochronological point of view, there is no evidence for this. Between c. 40 and c. 50 Ma, zircons of the subvolcanic dyke and monazites of the augen- and biotite-gneiss, indicate a change in the temperature and pressure conditions of the Lan Sang gneisses. The subrounded shape and a patchy zoning pattern of nearly all monazites strongly recommend a metamorphic growth. However, the process by which monazites grew is not clear

and therefore the interpretation remains difficult and uncertain (Palzer, 2013). It might be though related to the breakdown of allanite which could be found within the calc-silicates and the gneisses. The cause for allanite breakdown itself might be due to an isothermal decompression. Palzer (2013) questioned a post-stage 3 (amphibolite-facies overprint) age for the monazites but simultaneously missed an intrusion related age of the monazites and thus introduced a second metamorphic event. Indeed, most monazites yield Eocene ages. However, a Concordia age of 219 ± 8 Ma made up by monazites of the augen-gneiss could be identified. The question of how meaningful this age is, remains a matter of debate, as these monazites are probably preserved relics assimilated by the granitic intrusion.
The Eocene event is documented precisely by a monazite Tera-Wasserburg age of 48.6 ± 0.9 Ma, a monazite Concordia age of 40 ± 2 Ma, and two zircon Concordia ages of 50 ± 2 Ma and 42 ± 2 Ma, respectively, where the latter is ascribed to the intrusion of the subvolcanic dyke, based on ages obtained from soccer ball zircons. The time gap, however, between the older and younger ages is not unambiguous. Considering the exhumation of the Lan Sang gneisses between c. 40 and c. 50 Ma, this time gap might indicate a non-uniform stepwise exhumation. Palzer (2013) noted the Lan Sang gneisses already to be at a high level around 42 Ma and thus an intensive exhumation (and ductile deformation) between 30-40 Ma proposed by former authors can be excluded. The final exhumation, which Palzer (2013) considers to happen along the Bunopas normal fault, could be related to the 23.5 Ma age obtained by Lacassin et al. (1997), which they inferred to be coeval with the onset of E-W extension.

7.3 Comparison with the literature

7.3.1 Cretaceous metamorphism

Another extraordinary feature of the results presented in this work is that there is little evidence for the Cretaceous overprinting, which seems to be ubiquitous in nearly all crystalline rocks of SE-Asia, although 23 % of the entire ages obtained advocate such an event. Some zircons of the subvolcanic dyke (mount 285 and 290), though strongly scattered, and a monazite Concordia age (78 ± 24 Ma) of the augen-gneiss proof this, but no real age population, as in the case of the Indosinian and Eocene event, is evident. The question arises, why is there no Cretaceous fingerprint recorded in the zircons? Is it because zircons were not affected by this thermal overprint? The possibility of zircons having lost their „isotopical memory“ is valid in the case of the subvolcanic dyke. Zircons might have recrystallized partially retaining the information stored within the cores and reflecting the Eocene age in the newly grown remainder of grains with some exceptions still bearing evidence for the Cretaceous metamorphism. In zircons of the augen- and biotite-gneiss, however, there is only little evidence for an Eocene metamorphism (as recorded in zircons of the subvolcanite) that might have obscured Cretaceous ages by recrystallization.

However, the findings of Palin et al. (2013) could not be confirmed by zircons and monazites of the augen- and biotite-gneiss, both assumed to be orthogneisses. More to the south, Cretaceous ages in the rocks cropping out within the TPFZ are lacking too (Nantasin et al., 2012). Nantasin et al. (2012) also obtained U/Pb ages indicating a Late Triassic-Early Jurassic metamorphic event and additionally Eocene ages could be derived from zircons, though being slightly older as the ones found in this work. As both, MPFZ and TPFZ cut the CM-L belt, a genetic relation is evident. Simultaneously, assuming the CM-L belt exhibits the same rocks in the North as in the South, the question has to be posed why the gneisses in the North have suffered Cretaceous metamorphism, as described e.g. by Dunning et al. (1995), while more to the south of the CM-L belt, there is little or no evidence for this event. Is it due to a higher crustal level of the Lan Sang gneisses compared to other crystalline bodies where this Cretaceous metamorphism is obvious?

7.3.2 Timing of the MPFZ

The timing of the MPFZ, radiometrically investigated by several authors (Ahrendt et al., 1991, 1993; Mickein, 1997; Lacassin et al., 1997; Palin et al., 2013) still remains controversial. Ahrendt et al. (1991, 1993) and Mickein (1997) were the first to present radiometric data from the Lan Sang gneisses. Before, the age of the gneisses cropping out in Western Thailand was proposed to be of Precambrian age, based on geometrical relations (Brown et al., 1951; Buravas, 1952). However, their zircons obtained from paragneisses yield Late Triassic-Early Jurassic ages, which they interpreted as to reflect an amphibolite-facies metamorphism. They supported their interpretation with ϵ_TCHUR clearly classifying the gneiss protoliths to be of sedimentary origin. Lacassin et al. (1997) strongly influenced the idea of the MPFZ and its timing. With their $^{40}Ar/^{39}Ar$ results, obtained from biotites, they proposed left-lateral shearing along the MPFZ between c. 40-30 Ma with the last increments of sinistral shear taking place between 32.5 and 30.5 Ma. Furthermore, results suggested a second cooling phase, inferred to be coeval with the onset of E-W extension and final exhumation of the Lan Sang gneisses. Combining their results with the results obtained from Peltzer and Tapponnier (1988) and Tapponnier et al. (1986) they supported the idea of northward diachronism of strike-slip activity leading to the lateral extrusion of SE-Asia. Recent data from Palin et al. (2013) present for the first time U/Pb and Th/Pb ages of an orthogneiss sample within the Lan Sang gneisses, though Th/Pb ages have been favored by these authors for their interpretations. They interpreted Cretaceous monazite ages to represent the initial magmatic protolith emplacement, while monazite ages between c. 45 and c. 37 were considered to represent a maximum age of left-lateral motion and initiation of the MPFZ.
The data obtained from zircons and monazites in this work, however, conflict with some of the interpretations made by these authors. Referring to the data of Lacassin et al. (1997), a cessation of left-lateral shearing around 30 Ma cannot be supported by our dataset. The intrusion of the subvolcanic dyke at 42 ± 2 Ma

clearly is not in agreement with a model, assuming movement taken place more or less simultaneously along the entire shear zone. From field data alone, left-lateral shear must have taken place prior to the intrusion of the subvolcanic dyke, eventually as a consequence of the Cretaceous event or Indosinian orogeny. Palzer (2013) suggests the MPFZ to represent an Indosinian collision zone, which was reactivated during the Himalayan orogeny as a splay of the dextral Sagaing fault and which was exhumed by the collapse of a Tibetan-type plateau.
He further proposed, that the $^{40}Ar/^{39}Ar$ ages obtained from biotites by Lacassin et al. (1997), might not be related to the 300°C isotherm. His findings suggest that fluid activity lasted longer than shearing took place, and therefore mica ages are rather related to the last fluid activity than to shearing. Also Searle and Morley (2011) question the ages obtained by Lacassin et al. (1997) to be related to ductile shear along the MPFZ. According to these authors slightly younger mica cooling ages (29-23 Ma) from the Bhumipol Dam area strongly suggest, that cooling was regional and had nothing to do with strike-slip shearing. Furthermore, apatite fission track dating results confirm that there is no significant uplift and erosion pattern along the MPFZ. Moreover, Morley et al. (2007) doubt a purely strike-slip related exhumation and state, that the exhumation of mid-crustal rocks at Lan Sang is an atypical and localized feature of the fault zone that requires specific explanation.
However, the interpretations made by Palin et al. (2013) are also not in good agreement with our data. Interestingly, though in close spatial relation, their monazite ages obtained from an orthogneiss within the Lan Sang National Park only match partially with monazite ages of this work from an orthogneiss close by. Their monazites predominately yielded Cretaceous and Eocene (c. 45 and c. 37 Ma) ages. Eocene monazite ages are also evident in our samples. But, though having the same age, they interpreted the monazite ages to reflect the onset of left-lateral shearing whereas findings of this work suggest the ductile motion to end during Eocene times. Furthermore, Palin et al. (2013) proposed the Cretaceous event to mark the intrusion of the protolith of the orthogneiss which conflicts with our interpretation of a Triassic intrusion age.
Another subject of debate is whether the strike-slip faults in SE-Asia coincide with the timing of the India-Asia collision. Unfortunately, the timing of the ultimate India-Eurasia collision is still not well constrained, with an early collision of around 60 Ma being favored by some authors, and a much younger Eocene-Oligocene (c. 38 Ma) collision being proposed by others, who suggest that the collision at c. 60-55 Ma was between India and an intra-oceanic island arc (Metcalfe, 2013a). The same author noted a Middle Eocene age (45 Ma) for the initial collision of India (with accreted island arc) with Eurasia, temporally coincident with large-scale regional and global plate reorganizations at this time. Searle and Morley (2011) question these strike-slip faults to be coupled to the Himalayan orogeny and ascribe them to be purely crustal features with much lower finite offsets and thus to be much less important than originally assumed.
However, the findings of this work suggest the cessation of ductile motion along

the MPFZ roughly at 42 Ma. This could be in well accordance with the 45 Ma mentioned by Metcalfe (2013a). However, the question arises why ductile shearing apparently ended so soon after, while India even nowadays is pushing northwards. Is it due to a changing stress field proposed to be influencing Sundaland during Cenozoic times? Anyhow, a Himalayan influence is evident from our data, but the author prefers reactivation rather than initiation of the MPFZ at this time. As long as the exact timing of the strike-slip faults and the timing of the Himalayan orogeny is not well constrained, this discussion remains a matter of debate. The author of this work though favors the idea of Searle and Morley (2011) and others, who believe that the strike-slip faults are older in age, maybe as old as Cretaceous or even as old as Triassic.

8 Conclusions

Based on joint investigations (field investigations, thin sections, microprobe analyses, thermometry, pseudosections, geochemistry and geochronology analyses) of the Lan Sang gneisses and outcrops of adjacent regions, an attempt on modeling the history of these rocks was undertaken, in which this part of the work exhibits predominantly insights on the age of zircons and monazites and their internal and external morphology, constraining growth conditions and origin. By comparing results obtained in this work with results from the literature, conclusions could be drawn.

Three samples were taken in order to extract zircons and monazites for in-situ U-Th-Pb LA-ICP-Ms dating. The results were conceivable and surprising at the same time. In all samples evidence for the Indosinian orogeny could be found. Interestingly, the high-temperature, low-pressure Cretaceous metamorphism, documented in almost all igneous and metamorphic rocks in Thailand and adjacent countries, could not be confirmed based on our dataset. Furthermore, an Eocene event is clearly visible in predominantly monazite but also zircon data. Zircons of the subvolcanic dyke partially exhibit soccer ball shaped outlines and elongated prismatic zircons, indicating anatectic and magmatic growth, respectively. Zircons of the augen- and biotite-gneiss show only little evidence of an Eocene event, while monazites of the same sample clearly document such an event.

External morphology and internal texture of zircons and monazites are not always clear and sometimes rather ambiguous. However, trends may be inferred. While zircons of the augen- and biotite-gneiss exhibit Th/U and length-to-width ratios rather related to a metamorphic origin, zircons of the subvolcanic dyke are of igneous origin. Monazites of the augen- and biotite-gneiss also suggest a metamorphic origin. Studies of the internal texture do not exhibit a systematics for zircons, but a patchy zoning pattern of the majority of monazites of the augen- and biotite-gneiss also suggests a metamorphic origin.

A classification based on the QAPF or Streckeisen scheme yields granodioritic compositions of the biotite-gneiss, the subvolcanic dyke and the leucocratic dyke, while the augen-gneiss is marked by a granitic composition. Geochemical results and the timing of the climax of the Indosinian orogeny question a genetic relation to the rocks of the adjacent Tak batholith. However, more detailed investigations and more sophisticated methods would be required in order to prove the 'true' geochemical nature of the Lan Sang gneisses.

The integrated PTt-path summarizing results obtained by this and the accompanying work provides a potential history of the Lan Sang gneisses, which conflicts with the interpretation of former investigations. Unfortunately, geochronological investigations on zircons and monazites cannot fully support the PT-path proposed by Palzer (2013). Nevertheless, it provides some new insights of the evolution of these rocks.

Striking, however, is the appearance of an undeformed subvolcanic dyke within the strongly deformed, mylonitic gneisses. This subvolcanic dyke, which is clearly of intrusive nature, postdates the ductile motion along the MPFZ. A zircon Concordia age of 42 ± 2 Ma suggests deformation and shearing prior to c. 42 Ma and therefore conflicts with the $^{40}Ar/^{39}Ar$ biotite ages by Lacassin et al. (1997) who suggested the last increments of left-lateral ductile shear at 30.5 Ma. In the same manner, these results also contradict the lateral extrusion model of Peltzer and Tapponnier (1988) and Tapponnier et al. (1986). Furthermore, the assumption of Palin et al. (2013) considering Th/Pb ages, ranging between c. 45 and c. 37, of monazites to be related to the initiation of the MPFZ, cannot be supported, as our data suggest the MPFZ to be no longer affected by ductile shearing at this time.

Finally, the idea of the MPFZ to have initiated as a consequence of the Himalayan orogeny seems unlikely. Unfortunately, the timing of the ultimate collision between India and SE-Asia is still not well constrained. Assuming a collision at c. 45 Ma, it is however improbable that shearing along the MPFZ ended so soon after. We therefore suggest a Cretaceous or even Triassic (Indosinian) origin of the MPFZ, being reactivated by the resulting strain of the India-Eurasia collision.

Bibliography

Ahrendt, H., Chonglakmani, C., Hansen, B. T., and D., H. (1993). Geochronological cross section through Northern Thailand. *Journal of Southeast Asian Earth Sciences*, 8:1–4 and 207–217.

Ahrendt, H., Chonglakmani, C., Hansen, B. T., and Helmcke, D. (1991). First results from geochronological and structural investigations along the Tak - Mae Sot Highway/N-Thailand. In *Guidebook for the fieldtrip*, number 1, pages 69–76.

Assavapatchara, S., Charusiri, P., Charoentitirat, T., Chutakos, V., Hisada, K., and Ueno, K. (2006). On the Lithostratigraphy of Permian Rocks in Thailand: Implications for Depositional Environments and Tectonic Settings. *Journal of the Geological Society of Thailand*, 1(1):27–48.

Ayers, J. C., Miller, C., Gorisch, B., and Millman, J. (1999). Textural development of monazite during high-grade metamorphism: Hydrothermal growth kinetics, with implications for U-Th-Pb geochronology. *American Mineralogist*, 84(11-12):1766–1780.

Brown, G., Buravas, S., Charaljavanaphet, J., Jalichandra, W., Johnston, W., Sresthaputra, V., and Taylor, G. (1951). Geological reconnaissance of the mineral deposits in Thailand: Geologic investigations in Asia. *Bulletin of the Geological Survey*, 934:1–183.

Buravas, S. (1952). Preliminary notes on the geology of Thailand. *Thai Science Bulletin*, 7:7–43.

Campbell, K. V. (1975). Metamorphic and Deformational Events recorded in the Lan Sang Gneiss.

Cherniak, D. J., Watson, E. B., Grove, M., and Harrison, T. M. (2004). Pb diffusion in monazite: A combined RBS/SIMS study. *Geochimica et Cosmochimica Acta*, 68(4):829–840.

Cobbing, E. J. (2011). *The Geology of Thailand*, chapter Granitic Rocks, pages 441–457. The Geological Society of London.

Corfu, F., Hanchar, J. M., Hoskin, P. W. O., and Kinny, P. (2003). Atlas of zircon textures. In *Zircon*, volume 53 of *Reviews in Mineralogy & Geochemistry*, pages 469–500.

Dunning, G. R., Macdonald, A. S., and Barr, S. M. (1995). Zircon and monazite U-Pb dating of the Doi Inthanon core complex, northern Thailand: implications for extension within the Indosinian Orogen. *Tectonophysic*, 251:197–213.

Hansen, B. and Wemmer, K. (2011). *The Geology of Thailand*, chapter Age and evolution of the basement rocks in Thailand, pages 19–32. The Geological Society of London.

Harley, S. L. and Kelly, N. M. (2007). Zircon - Tiny but timely. *Elements*, 3(1):13–18.

Harley, S. L., Kelly, N. M., and Moeller, A. (2007). Zircon behaviour and the thermal histories of mountain chains. *Elements*, 3(1):25–30.

Klötzli, U., Klötzli, E., Günes, Z., and Košler, J. (2009). External accuracy of laser ablation U-Pb zircon dating: results from a test using five different reference zircons. *Geostandards and Geoanalytical Research*, 33(1):5–15.

Klötzli-Chowanetz, E., Klötzli, U., and Koller, F. (1997). Lower Ordovician migmatisation in the Oötztal crystalline basement (Eastern Alps, Austria): linking U-Pb and Pb-Pb dating with zircon morphology. *Schweizerische Mineralogische und Petrologische Mitteilungen*, 77(3):315–324.

Kohn, M. J. and Malloy, M. A. (2004). Formation of monazite via prograde metamorphic reactions among common silicates: Implications for age determinations. *Geochimica et Cosmochimica Acta*, 68(1):101–113.

Lacassin, R., Maluski, H., Leloup, P. H., Tapponnier, P., Hinthong, C., Siribhakdi, K., Chuaviroj, S., and Charoenravat, A. (1997). Tertiary diachronic extrusion and deformation of western Indochina: Structural and $^{40}Ar/^{39}Ar$ evidence from NW Thailand. *Journal of Geophysical Research*, 102:10,013–10,037.

Mahawat, C., Atherton, M. P., and Brotherton, M. S. (1990). The Tak Batholith, Thailand: the evolution of contrasting granite types and implications for tectonic setting. *Journal of Southeast Asian Earth Sciences*, 4(1):11–27.

Metcalfe, I. (2013a). Gondwana dispersion and Asian accretion: Tectonic and palaeogeographic evolution of eastern Tethys. *Journal of Asian Earth Sciences*, 66:1–33.

Metcalfe, I. (2013b). Tectonic evolution of the Malay Peninsula. *Journal of Asian Earth Sciences*, 76(SI):195–213.

Mickein, A. (1997). *U/Pb-, Rb/Sr- und K/Ar-Untersuchungen zur metamorphen Entwicklung und Altersstellung des "Präkambriums" in NW-Thailand.* PhD thesis, Göttingen.

Morley, C. K. (2001). Combined escape tectonics and subduction rollback-back arc extension: a model for the evolution of Tertiary rift basins in Thailand, Malaysia and Laos. *Journal of the Geological Society*, 158:461–474.

Morley, C. K., Charusiri, P., and Watkinson, I. M. (2011). *The Geology of Thailand*, chapter Structural geology of Thailand during the Cenozoic, pages 271–334. The Geological Society of London.

Morley, C. K., Smith, M., Carter, A., Charusiri, P., and Chantraprasert, S. (2007). Evolution of deformation styles at a major restraining bend, constraints from cooling histories, Mae Ping fault zone, western Thailand. *Geological Society, London, Special Publications*, 290:325–349.

Nantasin, P., Hauzenberger, C., Liu, X., Krenn, K., Dong, Y., Thöni, M., and Wathanakul, P. (2012). Occurrence of the high grade Thabsila metamorphic complex within the low grade Three Pagodas shear zone, Kanchanaburi Province, western Thailand: Petrology and geochronology. *Journal of Asian Earth Sciences*, 60:68–87.

Palin, R. M., Searle, M. P., Morley, C. K., Charusiri, P., Horstwood, M. S. A., and Roberts, N. M. W. (2013). Timing of metamorphism of the Lansang gneiss and implications for left-lateral motion along the Mae Ping (Wang Chao) strike-slip fault, Thailand. *Journal of Asian Earth Sciences*.

Palzer, M. (2013). New PTt–Constraints on the Mae Ping Core Complex, NW–Thailand: Is the Mae Ping Fault Zone an Indosinian relict? Master's thesis, University of Vienna.

Peltzer, G. and Tapponnier, P. (1988). Formation and evolution of strike-faults,rifts, and basins during the India-Asia collision: An experimental approach. *Journal of Geophysical Research*, 93(B12):15,085–15,117.

Polachan, S. and Sattayarak, N. (1989). *Strike-slip tectonics and the developement of Tertiary basins in Thailand*.

Ridd, M. F., Barber, A. J., and Crow, M. J. (2011). *The Geology of Thailand*, chapter Introduction to the geology of Thailand, pages 1–17. The Geological Society of London.

Schaltegger, U., Fanning, C. M., Gunther, D., Maurin, J. C., Schulmann, K., and Gebauer, D. (1999). Growth, annealing and recrystallization of zircon and preservation of monazite in high-grade metamorphism: conventional and in-situ U-Pb isotope, cathodoluminescence and microchemical evidence. *Contributions to Mineralogy and Petrology*, 134(2-3):186–201.

Scherrer, N. C., Engi, M., Gnos, E., Jakob, V., and Liechti, A. (2000). Monazite analysis; from sample preparation to microprobe age dating and REE quantification. *Schweizerische Mineralogische und Petrologische Mitteilungen*, 80:93–105.

Searle, M. P. and Morley, C. K. (2011). *The Geology of Thailand*, chapter Tectonic and thermal evolution of Thailand in the regional context of SE Asia, pages 539–571. The Geological Society of London.

Spear, F. S. and Pyle, J. M. (2002). Apatite, monazite, and xenotime in metamorphic rocks. In Kohn, M., Rakovan, J., and Hughes, J., editors, *Phosphates: Geochemical, Geobiological, and Materials Importance*, volume 48 of *Reviews in Mineralogy & Geochemistry*, pages 293–335.

Tapponnier, P., Peltzer, G., and Armijo, R. (1986). On the mechanics of the collision between India and Asia. *Collisional Tectonics, Geological Society Special Publications*, 19:115–157.

Vavra, G., Gebauer, D., Schmid, R., and Compston, W. (1996). Multiple zircon growth and recrystallization during polyphase Late Carboniferous to Triassic metamorphism in granulites of the Ivrea Zone (Southern Alps): An ion microprobe (SHRIMP) study. *Contributions to Mineralogy and Petrology*, 122(4):337–358.

List of Figures

Appendix

I. Abstract (Deutsch)

Die Mae Ping Störung repräsentiert eine der vier großen Störungszonen in Thailand, die, nach Meinung einiger Autoren, zur lateralen Extrusion SE-Asiens beitragen soll. Innerhalb dieser Störungszone tritt ein sogenannter Core Complex, der aus duktil deformierten amphibolitfaziellen Gesteinen besteht, zu Tage. Diese Gesteine werden auch, nach der Typlokalität, Lan Sang Gneise genannt. Trotz zahlreicher Untersuchungen dieser Gesteine bleiben Zeitpunkt und Ursache der Exhumation umstritten. Basierend auf strukturellen, petrologischen, geochemischen und geochronologischen Untersuchungen der Lan Sang Gneise wurde ein Versuch unternommen, die zeitabhängige Druck- und Temperaturentwicklung (PTt-Pfad) dieser Gesteine zu rekonstruieren. Im Zuge der Feldarbeit wurde ein diskordanter, undeformierter subvulkanischer Gang in den stark deformierten Lan Sang Gneisen gefunden. In-situ U-Th-Pb LA-ICP-MS Datierungen von 'Soccer ball'-Zirkonen, die unter anatektischen Bedingungen entstehen, ergeben ein Alter von 42 ± 2 Ma und schließen somit eine spätere Deformation aus. Diese Zirkonalter stehen den $^{40}Ar/^{39}Ar$ Biotitaltern von Lacassin et al. (1997) entgegen. Diese Autoren interpretierten die Abkühlalter (ca. 30 Ma) als die letzte Phase der sinistralen, duktilen Deformation. Zudem stellen die Zirkonalter eine direkte Verbindung bzw. die Initialisierung der Mae Ping Störung als Konsequenz der Himalaya-Gebirgsbildung in Frage. Die Deformation der Mae Ping Störung könnte daher schon viel früher, eventuell als Folge der Kollision zwischen Indochina und Sibumasu während der Trias, erfolgt sein.

II. Curriculum Vitae

PERSONAL DATA

Name:	Jürgen Österle
Nationality:	Austrian

EDUCATION

01/2012 -	MSc Earth Sciences at the University of Vienna Topic: New constraints on the timing of the Mae Ping fault zone, (NW-Thailand) Supervisor: Urs Klötzli Collaboration: Chulalongkorn University, Bangkok
09/2013 - 02/2014	Erasmus student exchange program, University of Barcelona
10/2008 - 01/2012	BSc Earth Sciences at the University of Vienna Topic: Petrography of the granulites along the Finero back thrust (Italy) Supervisor: Urs Klötzli
09/2001 - 07/2006	Buisness School in Bregenz, Austria
09/1997 - 07/2001	Grammar School in Bregenz, Austria
09/1993 - 07/1997	Elementary School in Bregenz, Austria

HONORS

- Scholarship of the University of Vienna (2012)
- Scholarship of the University of Vienna (2011)

PRESENTATIONS

Poster presentations

- Österle, J., Palzer, M., Klötzli, U. [2013]: New constraints on the timing of the Mae-Ping Core-Complex, NW Thailand. To be presented at the MinPet 2013, September 19-23, Graz, Austria
- Palzer, M., Österle, J., Klötzli, U. [2012]: Lithological and structural investigations of the Finero Back Thrust. To be presented at the European Geosciences Union General Assembly 2012, April 22-27, Vienna, Austria

PICO (Presenting Interactive COntent) presentation

- Palzer, M., Österle, J., Klötzli, U. [2013]: New constraints on the Mae-Ping Core-Complex NW-Thailand: Is the Mae-Ping an Indosinian relict? To be presented at the European Geosciences Union General Assembly 2013, April 7-12, Vienna, Austria

SKILLS

Languages:

- German: mother tongue
- English: fluent
- Spanish: basic proficiency

Computer skills:

- elementary knowledge: CorelDraw, Photoshop, ArcGIS, HTML, MatLab
- advanced knowledge: Microsoft Office programs

Technical skills:

- FEI Inspect S Scanning Electron Microscopy
- Nu Plasma LA-ICP-MS

TUTORIALS

07/2013	Mapping course: Ötztal, Austria
06/2012	Mapping course: Weyer, Austria
07/2011	Regional geology excursion: Eastern Alps cross section, Austria

WORK EXPERIENCE

03/2007 - 09/2008	Employee at Glas Marte GmbH (Bregenz)

III. Data

III. 1. Mass-spectrometry data zircon
III. 2. Mass-spectrometry data monazite
III. 3. SEM images
III. 3.1. Augen-gneiss
III. 3.1.1. 283 Monazite (small subrounded grains)
III. 3.1.2. 284 Monazite (large subrounded grains)
III. 3.1.3. 301 Zircon (small prismatic grains)
III. 3.1.4. 302 Zircon (medium-length prismatic grains)
III. 3.1.5. 303 Zircon (large prismatic grains)
III. 3.2. Biotite-gneiss
III. 3.2.1. 283 Monazite (small subrounded grains)
III. 3.2.2. 305 Zircon (prismatic grains)
III. 3.3. Subvolcanic dyke
III. 3.3.1. 285 Zircon (small soccer ball grains)
III. 3.3.2. 286 Zircon (large soccer ball grains)
III. 3.3.3. 287 Zircon (small euhedral and spherical grains)
III. 3.3.4. 288 Zircon (large euhedral grains)
III. 3.3.5. 289 Zircon (small anhedral grains)
III. 3.3.6. 290 Zircon (large anhedral grains)
III. 4. Geochemistry
III. 4.1. Raw data
III. 4.2. Ternplot data (06/01 II, 13/01 IV, 12/02 V)
III. 4.3. Ternplot data (01/01 IV, 12/02 II, 12/02 III)
III. 4.4. REE diagram data

SEM images contain SE and CL images of zircons and BSE images of monazites. For each zircon and monazite, which were measured using the in-situ laser ablation, the name of the measurement, the diameter of the laser (in μm) and the $^{238}U/^{206}Pb$ age is given.

Color code:

- pink: $<$ 35 Ma
- yellow: 35-60 Ma
- green: 60-190 Ma
- red: 190-220 Ma
- lightblue: $>$ 220 Ma

File name	std.	start	end	204Pb	206Pb	207Pb	208Pb	232Th	238U	206Pb/204Pb	2RSE (%)	207Pb/235U	2RSE (%)	206Pb/238U	2RSE (%)	Rho
130207_0293_plg_014	*	154	255	2.4E-07	1.6E-04	1.0E-05	2.6E-06	7.2E-04	7.5E-03	588	21	0.3970	3.01	0.0531	2.48	0.41
130207_0293_plg_015	*	142	237	2.4E-07	1.3E-04	8.3E-06	2.0E-06	5.7E-04	6.3E-03	743	#	0.3881	3.61	0.0541	1.48	0.20
130207_0293_plg_016	*	127	237	2.1E-07	1.5E-04	9.4E-06	1.9E-06	5.6E-04	7.2E-03	791	6	0.3957	1.58	0.0539	1.40	0.44
130207_0293_plg_017	*	129	250	2.1E-07	1.3E-04	8.6E-06	1.8E-06	5.5E-04	6.7E-03	805	6	0.3860	1.96	0.0522	1.96	0.50
130207_0293_plg_018	*	123	240	2.6E-07	1.6E-04	1.1E-05	2.3E-06	6.2E-04	8.1E-03	630	7	0.4004	1.91	0.0549	1.13	0.29
130207_0293_plg_019	*	133	244	2.1E-07	1.7E-04	1.1E-05	2.5E-06	6.8E-04	8.7E-03	1078	10	0.3998	3.11	0.0537	1.90	0.31
130207_0293_plg_020	*	118	243	2.9E-07	2.3E-04	1.4E-05	3.0E-06	8.7E-04	1.2E-02	772	5	0.3875	1.93	0.0536	1.33	0.35
130207_0285_06_01_II_A3_01		84	185	2.4E-07	2.7E-05	1.7E-06	3.5E-06	4.1E-03	6.2E-03	173	11	0.0868	6.03	0.0122	6.65	0.55
130207_0285_06_01_II_D1_01		80	142	4.3E-07	6.7E-05	5.9E-06	3.3E-06	1.2E-03	8.8E-03	320	41	0.2197	8.43	0.0222	3.67	0.22
130207_0285_06_01_II_D10_01		83	146	3.1E-07	5.6E-05	4.1E-06	6.0E-06	2.9E-03	5.8E-03	248	17	0.1871	15.48	0.0229	21.85	0.71
130207_0285_06_01_II_D4_01		77	193	2.6E-07	9.0E-05	6.7E-06	4.6E-06	2.8E-03	1.1E-02	869	13	0.1544	9.23	0.0246	10.04	0.54
130207_0285_06_01_II_D4_02		88	299	2.1E-07	1.7E-05	1.4E-06	1.0E-06	1.1E-03	4.4E-03	184	4	0.1105	4.33	0.0131	4.19	0.48
130207_0285_06_01_II_D6_01		80	320	#	#	#	#	#	#	#	#	#	#	#	#	#
130207_0285_06_01_II_D7_01		71	109	2.1E-07	3.2E-05	2.0E-06	2.1E-06	9.5E-04	2.8E-03	222	38	0.2330	22.69	0.0322	13.27	0.29
130207_0285_06_01_II_D8_01		88	212	2.2E-07	3.6E-05	2.2E-06	1.5E-06	1.4E-03	6.9E-03	253	4	0.1196	7.58	0.0175	6.85	0.45
130207_0285_06_01_II_D9_01		87	114	2.0E-07	1.7E-05	1.2E-06	1.2E-06	7.3E-04	2.4E-03	30	703	0.1259	142.19	0.0153	#	#
130207_0285_06_01_II_E4_01		140	334	3.5E-07	6.4E-05	4.2E-06	7.6E-06	6.7E-03	1.0E-02	141	21	0.0914	14.53	0.0120	14.84	0.51
130207_0285_06_01_II_E4_02		80	195	4.2E-07	2.1E-03	1.2E-04	2.7E-05	1.7E-02	2.3E-01	9134	12	0.1487	2.09	0.0234	1.77	0.42
130207_0285_06_01_II_E5_01		99	246	2.2E-07	1.5E-05	9.0E-07	1.4E-06	3.2E-03	6.1E-03	81	5	0.0426	5.40	0.0065	3.26	0.30
130207_0285_06_01_II_E6_01		73	233	2.8E-07	9.8E-05	5.6E-06	4.1E-06	5.0E-03	2.1E-02	673	5	0.0742	2.42	0.0117	1.23	0.25
130207_0285_06_01_II_E6_02		89	419	2.4E-07	9.8E-05	5.8E-06	3.4E-06	3.4E-03	1.7E-02	447	3	0.1503	3.96	0.0231	3.95	0.50
130205_0293_plg_015		121	241	8.8E-07	2.0E-03	1.2E-04	2.9E-05	5.4E-03	8.9E-02	2563	21	0.3683	2.63	0.0502	2.62	0.50
130205_0293_plg_016	*	110	236	8.7E-07	1.9E-03	1.1E-04	2.7E-05	4.8E-03	8.0E-02	2719	32	0.3908	5.97	0.0532	4.93	0.41
130205_0293_plg_017	*	134	245	1.0E-06	1.9E-03	1.1E-04	2.8E-05	4.6E-03	8.1E-02	2416	47	0.3962	7.13	0.0538	4.46	0.31
130205_0293_plg_018	*	112	235	9.5E-07	1.9E-03	1.1E-04	2.8E-05	4.6E-03	8.3E-02	2359	31	0.3946	2.86	0.0542	2.79	0.49

130205_0293_plg_019	*	125	175	6.6E-07	1.3E-03	8.4E-05	2.0E-05	3.1E-03	6.9E-02	2062	127	0.3883	10.83	0.0529	13.19	0.61
130205_0293_plg_021	*	130	180	4.7E-07	7.9E-04	5.0E-05	1.2E-05	1.7E-03	4.0E-02	1825	134	0.3980	12.30	0.0543	8.18	0.33
130205_0293_plg_022	*	165	238	4.5E-07	5.3E-04	3.6E-05	8.6E-06	1.1E-03	2.9E-02	1574	129	0.3925	25.88	0.0531	25.99	0.50
130205_0293_plg_023	*	160	225	4.9E-07	5.3E-04	3.5E-05	8.2E-06	1.1E-03	2.8E-02	1173	41	0.3942	34.47	0.0541	37.80	0.55
130205_0286_06_01_II_A01_1		120	270	1.1E-06	2.4E-03	1.8E-04	7.1E-05	4.7E-03	5.3E-02	2404	24	0.9112	17.47	0.0964	17.12	0.49
130205_0286_06_01_II_A02_1		127	300	7.0E-07	6.5E-05	4.0E-06	9.5E-06	2.6E-03	6.4E-03	117	14	0.1892	11.96	0.0253	10.22	0.43
130205_0286_06_01_II_A02_2		130	210	9.2E-07	6.8E-05	4.3E-06	1.3E-06	3.7E-04	4.8E-03	70	107	0.2357	92.31	0.0315	81.97	0.44
130205_0286_06_01_II_A03_1		123	175	9.6E-07	6.7E-05	4.2E-06	1.1E-05	1.0E-02	2.7E-02	90	174	0.0488	30.77	0.0065	7.09	0.12
130205_0286_06_01_II_A03_2		120	224	9.0E-07	2.8E-05	1.6E-06	3.7E-06	2.9E-03	8.0E-03	40	43	0.0614	23.86	0.0084	26.58	0.56
130205_0286_06_01_II_A04_1		155	240	1.1E-06	2.0E-05	1.2E-06	3.1E-06	3.4E-03	8.5E-03	20	49	0.0448	37.47	0.0061	26.82	0.36
130205_0286_06_01_II_A05_1		135	300	9.8E-07	3.1E-05	1.9E-06	3.3E-06	3.0E-03	1.1E-02	38	21	0.0572	10.89	0.0077	3.81	0.17
130205_0286_06_01_II_A06_1		150	290	6.2E-07	9.4E-06	5.7E-07	1.4E-06	1.4E-03	3.9E-03	17	14	0.0489	27.78	0.0067	8.00	0.14
130205_0286_06_01_II_A06_2		135	290	5.4E-07	8.6E-06	5.8E-07	1.3E-06	1.3E-03	3.6E-03	19	19	0.0538	25.40	0.0069	9.78	0.19
130205_0286_06_01_II_A07_1		150	250	4.4E-07	8.2E-06	5.1E-07	1.1E-06	1.2E-03	3.9E-03	16	88	0.0378	52.01	0.0058	24.56	0.24
130205_0286_06_01_II_A08_1		120	150	5.9E-07	3.6E-05	2.4E-06	6.3E-06	6.9E-03	1.8E-02	74	286	0.0390	359.76	0.0056	38.44	0.05
130205_0286_06_01_II_A08_2		100	280	6.2E-07	4.8E-05	3.1E-06	5.8E-06	5.5E-03	2.0E-02	80	20	0.0468	7.14	0.0062	8.57	0.60
130205_0286_06_01_II_A09_1		110	250	4.8E-07	1.2E-05	7.1E-07	1.9E-06	1.4E-03	3.8E-03	36	11	0.0591	22.65	0.0093	15.65	0.35
130205_0286_06_01_II_A09_2		110	195	3.6E-07	1.4E-05	9.1E-07	1.9E-06	1.6E-03	4.8E-03	37	27	0.0650	38.73	0.0081	12.88	0.17
130205_0286_06_01_II_A10_1		110	175	4.5E-07	5.5E-05	3.5E-06	5.5E-06	5.3E-03	2.5E-02	136	31	0.0409	48.70	0.0062	41.00	0.42
130205_0286_06_01_II_A10_2		120	280	4.9E-07	6.3E-05	3.9E-06	5.4E-06	5.6E-03	2.9E-02	169	21	0.0405	10.72	0.0057	11.68	0.54
130206_0293_plg_021	*	130	235	3.4E-07	6.0E-04	4.2E-05	1.1E-05	1.1E-03	3.9E-02	1921	28	0.4163	4.31	0.0569	4.25	0.49
130206_0293_plg_022	*	130	230	3.2E-07	6.6E-04	4.6E-05	1.4E-05	1.3E-03	4.1E-02	2288	30	0.3942	4.67	0.0538	3.07	0.33
130206_0293_plg_023	*	130	235	2.9E-07	6.6E-04	4.5E-05	1.4E-05	1.3E-03	4.1E-02	2325	58	0.3650	6.06	0.0496	#	#
130206_0293_plg_024	*	134	199	3.3E-07	4.8E-04	3.2E-05	1.2E-05	7.2E-04	2.0E-02	1450	74	0.3999	10.28	0.0540	19.19	0.93
130206_0293_plg_025	*	124	193	2.5E-07	4.9E-04	3.2E-05	1.3E-05	7.4E-04	1.9E-02	2543	68	0.3952	11.75	0.0544	#	#
130206_0293_plg_027	*	130	230	2.5E-07	4.1E-04	2.6E-05	9.2E-06	5.2E-04	1.6E-02	1674	22	0.3889	5.15	0.0527	4.06	0.39

130206_0293_plg_028	*	140	220	2.3E-07	4.0E-04	2.6E-05	9.5E-06	5.4E-04	1.5E-02	2230	50	0.3961	5.63	0.0542	5.12	0.45
130206_0287_06_01_II_1_1		75	220	2.1E-07	2.8E-05	2.1E-06	3.5E-06	3.6E-04	1.9E-03	260	24	0.5146	26.32	0.0601	26.08	0.50
130206_0287_06_01_II_2_1		100	200	2.9E-07	4.1E-04	3.9E-05	3.1E-05	1.6E-03	2.1E-02	1674	34	0.5049	40.92	0.0438	37.60	0.46
130206_0287_06_01_II_3_1		95	222	2.9E-07	3.8E-04	2.9E-05	3.3E-05	9.9E-04	1.4E-02	2148	34	0.6583	20.22	0.0693	15.46	0.38
130206_0287_06_01_II_5_1		80	162	2.2E-07	1.1E-05	6.7E-07	5.1E-07	3.6E-04	2.7E-03	77	35	0.0703	28.74	0.0096	18.36	0.32
130206_0287_06_01_II_5_2		85	277	2.4E-07	4.4E-05	3.6E-06	1.6E-06	3.2E-04	2.3E-03	520	19	0.7725	20.97	0.0787	20.36	0.49
130206_0287_06_01_II_A02_1		115	299	2.4E-07	2.1E-05	1.5E-06	3.8E-06	3.0E-03	1.4E-02	112	13	0.0384	12.35	0.0045	4.44	0.18
130206_0287_06_01_II_A05_1		120	300	3.9E-07	3.0E-05	2.3E-06	7.7E-06	6.4E-03	1.5E-02	120	32	0.0380	50.69	0.0046	45.84	0.45
130206_0287_06_01_II_A06_1		144	287	3.6E-07	2.1E-05	1.5E-06	4.8E-06	4.9E-03	1.0E-02	65	38	0.0444	21.58	0.0051	23.54	0.55
130206_0287_06_01_II_A08_1		125	298	5.8E-07	3.7E-05	5.0E-06	9.8E-06	5.6E-03	2.1E-02	69	38	0.0669	29.75	0.0044	4.65	0.08
130206_0287_06_01_II_B02_1		74	193	4.0E-07	8.2E-06	2.0E-06	3.1E-06	1.6E-03	4.0E-03	41	53	0.3058	26.52	0.0083	25.14	0.47
130206_0287_06_01_II_B03_1		70	233	4.4E-07	1.4E-05	3.1E-06	4.5E-06	2.8E-03	6.3E-03	76	33	0.2229	22.21	0.0079	14.57	0.33
130206_0287_06_01_II_B04_1		140	297	3.2E-07	2.8E-05	2.0E-06	5.4E-06	5.2E-03	1.4E-02	124	37	0.0353	12.83	0.0043	12.06	0.47
130206_0287_06_01_II_B05_1		76	207	3.5E-07	2.4E-05	1.5E-06	4.1E-06	3.4E-03	1.5E-02	56	28	0.0254	12.72	0.0036	5.17	0.20
130206_0287_06_01_II_B07_1		109	179	3.9E-07	1.1E-05	1.3E-06	2.3E-06	1.9E-03	4.3E-03	48	291	0.0673	90.94	0.0055	80.33	0.44
130206_0287_06_01_II_B09_1		102	214	4.0E-07	1.9E-05	2.0E-06	3.6E-06	2.8E-03	7.0E-03	72	72	0.0604	30.81	0.0044	60.16	0.98
130206_0287_06_01_II_B10_1		102	205	9.2E-07	3.6E-05	7.1E-06	1.1E-05	4.2E-03	1.7E-02	47	37	0.1015	40.72	0.0042	13.21	0.16
130206_0287_06_01_II_C01_1		83	276	1.0E-06	2.8E-05	9.3E-06	1.3E-05	3.8E-03	1.0E-02	36	26	0.2364	31.16	0.0051	12.96	0.21
130206_0287_06_01_II_C04_1		101	200	2.4E-07	8.0E-05	5.4E-06	8.7E-06	7.0E-04	5.0E-03	291	41	0.2485	13.19	0.0311	17.46	0.66
130206_0287_06_01_II_C05_1		120	290	3.5E-07	3.4E-04	2.1E-05	1.8E-05	2.2E-03	3.0E-02	1331	22	0.1528	9.50	0.0212	10.75	0.57
130206_0287_06_01_II_C06_1		96	190	2.8E-07	9.8E-05	6.0E-06	3.4E-06	6.2E-04	6.4E-03	550	56	0.2444	29.41	0.0334	26.11	0.44
130206_0287_06_01_II_C07_1		91	203	1.9E-07	1.3E-04	7.9E-06	1.9E-05	1.8E-03	8.0E-03	1004	25	0.2585	13.01	0.0355	12.52	0.48
130207_0293_plg_021	*	117	250	2.1E-07	1.1E-04	7.6E-06	1.5E-06	4.9E-04	6.1E-03	638	15	0.3858	12.01	0.0525	10.74	0.45
130207_0293_plg_022	*	148	250	2.2E-07	1.3E-04	8.6E-06	1.8E-06	5.2E-04	6.9E-03	973	73	0.4025	9.75	0.0552	8.17	0.42
130207_0293_plg_023	*	137	250	2.1E-07	1.2E-04	7.7E-06	1.6E-06	4.6E-04	6.3E-03	763	32	0.3934	11.41	0.0534	9.46	0.41
130207_0293_plg_024	*	140	245	1.9E-07	1.1E-04	7.4E-06	1.6E-06	4.9E-04	6.2E-03	638	13	0.3847	11.23	0.0525	10.31	0.46

130207_0293_plg_025	*	120	215	1.6E-07	1.1E-04	7.7E-06	1.7E-06	4.8E-04	6.2E-03	690	67	0.4012	11.41	0.0546	9.73	0.43
130207_0288_06_01_II_A3_01		82	300	5.6E-07	7.3E-05	7.6E-06	8.8E-06	2.6E-03	6.1E-03	186	21	0.3950	18.30	0.0341	3.13	0.09
130207_0288_06_01_II_A5_01		100	290	1.8E-07	2.2E-04	1.4E-05	2.3E-05	1.2E-02	2.3E-02	1623	11	0.1971	4.72	0.0274	4.55	0.48
130207_0288_06_01_II_A7_01		100	300	2.0E-07	2.1E-04	1.3E-05	4.6E-06	2.1E-03	1.8E-02	603	52	0.2318	4.15	0.0317	3.86	0.46
130207_0288_06_01_II_A7_02		100	294	2.5E-07	5.0E-05	3.0E-06	2.1E-06	4.8E-04	4.6E-03	230	3	0.2075	7.64	0.0311	5.29	0.35
130207_0288_06_01_II_A8_01		130	300	2.1E-07	4.6E-05	3.0E-06	3.0E-06	1.5E-03	4.7E-03	180	26	0.1989	13.60	0.0269	11.43	0.42
130207_0288_06_01_II_A8_02		100	270	1.9E-07	1.2E-04	7.2E-06	5.6E-06	2.7E-03	1.1E-02	704	8	0.2127	8.07	0.0302	6.88	0.43
130207_0288_06_01_II_A9_01		145	300	2.0E-07	3.1E-05	2.3E-06	1.4E-06	8.9E-04	4.6E-03	78	165	0.0971	91.50	0.0120	99.70	0.54
130207_0288_06_01_II_A9_02		81	160	2.2E-07	2.0E-04	1.4E-05	8.6E-06	1.9E-03	1.1E-02	1037	28	0.4203	10.23	0.0516	12.69	0.62
130207_0288_06_01_II_A9_03		195	286	2.1E-07	4.0E-04	2.8E-05	4.4E-05	7.6E-03	1.6E-02	2323	59	0.5585	14.59	0.0720	10.49	0.36
130207_0288_06_01_II_A10_01		94	226	2.1E-07	3.2E-05	2.1E-06	4.2E-06	1.9E-03	2.8E-03	201	18	0.2604	16.87	0.0336	9.71	0.29
130207_0288_06_01_II_A10_02		84	208	2.2E-07	1.1E-04	7.5E-06	1.7E-05	7.1E-03	9.8E-03	1374	#	0.2562	9.92	0.0366	8.86	0.45
130209_0293_plg_001	*	123	251	2.9E-07	2.9E-04	1.7E-05	6.1E-06	1.9E-03	1.3E-02	1350	9	0.3885	2.18	0.0525	2.68	0.61
130209_0293_plg_002	*	112	231	3.2E-07	3.2E-04	1.9E-05	7.1E-06	2.1E-03	1.4E-02	1233	4	0.3960	1.61	0.0542	1.51	0.47
130209_0293_plg_003	*	117	240	2.7E-07	3.2E-04	1.9E-05	7.2E-06	2.1E-03	1.4E-02	1340	5	0.3953	1.49	0.0540	1.84	0.62
130209_0293_plg_004	*	122	248	3.0E-07	3.7E-04	2.2E-05	8.3E-06	2.3E-03	1.6E-02	1319	4	0.3950	2.01	0.0537	2.43	0.61
130209_0293_plg_005	*	120	244	2.9E-07	3.8E-04	2.2E-05	8.4E-06	2.3E-03	1.7E-02	1510	5	0.3967	1.63	0.0549	1.69	0.52
130209_0293_plg_006	*	128	245	2.5E-07	1.9E-04	1.1E-05	2.7E-06	7.3E-04	8.6E-03	1061	10	0.3857	2.42	0.0526	3.10	0.64
130209_0293_plg_007	*	122	246	3.1E-07	2.3E-04	1.4E-05	3.5E-06	9.1E-04	1.0E-02	941	7	0.3950	1.75	0.0529	2.57	0.73
130209_0293_plg_008	*	122	244	3.0E-07	2.1E-04	1.3E-05	3.4E-06	8.2E-04	9.4E-03	745	5	0.3932	1.65	0.0538	1.85	0.56
130209_0293_plg_009	*	120	237	3.1E-07	2.6E-04	1.6E-05	4.2E-06	1.0E-03	1.1E-02	930	8	0.3962	1.18	0.0542	1.64	0.69
130209_0289_06_01_II_A1_1		80	360	1.6E-06	4.5E-04	3.5E-05	7.6E-05	3.2E-02	3.8E-02	788	13	0.3458	11.68	0.0284	3.92	0.17
130209_0289_06_01_II_A2_1		149	264	3.5E-07	3.4E-04	1.9E-05	1.0E-04	4.7E-02	2.7E-02	1077	8	0.2298	5.38	0.0320	3.32	0.31
130209_0289_06_01_II_A3_1		128	280	3.7E-07	1.7E-04	1.4E-05	5.5E-05	5.6E-03	3.1E-03	571	6	1.3469	2.85	0.1391	2.91	0.51
130209_0289_06_01_II_A4_1		148	271	3.8E-07	7.2E-04	3.9E-05	5.1E-05	2.3E-02	5.5E-02	2372	14	0.2169	3.76	0.0325	3.75	0.50
130209_0289_06_01_II_A5_1		104	289	3.5E-07	1.3E-05	1.2E-06	1.9E-06	4.7E-03	7.4E-03	54	6	0.0451	11.66	0.0041	2.68	0.12

130209_0289_06_01_II_A7_1		76	169	6.2E-07	4.2E-04	2.6E-05	1.5E-05	7.3E-03	4.1E-02	1328	19	0.2077	10.27	0.0279	10.30	0.50
130209_0289_06_01_II_A7_2		74	210	3.3E-07	1.5E-04	9.9E-06	7.0E-06	3.9E-03	1.6E-02	718	7	0.2723	8.09	0.0330	7.08	0.44
130209_0289_06_01_II_A7_3		76	138	3.5E-07	1.4E-03	7.5E-05	4.7E-05	2.0E-02	9.5E-02	7155	26	0.2216	4.30	0.0333	5.78	0.67
130209_0289_06_01_II_A8_1		112	229	2.7E-07	2.5E-05	1.5E-06	4.0E-06	2.6E-03	2.6E-03	118	4	0.2239	13.90	0.0291	11.04	0.40
130209_0289_06_01_II_A8_2		85	342	3.3E-07	1.7E-04	1.0E-05	1.2E-05	6.0E-03	1.3E-02	911	3	0.2379	1.32	0.0294	1.38	0.52
130209_0289_06_01_II_B2_1		82	156	4.7E-07	1.7E-04	1.0E-05	9.2E-06	3.6E-03	1.2E-02	956	#	0.2603	3.98	0.0355	4.91	0.62
130209_0289_06_01_II_B2_2		77	125	3.1E-07	4.4E-05	3.4E-06	4.3E-06	2.1E-03	4.2E-03	403	77	0.2969	24.75	0.0341	33.12	0.67
130209_0289_06_01_II_B4_1		110	319	3.3E-07	1.3E-05	1.1E-06	2.8E-06	2.7E-03	2.5E-03	78	8	0.1014	15.30	0.0144	5.08	0.17
130209_0289_06_01_II_B6_1		95	355	2.9E-07	4.5E-04	2.5E-05	3.1E-05	1.7E-02	3.7E-02	2223	3	0.2063	1.07	0.0293	1.18	0.55
130209_0289_06_01_II_B7_1		120	351	2.8E-07	1.8E-04	1.0E-05	2.6E-05	1.6E-02	2.3E-02	641	7	0.1341	2.11	0.0195	2.04	0.48
130209_0289_06_01_II_B8_1		82	206	3.1E-07	1.5E-04	8.5E-06	2.8E-05	1.5E-02	1.5E-02	1212	14	0.1955	4.87	0.0271	4.25	0.44
130209_0289_06_01_II_B9_1		113	310	2.7E-07	3.3E-05	1.8E-06	2.6E-06	5.2E-03	1.1E-02	158	3	0.0522	3.17	0.0075	1.21	0.19
130209_0289_06_01_II_B9_2		133	400	2.4E-07	5.1E-05	2.8E-06	2.9E-06	5.2E-03	1.2E-02	239	4	0.0760	5.55	0.0105	4.62	0.42
130209_0289_06_01_II_C1_1		119	325	3.0E-07	3.6E-05	2.1E-06	2.7E-06	1.9E-03	5.2E-03	169	4	0.1074	8.99	0.0149	7.82	0.44
130209_0289_06_01_II_C4_1		80	135	3.5E-07	5.0E-04	2.9E-05	4.9E-05	2.4E-02	4.1E-02	2055	31	0.2092	4.09	0.0295	6.51	0.79
130209_0289_06_01_II_C6_1		107	290	3.8E-07	4.8E-05	2.7E-06	5.2E-06	9.5E-03	1.5E-02	127	5	0.0500	3.22	0.0073	2.04	0.32
130207_0293_plg_029	*	129	240	2.4E-07	1.6E-04	1.0E-05	2.2E-06	6.8E-04	8.7E-03	836	5	0.3885	2.95	0.0534	1.73	0.29
130207_0293_plg_030	*	120	237	2.0E-07	1.6E-04	1.1E-05	2.5E-06	6.7E-04	8.9E-03	971	5	0.3996	1.85	0.0540	1.74	0.47
130207_0293_plg_031	*	120	238	2.1E-07	1.5E-04	1.0E-05	2.4E-06	7.0E-04	9.0E-03	964	8	0.3872	2.53	0.0533	2.15	0.42
130207_0293_plg_032	*	124	233	1.8E-07	1.5E-04	1.1E-05	2.4E-06	7.1E-04	9.1E-03	1097	7	0.3987	2.40	0.0539	1.57	0.33
130207_0290_06_01_II_A5_01		80	380	3.0E-07	3.5E-05	3.1E-06	5.3E-06	2.8E-03	4.6E-03	156	3	0.2890	3.99	0.0205	2.76	0.35
130207_0290_06_01_II_A5_02		88	254	2.5E-07	1.0E-05	8.6E-07	7.2E-07	3.8E-04	2.8E-03	55	3	0.1014	6.40	0.0095	6.90	0.54
130207_0290_06_01_II_A6_01		72	162	3.1E-07	7.8E-05	5.2E-06	1.4E-05	1.3E-02	1.4E-02	287	8	0.1160	4.05	0.0138	4.23	0.52
130207_0290_06_01_II_A6_02		78	151	3.8E-07	9.4E-05	6.5E-06	1.5E-05	1.3E-02	1.6E-02	278	10	0.1266	4.72	0.0150	7.01	0.74
130207_0290_06_01_II_A6_03		80	185	8.0E-07	4.5E-04	3.3E-05	3.1E-05	1.5E-02	5.2E-02	1580	13	0.2112	3.29	0.0268	1.46	0.22
130207_0290_06_01_II_A7_01		91	172	5.6E-07	2.9E-04	1.9E-05	3.3E-05	2.1E-02	4.4E-02	601	12	0.1450	2.96	0.0204	2.68	0.45

130207_0290_06_01_II_A8_01		80	500	3.9E-07	3.0E-04	1.9E-05	2.7E-05	1.3E-02	2.8E-02	837	3	0.2127	1.08	0.0239	1.01	0.46
130207_0290_06_01_II_A9_01		148	490	2.8E-07	5.3E-04	3.3E-05	3.1E-05	1.6E-02	5.5E-02	2128	7	0.2097	2.15	0.0232	1.95	0.45
130207_0290_06_01_II_B2_01		140	417	4.7E-07	1.4E-03	8.5E-05	2.7E-05	1.3E-02	1.4E-01	4299	9	0.1999	2.39	0.0319	2.17	0.45
130207_0290_06_01_II_B2_02		106	480	3.2E-07	2.6E-04	1.7E-05	8.6E-06	3.8E-03	2.5E-02	1207	4	0.2295	1.71	0.0351	1.50	0.44
130207_0290_06_01_II_B3_01		113	256	2.8E-07	1.2E-04	8.0E-06	7.7E-06	3.5E-03	1.2E-02	436	7	0.2303	2.02	0.0347	1.30	0.32
130207_0290_06_01_II_B3_02		88	231	2.6E-07	8.8E-05	5.9E-06	6.3E-06	2.5E-03	7.2E-03	676	6	0.2579	2.84	0.0380	2.52	0.44
130207_0290_06_01_II_B4_01		115	273	1.9E-07	5.9E-06	5.6E-07	7.3E-07	2.7E-03	5.0E-03	40	4	0.0347	6.80	0.0039	2.96	0.22
130207_0290_06_01_II_B5_01		129	357	1.7E-07	1.3E-04	8.5E-06	4.2E-06	2.1E-03	1.3E-02	877	2	0.2273	2.03	0.0335	1.85	0.46
130207_0290_06_01_II_B5_02		79	188	1.9E-07	1.1E-04	7.6E-06	7.4E-06	3.4E-03	1.1E-02	393	22	0.2315	2.42	0.0309	2.69	0.56
130521_0292_1255_plr_001	*	90	150	9.3E-07	4.2E-03	1.2E-04	2.5E-05	5.1E-03	9.2E-02	15686	212	0.4045	3.17	0.0540	3.04	0.48
130521_0292_1255_plr_002	*	82	120	1.1E-06	6.8E-03	1.9E-04	6.4E-05	1.5E-02	1.5E-01	14568	305	0.3940	13.08	0.0541	#	#
130521_0292_1255_plr_003	*	82	198	1.2E-06	6.7E-03	1.9E-04	6.4E-05	1.5E-02	1.5E-01	11745	97	0.4016	1.07	0.0557	1.17	0.55
130521_0292_1255_plr_004	*	84	205	5.5E-07	5.3E-03	1.5E-04	4.6E-05	1.0E-02	1.2E-01	18444	20	0.4008	1.16	0.0562	1.22	0.52
130521_0292_1255_plr_005	*	84	205	1.1E-06	3.3E-03	1.1E-04	3.3E-05	8.1E-03	1.1E-01	2903	22	0.3668	2.26	0.0474	2.38	0.53
130521_0292_1255_plr_006	*	82	200	1.0E-06	3.5E-03	1.2E-04	3.9E-05	9.4E-03	1.2E-01	-11761	-564	0.3753	1.50	0.0495	1.22	0.41
130521_0292_1255_plr_007	*	82	200	1.0E-06	3.8E-03	1.3E-04	4.2E-05	1.0E-02	1.3E-01	3610	54	0.3799	1.95	0.0509	1.67	0.43
130521_0292_1255_plr_008	*	84	200	1.0E-06	3.2E-03	1.2E-04	3.7E-05	9.8E-03	1.3E-01	3355	7	0.3902	1.68	0.0549	1.55	0.46
130521_0292_1255_plr_009	*	78	200	7.4E-07	2.7E-03	1.0E-04	3.0E-05	7.6E-03	1.1E-01	3999	12	0.3867	1.88	0.0536	1.36	0.36
130521_0292_1255_plr_010	*	78	200	1.0E-06	3.0E-03	1.1E-04	3.3E-05	8.2E-03	1.2E-01	5069	101	0.4000	3.74	0.0550	4.47	0.60
130521_0292_1255_plr_011	*	85	210	7.2E-07	2.3E-03	8.9E-05	2.1E-05	6.0E-03	1.0E-01	3558	10	0.4006	1.69	0.0603	1.48	0.44
130521_0292_1255_plr_012	*	44	200	6.3E-07	2.1E-03	8.8E-05	2.5E-05	5.2E-03	9.4E-02	8862	43	0.4580	4.12	0.0585	0.72	0.09
130521_0292_1255_plr_013	*	80	200	6.5E-07	1.9E-03	7.5E-05	1.8E-05	4.4E-03	8.4E-02	3261	18	0.4002	3.37	0.0572	1.99	0.30
130521_0292_1255_plr_014	*	83	200	6.2E-07	1.7E-03	6.7E-05	1.6E-05	4.4E-03	8.2E-02	2721	7	0.3871	3.45	0.0545	2.66	0.39
130521_0292_1255_plr_015	*	82	204	5.4E-07	1.4E-03	6.1E-05	1.7E-05	3.9E-03	7.5E-02	16027	41	0.3800	4.37	0.0493	2.70	0.31
130521_0292_1255_plr_016	*	80	200	7.6E-07	1.4E-03	6.2E-05	1.6E-05	3.9E-03	7.7E-02	1609	384	0.3720	7.19	0.0490	1.92	0.13
130521_0301_01_01_II_A02		88	249	#	4.9E-04	1.1E-05	1.1E-05	6.1E-03	2.3E-02	#	#	0.1844	13.63	0.0272	3.02	0.11

130521_0301_01_01_II_A03	56	140	9.1E-07	1.0E-03	3.1E-05	2.3E-06	8.2E-04	5.3E-02	#	#	0.2410	29.12	0.0329	27.59	0.47
130521_0301_01_01_II_A04	72	172	1.2E-06	1.5E-02	4.7E-04	4.2E-05	7.8E-03	7.1E-01	53491	109	0.2195	4.97	0.0298	6.50	0.65
130521_0301_01_01_II_A05	80	185	1.3E-06	8.8E-03	2.8E-04	4.6E-05	1.9E-02	4.5E-01	29960	152	0.2209	12.25	0.0292	11.68	0.48
130521_0301_01_01_II_A06	62	198	#	3.6E-04	1.1E-05	4.3E-06	7.3E-04	1.9E-02	#	#	0.2337	9.66	0.0318	9.47	0.49
130521_0301_01_01_II_A07	62	244	#	3.9E-04	1.2E-05	2.2E-05	9.5E-03	1.9E-02	#	#	0.2309	2.94	0.0309	1.48	0.25
130521_0301_01_01_II_A08	96	241	1.7E-06	7.7E-03	2.6E-04	9.9E-05	2.7E-02	4.1E-01	10058	192	0.2417	6.91	0.0317	5.94	0.43
130521_0301_01_01_II_A09	92	247	1.0E-06	2.2E-02	7.3E-04	9.5E-05	2.4E-02	1.1E+00	62905	69	0.2520	2.53	0.0353	2.82	0.56
130521_0301_01_01_II_A10	55	187	8.1E-07	1.1E-03	3.6E-05	8.3E-06	1.3E-03	5.9E-02	2870	5	0.2470	5.20	0.0350	5.48	0.53
130521_0301_01_01_II_B01	53	178	#	1.1E-03	3.8E-05	8.6E-06	2.4E-03	6.2E-02	#	#	0.2368	2.81	0.0335	2.25	0.40
130521_0301_01_01_II_B02	66	173	7.1E-07	1.8E-04	5.9E-06	8.1E-06	3.7E-03	9.8E-03	#	#	0.2359	5.22	0.0333	3.56	0.34
130521_0301_01_01_II_B03	81	180	#	5.0E-04	1.7E-05	7.2E-06	3.2E-03	2.9E-02	#	#	0.2383	6.34	0.0342	4.57	0.36
130521_0301_01_01_II_B04	59	186	6.6E-07	2.7E-04	9.8E-06	5.8E-06	2.6E-03	1.7E-02	#	#	0.2254	5.41	0.0314	3.11	0.29
130521_0301_01_01_II_B05	58	200	#	2.4E-04	8.6E-06	1.3E-06	5.4E-04	1.6E-02	#	#	0.2197	4.31	0.0305	3.68	0.43
130521_0301_01_01_II_B06	51	140	7.2E-07	6.8E-04	2.4E-05	1.8E-05	8.8E-03	4.2E-02	#	#	0.2319	3.36	0.0345	2.55	0.38
130521_0301_01_01_II_B07	75	200	7.1E-07	2.8E-03	9.5E-05	1.6E-05	6.8E-03	1.6E-01	1394	12	0.2424	4.75	0.0382	4.41	0.46
130521_0301_01_01_II_B08	78	222	#	2.4E-04	8.2E-06	4.0E-06	1.3E-03	1.5E-02	#	#	0.2196	5.78	0.0346	4.37	0.38
130521_0301_01_01_II_B09	64	211	1.9E-06	4.0E-04	1.4E-05	2.1E-05	9.4E-03	2.6E-02	1130	4	0.2399	3.37	0.0369	1.93	0.29
130521_0301_01_01_II_B10	78	231	4.7E-07	6.1E-04	2.2E-05	5.7E-06	2.4E-03	3.9E-02	1784	5	0.2391	2.85	0.0375	2.12	0.37
130521_0301_01_01_II_C01	65	200	#	3.3E-04	1.2E-05	1.1E-05	5.1E-03	2.1E-02	#	#	0.2405	4.13	0.0373	2.48	0.30
130521_0301_01_01_II_C02	63	181	5.4E-07	1.9E-04	6.7E-06	1.5E-06	7.1E-04	1.6E-02	535	7	0.2075	16.32	0.0321	14.91	0.46
130521_0301_01_01_II_C03_1	68	261	#	1.3E-04	4.7E-06	5.9E-06	2.1E-03	8.8E-03	#	#	0.2463	5.50	0.0361	2.95	0.27
130521_0301_01_01_II_C03_2	77	229	6.0E-07	2.2E-04	7.8E-06	1.3E-06	#	1.5E-02	377	1	0.2261	3.32	0.0353	2.71	0.41
130521_0301_01_01_II_C04	55	173	8.7E-07	6.9E-04	2.6E-05	1.1E-05	4.6E-03	5.0E-02	8817	7	0.2318	5.00	0.0357	4.02	0.40
130521_0301_01_01_II_C05	40	194	1.2E-06	1.9E-04	2.1E-05	1.5E-05	1.2E-03	2.8E-02	247	20	0.1739	51.26	0.0178	5.01	0.05
130521_0301_01_01_II_C06	51	131	1.5E-06	2.2E-04	8.5E-06	8.5E-06	4.3E-03	1.6E-02	483	12	0.2449	8.42	0.0366	4.02	0.24
130521_0301_01_01_II_C07	67	163	4.4E-07	3.0E-04	1.1E-05	1.1E-05	5.3E-03	2.2E-02	826	5	0.2364	4.20	0.0362	4.08	0.49

130521_0301_01_01_II_C08		54	200	5.3E-07	1.2E-03	4.4E-05	1.4E-05	7.7E-03	9.0E-02	2874	1	0.2231	3.05	0.0347	3.31	0.54
130521_0301_01_01_II_C09_1		55	114	#	3.2E-04	1.2E-05	1.3E-06	7.6E-04	2.5E-02	#	#	0.2237	7.48	0.0344	5.88	0.39
130521_0301_01_01_II_C09_2		45	93	#	1.4E-03	5.1E-05	3.6E-06	1.2E-03	1.1E-01	#	#	0.2189	10.56	0.0333	9.49	0.45
130524_0292_1255_plr_013	*	78	190	2.9E-06	6.6E-03	2.1E-04	4.5E-05	7.7E-03	1.4E-01	2481	15	0.3971	1.84	0.0541	1.92	0.52
130524_0292_1255_plr_014	*	83	200	2.7E-06	6.1E-03	2.0E-04	4.5E-05	7.5E-03	1.4E-01	2522	13	0.3937	2.07	0.0533	2.06	0.50
130524_0292_1255_plr_015	*	84	200	2.8E-06	5.9E-03	1.9E-04	4.4E-05	7.3E-03	1.3E-01	2381	16	0.3902	2.74	0.0536	2.70	0.49
130524_0292_1255_plr_016	*	95	200	2.5E-06	4.8E-03	1.7E-04	4.0E-05	6.4E-03	1.2E-01	2060	20	0.3801	5.46	0.0506	5.96	0.55
130524_0292_1255_plr_017	*	86	200	4.3E-06	5.1E-03	1.8E-04	4.2E-05	6.7E-03	1.3E-01	1184	6	0.3985	3.34	0.0548	4.47	0.67
130524_0292_1255_plr_018	*	93	200	#	5.2E-03	1.8E-04	4.4E-05	6.8E-03	1.3E-01	#	#	0.4008	4.71	0.0564	2.06	0.22
130524_0292_1255_plr_019	*	89	200	3.4E-06	4.6E-03	1.8E-04	5.6E-05	6.5E-03	1.3E-01	1473	13	0.4063	7.15	0.0513	3.58	0.25
130524_0292_1255_plr_020	*	90	200	2.5E-06	4.6E-03	1.7E-04	4.3E-05	6.6E-03	1.2E-01	2248	17	0.3857	5.69	0.0532	5.07	0.45
130524_0292_1255_plr_021	*	90	200	3.0E-06	5.2E-03	1.9E-04	5.6E-05	9.0E-03	1.4E-01	2838	19	0.3894	3.58	0.0556	1.67	0.23
130524_0302_01_01_II_A02_1		58	185	2.5E-06	6.5E-04	2.3E-05	5.6E-06	8.1E-04	3.4E-02	555	8	0.1970	16.36	0.0239	18.28	0.56
130524_0302_01_01_II_A02_2		53	186	3.8E-06	3.9E-03	1.3E-04	8.5E-06	1.7E-03	1.4E-01	-397	-32	0.2369	2.26	0.0325	2.83	0.63
130524_0302_01_01_II_B03_1		50	165	1.9E-06	1.1E-03	3.6E-05	4.1E-06	1.2E-03	4.3E-02	1534	5	0.2431	5.71	0.0326	3.29	0.29
130524_0302_01_01_II_B03_2		45	109	#	3.1E-03	1.0E-04	7.4E-06	1.4E-03	1.2E-01	#	#	0.2358	3.91	0.0327	3.34	0.43
130524_0302_01_01_II_B07_1		80	242	3.3E-06	1.2E-04	5.5E-06	5.0E-06	1.6E-03	2.2E-02	123	6	0.0565	16.87	0.0070	5.86	0.17
130524_0302_01_01_II_B07_2		53	184	1.8E-06	9.7E-04	4.2E-05	3.4E-05	2.6E-03	1.0E-02	599	3	1.1751	6.30	0.1206	6.58	0.52
130524_0302_01_01_II_C01_1		53	161	1.8E-06	2.5E-03	7.8E-05	4.7E-06	1.2E-03	9.2E-02	2791	12	0.2391	2.32	0.0347	2.02	0.43
130524_0302_01_01_II_C01_2		45	151	6.9E-06	4.2E-03	4.2E-04	1.1E-04	3.5E-03	2.0E-02	518	123	6.2164	18.26	0.2837	16.98	0.46
130524_0302_01_01_II_C02_1		69	293	2.4E-06	9.5E-04	3.3E-05	5.8E-06	6.9E-04	4.9E-02	1243	2	0.1963	3.83	0.0259	3.33	0.43
130524_0302_01_01_II_C02_2		67	295	2.0E-06	1.0E-03	3.4E-05	6.5E-06	1.3E-03	3.8E-02	276	7	0.2618	2.29	0.0343	0.95	0.21
130524_0302_01_01_II_D02		38	136	4.8E-06	4.6E-04	3.5E-05	2.1E-05	1.2E-03	2.9E-02	174	13	0.2857	51.86	0.0245	15.43	0.15
130524_0302_01_01_II_D06		70	290	#	3.6E-04	1.3E-05	2.0E-05	4.9E-03	1.5E-02	#	#	0.2673	4.83	0.0353	1.44	0.15
130524_0302_01_01_II_E02_1		54	129	#	1.2E-04	7.9E-06	1.4E-05	1.5E-03	2.3E-02	#	#	0.0688	44.05	0.0070	6.96	0.08
130524_0302_01_01_II_E02_2		49	120	#	5.6E-04	1.9E-05	1.5E-05	2.6E-03	2.4E-02	#	#	0.2376	11.76	0.0327	5.87	0.25

130524_0302_01_01_II_E07		62	182	2.0E-06	4.4E-04	1.6E-05	2.9E-05	7.6E-03	1.9E-02	516	5	0.2404	4.83	0.0320	3.46	0.36
130524_0302_01_01_II_F01_1		59	233	1.6E-06	3.6E-03	1.2E-04	1.1E-05	1.5E-03	1.6E-01	4716	5	0.2333	6.62	0.0332	6.64	0.50
130524_0302_01_01_II_F01_2		47	105	#	2.1E-03	7.1E-05	5.7E-06	1.1E-03	8.6E-02	#	#	0.2447	5.40	0.0342	8.52	0.79
130524_0302_01_01_II_F03		47	109	#	3.4E-04	1.2E-05	2.4E-05	6.1E-03	1.5E-02	#	#	0.2625	17.18	0.0334	4.40	0.13
130524_0302_01_01_II_F04		70	253	2.1E-06	6.1E-04	2.6E-05	6.6E-06	7.2E-04	3.2E-02	351	7	0.2495	8.02	0.0283	2.73	0.17
130524_0302_01_01_II_F06		45	102	#	2.6E-04	9.5E-06	9.9E-06	2.6E-03	1.2E-02	#	#	0.2357	19.31	0.0307	17.42	0.45
130524_0292_1255_plr_001	*	45	200	4.7E-06	5.6E-03	1.8E-04	3.8E-05	6.1E-03	1.2E-01	1066	10	0.4016	1.21	0.0544	1.42	0.59
130524_0292_1255_plr_002	*	45	200	4.1E-06	6.7E-03	2.1E-04	4.7E-05	7.8E-03	1.4E-01	1511	13	0.3889	0.81	0.0535	1.41	0.87
130524_0292_1255_plr_003	*	45	200	3.7E-06	5.7E-03	1.8E-04	3.8E-05	6.3E-03	1.2E-01	1311	13	0.3908	0.91	0.0532	1.54	0.85
130524_0292_1255_plr_004	*	45	200	3.8E-06	5.3E-03	1.7E-04	3.7E-05	5.9E-03	1.2E-01	1312	13	0.3899	1.36	0.0532	1.67	0.61
130524_0292_1255_plr_005	*	45	200	2.8E-06	5.4E-03	1.7E-04	3.7E-05	6.1E-03	1.2E-01	1655	14	0.3939	1.05	0.0535	1.66	0.79
130524_0292_1255_plr_006	*	45	200	3.0E-06	5.6E-03	1.8E-04	3.8E-05	6.4E-03	1.2E-01	1588	15	0.3918	1.20	0.0537	1.62	0.68
130524_0292_1255_plr_007	*	45	200	3.2E-06	6.2E-03	2.0E-04	4.3E-05	7.0E-03	1.4E-01	1745	13	0.3936	0.96	0.0538	1.55	0.80
130524_0292_1255_plr_008	*	45	197	3.0E-06	6.5E-03	2.1E-04	4.7E-05	7.4E-03	1.5E-01	2102	11	0.3953	1.32	0.0537	1.70	0.65
130524_0292_1255_plr_009	*	45	200	#	6.9E-03	2.3E-04	5.6E-05	8.2E-03	1.5E-01	#	#	0.3991	1.72	0.0541	1.57	0.46
130524_0292_1255_plr_010	*	45	200	3.1E-06	6.5E-03	2.1E-04	5.2E-05	8.7E-03	1.4E-01	2050	11	0.3915	1.05	0.0535	1.49	0.71
130524_0292_1255_plr_011	*	45	200	2.7E-06	6.2E-03	2.0E-04	5.3E-05	9.0E-03	1.4E-01	2120	12	0.3921	1.04	0.0539	1.36	0.66
130524_0292_1255_plr_012	*	45	200	3.3E-06	5.9E-03	1.9E-04	4.6E-05	7.5E-03	1.3E-01	1943	7	0.3936	1.13	0.0532	1.54	0.68
130524_0303_01_01_II_A01_1		70	276	5.8E-06	2.3E-04	7.4E-06	9.9E-06	2.3E-03	8.0E-03	168	3	0.2559	8.52	0.0353	2.76	0.16
130524_0303_01_01_II_A01_2		55	163	4.2E-06	2.3E-03	7.2E-05	8.6E-06	9.3E-04	8.6E-02	1244	1	0.2377	14.28	0.0333	13.37	0.47
130524_0303_01_01_II_A05_1		50	130	4.3E-06	3.2E-03	9.5E-05	4.5E-06	1.1E-03	1.1E-01	#	#	0.2393	2.98	0.0358	2.82	0.47
130524_0303_01_01_II_A05_2		47	129	#	1.4E-03	4.4E-05	6.3E-05	1.7E-02	5.0E-02	#	#	0.2338	5.27	0.0344	5.16	0.49
130524_0303_01_01_II_A06_1		48	120	2.3E-06	5.6E-04	2.0E-05	6.4E-05	1.1E-02	1.4E-02	-106	-50	0.4142	14.92	0.0499	9.53	0.32
130524_0303_01_01_II_A06_2		45	155	3.4E-06	6.9E-03	2.1E-04	6.1E-06	1.1E-03	2.3E-01	2097	10	0.2361	3.17	0.0353	3.17	0.50
130524_0303_01_01_II_A07_1		54	175	2.9E-06	8.3E-04	2.7E-05	3.5E-06	6.4E-04	3.3E-02	612	5	0.2320	10.45	0.0319	9.36	0.45
130524_0303_01_01_II_A07_2		45	125	#	1.8E-03	5.4E-05	2.6E-06	9.3E-04	6.5E-02	#	#	0.2196	4.92	0.0333	5.42	0.55

130524_0303_01_01_II_A10_1		59	191	2.1E-06	3.0E-04	9.4E-06	2.7E-06	6.0E-04	4.5E-02	143	0	0.0591	8.11	0.0081	2.83	0.17
130524_0303_01_01_II_A10_2		50	124	5.3E-06	5.0E-04	1.6E-05	1.2E-05	2.7E-03	1.7E-02	-1367	-23	0.2667	10.94	0.0351	10.36	0.47
130524_0303_01_01_II_B02		60	160	#	2.9E-04	9.7E-06	1.4E-05	3.1E-03	9.4E-03	#	#	0.2817	11.70	0.0369	6.85	0.29
130524_0303_01_01_II_B03_1		58	150	1.9E-06	7.9E-04	2.7E-05	4.9E-06	8.0E-04	3.2E-02	527	3	0.2235	10.48	0.0317	5.89	0.28
130524_0303_01_01_II_B03_2		57	206	2.2E-06	7.8E-04	2.4E-05	3.2E-05	8.0E-03	2.6E-02	455	4	0.2503	3.17	0.0358	2.12	0.33
130524_0303_01_01_II_B04_1		57	197	2.1E-06	1.6E-04	6.8E-06	4.1E-06	2.2E-03	2.6E-02	110	3	0.0506	40.88	0.0075	4.81	0.06
130524_0303_01_01_II_B04_2		47	103	#	3.8E-04	1.2E-05	1.3E-05	3.4E-03	1.3E-02	#	#	0.2405	12.86	0.0356	6.31	0.25
130524_0303_01_01_II_B05_1		50	150	7.1E-06	1.5E-03	4.7E-05	3.2E-06	6.8E-04	5.5E-02	279	4	0.2327	7.56	0.0339	5.10	0.34
130524_0303_01_01_II_B05_2		58	240	1.7E-06	3.4E-03	1.0E-04	1.9E-05	4.6E-03	1.2E-01	2152	3	0.2453	1.87	0.0358	1.57	0.42
130524_0303_01_01_II_B06_1		52	175	4.1E-06	1.3E-03	3.9E-05	1.2E-05	7.2E-04	4.4E-02	#	#	0.2388	2.77	0.0358	2.00	0.36
130524_0303_01_01_II_B06_2		53	130	1.9E-06	1.1E-04	3.5E-06	8.7E-06	2.2E-03	3.6E-03	#	#	0.2823	17.64	0.0370	9.54	0.27
130524_0303_01_01_II_B08_1		45	187	3.5E-06	8.2E-03	3.5E-04	8.0E-06	8.0E-04	8.6E-02	2461	1	1.0916	3.48	0.1152	3.37	0.48
130524_0303_01_01_II_B08_2		73	298	4.0E-06	2.5E-04	8.6E-06	2.9E-06	2.0E-03	3.0E-02	81	3	0.0868	10.37	0.0097	7.51	0.36
130524_0303_01_01_II_B09		50	153	3.3E-06	1.3E-03	4.6E-05	5.9E-05	8.0E-03	2.4E-02	167	13	0.5822	7.91	0.0753	6.50	0.41
130521_0292_1255_plr_017		82	200	#	2.2E-03	1.1E-04	3.3E-05	1.1E-02	1.8E-01	#	#	0.2774	#	0.0298	#	#
130521_0292_1255_plr_018	*	82	200	5.4E-07	2.2E-03	9.0E-05	2.4E-05	7.2E-03	1.2E-01	4154	10	0.3785	2.48	0.0530	2.04	0.41
130521_0292_1255_plr_019	*	83	200	6.1E-07	1.9E-03	8.2E-05	2.4E-05	7.0E-03	1.1E-01	2644	12	0.3938	3.42	0.0532	1.94	0.28
130521_0292_1255_plr_020	*	45	200	5.9E-07	1.9E-03	8.1E-05	2.3E-05	6.4E-03	1.0E-01	2973	12	0.4164	1.73	0.0554	0.92	0.27
130521_0292_1255_plr_021	*	84	200	3.1E-07	1.4E-03	6.3E-05	1.7E-05	5.6E-03	9.9E-02	4925	10	0.3789	1.57	0.0514	1.44	0.46
130521_0292_1255_plr_022	*	82	200	5.7E-07	1.5E-03	6.6E-05	1.8E-05	5.8E-03	1.0E-01	4038	7	0.3906	1.92	0.0536	1.79	0.47
130521_0292_1255_plr_023	*	81	200	3.2E-07	1.5E-03	6.6E-05	1.9E-05	5.9E-03	1.0E-01	4905	5	0.3991	1.65	0.0551	1.80	0.55
130521_0292_1255_plr_024	*	83	200	2.8E-07	1.2E-03	5.5E-05	1.7E-05	5.6E-03	9.5E-02	3626	3	0.3864	2.56	0.0521	1.94	0.38
130521_0292_1255_plr_025	*	81	200	2.8E-07	1.1E-03	5.0E-05	1.3E-05	4.2E-03	8.5E-02	3928	4	0.3957	2.65	0.0532	3.24	0.61
130521_0292_1255_plr_026	*	84	200	2.1E-07	1.1E-03	5.3E-05	1.4E-05	4.5E-03	8.7E-02	-6485	-44	0.4001	3.72	0.0551	3.24	0.44
130521_0292_1255_plr_027	*	86	200	2.7E-07	1.0E-03	5.0E-05	1.3E-05	4.4E-03	8.8E-02	3229	3	0.4122	2.16	0.0582	2.14	0.49
130521_0292_1255_plr_028	*	82	200	1.7E-07	9.3E-04	4.6E-05	1.2E-05	4.2E-03	8.7E-02	5856	5	0.3994	3.97	0.0546	4.54	0.57

130521_0292_1255_plr_029	*	85	200	2.3E-07	8.4E-04	4.3E-05	1.1E-05	4.1E-03	8.6E-02	5872	6	0.3711	2.02	0.0490	1.94	0.48
130521_0305_01_01_IV_A01_1		73	185	#	6.8E-05	2.9E-06	3.2E-06	1.7E-03	6.8E-03	#	#	0.2403	29.01	0.0333	23.78	0.41
130521_0305_01_01_IV_A01_2		45	122	5.4E-07	9.2E-04	4.4E-05	7.0E-06	2.0E-03	6.1E-02	-304	-127	0.3539	17.96	0.0432	17.33	0.48
130521_0305_01_01_IV_A02		52	120	#	1.9E-04	8.1E-06	1.0E-05	5.6E-03	2.3E-02	#	#	0.2054	19.85	0.0280	17.87	0.45
130521_0305_01_01_IV_A03		52	140	#	9.2E-05	4.2E-06	1.6E-06	8.4E-04	6.7E-03	#	#	0.3036	25.89	0.0380	29.17	0.56
130521_0305_01_01_IV_A04		65	245	1.4E-07	2.4E-04	1.1E-05	1.3E-05	5.5E-03	1.9E-02	-15691	-14	0.3248	8.95	0.0415	8.86	0.50
130521_0305_01_01_IV_A05		51	122	#	1.2E-04	5.8E-06	7.1E-06	2.9E-03	1.1E-02	#	#	0.2887	46.38	0.0387	39.37	0.42
130521_0305_01_01_IV_A06_1		48	125	2.6E-07	2.4E-04	4.0E-05	1.2E-05	8.6E-04	2.5E-03	1242	4	9.8916	16.16	0.3523	15.27	0.47
130521_0305_01_01_IV_A06_2		45	111	#	8.3E-04	1.4E-04	8.2E-05	3.8E-03	6.3E-03	#	#	12.5674	6.97	0.4644	6.50	0.47
130521_0305_01_01_IV_A07		51	131	3.1E-07	3.4E-04	1.7E-05	2.9E-05	7.0E-03	3.0E-02	#	#	0.3435	35.16	0.0410	31.79	0.45
130521_0305_01_01_IV_A08		47	109	#	9.3E-05	4.8E-06	3.3E-06	1.1E-03	5.8E-03	#	#	0.4624	34.47	0.0508	43.77	0.63
130521_0305_01_01_IV_A09		77	217	#	8.9E-05	3.9E-06	4.7E-06	1.0E-02	4.2E-02	#	#	0.0597	9.64	0.0084	4.90	0.25
130521_0305_01_01_IV_A10		54	178	4.4E-07	9.9E-04	5.9E-05	9.6E-05	3.6E-02	1.4E-01	4624	31	0.2519	19.17	0.0289	14.17	0.37
130521_0305_01_01_IV_B01		41	74	9.7E-07	2.8E-04	7.7E-05	8.0E-05	3.2E-02	1.1E-01	275	584	0.7265	211.95	0.0116	60.27	0.14
130521_0305_01_01_IV_B02		45	103	#	9.6E-05	5.0E-06	1.9E-06	8.2E-04	1.7E-02	#	#	0.1963	49.66	0.0272	52.44	0.53
130521_0305_01_01_IV_B03		45	114	#	3.3E-03	3.0E-04	1.1E-04	8.6E-03	5.5E-02	#	#	3.5161	2.65	0.2464	2.50	0.47
130521_0305_01_01_IV_B04_1		52	172	#	3.2E-04	1.4E-05	2.2E-05	1.3E-02	4.1E-02	#	#	0.2226	4.14	0.0314	3.33	0.40
130521_0305_01_01_IV_B04_2		54	131	#	1.1E-05	2.0E-06	2.3E-06	9.6E-04	7.2E-03	#	#	0.1225	26.26	0.0051	11.99	0.23
130521_0305_01_01_IV_C01		59	136	2.5E-07	6.1E-06	1.1E-06	1.2E-06	1.5E-03	4.3E-03	#	#	0.2290	35.39	0.0066	23.27	0.33
130521_0305_01_01_IV_C02		54	110	#	1.7E-05	1.4E-06	1.2E-06	6.7E-04	8.7E-03	#	#	0.0767	41.43	0.0092	26.15	0.32
130521_0305_01_01_IV_C03		70	170	2.3E-07	4.9E-05	2.6E-06	3.9E-06	1.1E-02	3.6E-02	220	0	0.0459	28.55	0.0059	20.08	0.35
130521_0305_01_01_IV_C05		92	149	#	2.5E-05	2.5E-06	3.3E-06	7.3E-03	1.6E-02	#	#	0.0720	179.54	0.0062	35.89	0.10
130521_0305_01_01_IV_C07		69	226	3.0E-07	1.5E-04	1.0E-05	1.5E-05	3.8E-02	9.7E-02	755	12	0.0522	30.87	0.0065	10.53	0.17

#: no data, wrong data

207Pb 206Pb	2RSE (%)	208Pb 206Pb	2RSE (%)	208Pb 232Th	2RSE (%)	238U 206Pb	2RSE (%)	207Pb 206Pb	2RSE (%)	Age 235U	Error 235U	Age 238U	Error 238U	Age 232Th	Error 232Th	L-W-ratio	232Th 238U
0.0535	2.12	0.1154	11.69	0.0171	14.41	18.834	2.48	0.0535	1.62	339.45	8.74	333.50	8.07	342.97	49.06		
0.0532	2.55	0.0938	6.97	0.0178	17.42	18.472	1.48	0.0532	0.61	332.98	10.30	339.86	4.89	355.73	61.51		
0.0529	1.57	0.0867	4.62	0.0159	10.38	18.557	1.40	0.0529	3.08	338.51	4.56	338.34	4.63	318.70	32.84		
0.0535	1.87	0.0969	4.89	0.0158	8.93	19.147	1.96	0.0535	5.04	331.46	5.54	328.18	6.28	315.96	28.00		
0.0529	1.55	0.1093	7.11	0.0184	9.00	18.199	1.13	0.0529	1.57	341.96	5.57	344.82	3.78	367.86	32.85		
0.0537	1.58	0.1048	5.10	0.0176	10.32	18.622	1.90	0.0537	2.55	341.53	9.05	337.19	6.24	352.56	36.10		
0.0528	1.25	0.0932	3.67	0.0162	6.59	18.667	1.33	0.0528	2.12	332.56	5.48	336.41	4.37	325.65	21.32		
0.0511	6.93	1.0943	9.60	0.0036	4.42	81.941	6.65	0.0511	1.25	84.49	4.90	78.20	5.17	72.97	3.22	1:1	0.67
0.0652	14.46	0.3345	13.29	0.0165	30.61	44.959	3.67	0.0652	1.58	201.69	15.54	141.81	5.15	330.88	100.71	2:1	0.14
0.0586	7.49	0.7218	4.79	0.0083	11.00	43.639	21.85	0.0586	6.93	174.15	25.09	146.05	31.63	166.98	18.30	1:1	0.50
0.0411	19.08	0.1695	34.52	0.0089	13.50	40.579	10.04	0.0411	7.49	145.78	12.61	156.93	15.59	178.11	23.95	1,5:1	0.25
0.0493	5.72	0.1932	15.08	0.0049	4.30	76.258	4.19	0.0493	30.77	106.42	4.38	83.99	3.50	99.05	4.25	1,5:1	0.26
#	#	#	#	#	#	#	#	#	3.16	#	#	#	#	#	#	2:1	#
0.0533	10.06	0.4169	42.21	0.0096	17.58	31.012	13.27	0.0533	10.06	212.69	44.49	204.59	26.78	194.11	34.00	1:1	0.34
0.0490	3.16	0.3123	6.23	0.0063	9.25	57.302	6.85	0.0490	1.55	114.75	8.26	111.53	7.58	126.68	11.69	1,5:1	0.20
0.0526	30.77	0.4644	67.14	0.0083	66.47	65.166	#	0.0526	1.87	120.40	175.82	98.17	#	167.58	111.23	2,5:1	0.30
0.0539	3.08	0.8222	2.53	0.0037	13.01	83.205	14.84	0.0539	#	88.76	12.42	77.01	11.37	73.83	9.59	1,5:1	0.66
0.0471	0.61	0.0495	32.81	0.0076	3.99	42.739	1.77	0.0471	14.46	140.77	2.75	149.09	2.60	153.60	6.11	1,5:1	0.07
0.0468	5.04	0.6534	4.34	0.0020	4.99	154.162	3.26	0.0468	5.72	42.35	2.24	41.68	1.36	39.71	1.98	1,5:1	0.52
0.0467	1.62	0.2318	5.44	0.0035	2.39	85.165	1.23	0.0467	19.08	72.66	1.70	75.25	0.92	71.34	1.70	1,5:1	0.24
0.0502	1.18	0.2256	5.33	0.0087	5.03	43.235	3.95	0.0502	1.18	142.16	5.27	147.41	5.77	174.62	8.74	1,5:1	0.20
0.0530	1.54	0.0980	5.44	0.0158	5.01	19.911	2.62	0.0530	1.54	318.38	7.22	315.89	8.09	317.23	15.77		
0.0534	2.37	0.1000	5.57	0.0166	6.65	18.803	4.93	0.0534	2.37	334.92	17.19	334.04	16.07	333.45	22.00		
0.0533	3.69	0.1003	6.17	0.0171	6.41	18.594	4.46	0.0533	3.69	338.91	20.76	337.69	14.69	343.25	21.82		
0.0529	1.90	0.1001	5.09	0.0174	7.19	18.449	2.79	0.0529	1.90	337.74	8.24	340.28	9.26	347.85	24.80		

0.0531	10.71	0.0972	38.54	0.0158	36.87	18.905	13.19	0.0531	10.71	333.11	31.23	332.28	42.87	316.81	116.24		
0.0533	7.28	0.1024	67.32	0.0180	62.49	18.425	8.18	0.0533	7.28	340.19	36.20	340.71	27.21	359.64	223.97		
0.0538	5.59	0.1015	18.22	0.0170	42.72	18.836	25.99	0.0538	5.59	336.22	76.93	333.46	85.03	340.05	144.56		
0.0527	7.87	0.0985	35.61	0.0169	56.18	18.473	37.80	0.0527	7.87	337.41	104.12	339.85	126.35	338.93	189.72		
0.0684	1.06	0.1930	4.91	0.0361	18.07	10.369	17.12	0.0684	1.06	657.70	88.29	593.51	97.82	716.45	127.59	1:1	0.09
0.0552	6.60	0.9901	5.36	0.0099	9.52	39.555	10.22	0.0552	6.60	175.97	19.50	160.95	16.26	199.22	18.88	1,5:1	0.40
0.0555	14.42	0.1097	99.87	0.0060	233.75	31.772	81.97	0.0555	14.42	214.92	196.67	199.77	163.29	121.21	284.47	1,5:1	0.08
0.0549	44.59	1.0994	32.13	0.0028	32.45	153.713	7.09	0.0549	44.59	48.41	14.65	41.80	2.96	56.70	18.38	1:1	0.39
0.0522	21.17	0.9758	31.34	0.0033	16.14	118.912	26.58	0.0522	21.17	60.55	14.12	53.99	14.30	67.24	10.84	1:1	0.37
0.0520	40.94	0.9986	38.59	0.0023	44.98	165.072	26.82	0.0520	40.94	44.47	16.43	38.93	10.42	45.46	20.43	1:1	0.40
0.0537	11.24	0.7170	8.40	0.0029	8.51	129.643	3.81	0.0537	11.24	56.45	6.00	49.53	1.88	57.57	4.89	1:1	0.28
0.0522	27.22	0.9574	15.53	0.0024	16.61	148.954	8.00	0.0522	27.22	48.45	13.23	43.13	3.44	47.72	7.92	1,5:1	0.36
0.0554	22.52	0.9243	15.34	0.0023	18.25	144.831	9.78	0.0554	22.52	53.20	13.25	44.36	4.32	46.92	8.56	1,5:1	0.36
0.0480	48.73	0.8460	29.95	0.0022	46.73	171.903	24.56	0.0480	48.73	37.65	19.41	37.39	9.16	43.46	20.30	1,5:1	0.32
0.0500	296.23	0.9332	#	0.0020	267.19	177.904	38.44	0.0500	296.23	38.82	147.21	36.13	13.86	39.44	105.55	1:1	0.38
0.0549	6.80	0.7383	5.36	0.0022	8.81	161.165	8.57	0.0549	6.80	46.47	3.25	39.88	3.41	43.84	3.86	1:1	0.28
0.0468	18.66	1.0253	16.67	0.0033	21.88	107.916	15.65	0.0468	18.66	58.32	12.92	59.46	9.27	66.82	14.60	1:1	0.36
0.0577	34.37	0.9009	22.27	0.0027	30.49	123.084	12.88	0.0577	34.37	63.90	24.27	52.16	6.70	55.10	16.79	1:1	0.34
0.0522	23.87	0.6062	29.52	0.0022	35.99	162.274	41.00	0.0522	23.87	40.68	19.61	39.60	16.21	44.70	16.08	1:1	0.21
0.0508	6.74	0.4107	39.74	0.0022	11.44	175.419	11.68	0.0508	6.74	40.31	4.25	36.64	4.27	44.77	5.11	1:1	0.19
0.0532	4.79	0.1012	6.75	0.0180	25.62	17.561	4.25	0.0532	4.79	353.43	12.94	357.03	14.79	361.50	91.99		
0.0531	3.32	0.1001	24.28	0.0164	19.55	18.587	3.07	0.0531	3.32	337.41	13.48	337.81	10.11	329.74	64.05		
0.0533	7.90	0.0989	23.42	0.0160	17.37	20.179	#	0.0533	7.90	315.92	16.58	311.80	#	319.92	55.22		
0.0533	10.52	0.0953	54.39	0.0173	58.26	18.502	19.19	0.0533	10.52	341.57	30.27	339.33	63.74	347.23	201.58		
0.0530	16.24	0.1045	17.67	0.0168	62.77	18.378	#	0.0530	16.24	338.16	34.38	341.55	#	337.04	210.90		
0.0534	4.99	0.1029	33.68	0.0165	46.17	18.965	4.06	0.0534	4.99	333.58	14.76	331.25	13.13	331.02	152.15		

0.0531	4.56	0.0970	162.12	0.0172	59.33	18.436	5.12	0.0531	4.56	338.79	16.34	340.51	17.00	344.10	203.44		
0.0500	34.91	1.3097	30.08	0.0225	25.82	16.630	26.08	0.0500	34.91	421.52	95.14	376.43	96.08	449.00	114.99	1:1	0.19
0.0796	6.00	0.6702	26.87	0.0187	39.80	22.811	37.60	0.0796	6.00	414.98	149.94	276.58	102.60	375.36	148.57	1,5:1	0.07
0.0670	7.26	1.1102	38.21	0.0437	28.32	14.435	15.46	0.0670	7.26	513.60	84.96	431.79	64.88	864.93	241.18	1,5:1	0.07
0.0499	22.52	0.2233	447.16	0.0016	39.01	104.704	18.36	0.0499	22.52	69.01	19.36	61.28	11.21	32.94	12.84	2:1	0.13
0.0668	8.57	0.5010	19.27	0.0142	19.37	12.700	20.36	0.0668	8.57	581.19	97.34	488.61	96.50	284.13	54.72	2:1	0.14
0.0616	12.83	0.9426	13.15	0.0018	8.75	224.171	4.44	0.0616	12.83	38.28	4.65	28.69	1.27	36.48	3.19	6:1	0.22
0.0589	18.41	1.2098	9.94	0.0015	15.41	217.282	45.84	0.0589	18.41	37.83	19.00	29.60	13.55	30.51	4.70	6:1	0.43
0.0623	23.19	1.0644	17.08	0.0013	19.21	195.859	23.54	0.0623	23.19	44.13	9.36	32.83	7.71	26.24	5.04	4,5:1	0.48
0.1059	25.41	1.1943	14.32	0.0022	24.00	226.092	4.65	0.1059	25.41	65.79	19.13	28.45	1.32	44.12	10.58	6:1	0.27
0.2444	45.66	1.7531	34.57	0.0044	23.07	120.735	25.14	0.2444	45.66	270.90	65.11	53.17	13.32	87.88	20.24	6:1	0.41
0.0984	193.56	1.4437	47.00	0.0031	18.27	127.231	14.57	0.0984	193.56	204.34	41.96	50.47	7.33	62.24	11.36	11:1	0.44
0.0584	15.59	0.8759	20.50	0.0011	10.86	231.190	12.06	0.0584	15.59	35.20	4.45	27.82	3.35	22.92	2.49	6,5:1	0.36
0.0531	11.46	0.7306	7.00	0.0013	9.19	281.519	5.17	0.0531	11.46	25.43	3.20	22.86	1.18	25.79	2.37	4:1	0.23
0.0886	190.06	0.8435	224.47	0.0019	134.94	180.501	80.33	0.0886	190.06	66.10	59.93	35.62	28.59	37.54	50.68	2:1	0.44
0.0951	21.06	1.0240	24.68	0.0016	32.17	226.073	60.16	0.0951	21.06	59.58	17.99	28.45	17.10	32.26	10.37	3,5:1	0.40
0.1764	41.88	1.5343	41.18	0.0026	30.36	237.760	13.21	0.1764	41.88	98.14	38.82	27.06	3.57	52.55	15.94	4:1	0.25
0.2878	19.43	2.1243	13.90	0.0038	23.55	195.638	12.96	0.2878	19.43	215.44	62.36	32.87	4.25	77.47	18.22	4,5:1	0.36
0.0585	15.23	0.4402	35.85	0.0113	28.79	32.141	17.46	0.0585	15.23	225.33	27.01	197.51	34.04	226.52	64.95	4:1	0.14
0.0520	3.00	0.2509	10.65	0.0067	25.69	47.133	10.75	0.0520	3.00	144.36	12.87	135.34	14.41	134.57	34.49	4:1	0.07
0.0537	12.78	0.3003	85.79	0.0095	81.48	29.934	26.11	0.0537	12.78	222.00	60.41	211.84	54.64	190.94	155.45	3,5:1	0.10
0.0527	7.25	1.2031	36.30	0.0117	19.18	28.189	12.52	0.0527	7.25	233.47	27.51	224.72	27.71	235.93	45.03	2:1	0.23
0.0534	6.41	0.1021	24.08	0.0174	34.14	19.056	10.74	0.0534	6.41	331.30	34.54	329.71	34.62	348.72	118.39		
0.0530	9.38	0.0997	29.21	0.0156	42.08	18.109	8.17	0.0530	9.38	343.46	28.83	346.49	27.60	312.74	131.02		
0.0532	7.30	0.0973	23.83	0.0180	42.46	18.729	9.46	0.0532	7.30	336.83	33.24	335.32	30.97	360.02	152.08		
0.0534	8.45	0.1050	29.94	0.0165	51.02	19.034	10.31	0.0534	8.45	330.50	32.18	330.09	33.26	331.01	168.20		

0.0530	9.39	0.0959	32.95	0.0173	51.87	18.304	9.73	0.0530	9.39	342.49	33.72	342.91	32.57	347.16	179.32		
0.0839	15.76	0.9303	14.15	0.0146	20.46	29.305	3.13	0.0839	15.76	338.03	54.03	216.31	6.66	293.04	59.60	5:1	0.43
0.0524	2.61	0.8499	10.69	0.0093	6.13	36.452	4.55	0.0524	2.61	182.64	7.92	174.46	7.84	187.26	11.43	3:1	0.54
0.0530	2.80	0.1401	13.84	0.0108	10.14	31.509	3.86	0.0530	2.80	211.65	7.96	201.41	7.66	217.78	21.97	2:1	0.12
0.0478	5.86	#	#	#	#	32.105	5.29	0.0478	5.86	191.46	13.42	197.73	10.31	#	#	2:1	0.11
0.0527	8.94	0.5392	10.94	0.0102	15.90	37.197	11.43	0.0527	8.94	184.23	23.17	171.02	19.33	204.87	32.43	2:1	0.32
0.0520	4.77	0.3538	13.74	0.0104	10.49	33.152	6.88	0.0520	4.77	195.78	14.48	191.58	13.01	209.69	21.88	2:1	0.25
0.0601	20.95	0.3791	33.21	0.0049	104.03	83.435	99.70	0.0601	20.95	94.10	85.76	76.80	76.57	98.71	102.69	1,5:1	0.19
0.0595	7.20	0.2764	65.02	0.0201	48.08	19.396	12.69	0.0595	7.20	356.29	31.21	324.07	40.22	402.18	192.38	1,5:1	0.17
0.0564	11.35	0.8117	37.45	0.0279	11.89	13.882	10.49	0.0564	11.35	450.54	54.51	448.42	45.60	557.08	65.41	1,5:1	0.47
0.0556	13.01	0.9001	14.75	0.0103	14.28	29.740	9.71	0.0556	13.01	234.99	36.01	213.19	20.39	206.95	29.43	1,5:1	0.67
0.0508	8.28	1.3680	36.81	0.0110	9.93	27.298	8.86	0.0508	8.28	231.64	20.75	231.93	20.22	221.16	21.85	1,5:1	0.72
0.0538	1.61	0.0933	2.58	0.0169	4.53	19.049	2.68	0.0538	1.61	333.28	6.21	329.83	8.63	337.83	15.20		
0.0531	1.10	0.1013	3.20	0.0174	4.02	18.442	1.51	0.0531	1.10	338.71	4.64	340.41	5.02	347.73	13.87		
0.0528	1.04	0.1007	2.03	0.0168	4.30	18.517	1.84	0.0528	1.04	338.25	4.29	339.07	6.09	336.35	14.34		
0.0535	1.36	0.1129	3.81	0.0167	3.03	18.628	2.43	0.0535	1.36	337.99	5.79	337.09	7.99	335.14	10.09		
0.0524	1.22	0.1063	3.74	0.0169	2.89	18.217	1.69	0.0524	1.22	339.28	4.71	344.50	5.68	338.20	9.71		
0.0536	2.30	0.0825	5.17	0.0177	9.88	19.009	3.10	0.0536	2.30	331.24	6.87	330.50	9.99	354.33	34.72		
0.0538	1.62	0.0889	4.66	0.0164	8.97	18.914	2.57	0.0538	1.62	338.05	5.04	332.13	8.32	329.30	29.33		
0.0527	1.47	0.1050	5.01	0.0176	7.04	18.573	1.85	0.0527	1.47	336.68	4.73	338.06	6.10	353.28	24.67		
0.0533	1.59	0.1094	4.91	0.0163	5.98	18.434	1.64	0.0533	1.59	338.87	3.40	340.55	5.44	327.14	19.41		
0.0896	7.79	1.1078	4.65	0.0113	7.90	35.197	3.92	0.0896	7.79	301.56	30.94	180.60	6.98	227.99	17.91	2,5:1	0.84
0.0520	2.39	1.6109	1.49	0.0096	2.41	31.265	3.32	0.0520	2.39	210.07	10.25	202.96	6.63	192.77	4.63	2,5:1	1.75
0.0706	1.75	1.8322	1.65	0.0412	2.09	7.191	2.91	0.0706	1.75	866.24	16.77	839.38	22.94	816.79	16.77	2,5:1	1.82
0.0493	1.18	0.4015	4.94	0.0096	3.03	30.757	3.75	0.0493	1.18	199.35	6.82	206.26	7.62	192.76	5.82	4:1	0.42
0.0757	8.24	0.8585	5.90	0.0015	7.79	243.374	2.68	0.0757	8.24	44.79	5.12	26.43	0.71	31.05	2.42	2,5:1	0.64

0.0547	3.54	0.1926	11.86	0.0098	13.69	35.832	10.30	0.0547	3.54	191.64	18.09	177.44	18.04	197.35	26.90	2,5:1	0.18
0.0567	4.67	0.2485	13.07	0.0103	6.97	30.290	7.08	0.0567	4.67	244.57	17.73	209.38	14.60	207.43	14.38	2,5:1	0.24
0.0485	1.79	0.2285	5.50	0.0094	2.39	29.991	5.78	0.0485	1.79	203.28	7.95	211.44	12.04	189.09	4.51	2,5:1	0.21
0.0539	5.92	0.7346	3.54	0.0095	11.91	34.400	11.04	0.0539	5.92	205.12	26.15	184.72	20.14	190.30	22.57	2,5:1	1.01
0.0572	1.25	0.2714	5.21	0.0108	1.49	34.050	1.38	0.0572	1.25	216.69	2.58	186.59	2.54	216.23	3.21	2,5:1	0.44
0.0529	4.73	0.2073	17.23	0.0109	10.17	28.135	4.91	0.0529	4.73	234.87	8.38	225.14	10.87	219.21	22.19	2,5:1	0.31
0.0522	94.93	0.3565	95.22	0.0127	34.11	29.356	33.12	0.0522	94.93	263.98	59.23	215.94	70.71	256.00	86.96	2,5:1	0.49
0.0400	36.65	0.7997	6.84	0.0044	14.35	69.519	5.08	0.0400	36.65	98.08	14.41	92.07	4.64	88.29	12.65	3:1	1.05
0.0506	0.59	0.3811	3.98	0.0089	1.27	34.074	1.18	0.0506	0.59	190.46	1.86	186.47	2.17	179.15	2.27	4:1	0.46
0.0510	1.09	0.5591	6.42	0.0067	3.42	51.411	2.04	0.0510	1.09	127.75	2.54	124.19	2.51	134.35	4.58	2:1	0.70
0.0506	3.16	0.8181	7.44	0.0093	3.75	36.852	4.25	0.0506	3.16	181.32	8.12	172.59	7.24	187.63	7.01	3:1	1.04
0.0476	2.70	0.3822	2.59	0.0023	2.90	132.846	1.21	0.0476	2.70	51.68	1.60	48.34	0.58	46.78	1.35	3:1	0.48
0.0510	3.08	0.3010	4.88	0.0026	3.34	95.625	4.62	0.0510	3.08	74.37	3.98	67.06	3.08	51.58	1.72	3:1	0.45
0.0522	2.99	0.1547	43.97	0.0064	4.03	66.954	7.82	0.0522	2.99	103.54	8.88	95.57	7.42	128.75	5.17	4,5:1	0.36
0.0520	4.91	0.7215	#	0.0090	3.16	33.937	6.51	0.0520	4.91	192.88	7.21	187.21	12.02	181.39	5.70	2:1	0.59
0.0502	2.46	0.5768	1.94	0.0023	2.42	136.794	2.04	0.0502	2.46	49.52	1.56	46.95	0.96	46.25	1.12	1,5:1	0.62
0.0527	1.82	0.0987	5.49	0.0164	8.63	18.730	1.73	0.0527	1.82	333.27	8.41	335.31	5.64	327.92	28.10		
0.0538	1.24	0.1014	3.92	0.0176	8.30	18.525	1.74	0.0538	1.24	341.39	5.37	338.91	5.76	352.94	29.07		
0.0526	1.34	0.0986	4.47	0.0163	7.27	18.759	2.15	0.0526	1.34	332.34	7.18	334.79	7.00	326.89	23.57		
0.0537	1.31	0.1012	4.68	0.0176	8.09	18.543	1.57	0.0537	1.31	340.68	6.97	338.60	5.18	351.95	28.25		
0.1028	3.40	2.9419	2.55	-0.5552	2.99	48.809	2.76	0.1028	3.40	257.78	9.11	130.74	3.57	#	-741.01	4:1	0.61
0.0667	5.90	0.6242	5.26	0.0463	5.15	105.810	6.90	0.0667	5.90	98.06	6.00	60.64	4.17	914.85	46.07	4:1	0.13
0.0618	2.62	1.8635	1.24	0.0110	4.43	72.598	4.23	0.0618	2.62	111.41	4.29	88.19	3.71	221.24	9.75	2,5:1	0.89
0.0613	4.10	1.4232	2.31	0.0079	8.38	66.703	7.01	0.0613	4.10	121.07	5.40	95.93	6.68	159.58	13.33	2,5:1	0.81
0.0581	3.62	0.4069	12.92	0.0124	4.62	37.362	1.46	0.0581	3.62	194.60	5.84	170.27	2.45	248.14	11.39	2,5:1	0.28
0.0517	1.94	0.6620	3.33	0.0057	#	49.032	2.68	0.0517	1.94	137.49	3.81	130.15	3.45	114.06	#	1,5:1	0.47

0.0697	0.64	2.8394	1.06	-0.0326	1.07	41.877	1.01	0.0697	0.64	195.78	1.93	152.13	1.52	-670.41	-7.32	2,5:1	0.46
0.0719	0.64	8.8279	4.01	-0.0168	2.84	43.148	1.95	0.0719	0.64	193.30	3.80	147.70	2.84	-342.69	-9.82	2:1	0.29
0.0462	0.46	0.0981	8.31	0.0070	2.98	31.393	2.17	0.0462	0.46	185.01	4.05	202.14	4.32	141.60	4.20	3,5:1	0.10
0.0479	0.69	0.1539	5.19	0.0081	1.88	28.529	1.50	0.0479	0.69	209.76	3.24	222.09	3.28	162.69	3.05	3,5:1	0.15
0.0486	1.53	0.3493	2.43	0.0073	3.28	28.841	1.30	0.0486	1.53	210.46	3.84	219.72	2.80	147.93	4.84	2,5:1	0.29
0.0487	1.88	0.3748	1.87	0.0083	3.24	26.299	2.52	0.0487	1.88	233.01	5.92	240.57	5.95	167.14	5.39	2,5:1	0.35
0.0620	7.75	0.6678	7.05	0.0009	7.88	253.717	2.96	0.0620	7.75	34.66	2.32	25.36	0.75	18.01	1.42	1,5:1	0.55
0.0496	1.20	0.1776	3.55	0.0075	3.47	29.884	1.85	0.0496	1.20	207.94	3.83	212.18	3.87	150.93	5.21	2:1	0.16
0.0542	2.63	0.4625	5.79	0.0091	3.72	32.359	2.69	0.0542	2.63	211.45	4.63	196.20	5.20	182.68	6.76	2:1	0.30
0.0550	4.15	0.0209	12.85	0.0002	13.07	18.531	3.04	0.0550	4.15	344.88	9.30	338.82	10.03	3.46	0.45		
0.0529	3.73	0.0328	22.69	0.0002	14.50	18.492	#	0.0529	3.73	337.31	38.25	339.50	#	3.03	0.44		
0.0521	0.88	0.0323	4.14	0.0002	2.96	17.959	1.17	0.0521	0.88	342.83	3.11	349.31	3.98	3.10	0.09		
0.0515	1.29	0.0285	14.37	0.0002	6.58	17.808	1.22	0.0515	1.29	342.25	3.39	352.20	4.18	3.27	0.22		
0.0551	1.34	0.0286	11.94	0.0001	6.74	21.095	2.38	0.0551	1.34	317.25	6.18	298.57	6.96	2.94	0.20		
0.0540	0.97	0.0311	11.51	0.0002	5.64	20.214	1.22	0.0540	0.97	323.55	4.16	311.27	3.71	3.05	0.17		
0.0533	1.12	0.0312	6.24	0.0001	5.27	19.664	1.67	0.0533	1.12	327.00	5.46	319.76	5.22	3.01	0.16		
0.0520	1.27	0.0296	6.08	0.0001	3.84	18.209	1.55	0.0520	1.27	334.49	4.80	344.64	5.20	2.87	0.11		
0.0530	1.38	0.0284	13.66	0.0002	7.26	18.671	1.36	0.0530	1.38	331.94	5.33	336.34	4.44	3.05	0.22		
0.0528	2.95	0.0267	11.85	0.0002	7.99	18.169	4.47	0.0528	2.95	341.66	10.91	345.38	15.05	3.05	0.24		
0.0498	1.22	0.0223	11.42	0.0001	5.83	16.584	1.48	0.0498	1.22	342.10	4.93	377.45	5.45	2.77	0.16		
0.0590	3.83	0.0378	10.82	0.0002	10.20	17.100	0.72	0.0590	3.83	382.85	13.24	366.37	2.57	4.67	0.48		
0.0520	3.07	0.0257	15.48	0.0002	12.16	17.493	1.99	0.0520	3.07	341.82	9.83	358.36	6.95	3.17	0.39		
0.0510	2.76	0.0252	16.92	0.0001	9.91	18.345	2.66	0.0510	2.76	332.26	9.83	342.15	8.88	2.83	0.28		
0.0548	5.08	0.0337	23.94	0.0002	16.98	20.277	2.70	0.0548	5.08	327.01	12.28	310.33	8.19	3.20	0.54		
0.0533	5.95	0.0291	24.30	0.0001	27.61	20.397	1.92	0.0533	5.95	321.14	19.99	308.54	5.80	2.84	0.78		
0.0487	14.49	0.1058	22.12	0.0001	13.56	36.824	3.02	0.0487	14.49	171.84	21.79	172.73	5.15	1.53	0.21	5:1	0.26

0.0529	5.78	0.0024	#	0.0001	11.52	30.412	27.59	0.0529	5.78	219.23	59.11	208.56	56.88	1.80	0.21	5:1	0.02
0.0531	4.91	0.0063	90.42	0.0001	60.31	33.595	6.50	0.0531	4.91	201.46	9.13	189.08	12.13	2.98	1.80	4:1	0.01
0.0539	2.37	0.0214	43.07	0.0001	24.59	34.284	11.68	0.0539	2.37	202.65	22.75	185.34	21.38	1.97	0.48	6:1	0.04
0.0514	6.21	0.0237	7.84	#	#	31.429	9.47	0.0514	6.21	213.26	18.75	201.92	18.85	#	#	4:1	0.04
0.0531	2.47	0.1727	2.05	0.0001	2.11	32.372	1.48	0.0531	2.47	210.91	5.62	196.12	2.87	1.74	0.04	7:1	0.49
0.0539	1.49	0.0535	29.59	0.0001	24.38	31.536	5.94	0.0539	1.49	219.79	13.75	201.24	11.78	2.42	0.59	7:1	0.07
0.0511	0.59	0.0176	25.46	0.0001	8.03	28.330	2.82	0.0511	0.59	228.21	5.17	223.62	6.19	2.83	0.23	5:1	0.02
0.0506	2.92	0.0039	213.14	0.0000	171.10	28.566	5.48	0.0506	2.92	224.18	10.51	221.81	11.95	0.95	1.63	4:1	0.02
0.0506	1.63	0.0213	15.64	0.0001	11.77	29.814	2.25	0.0506	1.63	215.80	5.48	212.67	4.70	1.72	0.20	3,5:1	0.04
0.0511	5.85	0.1392	11.69	0.0001	6.43	30.017	3.56	0.0511	5.85	215.03	10.17	211.26	7.39	1.67	0.11	3:1	0.37
0.0506	4.42	0.1499	82.11	0.0001	10.34	29.230	4.57	0.0506	4.42	217.06	12.47	216.85	9.76	1.64	0.17	3,5:1	0.11
0.0522	4.35	0.0569	18.61	0.0001	8.61	31.837	3.11	0.0522	4.35	206.37	10.15	199.37	6.12	1.61	0.14	4:1	0.15
0.0518	3.28	0.0125	6.30	0.0002	7.07	32.773	3.68	0.0518	3.28	201.64	7.91	193.76	7.03	3.11	0.22	3:1	0.03
0.0492	2.51	0.0741	14.98	0.0001	7.48	28.988	2.55	0.0492	2.51	211.80	6.45	218.64	5.47	1.52	0.11	3:1	0.21
0.0470	1.13	0.0220	27.23	0.0001	7.85	26.150	4.41	0.0470	1.13	220.42	9.46	241.92	10.49	1.84	0.14	3,5:1	0.04
0.0464	3.94	0.0574	16.76	0.0001	16.31	28.938	4.37	0.0464	3.94	201.56	10.63	219.01	9.41	1.57	0.26	5:1	0.09
0.0486	3.44	0.1262	7.45	0.0001	4.36	27.114	1.93	0.0486	3.44	218.36	6.65	233.47	4.42	1.80	0.08	3,5:1	0.37
0.0477	1.69	0.0198	14.41	0.0001	9.49	26.634	2.12	0.0477	1.69	217.66	5.60	237.60	4.95	1.84	0.17	3:1	0.06
0.0483	3.12	0.1117	16.11	0.0001	5.92	26.797	2.48	0.0483	3.12	218.84	8.15	236.18	5.74	1.67	0.10	3,5:1	0.24
0.0488	6.44	0.0110	37.69	0.0001	3.25	31.181	14.91	0.0488	6.44	191.46	28.88	203.50	29.94	1.32	0.04	4:1	0.04
0.0509	5.40	0.1821	4.25	0.0001	3.02	27.738	2.95	0.0509	5.40	223.54	11.10	228.32	6.63	1.55	0.05	3,5:1	0.24
0.0477	3.12	0.0137	8.34	#	#	28.354	2.71	0.0477	3.12	206.95	6.24	223.44	5.96	#	#	3,5:1	#
0.0483	3.64	0.0515	19.65	0.0001	22.90	28.042	4.02	0.0483	3.64	211.71	9.59	225.88	8.93	1.44	0.33	4:1	0.09
0.0654	51.68	0.0549	118.51	0.0013	9.15	56.140	5.01	0.0654	51.68	162.78	80.17	113.82	5.65	25.37	2.32	4:1	0.04
0.0494	8.95	0.0782	31.32	0.0001	10.69	27.328	4.02	0.0494	8.95	222.40	16.96	231.68	9.16	1.50	0.16	3,5:1	0.27
0.0479	4.43	0.1212	32.13	0.0001	8.38	27.617	4.08	0.0479	4.43	215.48	8.19	229.30	9.21	1.59	0.13	4:1	0.24

0.0477	1.27	0.0469	23.83	0.0001	9.15	28.843	3.31	0.0477	1.27	204.50	5.67	219.71	7.16	1.54	0.14	4:1	0.08
0.0468	5.01	0.0140	55.60	0.0001	25.01	29.031	5.88	0.0468	5.01	205.02	13.99	218.31	12.64	1.41	0.35	3,5:1	0.03
0.0475	3.11	0.0074	42.97	0.0001	45.27	30.060	9.49	0.0475	3.11	201.02	19.45	210.96	19.72	1.91	0.87	3,5:1	0.01
0.0532	1.01	0.0274	3.96	0.0002	4.35	18.488	1.92	0.0532	1.01	339.51	5.32	339.57	6.34	3.06	0.13		
0.0536	1.24	0.0298	4.16	0.0002	5.26	18.764	2.06	0.0536	1.24	337.04	5.94	334.71	6.73	3.23	0.17		
0.0529	1.26	0.0303	4.22	0.0002	5.93	18.670	2.70	0.0529	1.26	334.49	7.85	336.36	8.85	3.21	0.19		
0.0544	1.56	0.0300	6.93	0.0002	7.95	19.774	5.96	0.0544	1.56	327.14	15.38	318.04	18.53	3.06	0.24		
0.0525	1.74	0.0279	5.58	0.0002	6.38	18.257	4.47	0.0525	1.74	340.57	9.71	343.77	14.97	3.06	0.20		
0.0517	3.63	0.0277	14.60	0.0002	16.63	17.716	2.06	0.0517	3.63	342.21	13.78	353.97	7.09	3.07	0.51		
0.0573	5.86	0.0341	21.13	0.0002	21.48	19.502	3.58	0.0573	5.86	346.19	21.19	322.36	11.28	3.99	0.86		
0.0524	2.37	0.0254	10.94	0.0001	14.17	18.787	5.07	0.0524	2.37	331.19	16.20	334.31	16.53	2.91	0.41		
0.0508	2.59	0.0285	13.28	0.0001	11.51	17.978	1.67	0.0508	2.59	333.90	10.23	348.96	5.67	2.71	0.31		
0.0625	9.48	0.0235	84.43	0.0003	10.43	41.918	18.28	0.0625	9.48	182.55	27.71	151.98	27.52	6.62	0.69	2:1	0.02
0.0523	1.19	0.0098	16.05	0.0002	13.56	30.736	2.83	0.0523	1.19	215.88	4.40	206.40	5.75	3.17	0.43	2:1	0.01
0.0534	3.17	0.0137	28.01	0.0002	12.48	30.654	3.29	0.0534	3.17	220.97	11.41	206.94	6.70	3.12	0.39	1,5:1	0.03
0.0524	2.66	0.0092	30.92	0.0001	24.38	30.540	3.34	0.0524	2.66	214.94	7.60	207.70	6.84	2.88	0.70	1,5:1	0.01
0.0579	14.96	0.0829	23.62	0.0000	19.93	142.726	5.86	0.0579	14.96	55.85	9.21	45.01	2.63	0.98	0.20	2,5:1	0.07
0.0702	2.41	0.1415	14.83	0.0003	7.43	8.290	6.58	0.0702	2.41	789.02	35.17	734.14	45.80	6.94	0.52	2,5:1	0.26
0.0498	1.51	0.0086	25.64	0.0002	20.29	28.850	2.02	0.0498	1.51	217.70	4.55	219.66	4.35	3.19	0.65	3:1	0.01
0.1559	3.34	0.1009	17.85	0.0009	16.51	3.524	16.98	0.1559	3.34	2006.76	173.72	1610.18	246.53	17.18	2.84	3:1	0.17
0.0547	2.19	0.0195	7.00	0.0002	0.99	38.632	3.33	0.0547	2.19	181.99	6.40	164.74	5.41	4.17	0.04	5:1	0.01
0.0555	2.18	0.0482	13.47	0.0001	9.71	29.188	0.95	0.0555	2.18	236.13	4.83	217.16	2.02	2.92	0.28	5:1	0.03
0.0702	86.16	0.0486	306.94	0.0003	52.78	40.753	15.43	0.0702	86.16	255.13	124.31	156.27	23.86	6.77	3.57	3:1	0.04
0.0552	4.31	0.2157	4.42	0.0001	3.48	28.355	1.44	0.0552	4.31	240.56	10.40	223.43	3.16	2.12	0.07	2,5:1	0.33
0.0695	18.84	0.2855	2.38	0.0001	38.03	143.357	6.96	0.0695	18.84	67.52	29.19	44.81	3.11	2.14	0.81	3:1	0.06
0.0525	8.56	0.0930	18.27	0.0001	14.63	30.578	5.87	0.0525	8.56	216.42	23.19	207.45	11.99	2.28	0.33	3:1	0.11

0.0555	5.90	0.2152	5.64	0.0001	3.91	31.260	3.46	0.0555	5.90	218.71	9.55	202.99	6.91	1.92	0.08	2,5:1	0.40
0.0512	1.65	0.0070	13.93	0.0002	12.56	30.093	6.64	0.0512	1.65	212.94	12.80	210.73	13.79	4.13	0.52	2,5:1	0.01
0.0517	7.61	0.0208	98.82	0.0001	31.14	29.282	8.52	0.0517	7.61	222.30	10.83	216.48	18.17	2.63	0.82	2,5:1	0.01
0.0567	15.75	0.2432	17.74	0.0001	11.92	29.924	4.40	0.0567	15.75	236.66	36.94	211.91	9.17	1.96	0.23	3:1	0.42
0.0646	7.71	0.0379	26.61	0.0003	8.85	35.397	2.73	0.0646	7.71	226.19	16.38	179.59	4.84	5.14	0.45	3:1	0.02
0.0580	19.80	0.1326	48.13	0.0001	17.67	32.521	17.42	0.0580	19.80	214.85	38.10	195.24	33.58	1.92	0.34	3:1	0.22
0.0536	1.67	0.0287	6.14	0.0002	5.44	18.372	1.42	0.0536	1.67	342.80	3.52	341.67	4.73	3.22	0.17		
0.0528	1.29	0.0294	5.21	0.0002	4.17	18.709	1.41	0.0528	1.29	333.57	2.31	335.67	4.62	3.07	0.13		
0.0532	1.41	0.0285	5.65	0.0002	5.13	18.813	1.54	0.0532	1.41	334.94	2.59	333.86	5.01	3.16	0.16		
0.0533	1.49	0.0291	6.19	0.0002	5.72	18.785	1.67	0.0533	1.49	334.31	3.89	334.34	5.46	3.11	0.18		
0.0531	1.37	0.0293	5.79	0.0002	5.09	18.679	1.66	0.0531	1.37	337.19	3.02	336.20	5.43	3.12	0.16		
0.0532	1.52	0.0297	6.11	0.0002	5.20	18.639	1.62	0.0532	1.52	335.65	3.43	336.90	5.33	3.14	0.16		
0.0531	1.31	0.0279	5.35	0.0002	4.26	18.570	1.55	0.0531	1.31	336.98	2.77	338.11	5.10	3.06	0.13		
0.0533	1.34	0.0284	5.92	0.0002	5.07	18.613	1.70	0.0533	1.34	338.25	3.80	337.36	5.60	3.17	0.16		
0.0535	1.42	0.0294	7.94	0.0002	5.79	18.486	1.57	0.0535	1.42	341.01	4.98	339.61	5.20	3.31	0.19		
0.0531	1.08	0.0287	5.73	0.0002	3.47	18.683	1.49	0.0531	1.08	335.50	2.99	336.13	4.88	3.06	0.11		
0.0527	1.02	0.0305	4.54	0.0002	2.82	18.537	1.36	0.0527	1.02	335.91	2.96	338.70	4.50	3.06	0.09		
0.0537	1.18	0.0281	4.63	0.0002	3.83	18.788	1.54	0.0537	1.18	337.02	3.25	334.29	5.01	3.25	0.12		
0.0524	7.27	0.1767	10.55	0.0001	7.44	28.311	2.76	0.0524	7.27	231.40	17.79	223.77	6.08	2.06	0.15	2:1	0.28
0.0503	3.62	0.0123	33.87	0.0003	24.26	29.987	13.37	0.0503	3.62	216.51	28.22	211.47	27.88	6.21	1.51	2:1	0.01
0.0484	1.99	0.0062	34.84	0.0001	27.84	27.897	2.82	0.0484	1.99	217.84	5.86	227.04	6.30	2.33	0.65	1,5:1	0.01
0.0491	3.22	0.0875	78.73	0.0001	5.89	29.047	5.16	0.0491	3.22	213.35	10.20	218.20	11.08	1.75	0.10	1,5:1	0.33
0.0603	12.17	0.4683	17.04	0.0001	9.11	20.034	9.53	0.0603	12.17	351.87	45.38	313.99	29.28	2.77	0.25	2:1	0.76
0.0482	1.08	0.0033	35.62	0.0001	21.07	28.296	3.17	0.0482	1.08	215.21	6.16	223.89	6.99	2.86	0.60	2:1	0.00
0.0532	6.05	0.0169	38.37	0.0002	10.31	31.377	9.36	0.0532	6.05	211.86	20.18	202.24	18.67	3.82	0.39	1,5:1	0.02
0.0478	1.84	0.0053	16.51	0.0001	12.77	29.999	5.42	0.0478	1.84	201.56	9.03	211.39	11.27	1.48	0.19	1,5:1	0.01

0.0521	7.73	0.0248	19.47	#	#	123.138	2.83	0.0521	7.73	58.31	4.61	52.14	1.47	#	#	1:1	0.01
0.0549	12.37	0.1187	30.76	0.0001	19.38	28.508	10.36	0.0549	12.37	240.08	23.67	222.25	22.67	2.15	0.42	1:1	0.16
0.0542	9.23	0.2391	27.90	0.0001	9.57	27.113	6.85	0.0542	9.23	252.04	26.45	233.49	15.73	2.05	0.20	1,5:1	0.32
0.0527	9.50	0.0179	67.78	0.0001	30.54	31.521	5.89	0.0527	9.50	204.78	19.63	201.34	11.69	2.52	0.77	1,5:1	0.02
0.0508	2.70	0.1551	3.46	0.0001	3.00	27.907	2.12	0.0508	2.70	226.80	6.46	226.95	4.73	1.89	0.06	1,5:1	0.30
0.0468	35.66	0.0476	74.40	0.0000	81.50	133.496	4.81	0.0468	35.66	50.15	20.20	48.11	2.30	0.43	0.35	2:1	0.09
0.0516	15.57	0.1231	10.86	0.0001	16.97	28.124	6.31	0.0516	15.57	218.80	25.63	225.24	13.98	1.78	0.30	2:1	0.26
0.0505	4.00	0.0089	43.25	0.0001	4.12	29.457	5.10	0.0505	4.00	212.43	14.59	215.21	10.80	2.15	0.09	2:1	0.01
0.0496	1.04	0.0156	20.24	0.0001	9.84	27.913	1.57	0.0496	1.04	222.72	3.74	226.91	3.51	2.70	0.27	2:1	0.04
0.0486	1.86	0.0255	10.86	#	#	27.952	2.00	0.0486	1.86	217.45	5.43	226.60	4.45	#	#	2,5:1	0.02
0.0555	17.70	0.3079	17.73	0.0001	10.92	27.048	9.54	0.0555	17.70	252.46	40.21	234.04	21.96	1.98	0.22	2,5:1	0.60
0.0677	0.54	0.0030	14.48	0.0003	8.47	8.684	3.37	0.0677	0.54	749.27	18.60	702.61	22.46	5.97	0.51	2,5:1	0.01
0.0573	5.91	0.0429	16.26	0.0000	15.15	102.623	7.51	0.0573	5.91	84.54	8.45	62.51	4.67	0.87	0.13	2,5:1	0.06
0.0567	3.36	0.1429	11.68	0.0002	8.67	13.286	6.50	0.0567	3.36	465.89	29.98	467.80	29.39	3.96	0.34	2:1	0.34
0.0664	7.05	0.0368	7.32	0.0001	12.97	33.602	#	0.0664	7.05	248.60	#	189.05	#	2.34	0.30		
0.0518	1.11	0.0262	7.35	0.0001	3.68	18.858	2.04	0.0518	1.11	325.93	6.94	333.08	6.62	2.88	0.11		
0.0532	2.91	0.0295	10.54	0.0002	5.01	18.800	1.94	0.0532	2.91	337.17	9.86	334.08	6.31	3.05	0.15		
0.0550	1.73	0.0323	7.13	0.0002	6.46	18.036	0.92	0.0550	1.73	353.47	5.17	347.85	3.11	3.65	0.24		
0.0534	1.36	0.0277	6.91	0.0001	4.63	19.452	1.44	0.0534	1.36	326.25	4.38	323.17	4.56	2.98	0.14		
0.0528	1.39	0.0283	6.68	0.0002	5.16	18.643	1.79	0.0528	1.39	334.81	5.48	336.83	5.86	3.08	0.16		
0.0527	1.42	0.0291	7.58	0.0002	4.40	18.151	1.80	0.0527	1.42	340.96	4.78	345.71	6.08	3.11	0.14		
0.0539	1.61	0.0334	10.54	0.0002	5.55	19.197	1.94	0.0539	1.61	331.70	7.26	327.34	6.20	3.14	0.17		
0.0540	2.01	0.0272	7.39	0.0002	5.94	18.815	3.24	0.0540	2.01	338.51	7.65	333.83	10.56	3.21	0.19		
0.0526	1.42	0.0275	7.71	0.0002	6.30	18.145	3.24	0.0526	1.42	341.75	10.84	345.83	10.92	3.25	0.20		
0.0512	2.14	0.0278	8.80	0.0002	7.37	17.194	2.14	0.0512	2.14	350.44	6.42	364.43	7.58	3.18	0.23		
0.0529	2.13	0.0288	8.78	0.0002	7.71	18.327	4.54	0.0529	2.13	341.24	11.58	342.48	15.15	3.18	0.25		

0.0550	2.43	0.0301	9.22	0.0002	7.06	20.428	1.94	0.0550	2.43	320.45	5.56	308.09	5.83	3.03	0.21		
0.0513	9.89	0.1100	10.46	0.0001	27.58	30.005	23.78	0.0513	9.89	218.64	58.73	211.34	49.64	1.87	0.52	3:1	0.25
0.0595	8.09	0.0225	41.82	0.0002	41.14	23.138	17.33	0.0595	8.09	307.67	48.82	272.76	46.45	3.42	1.41	3:1	0.03
0.0527	5.52	0.1693	69.57	0.0001	16.43	35.732	17.87	0.0527	5.52	189.70	34.95	177.93	31.44	1.65	0.27	3:1	0.24
0.0557	7.35	0.0355	24.84	0.0001	13.85	26.293	29.17	0.0557	7.35	269.20	63.16	240.63	69.27	2.06	0.29	2,5:1	0.12
0.0562	2.02	0.1239	5.50	0.0001	8.96	24.096	8.86	0.0562	2.02	285.62	22.53	262.12	22.81	2.16	0.19	3:1	0.29
0.0551	7.31	0.1207	28.25	0.0001	32.27	25.846	39.37	0.0551	7.31	257.57	111.40	244.72	95.24	2.10	0.68	3:1	0.26
0.2010	2.12	0.1196	3.90	0.0008	23.20	2.838	15.27	0.2010	2.12	2424.73	161.15	1945.64	261.75	16.44	3.81	1,5:1	0.34
0.1956	1.57	0.2274	3.95	0.0010	7.00	2.153	6.50	0.1956	1.57	2647.79	67.77	2458.99	134.30	21.00	1.47	1,5:1	0.61
0.0585	6.18	0.2212	33.58	0.0002	8.61	24.372	31.79	0.0585	6.18	299.82	95.64	259.22	81.29	4.10	0.35	2:1	0.23
0.0626	11.45	0.0839	17.66	0.0001	47.77	19.667	43.77	0.0626	11.45	385.93	117.18	319.71	137.98	2.65	1.27	3:1	0.19
0.0515	6.38	0.1345	10.13	0.0000	9.23	119.501	4.90	0.0515	6.38	58.89	5.53	53.72	2.62	0.48	0.04	3:1	0.24
0.0603	14.32	0.2076	28.75	0.0002	16.92	34.582	14.17	0.0603	14.32	228.09	39.94	183.77	25.73	3.20	0.54	2:1	0.26
0.4691	197.56	0.9335	178.56	0.0002	222.21	86.279	60.27	0.4691	197.56	554.51	2258.90	74.29	44.67	4.26	9.46	3:1	0.30
0.0523	9.62	0.0200	2.33	#	#	36.736	52.44	0.0523	9.62	182.03	86.33	173.13	90.21	#	#	2,5:1	0.05
0.1036	0.81	0.0757	4.61	0.0006	3.33	4.059	2.50	0.1036	0.81	1530.84	21.17	1419.66	31.93	12.90	0.43	2:1	0.16
0.0515	2.31	0.1576	6.24	0.0001	4.47	31.896	3.33	0.0515	2.31	204.09	7.68	199.00	6.52	1.73	0.08	1,5:1	0.32
0.1350	26.57	0.2601	31.69	0.0001	31.83	194.176	11.99	0.1350	26.57	117.38	29.53	33.11	3.96	2.39	0.76	1,5:1	0.13
0.1918	29.24	0.3936	23.51	0.0001	32.22	151.707	23.27	0.1918	29.24	209.37	69.26	42.35	9.83	1.07	0.34	3:1	0.35
0.0623	27.84	0.0141	2667.16	#	#	108.283	26.15	0.0623	27.84	75.06	30.43	59.26	15.44	#	#	3:1	0.08
0.0554	16.43	0.2057	22.90	0.0000	20.99	169.711	20.08	0.0554	16.43	45.58	12.81	37.87	7.59	0.39	0.08	3:1	0.31
0.0822	139.53	0.2663	84.87	0.0000	115.45	160.414	35.89	0.0822	139.53	70.58	130.46	40.06	14.35	0.39	0.45	4:1	0.45
0.0599	16.50	0.2193	8.71	0.0000	46.06	153.627	10.53	0.0599	16.50	51.69	15.68	41.83	4.39	0.27	0.12	4:1	0.39

File name	std.	start	end	204Pb	206Pb	207Pb	208Pb	232Th	238U	206Pb/204Pb	2RSE (%)	207Pb/235U	2RSE (%)	206Pb/238U	2RSE (%)	Rho
130201_0198_1240_Dobragneis_010	*	50	95	1.1E-06	1.7E-03	7.8E-05	2.5E-03	3.0E-01	5.9E-02	#	#	0.4079	8.42	0.0536	16.08	0.96
130201_0198_1240_Dobragneis_011	*	49	97	#	2.0E-03	9.0E-05	2.6E-03	2.9E-01	6.9E-02	#	#	0.4015	8.47	0.0548	12.13	0.72
130201_0198_1240_Dobragneis_012	*	50	98	#	1.9E-03	8.6E-05	2.5E-03	2.8E-01	6.6E-02	#	#	0.3954	7.21	0.0552	7.77	0.54
130201_0198_1240_Dobragneis_013	*	48	99	1.1E-06	1.0E-03	4.9E-05	3.6E-03	4.2E-01	3.7E-02	#	#	0.3880	8.72	0.0530	12.11	0.69
130201_0198_1240_Dobragneis_014	*	50	99	1.3E-06	1.2E-03	5.7E-05	4.3E-03	5.1E-01	4.4E-02	#	#	0.3825	10.87	0.0540	8.67	0.40
130201_0198_1240_Dobragneis_015	*	54	95	3.3E-07	3.3E-03	1.7E-04	4.6E-03	5.0E-01	1.2E-01	9079	142	0.4211	10.11	0.0552	11.94	0.59
130201_0198_1240_Dobragneis_016	*	46	92	#	3.4E-03	1.8E-04	5.4E-03	5.9E-01	1.3E-01	#	#	0.3831	19.36	0.0515	21.02	0.54
130201_0198_1240_Dobragneis_018	*	50	90	6.9E-07	1.5E-02	7.9E-04	4.7E-04	5.1E-02	5.7E-01	30133	106	0.4047	8.30	0.0564	6.64	0.40
130201_0198_1240_Dobragneis_019	*	57	110	6.8E-07	2.9E-03	1.6E-04	6.4E-03	6.5E-01	1.2E-01	7826	110	0.3966	17.84	0.0529	#	#
130201_0198_1240_Dobragneis_020	*	53	98	2.7E-07	2.4E-03	1.3E-04	5.6E-03	5.8E-01	1.0E-01	7358	152	0.3981	11.81	0.0542	16.85	0.71
130201_0198_1240_Dobragneis_021	*	58	122	3.6E-07	2.9E-03	1.6E-04	7.9E-03	8.2E-01	1.2E-01	18859	86	0.3961	13.72	0.0549	14.85	0.54
130201_0283_01_01_II_D01_1		43	102	7.2E-07	2.4E-04	1.6E-05	1.9E-03	1.5E+00	6.5E-02	357	34	0.0763	24.79	0.0079	37.82	0.76
130201_0283_01_01_II_D01_2		44	93	6.4E-07	7.2E-04	4.2E-05	3.1E-03	2.1E+00	1.2E-01	1023	243	0.0796	125.64	0.0095	144.68	0.58
130201_0283_01_01_II_E01_1		51	130	7.1E-07	5.2E-03	2.6E-04	8.2E-03	1.4E+00	3.4E-01	8807	28	0.2526	14.39	0.0365	14.50	0.50
130201_0283_01_01_II_E01_2		41	104	8.1E-06	6.2E-03	3.8E-04	8.2E-03	1.2E+00	3.9E-01	1042	76	0.2748	11.63	0.0321	14.27	0.61
130201_0283_01_01_II_E03_1		50	92	8.0E-07	5.5E-03	2.8E-04	8.5E-03	1.5E+00	3.7E-01	6701	49	0.2208	23.82	0.0320	21.85	0.46
130201_0283_01_01_II_E03_2		44	78	8.3E-07	2.7E-03	1.4E-04	3.8E-03	1.3E+00	3.4E-01	3640	110	0.1081	129.72	0.0155	136.47	0.53
130201_0283_01_01_II_E04_1		45	67	1.2E-06	5.7E-04	2.7E-05	1.6E-03	9.7E-01	7.0E-02	432	115	0.1136	84.82	0.0152	71.04	0.42
130201_0283_01_01_II_E04_2		30	58	1.3E-06	1.8E-03	8.6E-05	4.4E-03	3.1E+00	2.6E-01	2571	139	0.1511	169.24	0.0220	176.40	0.52
130201_0283_01_01_II_E04_3		39	96	#	7.6E-04	3.6E-05	1.5E-03	8.6E-01	7.9E-02	#	#	0.1369	33.52	0.0199	35.05	0.52
130521_0198_1240_020	*	49	247	1.8E-06	1.0E-02	2.8E-04	5.5E-03	1.2E+00	2.1E-01	7679	7	0.4103	1.33	0.0557	1.13	0.43
130521_0198_1240_021	*	58	200	#	4.0E-03	1.1E-04	2.1E-03	5.1E-01	8.8E-02	#	#	0.3872	2.34	0.0527	2.45	0.52
130521_0198_1240_022	*	59	200	1.4E-06	2.3E-03	6.2E-05	1.9E-03	4.7E-01	5.0E-02	1808	4	0.3906	2.78	0.0535	2.83	0.51
130521_0198_1240_023	*	59	200	2.4E-06	2.1E-03	5.9E-05	1.9E-03	4.7E-01	4.6E-02	826	9	0.4113	3.87	0.0558	2.56	0.33
130521_0198_1240_025	*	61	142	1.4E-06	3.3E-03	9.1E-05	1.2E-03	3.1E-01	7.4E-02	-15	-4205	0.3893	2.47	0.0532	3.14	0.64

130521_0283_01_01_IV_01_1		52	96	1.1E-06	4.5E-05	1.4E-06	2.0E-04	4.9E-01	9.7E-03	41	5	0.0471	21.45	0.0058	7.93	0.18
130521_0283_01_01_IV_01_2		60	106	1.1E-06	6.0E-05	2.1E-06	2.5E-04	6.2E-01	1.3E-02	68	7	0.0594	63.57	0.0059	6.08	0.05
130521_0283_01_01_IV_02_1		59	117	1.5E-06	5.2E-05	3.1E-06	1.9E-04	4.7E-01	1.0E-02	#	#	0.1014	72.07	0.0064	9.36	0.06
130521_0283_01_01_IV_02_2		54	112	1.5E-06	8.5E-05	2.6E-06	9.1E-04	2.2E+00	1.6E-02	#	#	0.0543	23.00	0.0066	5.49	0.12
130521_0283_01_01_IV_03_1		55	88	1.2E-06	5.0E-05	1.8E-06	2.1E-04	5.1E-01	1.1E-02	32	82	0.0543	70.85	0.0061	10.16	0.07
130521_0283_01_01_IV_03_2		54	99	#	8.3E-05	2.7E-06	2.6E-04	6.8E-01	1.7E-02	#	#	0.0573	39.86	0.0063	8.24	0.10
130521_0198_1240_007	*	50	110	1.3E-06	5.2E-03	1.4E-04	2.7E-03	7.1E-01	1.1E-01	#	#	0.3957	5.41	0.0541	6.19	0.57
130521_0198_1240_008	*	50	110	1.7E-06	5.7E-03	1.5E-04	3.0E-03	7.6E-01	1.2E-01	3657	37	0.4008	4.01	0.0542	5.67	0.71
130521_0198_1240_009	*	50	110	4.7E-06	5.1E-03	1.4E-04	2.8E-03	7.2E-01	1.1E-01	-111	-602	0.3967	5.05	0.0541	5.17	0.51
130521_0198_1240_010	*	50	110	1.4E-06	3.3E-03	8.9E-05	1.7E-03	4.3E-01	7.1E-02	2719	11	0.4007	5.40	0.0542	6.08	0.56
130521_0198_1240_011	*	50	110	1.7E-06	4.3E-03	1.1E-04	2.2E-03	5.6E-01	9.1E-02	3115	8	0.3973	5.88	0.0544	5.33	0.45
130521_0198_1240_012	*	50	110	2.1E-06	3.3E-03	8.7E-05	2.1E-03	5.4E-01	6.9E-02	2989	17	0.3951	7.34	0.0541	6.20	0.42
130521_0198_1240_013	*	50	108	1.3E-06	3.5E-03	9.3E-05	2.0E-03	5.2E-01	7.4E-02	3166	14	0.3962	8.61	0.0542	6.68	0.39
130521_0198_1240_014	*	50	110	1.3E-06	3.5E-03	9.5E-05	2.0E-03	5.0E-01	7.5E-02	#	#	0.3980	8.86	0.0541	7.45	0.42
130521_0198_1240_015	*	50	99	1.4E-06	2.7E-03	7.3E-05	1.4E-03	3.6E-01	5.7E-02	-1382	-99	0.3993	8.32	0.0538	8.91	0.54
130521_0198_1240_016	*	50	93	1.3E-06	2.1E-03	5.7E-05	1.3E-03	3.3E-01	4.5E-02	#	#	0.3972	6.02	0.0544	9.65	0.80
130521_0198_1240_017	*	52	93	2.3E-06	2.0E-03	5.5E-05	1.2E-03	2.9E-01	4.3E-02	699	75	0.3985	6.01	0.0542	10.98	0.91
130521_0198_1240_019	*	55	102	1.4E-06	2.0E-03	5.4E-05	4.6E-03	1.1E+00	4.2E-02	#	#	0.3974	10.87	0.0540	13.23	0.61
130521_0284_01_01_II_A02_1		50	140	2.2E-06	4.2E-04	1.5E-05	1.6E-03	2.8E+00	5.2E-02	183	11	0.0919	17.53	0.0095	6.21	0.18
130521_0284_01_01_II_A02_2		50	142	2.2E-06	3.8E-04	1.2E-05	1.8E-03	3.2E+00	4.9E-02	179	22	0.0726	14.46	0.0084	8.94	0.31
130521_0284_01_01_II_A06		50	190	1.4E-06	3.0E-04	1.0E-05	1.5E-03	2.9E+00	4.2E-02	257	3	0.0786	8.96	0.0080	4.26	0.24
130521_0284_01_01_II_A07		50	217	1.6E-06	2.8E-04	8.8E-06	1.5E-03	2.7E+00	3.9E-02	204	1	0.0718	8.09	0.0080	3.01	0.19
130521_0284_01_01_II_A08_1		44	172	1.9E-06	3.0E-04	1.0E-05	1.4E-03	2.7E+00	4.1E-02	206	9	0.0735	13.58	0.0079	5.29	0.19
130521_0284_01_01_II_A08_2		50	145	2.2E-06	2.8E-04	9.1E-06	1.5E-03	2.8E+00	4.0E-02	171	3	0.0693	11.02	0.0079	5.58	0.25
130521_0284_01_01_II_A10		50	175	2.4E-06	3.2E-04	1.0E-05	1.7E-03	3.0E+00	4.5E-02	203	2	0.0715	9.76	0.0080	3.69	0.19
130521_0284_01_01_II_B03		50	190	2.9E-06	6.6E-04	1.7E-05	3.5E-05	8.7E-03	2.2E-02	274	6	0.2431	4.94	0.0344	1.99	0.20

130521_0284_01_01_II_B04		50	128	1.5E-06	4.2E-04	1.2E-05	1.0E-03	2.1E+00	6.9E-02	391	9	0.0530	9.96	0.0068	8.44	0.42
130521_0284_01_01_II_B09		50	192	1.8E-06	2.6E-04	8.4E-06	1.5E-03	2.8E+00	3.7E-02	121	4	0.0679	8.54	0.0078	3.32	0.19
130521_0284_01_01_II_B10		50	133	1.5E-06	2.9E-04	9.0E-06	1.4E-03	2.6E+00	4.0E-02	217	3	0.0658	12.96	0.0080	7.23	0.28
130521_0284_01_01_II_C01		50	173	1.6E-06	2.9E-04	9.5E-06	1.4E-03	2.5E+00	4.1E-02	164	2	0.0711	8.32	0.0081	3.58	0.22
130521_0284_01_01_II_C05		50	110	3.0E-06	1.4E-03	3.8E-05	1.8E-03	2.4E+00	9.0E-02	1986	51	0.1617	51.29	0.0223	55.80	0.54
130521_0284_01_01_II_C07		50	170	4.1E-06	9.0E-03	2.5E-04	6.2E-03	2.5E+00	3.1E-01	3079	38	0.2737	9.48	0.0352	5.62	0.30
130521_0284_01_01_II_D03_1		50	132	1.6E-06	3.8E-04	1.2E-05	1.3E-03	2.3E+00	5.3E-02	314	12	0.0718	14.64	0.0081	8.15	0.28
130521_0284_01_01_II_D03_2		50	170	2.7E-06	2.8E-04	9.1E-06	1.4E-03	2.6E+00	3.8E-02	186	6	0.0701	7.95	0.0081	5.23	0.33
130521_0284_01_01_II_D03_3		50	168	2.7E-06	4.1E-04	1.3E-05	1.1E-03	2.3E+00	6.7E-02	352	6	0.0546	15.75	0.0067	4.13	0.13
130521_0284_01_01_II_D05		50	163	3.0E-06	2.9E-04	9.3E-06	1.4E-03	2.6E+00	4.4E-02	190	6	0.0659	7.38	0.0081	3.98	0.27
130521_0284_01_01_II_D06_1		50	148	1.4E-06	5.5E-04	1.5E-05	1.4E-03	2.7E+00	8.5E-02	360	2	0.0608	5.74	0.0075	2.69	0.23
130521_0284_01_01_II_D06_2		50	143	1.5E-06	3.4E-04	1.0E-05	1.2E-03	2.4E+00	5.5E-02	#	#	0.0638	9.01	0.0077	6.44	0.36
130521_0284_01_01_II_D07		50	165	1.8E-06	3.1E-04	1.0E-05	1.5E-03	2.7E+00	4.5E-02	210	7	0.0658	9.21	0.0077	4.35	0.24
130521_0284_01_01_II_D09		50	163	1.4E-06	4.1E-04	1.3E-05	1.4E-03	2.6E+00	6.1E-02	304	6	0.0641	5.91	0.0076	3.54	0.30
130521_0284_01_01_II_E02		50	160	1.5E-06	2.9E-04	9.5E-06	1.3E-03	2.4E+00	4.1E-02	200	3	0.0694	7.65	0.0078	4.32	0.28
130521_0284_01_01_II_E03_1		50	105	1.4E-06	3.3E-04	1.0E-05	1.3E-03	2.4E+00	4.8E-02	255	6	0.0653	14.59	0.0077	16.75	0.57
130521_0284_01_01_II_E03_2		50	102	1.6E-06	4.6E-04	1.4E-05	1.2E-03	2.5E+00	8.0E-02	1010	29	0.0566	17.14	0.0070	13.59	0.40
130521_0284_01_01_II_E06		51	289	1.4E-06	2.4E-04	7.9E-06	1.3E-03	2.4E+00	3.5E-02	218	2	0.0679	4.77	0.0077	1.76	0.18
130521_0284_01_01_II_E07_1		40	155	2.4E-06	2.4E-04	1.2E-05	1.2E-03	2.3E+00	3.4E-02	156	8	0.1044	20.45	0.0080	4.30	0.11
130521_0284_01_01_II_E07_2		54	178	7.2E-06	2.8E-04	7.7E-06	1.4E-03	2.7E+00	4.3E-02	-633	-4	0.0554	12.62	0.0074	2.86	0.11
130521_0284_01_01_II_E08		50	193	#	3.3E-04	1.0E-05	1.4E-03	2.5E+00	5.0E-02	#	#	0.0634	4.73	0.0074	2.93	0.31
130521_0284_01_01_II_E09_1		58	195	1.9E-06	3.3E-04	1.5E-05	1.2E-03	2.2E+00	4.9E-02	191	10	0.0883	19.44	0.0076	3.25	0.08
130521_0284_01_01_II_E09_2		50	196	1.2E-06	3.4E-04	1.1E-05	1.4E-03	2.5E+00	5.2E-02	301	3	0.0638	4.99	0.0073	1.99	0.20

207Pb 206Pb	2RSE (%)	208Pb 206Pb	2RSE (%)	208Pb 232Th	2RSE (%)	238U 206Pb	2RSE (%)	207Pb 206Pb	2RSE (%)	Age 235U	Error 235U	Age 238U	Error 238U	Age 232Th	Error 232Th	L-W-ratio	232Th 238U
0.0550	7.31	0.0661	9.71	0.0163	29.95	18.640	16.08	0.0550	7.31	347.33	25.06	336.87	53.00	326.93	97.35		
0.0527	2.53	0.0624	19.94	0.0178	5.09	18.249	12.13	0.0527	2.53	342.76	24.93	343.90	40.75	355.77	17.95		
0.0521	2.33	0.0642	17.50	0.0175	6.19	18.117	7.77	0.0521	2.33	338.31	20.95	346.35	26.25	350.92	21.54		
0.0534	6.37	0.1879	20.69	0.0166	7.07	18.874	12.11	0.0534	6.37	332.92	25.06	332.81	39.40	331.96	23.29		
0.0518	3.62	0.2054	21.19	0.0165	5.07	18.504	8.67	0.0518	3.62	328.85	31.01	339.29	28.70	331.43	16.68		
0.0554	4.17	0.0907	12.09	0.0174	12.34	18.129	11.94	0.0554	4.17	356.87	30.90	346.13	40.37	349.61	42.80		
0.0537	1.39	0.1023	9.32	0.0167	11.61	19.406	21.02	0.0537	1.39	329.32	55.96	323.91	66.73	333.79	38.48		
0.0520	2.52	0.0019	7.50	0.0169	14.51	17.715	6.64	0.0520	2.52	345.05	24.58	353.99	22.92	338.17	48.71		
0.0537	3.91	0.1023	8.10	0.0172	7.16	18.918	#	0.0537	3.91	339.20	52.79	332.06	#	344.16	24.45		
0.0534	4.78	0.1027	12.82	0.0169	13.15	18.449	16.85	0.0534	4.78	340.29	34.73	340.27	56.09	339.54	44.33		
0.0529	2.03	0.1120	9.19	0.0168	7.77	18.225	14.85	0.0529	2.03	338.79	40.31	344.35	49.97	337.69	26.05		
0.0680	12.69	0.4405	26.14	0.0021	12.80	126.673	37.82	0.0680	12.69	74.68	18.01	50.69	19.12	42.50	5.44	1:1	23.46
0.0612	13.75	0.3021	72.40	0.0020	132.15	105.545	144.68	0.0612	13.75	77.76	98.69	60.79	88.14	39.59	52.34	1:1	17.75
0.0502	0.87	0.1005	7.74	0.0134	23.77	27.398	14.50	0.0502	0.87	228.69	29.90	231.09	33.00	268.08	63.40	1,5:1	4.04
0.0608	9.92	0.0781	5.69	0.0114	11.28	31.132	14.27	0.0608	9.92	246.49	25.78	203.81	28.69	229.10	25.71	1,5:1	3.21
0.0507	2.92	0.0849	19.69	0.0101	23.72	31.291	21.85	0.0507	2.92	202.61	44.73	202.79	43.76	202.67	47.89	1:1	4.04
0.0511	11.63	0.0800	30.11	0.0047	167.12	64.382	136.47	0.0511	11.63	104.26	137.43	99.36	135.98	95.36	159.63	1:1	3.70
0.0540	47.53	0.1590	219.49	0.0030	65.38	65.628	71.04	0.0540	47.53	109.28	91.92	97.49	69.11	61.19	39.98	1:1	13.98
0.0501	11.13	0.0556	1091.50	0.0037	112.47	45.486	176.40	0.0501	11.13	142.89	255.10	140.19	249.39	74.90	84.26	1:1	12.03
0.0498	4.30	0.1142	81.30	0.0036	31.25	50.144	35.05	0.0498	4.30	130.31	41.84	127.29	44.33	71.80	22.41	1:1	10.90
0.0535	0.41	1.2598	1.12	0.0176	1.43	17.957	1.13	0.0535	0.41	349.10	3.94	349.36	3.85	352.86	5.01		
0.0532	0.92	0.7728	1.44	0.0163	2.79	18.970	2.45	0.0532	0.92	332.34	6.66	331.17	7.93	326.73	9.03		
0.0529	1.22	1.0223	4.42	0.0167	2.74	18.700	2.83	0.0529	1.22	334.80	7.97	335.83	9.26	335.50	9.11		
0.0536	2.76	1.0754	1.96	0.0176	2.90	17.935	2.56	0.0536	2.76	349.80	11.51	349.76	8.71	353.02	10.16		
0.0530	1.42	0.8992	2.66	0.0166	4.96	18.809	3.14	0.0530	1.42	333.84	7.05	333.92	10.24	332.01	16.34		

0.0599	20.70	4.2518	11.38	0.0017	10.78	171.978	7.93	0.0599	20.70	46.77	9.85	37.38	2.96	35.07	3.78	1,5:1	50.07
0.0720	62.49	3.6739	17.85	0.0018	13.35	168.627	6.08	0.0720	62.49	58.58	36.84	38.12	2.31	35.55	4.74	1,5:1	48.47
0.1107	65.13	3.1613	9.28	0.0018	4.88	155.424	9.36	0.1107	65.13	98.06	69.70	41.34	3.86	36.67	1.79	1,5:1	45.72
0.0597	24.56	9.0151	11.18	0.0019	#	151.775	5.49	0.0597	24.56	53.65	12.09	42.33	2.32	37.41	#	1,5:1	132.89
0.0655	63.38	3.6673	22.47	0.0018	24.72	163.704	10.16	0.0655	63.38	53.69	37.75	39.26	3.98	36.98	9.13	1:1	47.89
0.0655	41.88	3.2134	18.22	0.0018	#	157.615	8.24	0.0655	41.88	56.55	22.17	40.77	3.35	35.36	#	1:1	40.42
0.0532	2.21	0.8658	16.72	0.0165	11.03	18.490	6.19	0.0532	2.21	338.49	15.69	339.55	20.49	329.82	36.11		
0.0535	2.08	0.8715	23.67	0.0171	7.90	18.447	5.67	0.0535	2.08	342.24	11.72	340.31	18.82	342.31	26.83		
0.0532	1.99	1.0086	20.88	0.0172	6.65	18.482	5.17	0.0532	1.99	339.22	14.67	339.68	17.11	344.01	22.70		
0.0532	1.94	1.2181	4.34	0.0171	8.57	18.443	6.08	0.0532	1.94	342.13	15.82	340.39	20.19	342.15	29.11		
0.0530	1.53	1.2422	9.41	0.0172	8.91	18.392	5.33	0.0530	1.53	339.69	17.11	341.30	17.74	344.78	30.48		
0.0532	2.35	1.5291	30.09	0.0173	8.00	18.472	6.20	0.0532	2.35	338.10	21.34	339.87	20.55	346.62	27.52		
0.0531	2.28	1.0352	19.58	0.0167	9.38	18.445	6.68	0.0531	2.28	338.89	25.10	340.35	22.18	334.49	31.13		
0.0534	2.04	0.9873	29.25	0.0170	7.19	18.494	7.45	0.0534	2.04	340.16	25.94	339.46	24.70	341.13	24.34		
0.0538	4.32	0.8195	3.22	0.0168	15.31	18.571	8.91	0.0538	4.32	341.14	24.39	338.10	29.41	337.63	51.33		
0.0527	4.48	0.5248	13.81	0.0161	#	18.386	9.65	0.0527	4.48	339.61	17.52	341.41	32.16	322.15	#		
0.0533	7.38	0.4681	7.95	0.0165	#	18.447	10.98	0.0533	7.38	340.57	17.55	340.31	36.52	330.64	#		
0.0535	6.03	1.7699	7.82	0.0182	12.36	18.506	13.23	0.0535	6.03	339.75	31.89	339.26	43.88	364.24	44.65		
0.0690	11.11	7.2164	6.09	0.0024	6.65	105.297	6.21	0.0690	11.11	89.28	15.10	60.93	3.77	49.27	3.27	1,5:1	54.47
0.0629	8.53	9.5686	4.31	0.0024	7.15	119.230	8.94	0.0629	8.53	71.21	9.99	53.84	4.80	47.63	3.40	1,5:1	66.23
0.0692	6.39	10.6080	2.28	0.0023	3.41	125.736	4.26	0.0692	6.39	76.82	6.65	51.07	2.17	46.19	1.57	1:1	68.45
0.0646	6.39	11.6160	2.11	0.0023	2.21	124.775	3.01	0.0646	6.39	70.42	5.52	51.46	1.54	46.77	1.03	1:1	70.10
0.0650	8.47	11.3311	3.57	0.0023	4.46	125.787	5.29	0.0650	8.47	72.05	9.49	51.05	2.69	45.61	2.03	1,5:1	65.59
0.0655	14.54	12.4520	2.69	0.0023	4.98	126.774	5.58	0.0655	14.54	68.08	7.29	50.65	2.81	46.32	2.31	1,5:1	70.05
0.0637	6.36	12.3647	2.26	0.0024	3.54	124.793	3.69	0.0637	6.36	70.16	6.64	51.45	1.89	47.65	1.69	2:1	68.05
0.0513	4.38	0.1029	24.93	0.0163	25.83	29.073	1.99	0.0513	4.38	220.94	9.86	218.01	4.26	327.77	84.17	1:1	0.39

0.0559	6.98	5.6518	5.32	0.0020	12.04	147.180	8.44	0.0559	6.98	52.46	5.11	43.65	3.67	40.87	4.92	1:1	30.05
0.0631	7.44	14.2988	2.03	0.0023	3.22	127.937	3.32	0.0631	7.44	66.73	5.53	50.19	1.66	46.10	1.48	2,5:1	74.10
0.0600	7.39	11.3184	2.30	0.0023	7.40	124.931	7.23	0.0600	7.39	64.69	8.15	51.39	3.70	45.81	3.39	1,5:1	63.58
0.0637	6.08	11.8819	4.89	0.0024	3.90	123.594	3.58	0.0637	6.08	69.73	5.62	51.95	1.85	47.93	1.87	1:1	61.60
0.0510	22.80	1.3994	382.28	0.0039	40.61	44.922	55.80	0.0510	22.80	152.15	75.19	141.93	78.80	79.60	32.29	1:1	27.06
0.0545	5.15	1.6148	5.69	0.0120	6.41	28.408	5.62	0.0545	5.15	245.61	20.90	223.02	12.32	241.32	15.39	1:1	7.98
0.0621	7.36	7.0453	2.50	0.0023	9.03	122.887	8.15	0.0621	7.36	70.40	10.01	52.25	4.24	47.37	4.27	1:1	44.18
0.0620	4.91	10.2530	3.09	0.0023	4.54	123.080	5.23	0.0620	4.91	68.76	5.30	52.16	2.72	45.90	2.08	1:1	69.63
0.0584	11.96	5.1268	2.47	0.0021	3.80	148.248	4.13	0.0584	11.96	53.94	8.31	43.34	1.78	42.44	1.61	1:1	33.62
0.0588	6.74	10.2895	11.27	0.0023	3.03	123.441	3.98	0.0588	6.74	64.77	4.64	52.01	2.06	46.57	1.41	1:1	59.01
0.0583	5.46	6.0266	26.31	0.0022	6.00	132.639	2.69	0.0583	5.46	59.94	3.35	48.42	1.30	44.07	2.64	1:1	31.45
0.0600	5.18	6.5627	21.12	0.0023	5.10	130.030	6.44	0.0600	5.18	62.77	5.50	49.39	3.17	45.55	2.32	1:1	44.85
0.0615	6.75	6.1732	2.15	0.0023	4.46	129.884	4.35	0.0615	6.75	64.74	5.79	49.44	2.14	45.67	2.03	1:1	59.93
0.0610	3.57	4.2883	1.16	0.0023	3.87	131.658	3.54	0.0610	3.57	63.08	3.62	48.78	1.72	45.44	1.76	1,5:1	43.71
0.0640	5.35	5.3123	1.99	0.0023	4.51	128.107	4.32	0.0640	5.35	68.18	5.06	50.12	2.16	46.41	2.09	1:1	57.26
0.0616	11.88	4.2061	10.07	0.0022	21.10	130.244	16.75	0.0616	11.88	64.25	9.13	49.31	8.23	44.98	9.48	1:1	49.57
0.0584	7.97	3.3575	52.86	0.0022	8.99	142.570	13.59	0.0584	7.97	55.91	9.37	45.06	6.10	43.60	3.92	1:1	31.00
0.0634	3.77	5.2352	1.10	0.0022	1.52	130.454	1.76	0.0634	3.77	66.73	3.08	49.23	0.86	44.92	0.68	1:1	67.98
0.0921	16.65	4.5678	3.13	0.0022	4.32	124.268	4.30	0.0921	16.65	100.87	19.83	51.67	2.21	43.78	1.89	1,5:1	66.62
0.0541	11.92	3.4226	5.17	0.0020	5.82	134.470	2.86	0.0541	11.92	54.70	6.74	47.76	1.36	40.71	2.37	1,5:1	62.61
0.0626	4.02	2.7547	1.02	0.0021	3.48	136.053	2.93	0.0626	4.02	62.45	2.87	47.21	1.38	43.02	1.50	2:1	50.27
0.0832	16.10	2.3499	1.73	0.0022	3.00	131.589	3.25	0.0832	16.10	85.89	16.13	48.80	1.58	43.81	1.31	1:1	45.97
0.0635	4.16	2.4633	1.16	0.0022	2.12	136.761	1.99	0.0635	4.16	62.78	3.04	46.96	0.93	43.62	0.93	1:1	48.89

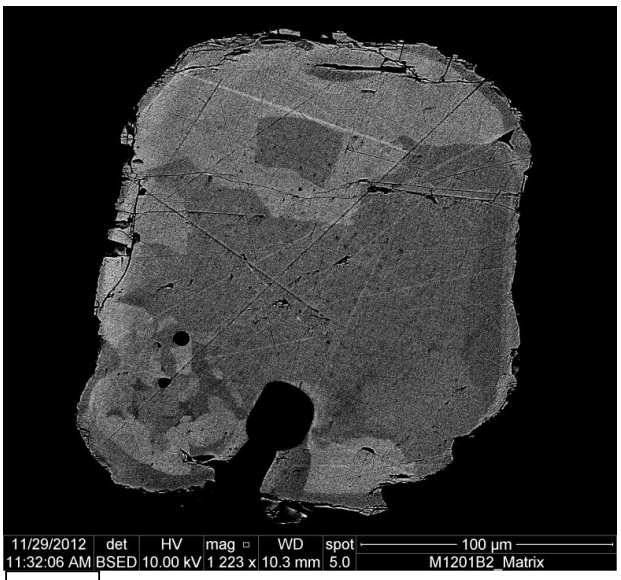

A02

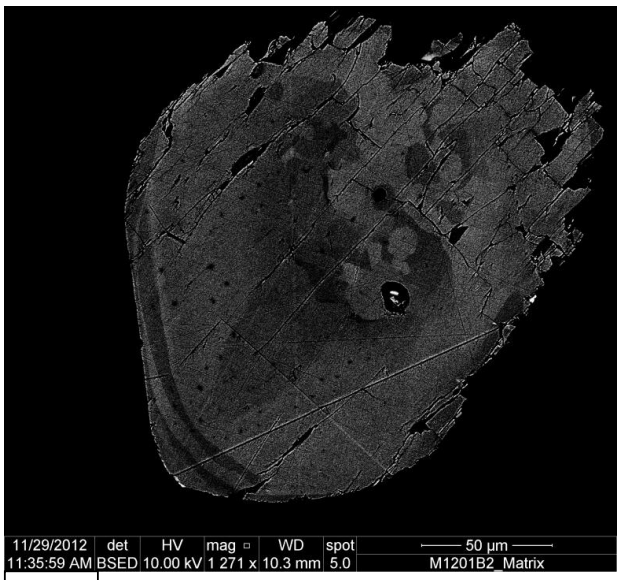

A03

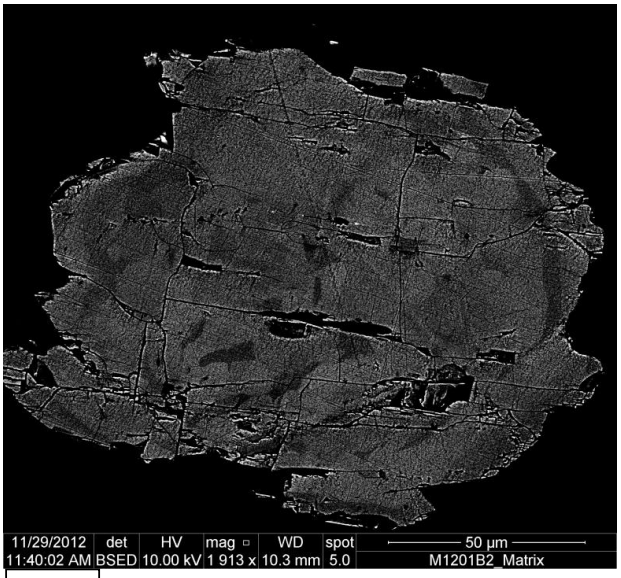

A04

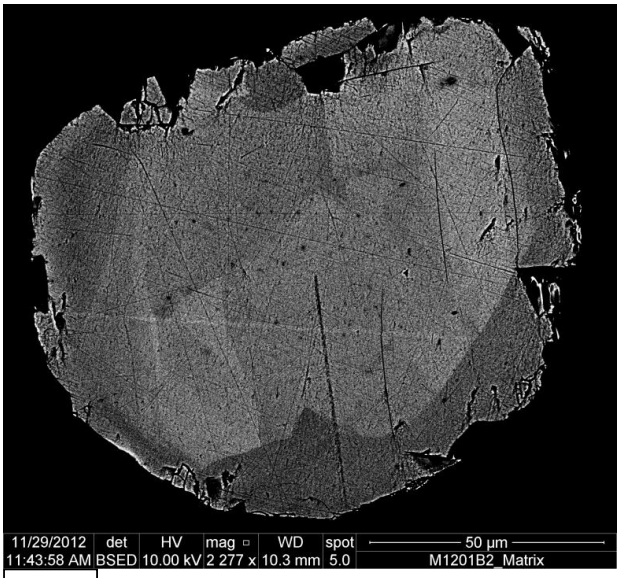

A07

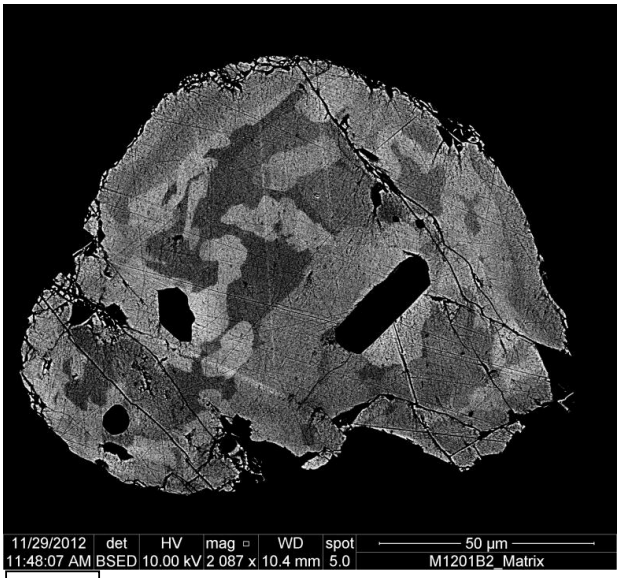

A08

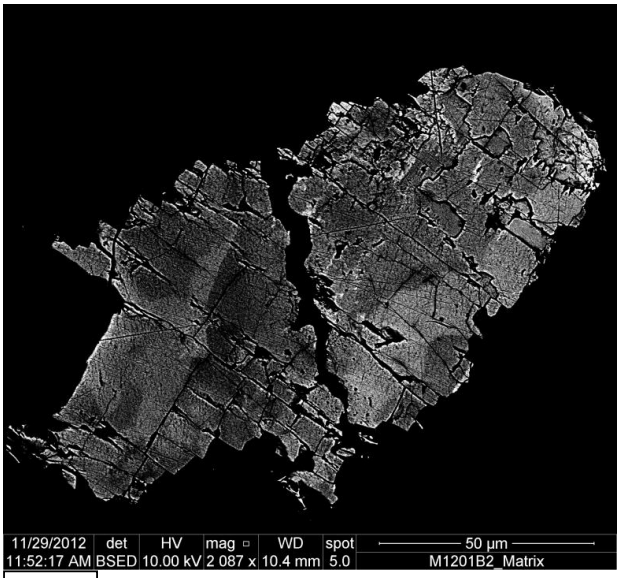

A09

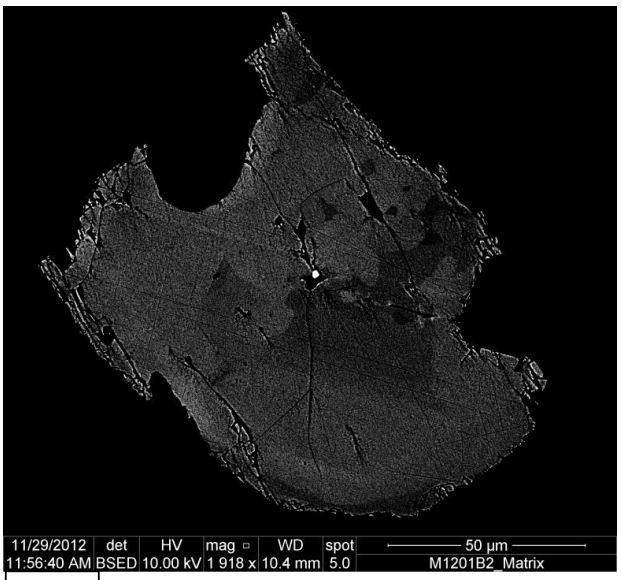

A10

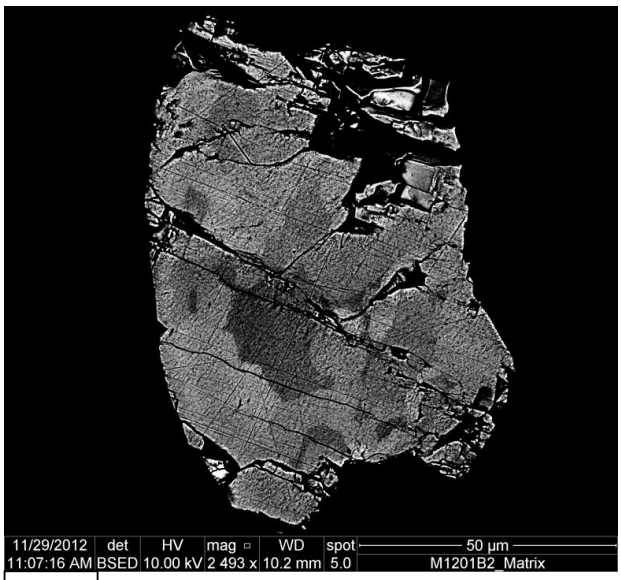

B01

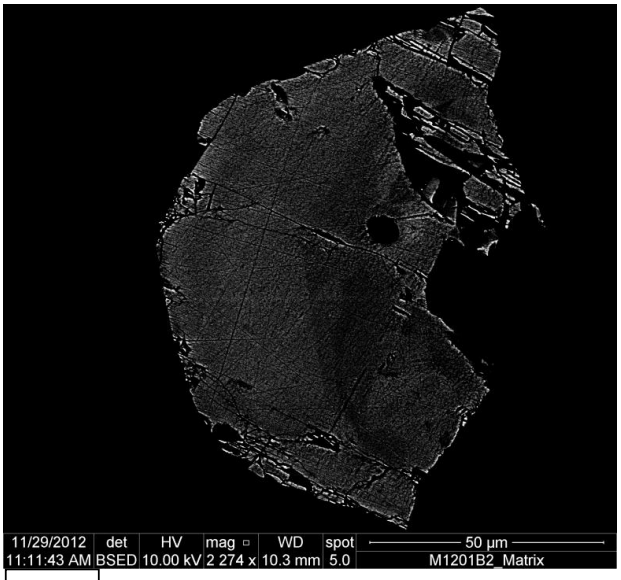

B02

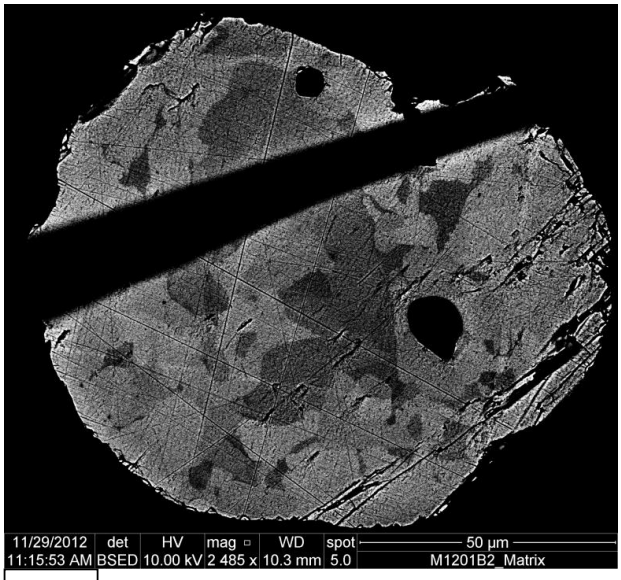

B04

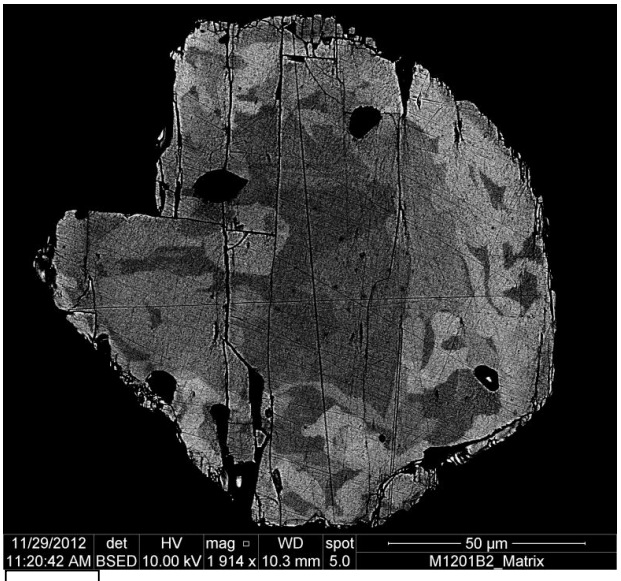

B06

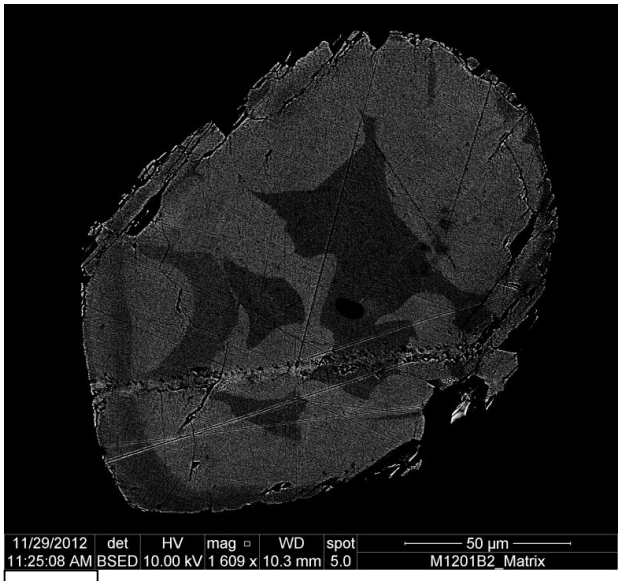

B07

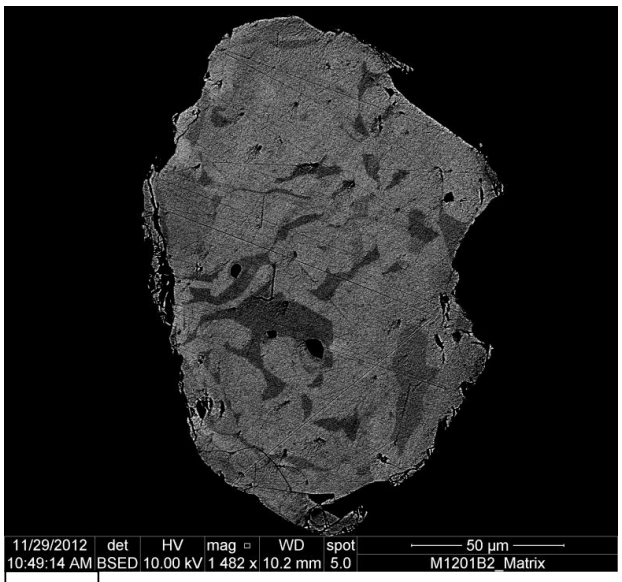

C01

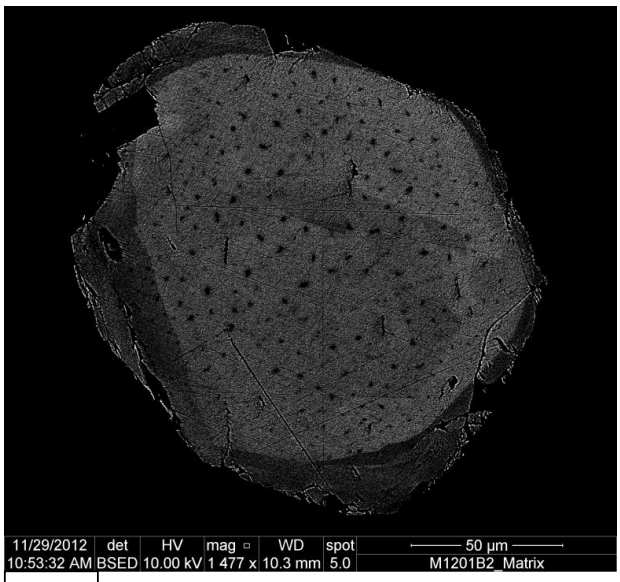

C03

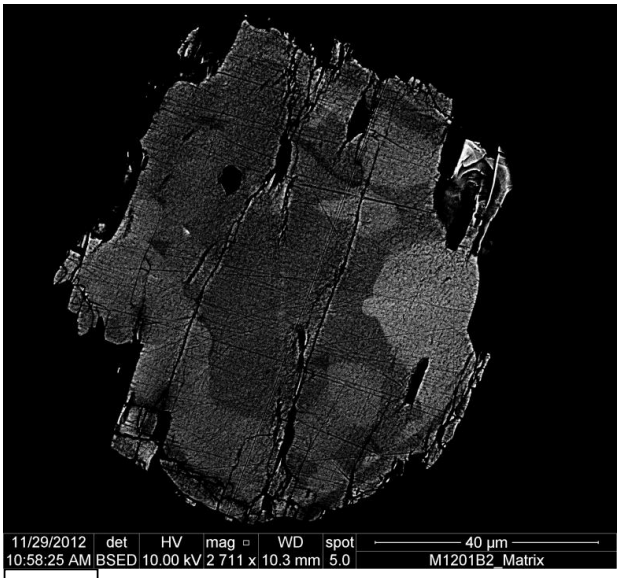

C04

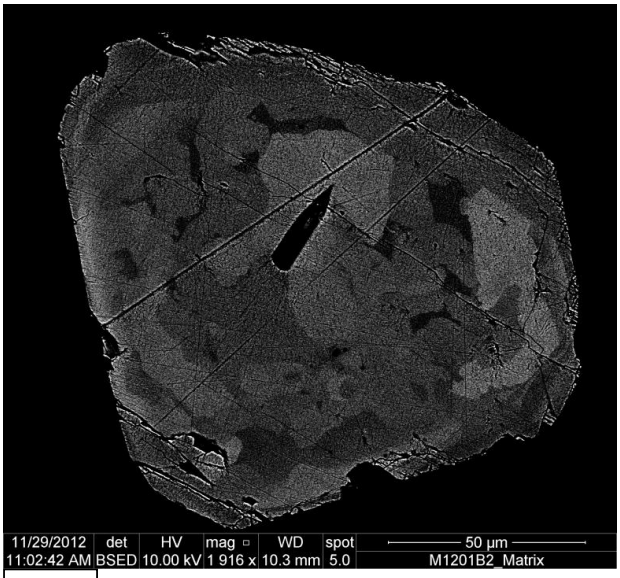

C06

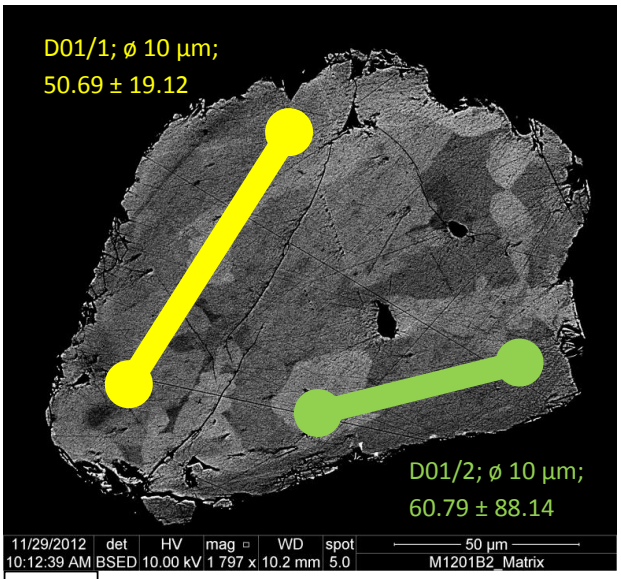

D01

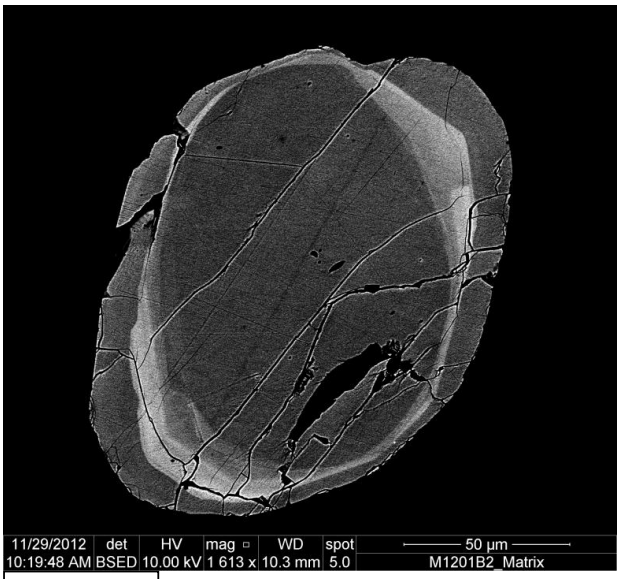

D02 Zirkon

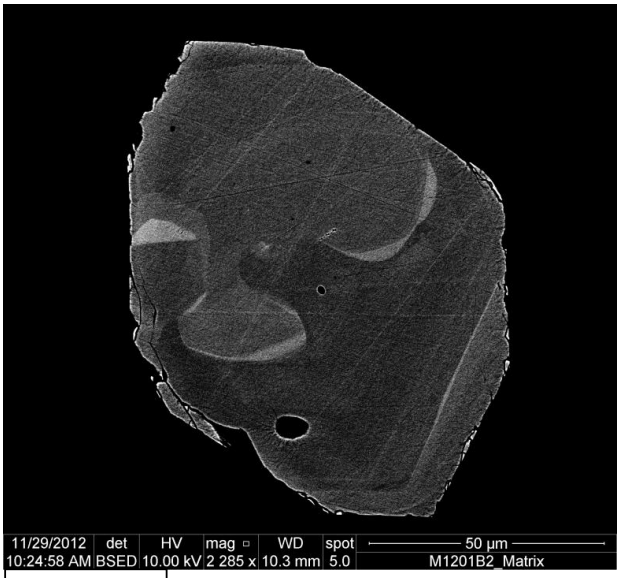

D03 Zirkon

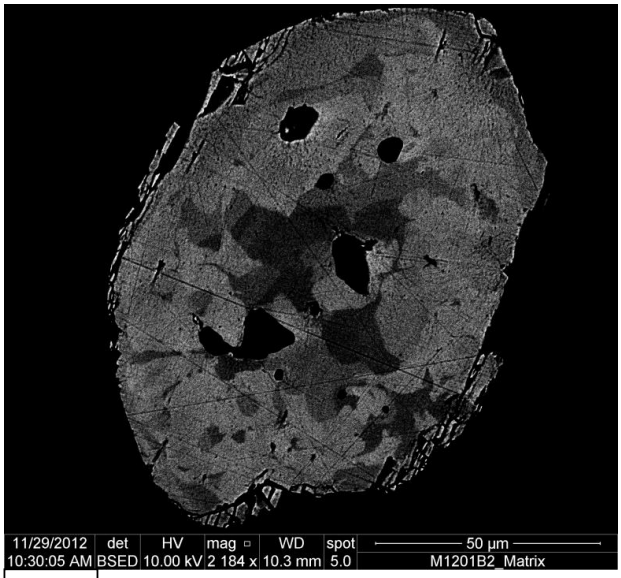

D07

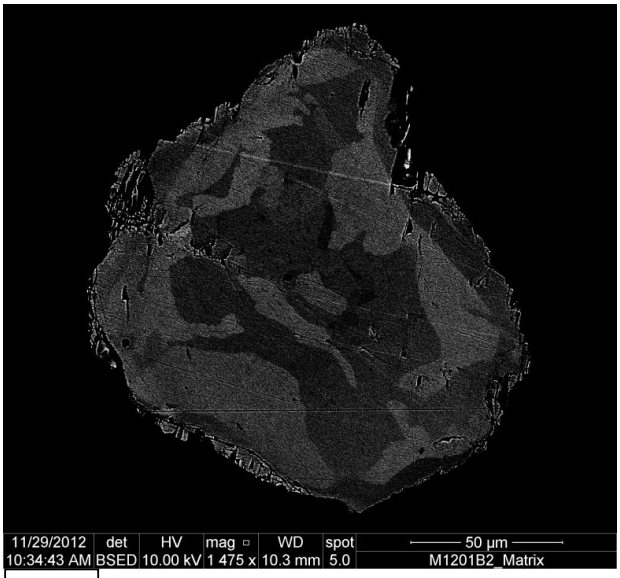

D10

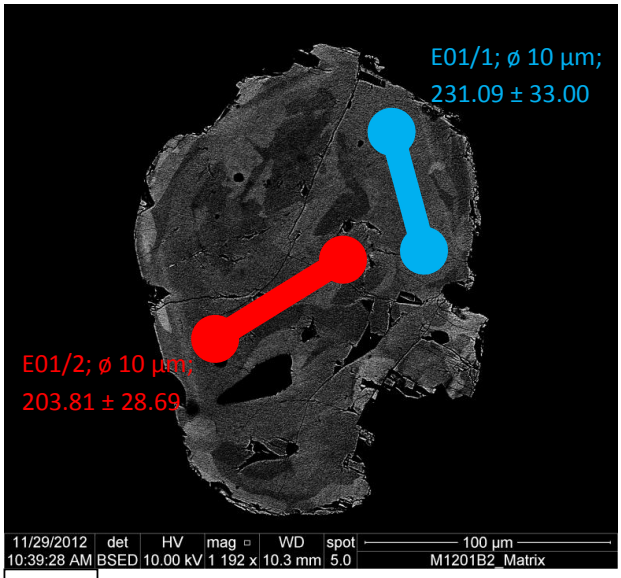

E01

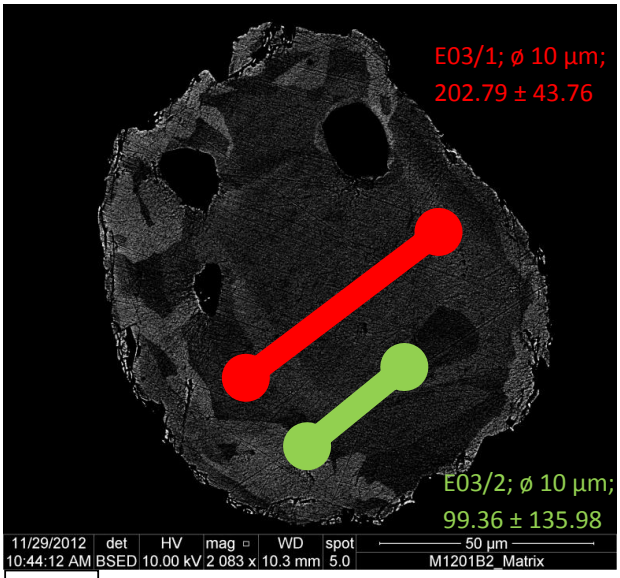

E03

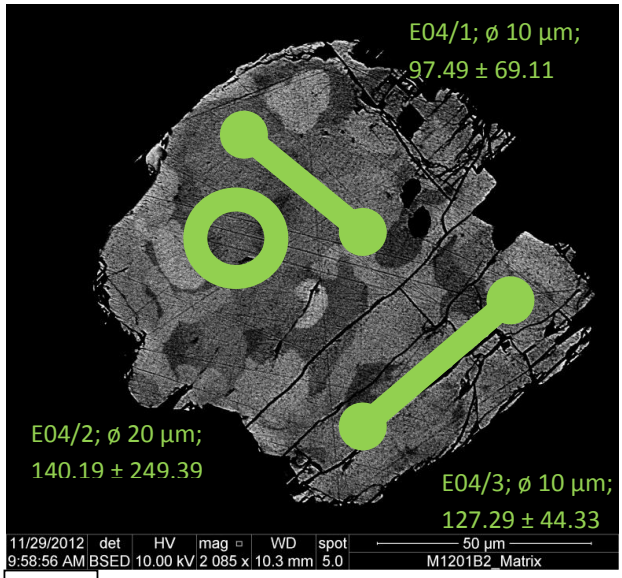

E04

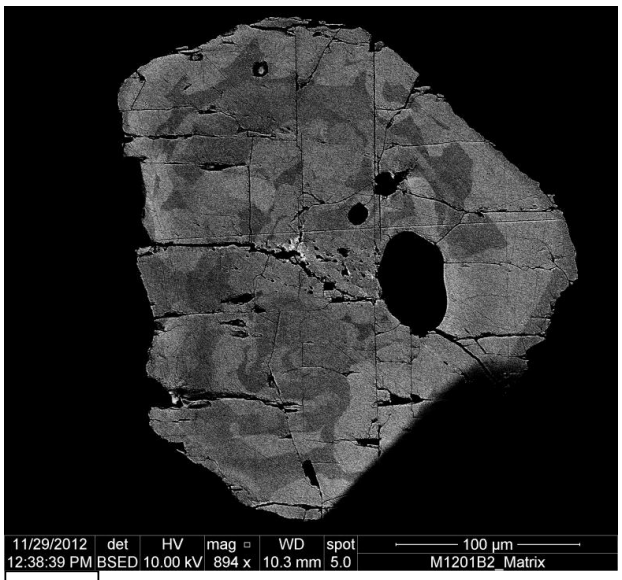

A01

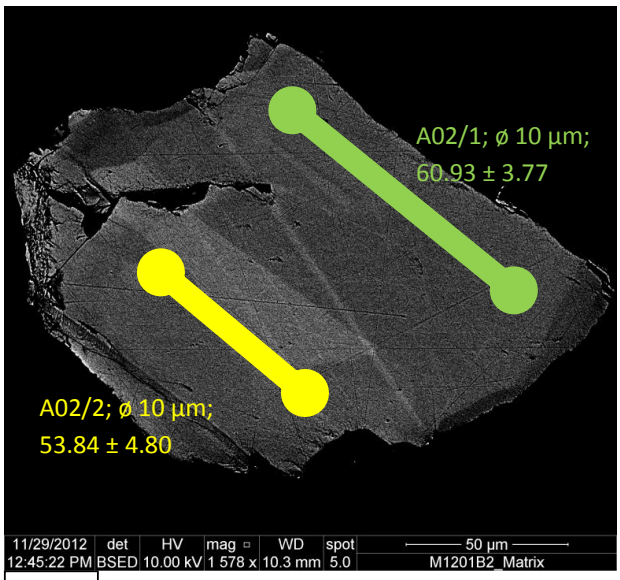

A02

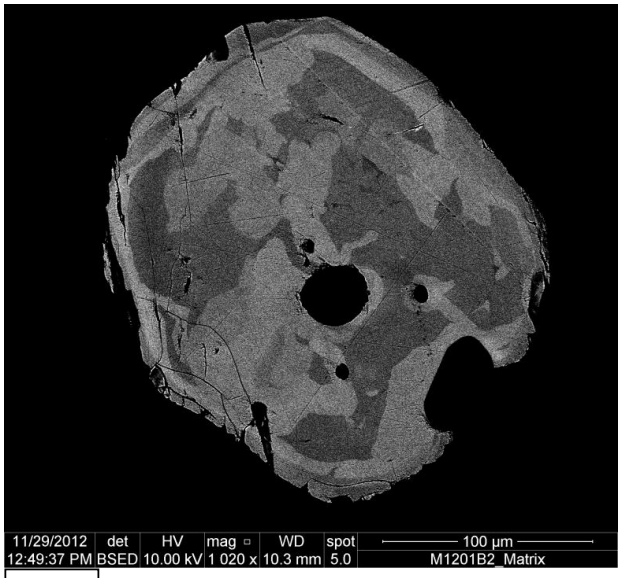

A05

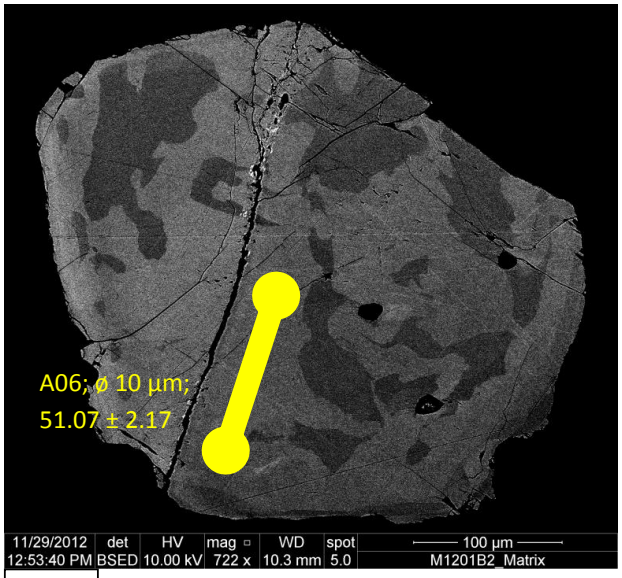

A06

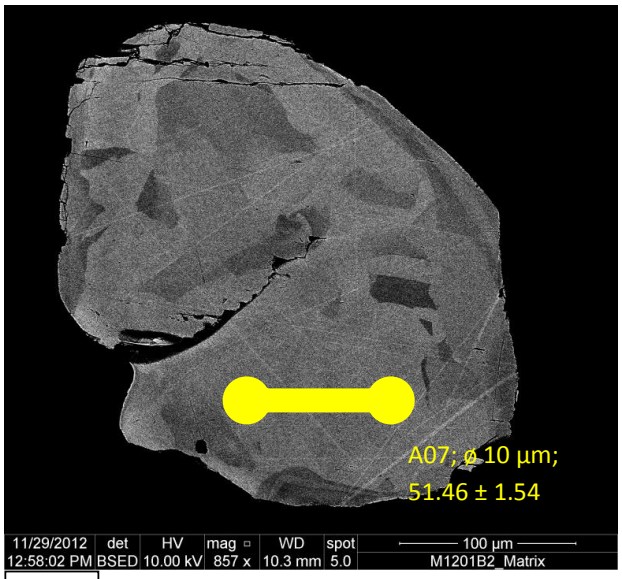

A07

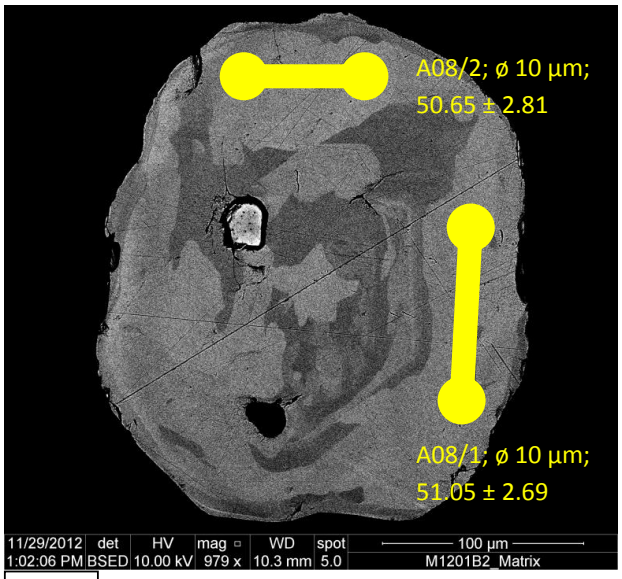

A08

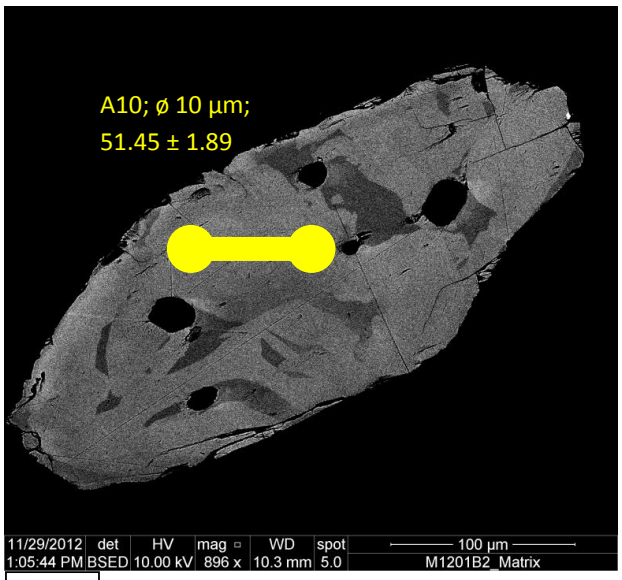

A10

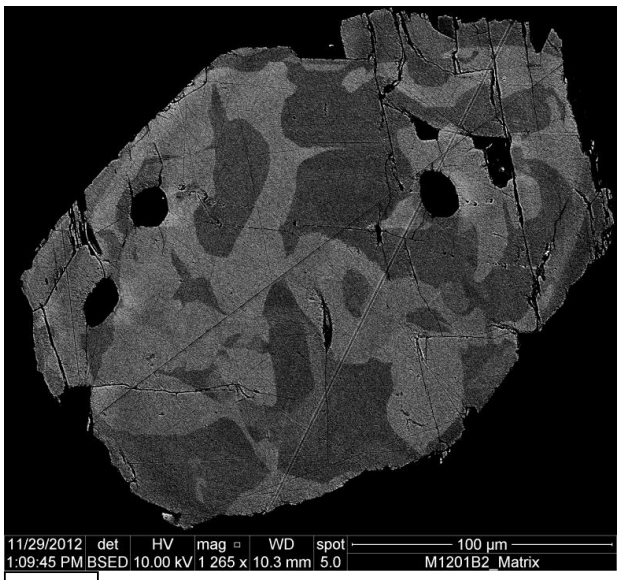

B02

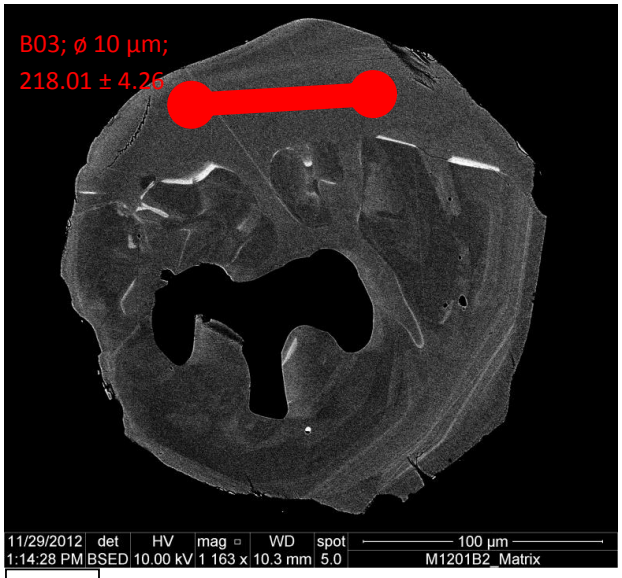

B03

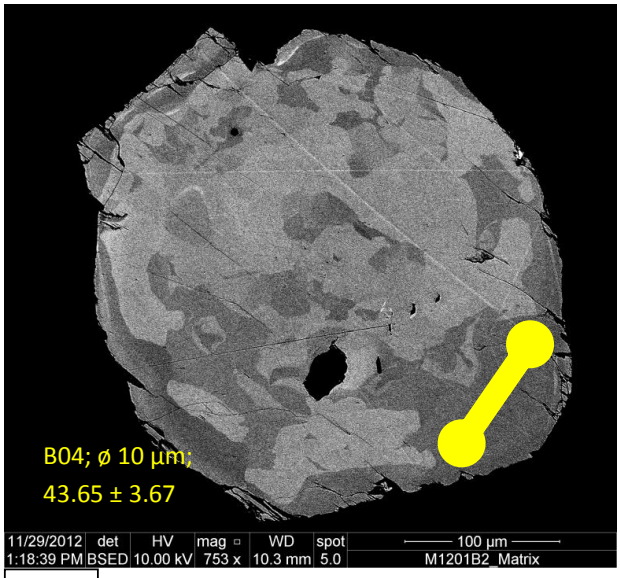

B04

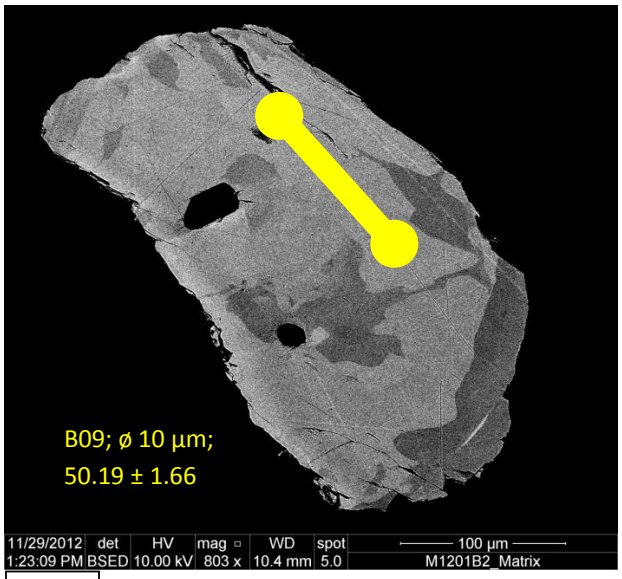

B09

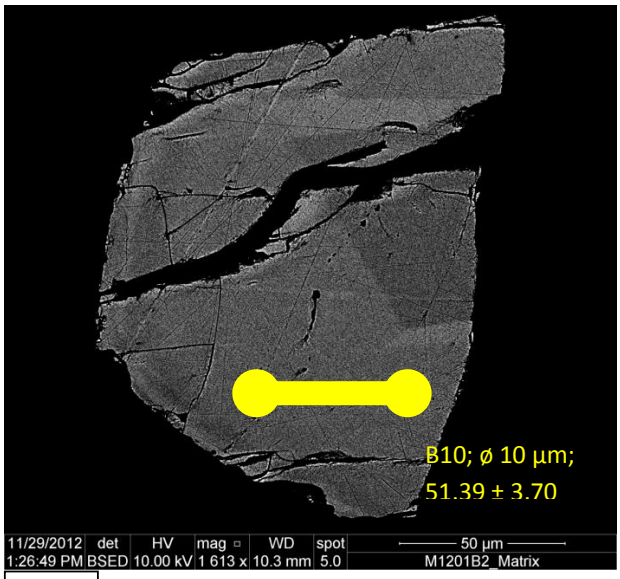

B10

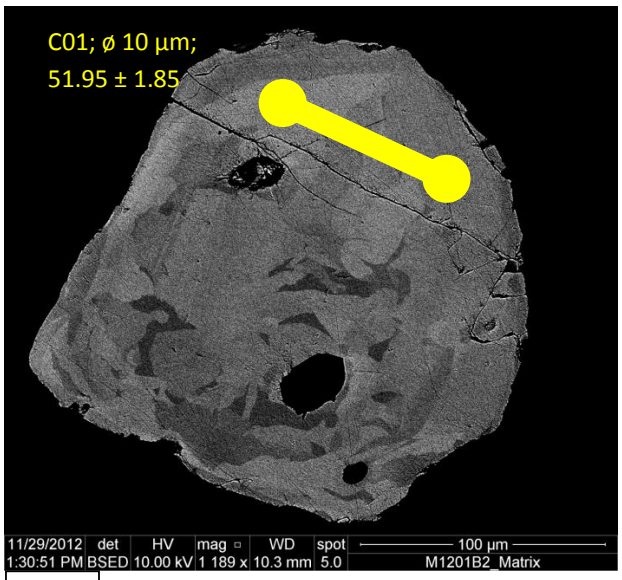

C01

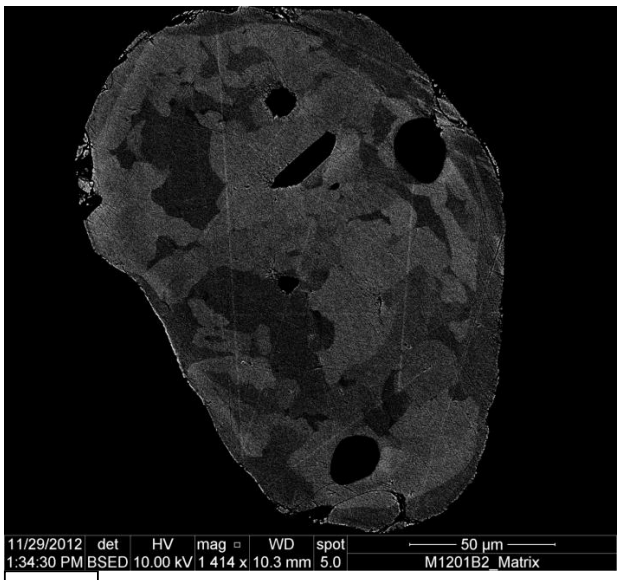

C03

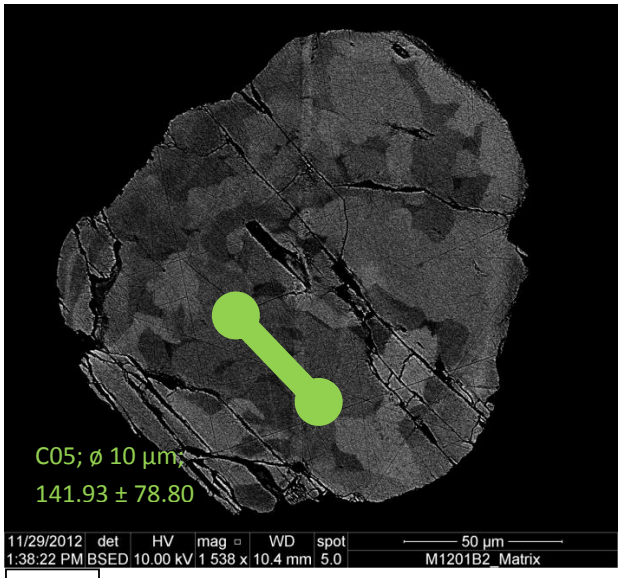

C05

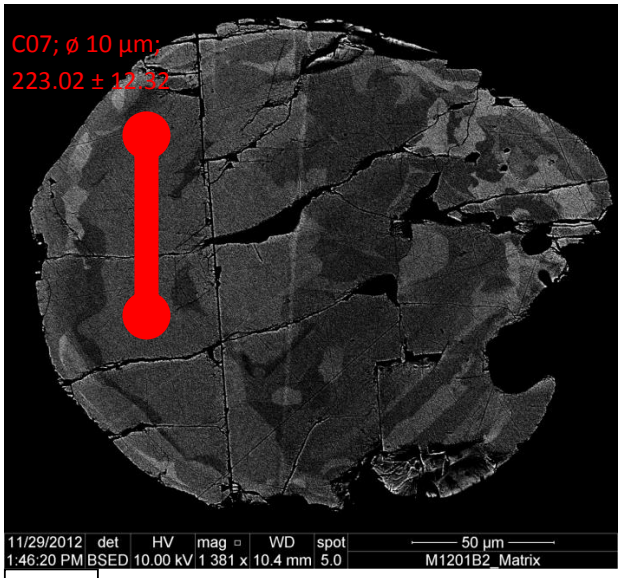

C07

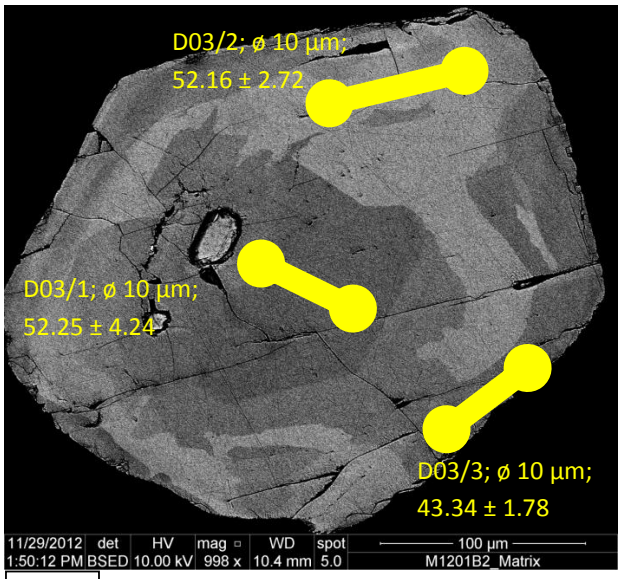

D03

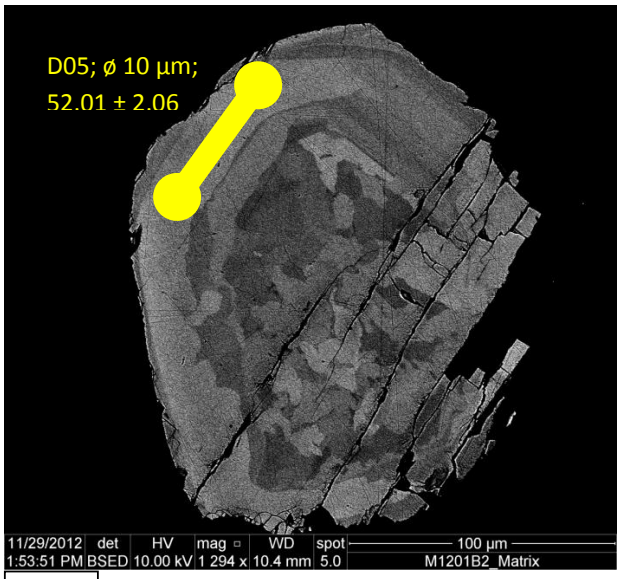

D05

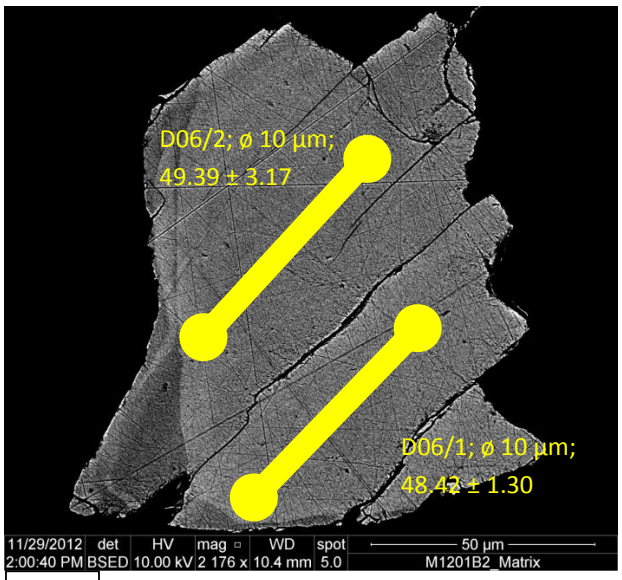

D06

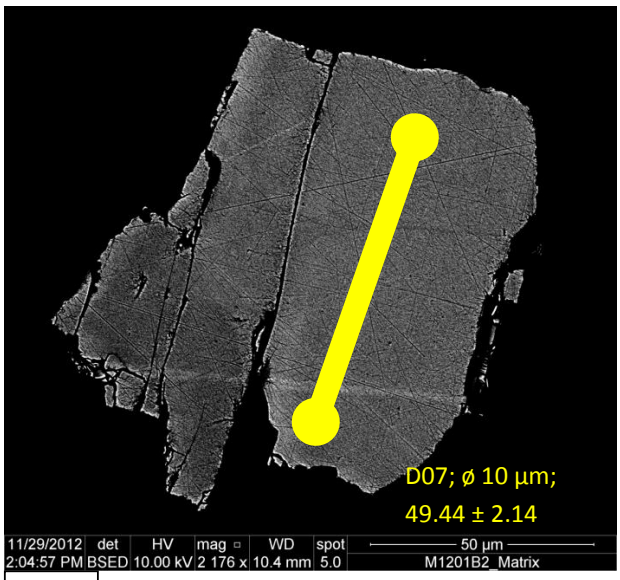

D07

D08

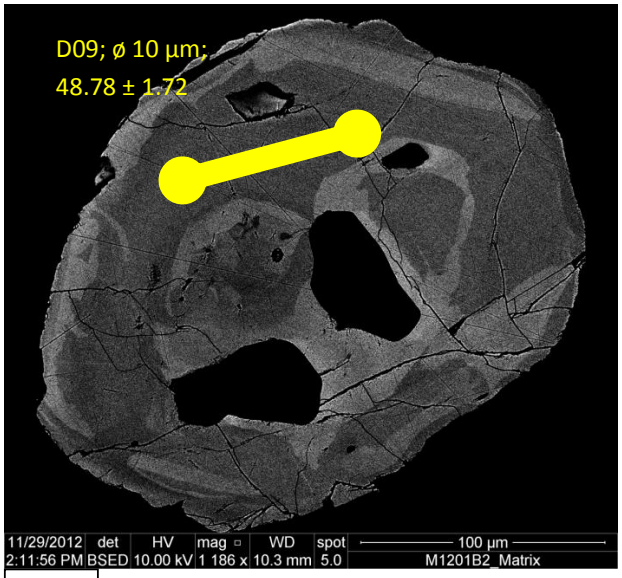

D09

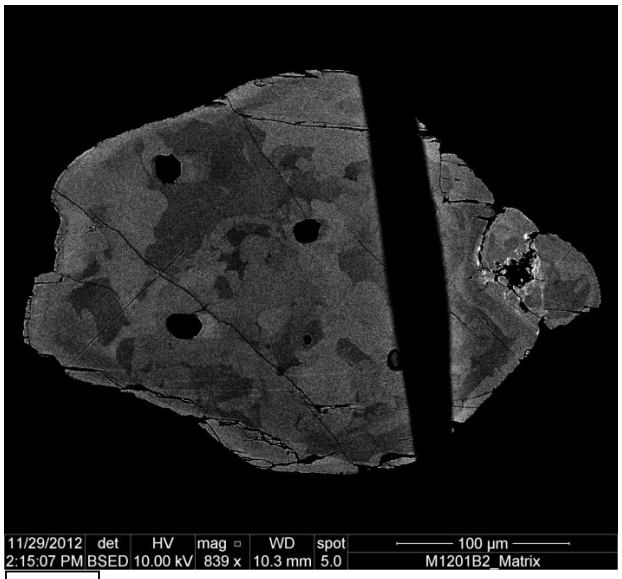

D10

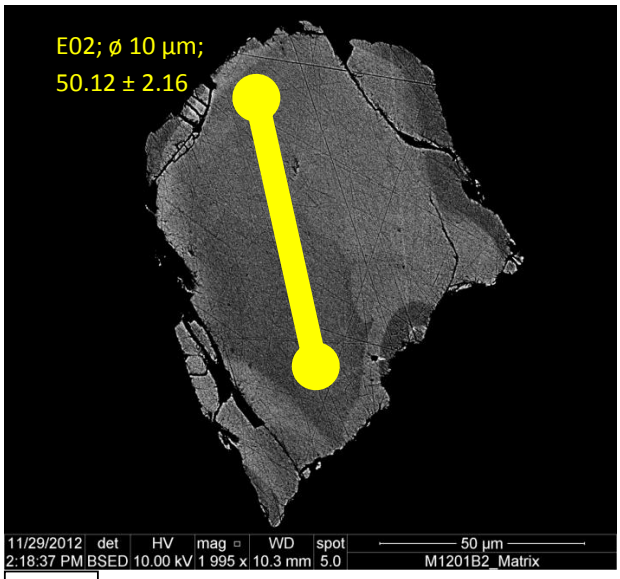

E02

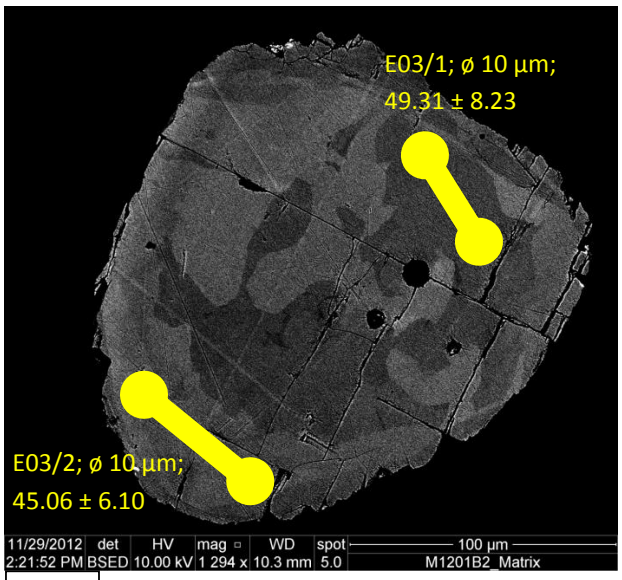

E03

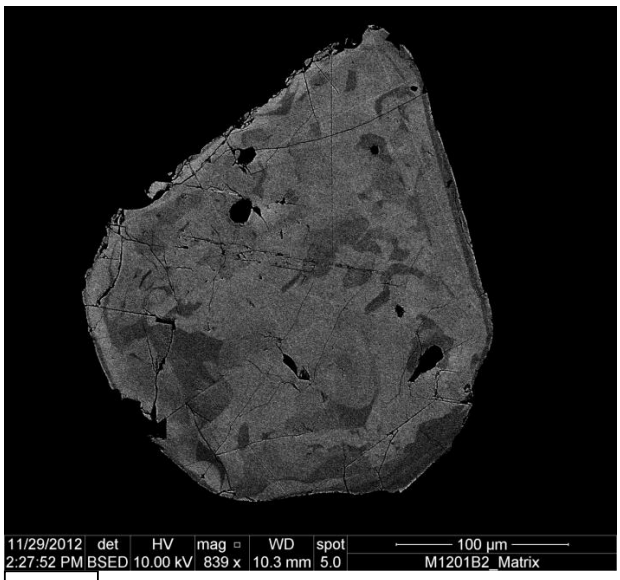

E05

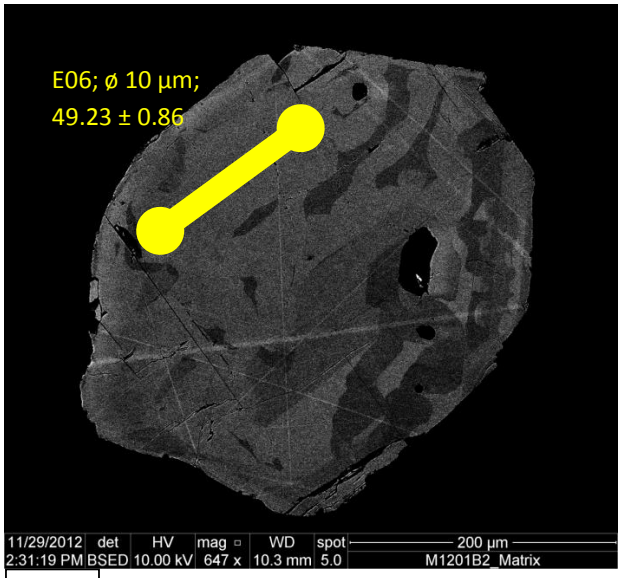

E06

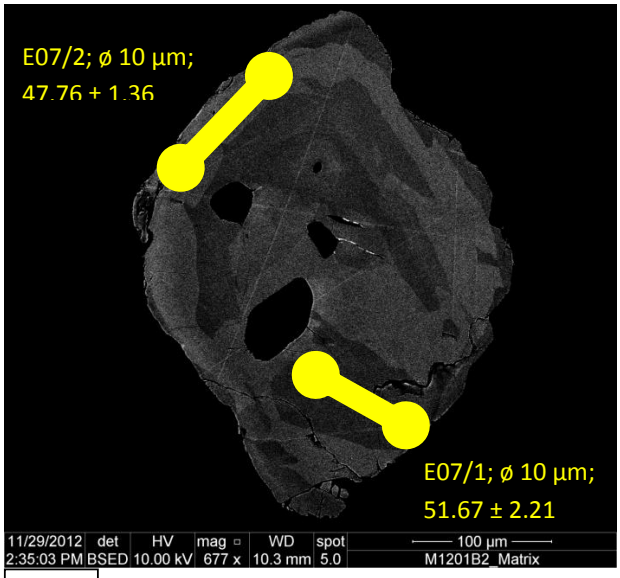

E07

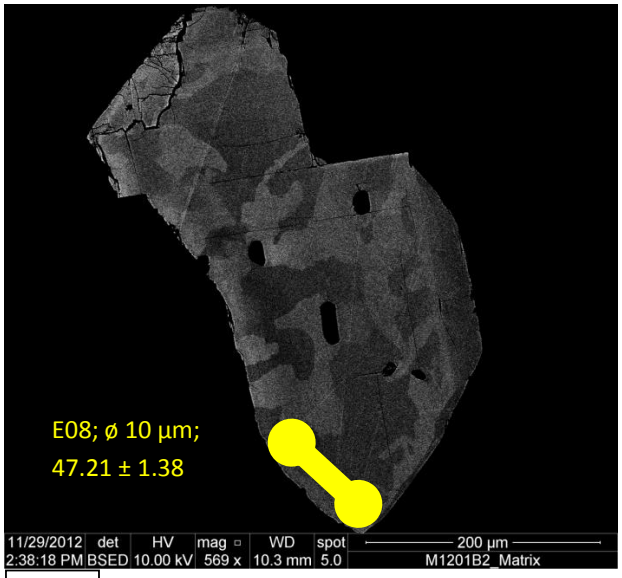

E08

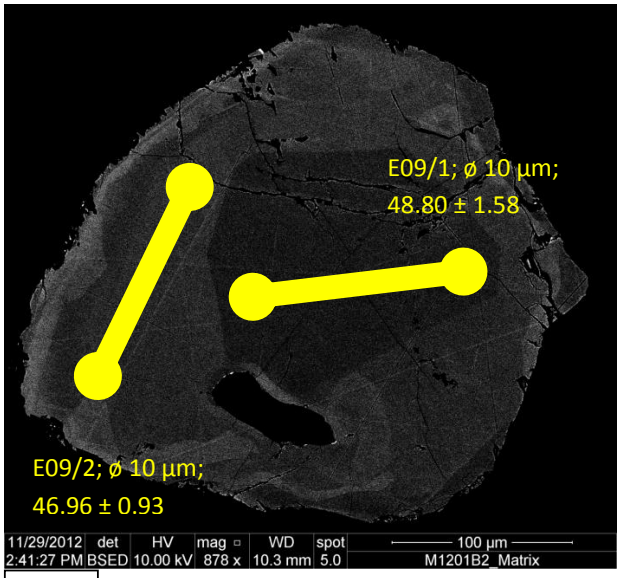

E09

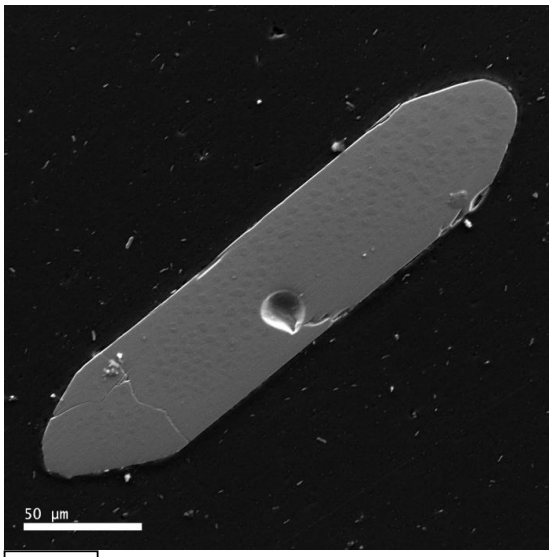
50 µm

A01

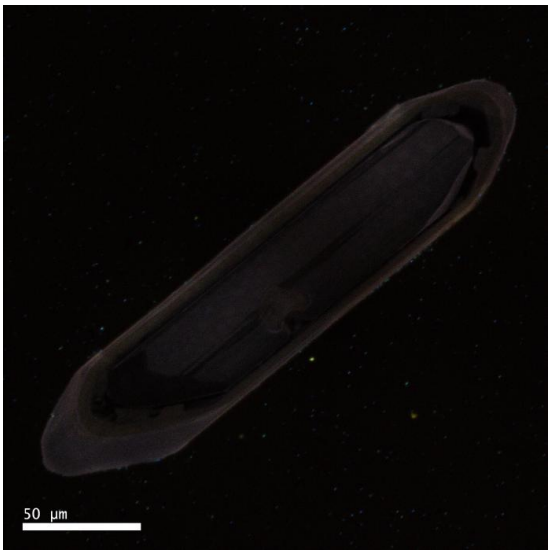
50 µm

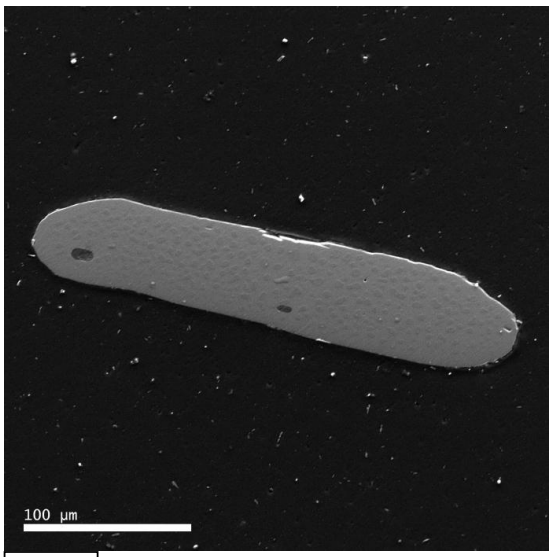
100 µm

A02

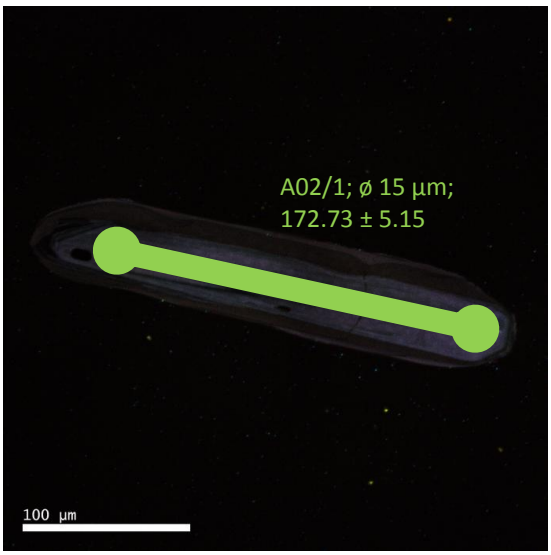
A02/1; ø 15 µm;
172.73 ± 5.15
100 µm

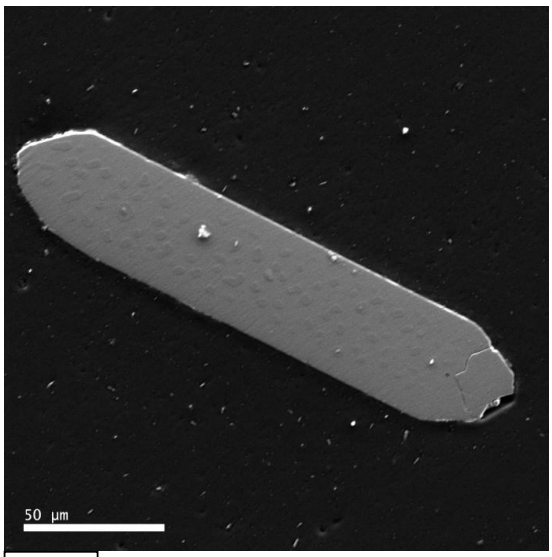
50 µm

A03

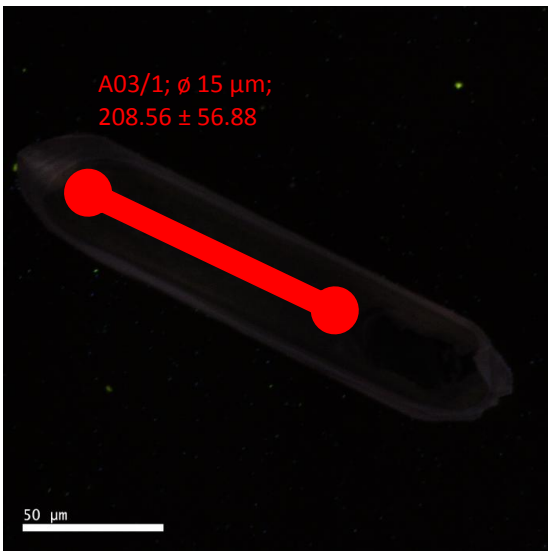
A03/1; ø 15 µm;
208.56 ± 56.88
50 µm

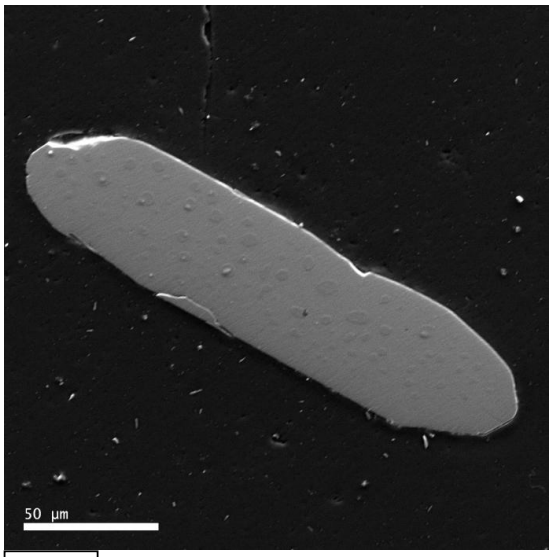
50 µm

A04

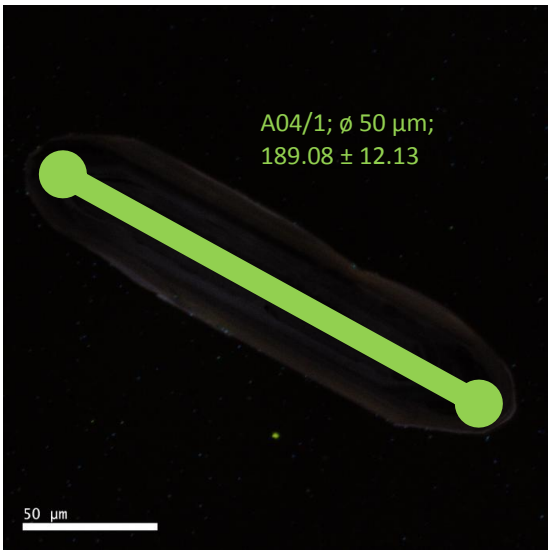
A04/1; ø 50 µm;
189.08 ± 12.13
50 µm

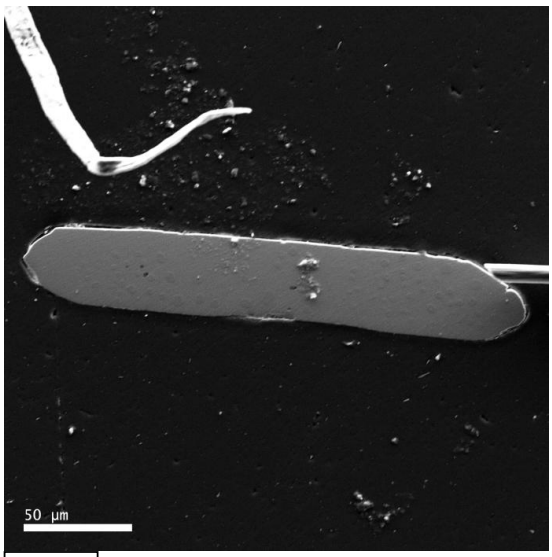
50 µm

A05

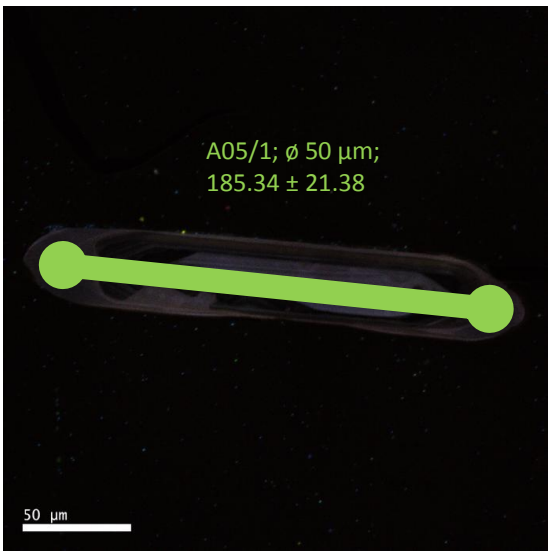
A05/1; ø 50 µm;
185.34 ± 21.38
50 µm

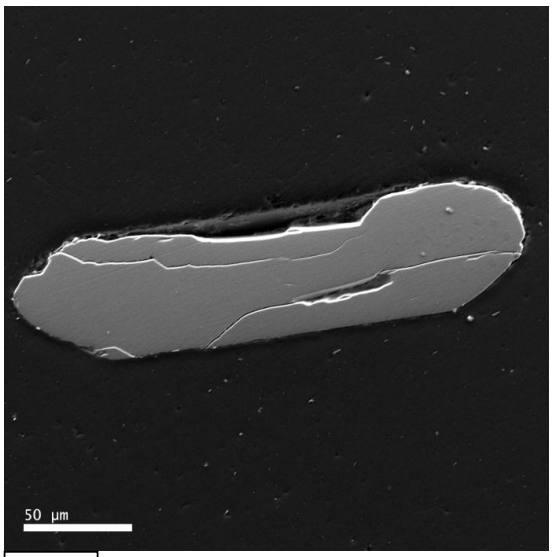
50 µm

A06

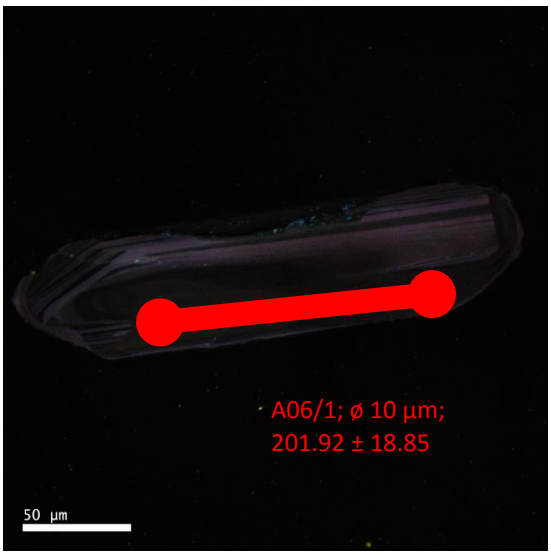
A06/1; ø 10 µm;
201.92 ± 18.85
50 µm

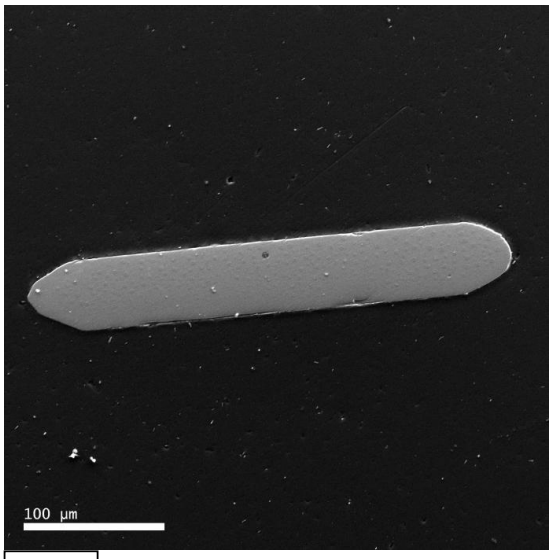
100 µm

A07

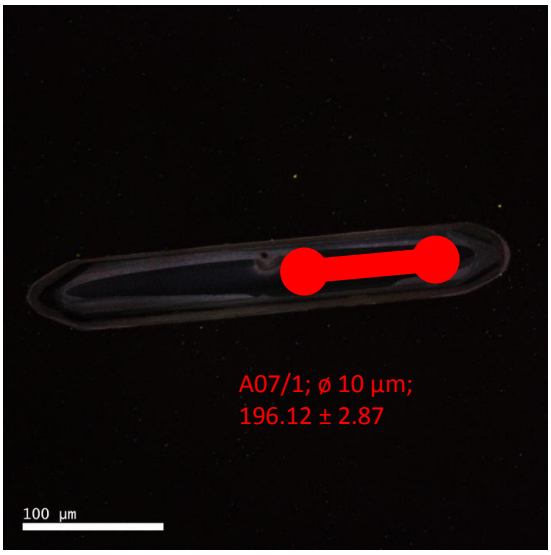
A07/1; ø 10 µm;
196.12 ± 2.87
100 µm

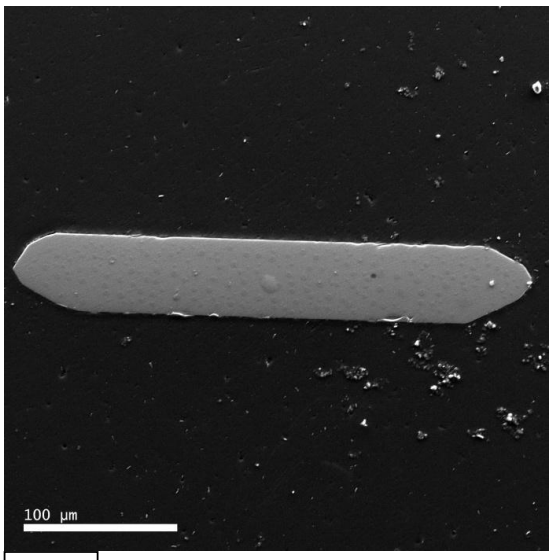
100 µm

A08

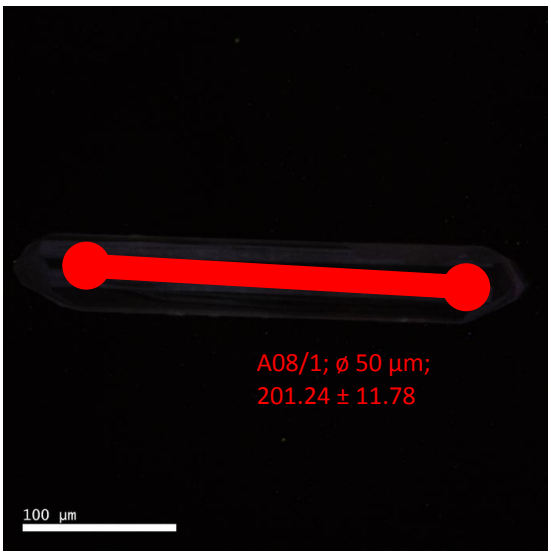
A08/1; ø 50 µm;
201.24 ± 11.78
100 µm

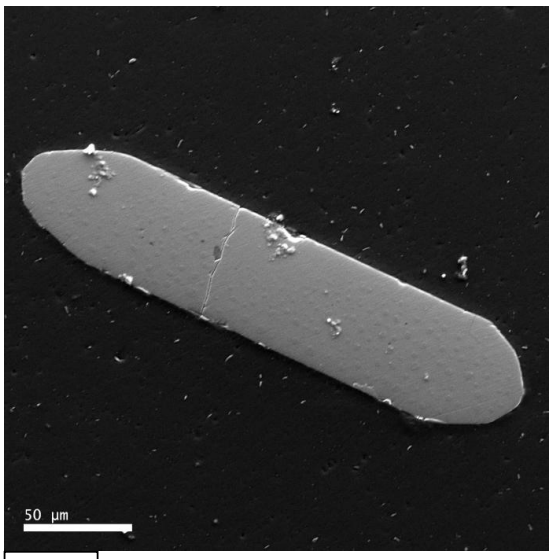
50 µm

A09

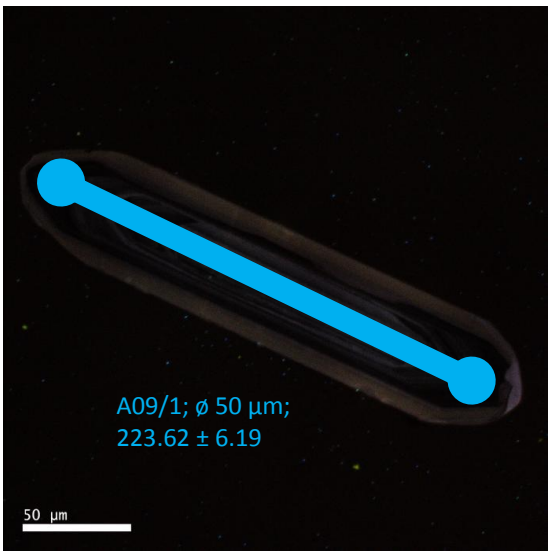
A09/1; ø 50 µm;
223.62 ± 6.19
50 µm

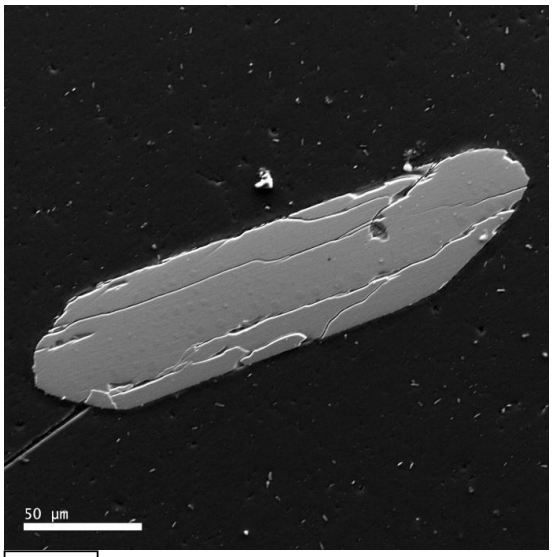
50 µm

A10

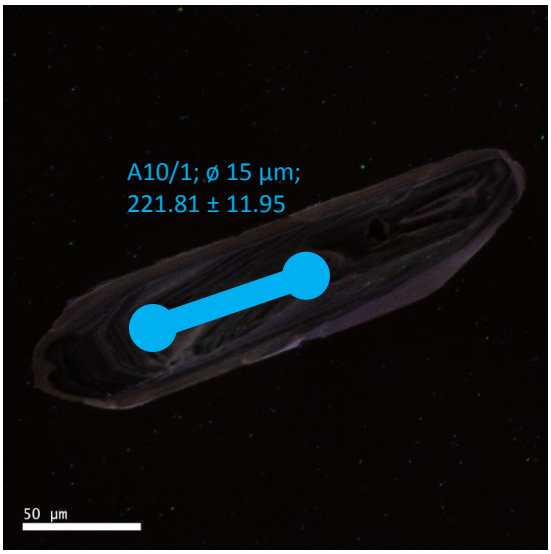
A10/1; ø 15 µm;
221.81 ± 11.95
50 µm

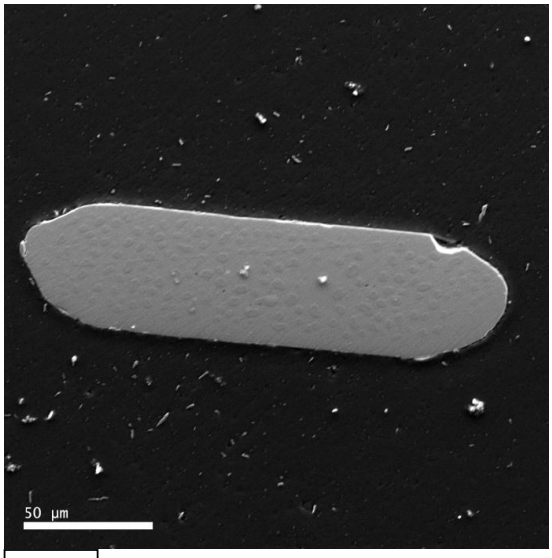
50 µm

B01

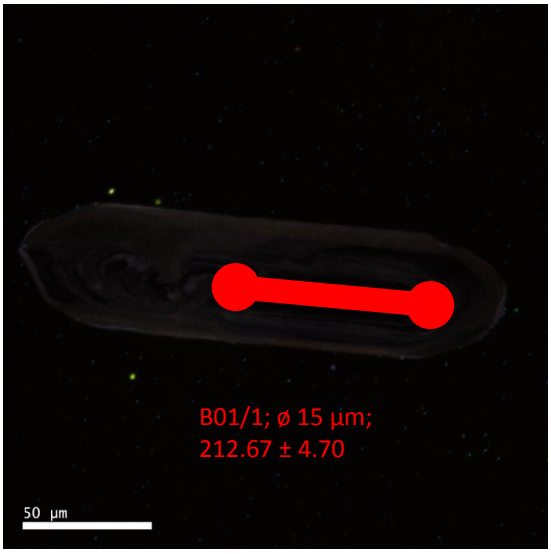
B01/1; ø 15 µm;
212.67 ± 4.70
50 µm

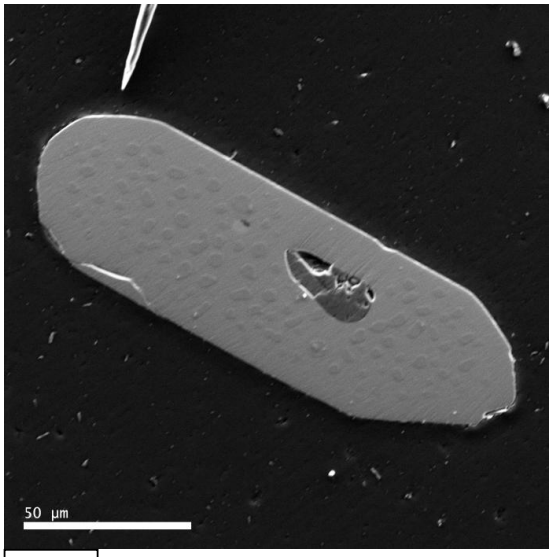
50 µm

B02

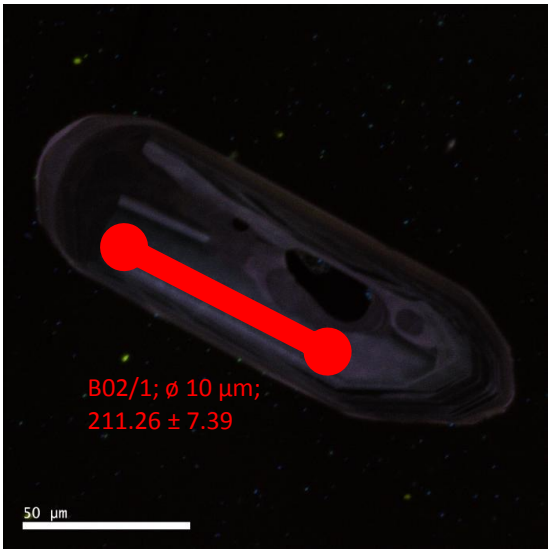
B02/1; ø 10 µm;
211.26 ± 7.39
50 µm

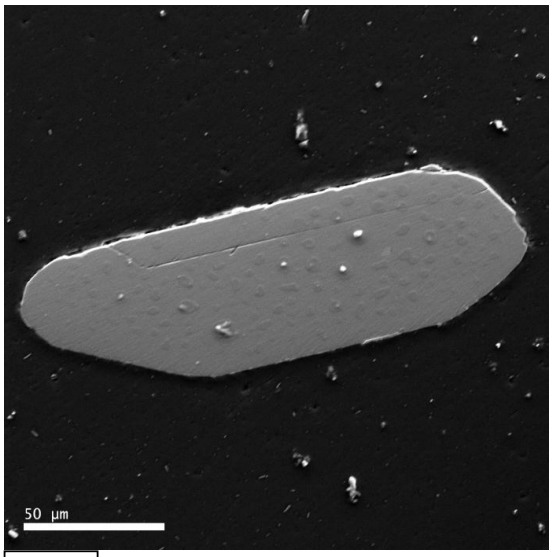
50 µm

B03

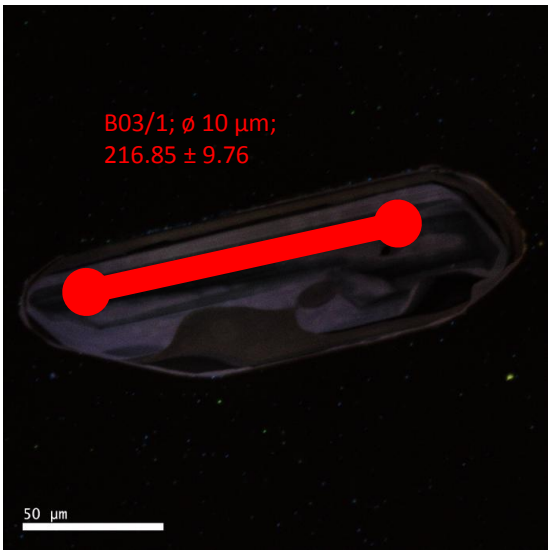
B03/1; ø 10 µm;
216.85 ± 9.76
50 µm

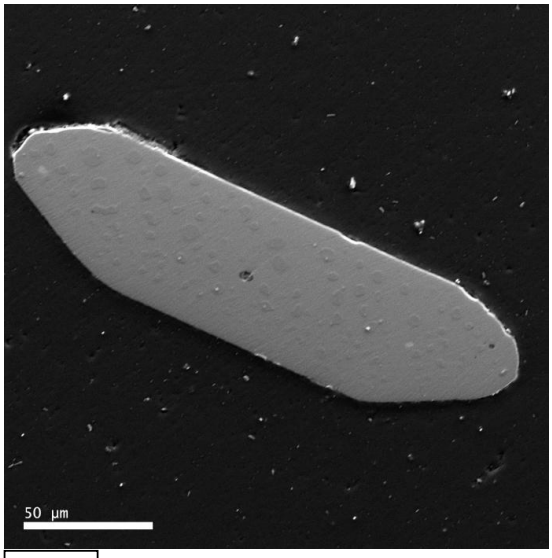
50 µm

B04

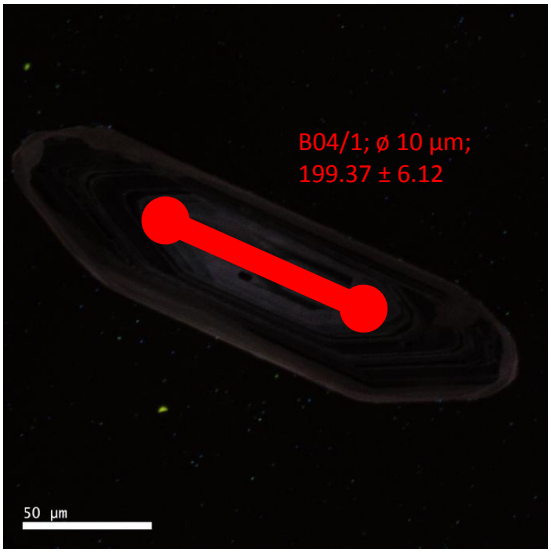
B04/1; ø 10 µm;
199.37 ± 6.12
50 µm

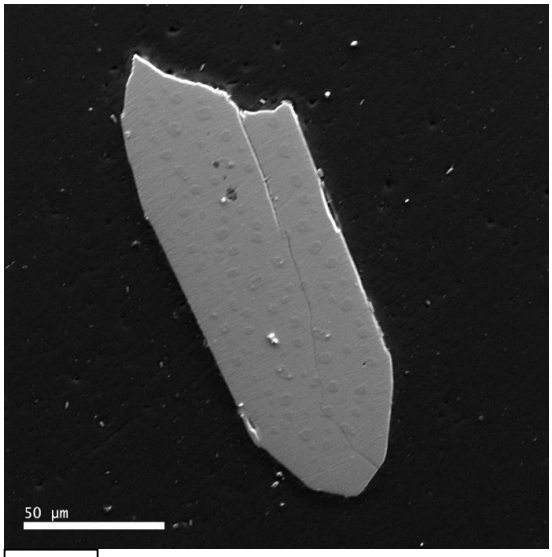
50 µm

B05


B05/1; ø 10 µm;
193.76 ± 7.03
50 µm

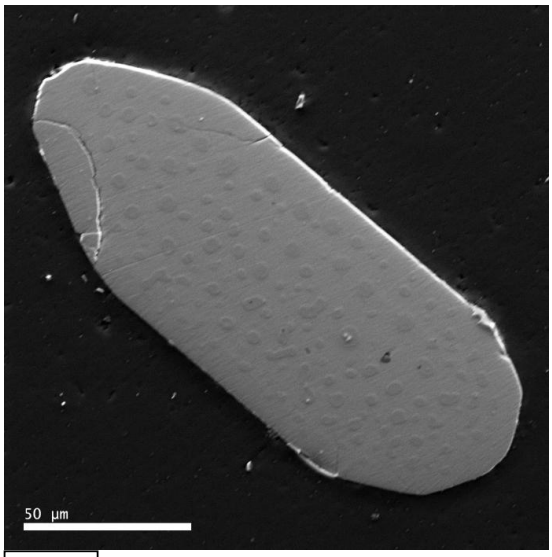
50 µm

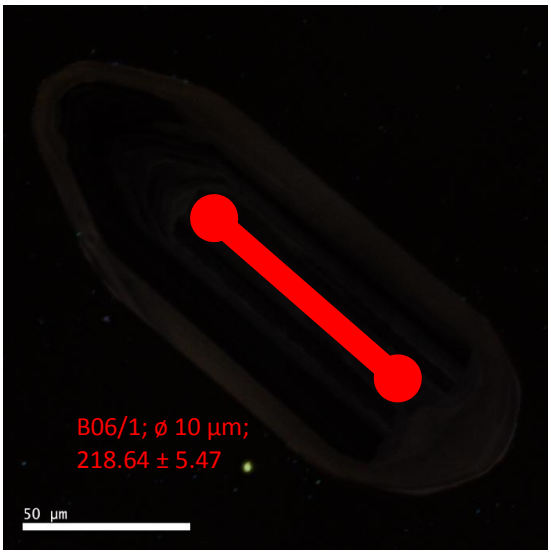
B06/1; ø 10 µm;
218.64 ± 5.47
50 µm

B06

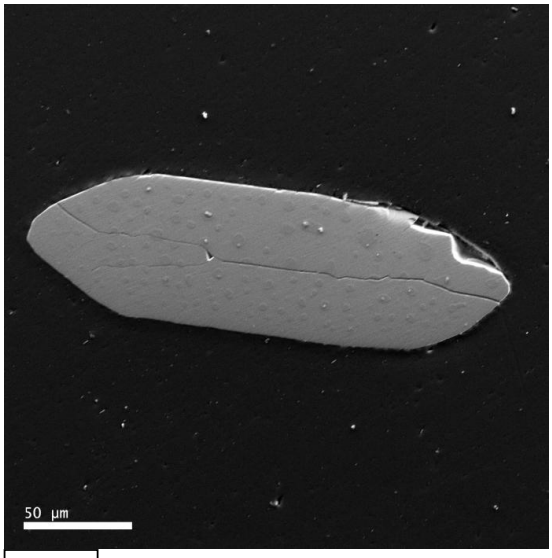
50 µm

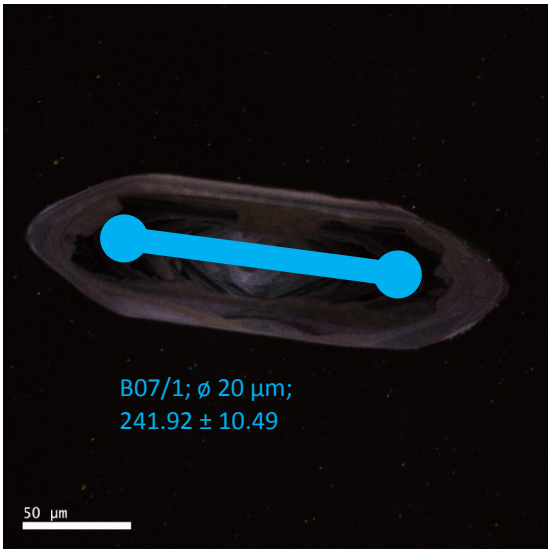
B07/1; ø 20 µm;
241.92 ± 10.49
50 µm

B07

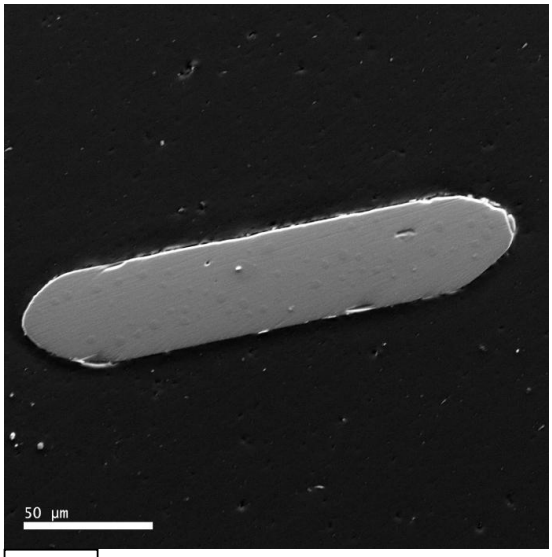
50 µm

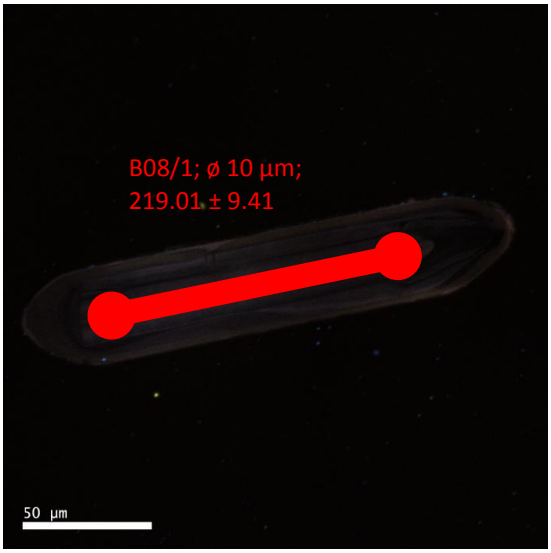
B08/1; ø 10 µm;
219.01 ± 9.41
50 µm

B08

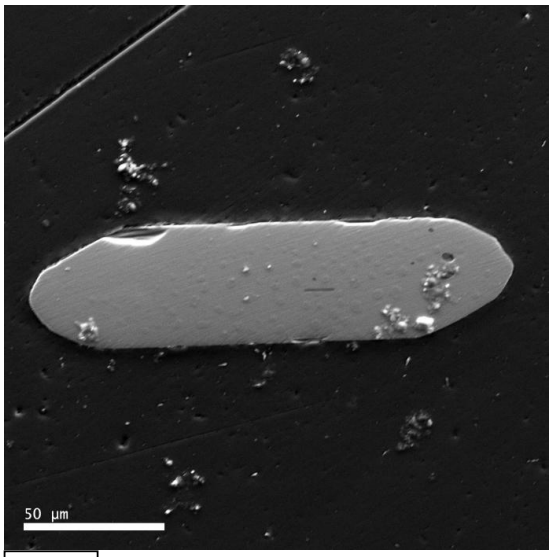
50 µm

B09

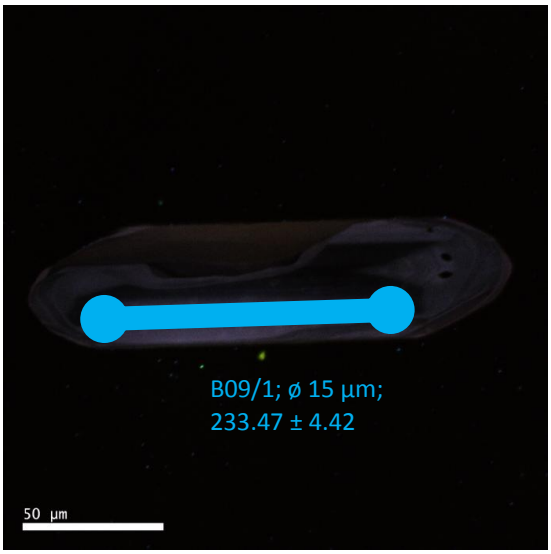
B09/1; ø 15 µm;
233.47 ± 4.42
50 µm

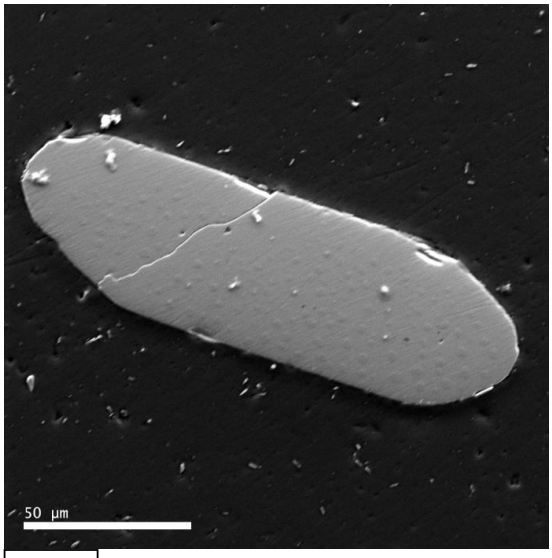
50 µm

B10

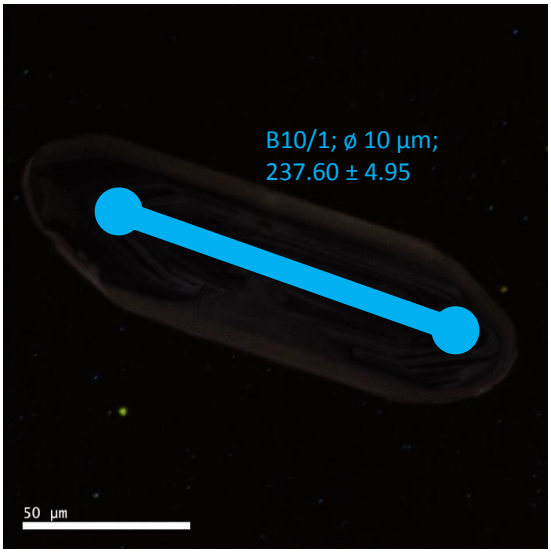
B10/1; ø 10 µm;
237.60 ± 4.95
50 µm

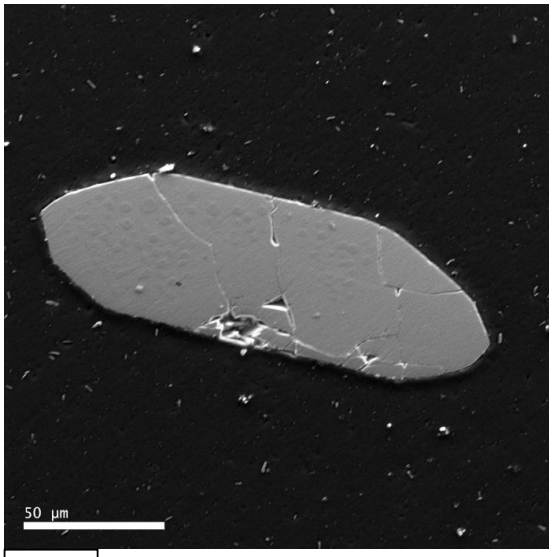
50 µm

C01

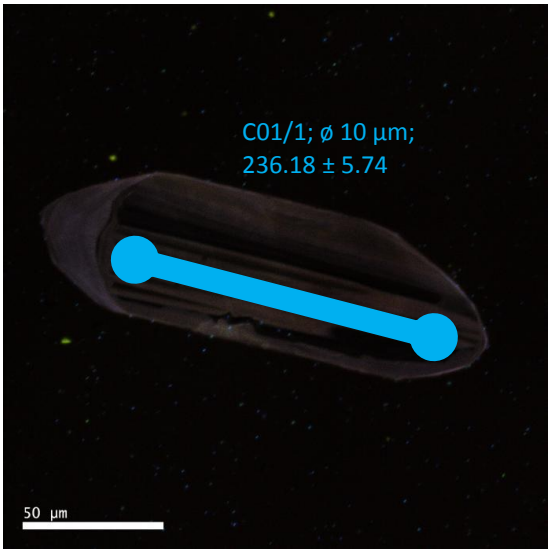
C01/1; ø 10 µm;
236.18 ± 5.74
50 µm

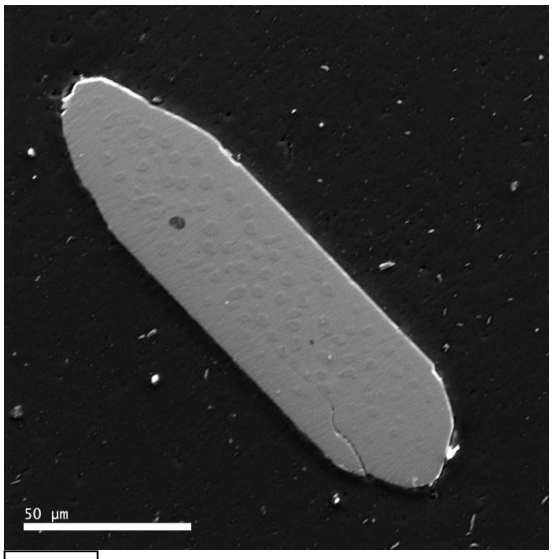
50 µm

C02

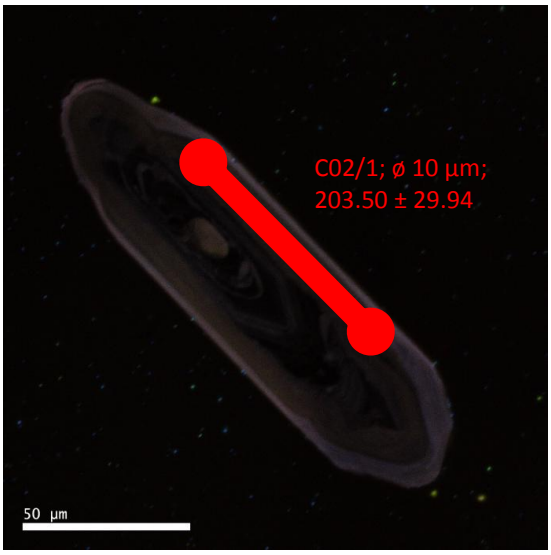
C02/1; ø 10 µm;
203.50 ± 29.94
50 µm

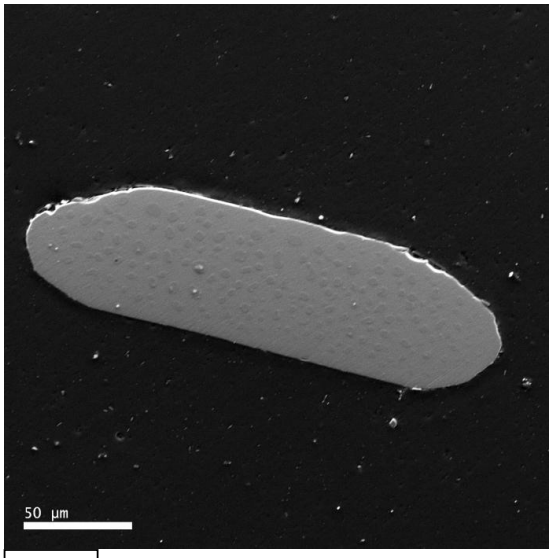
50 µm

C03

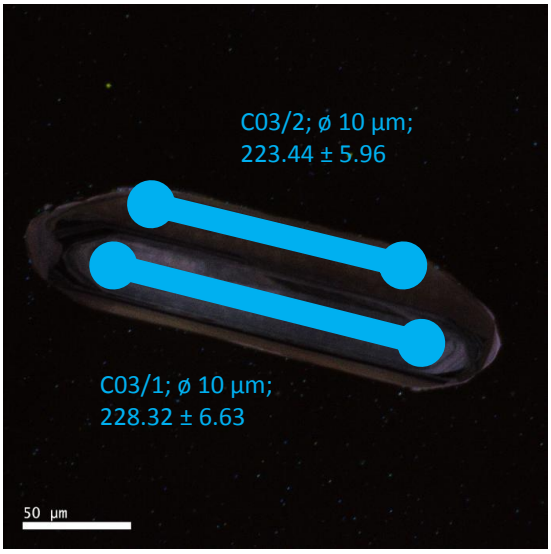
C03/2; ø 10 µm;
223.44 ± 5.96
C03/1; ø 10 µm;
228.32 ± 6.63
50 µm

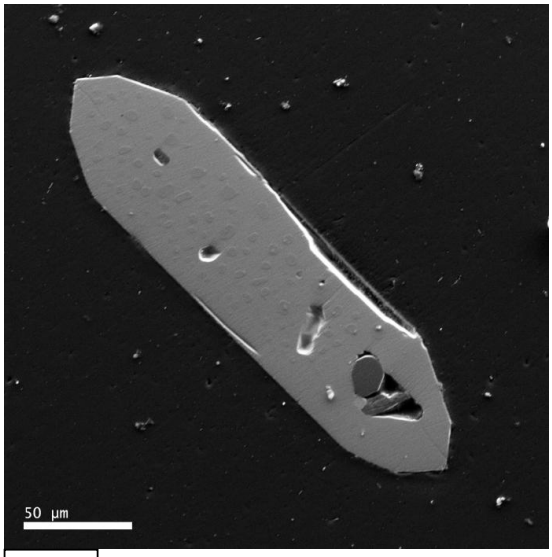
50 µm

C04

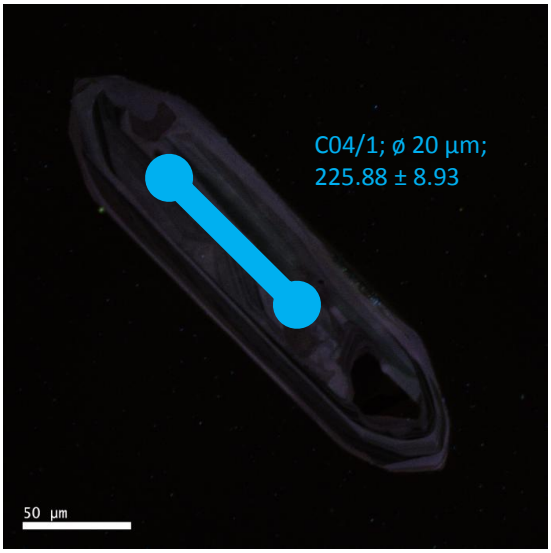
C04/1; ø 20 µm;
225.88 ± 8.93
50 µm

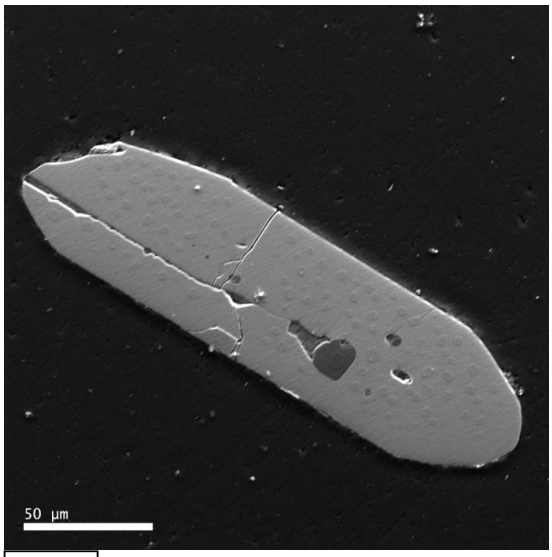
50 µm

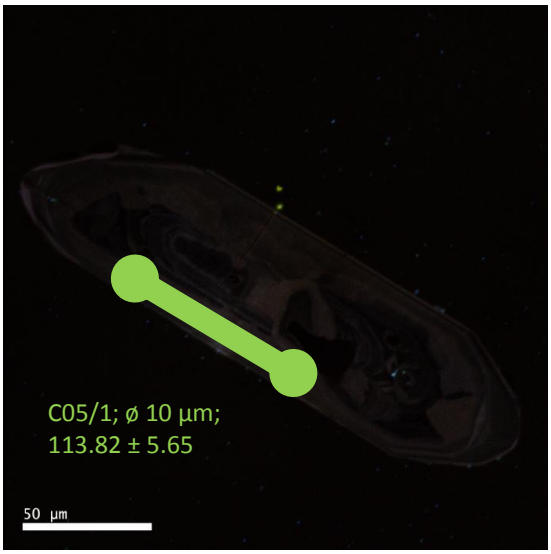
C05/1; ø 10 µm;
113.82 ± 5.65
50 µm

C05

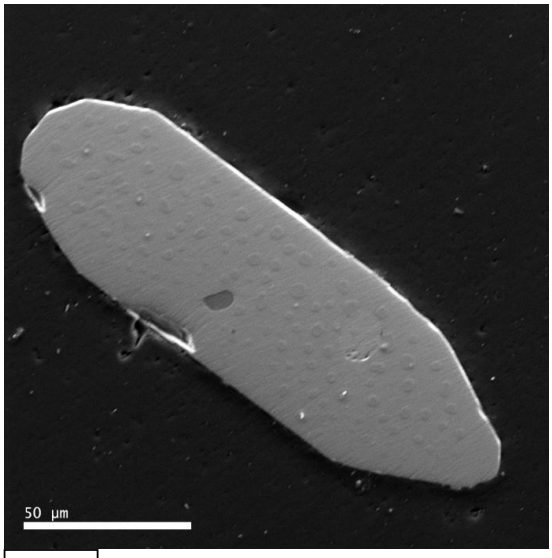
50 µm

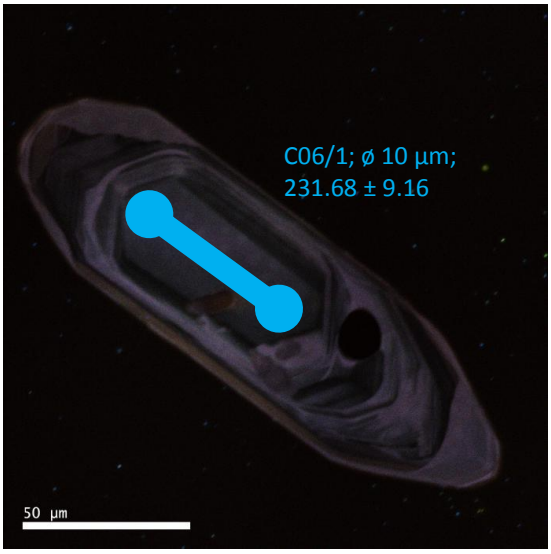
C06/1; ø 10 µm;
231.68 ± 9.16
50 µm

C06

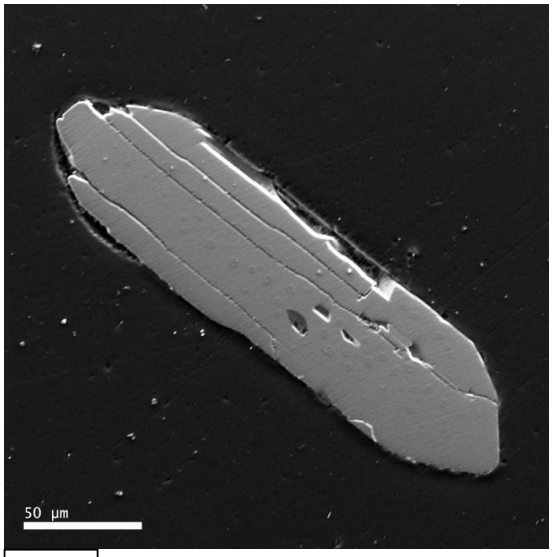
50 µm

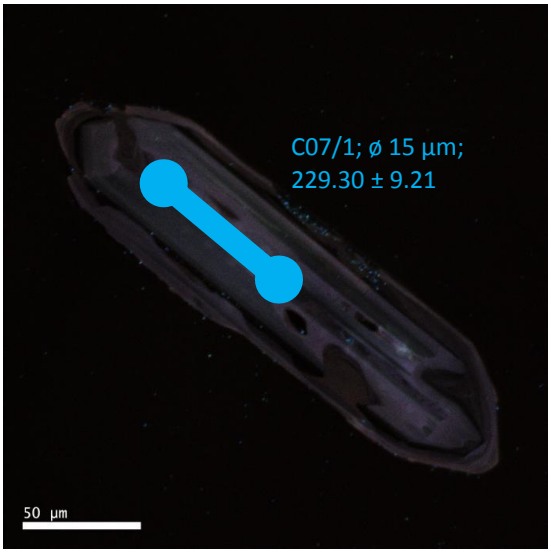
C07/1; ø 15 µm;
229.30 ± 9.21
50 µm

C07

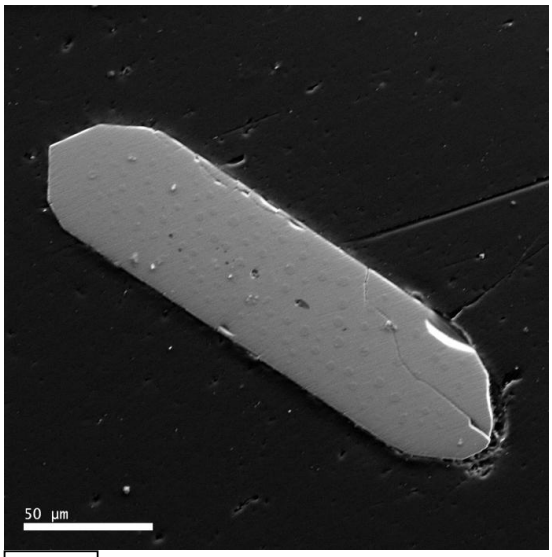
50 µm

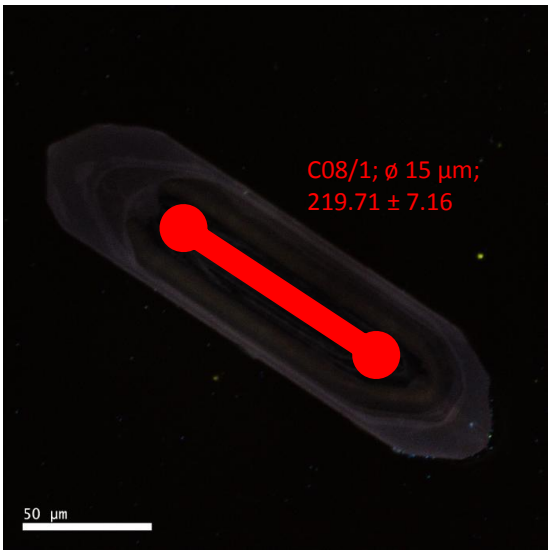
C08/1; ø 15 µm;
219.71 ± 7.16
50 µm

C08

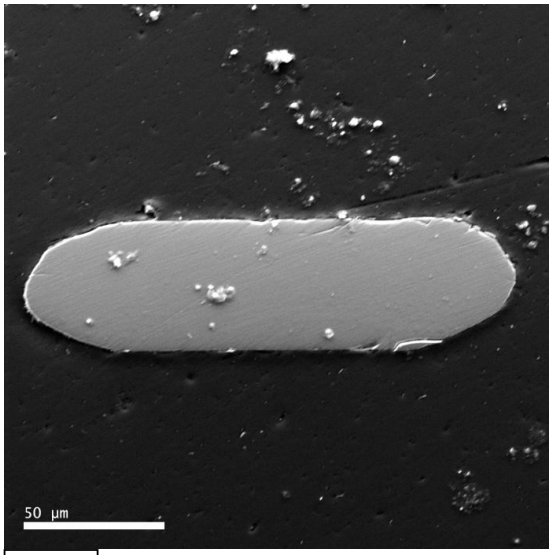
50 µm

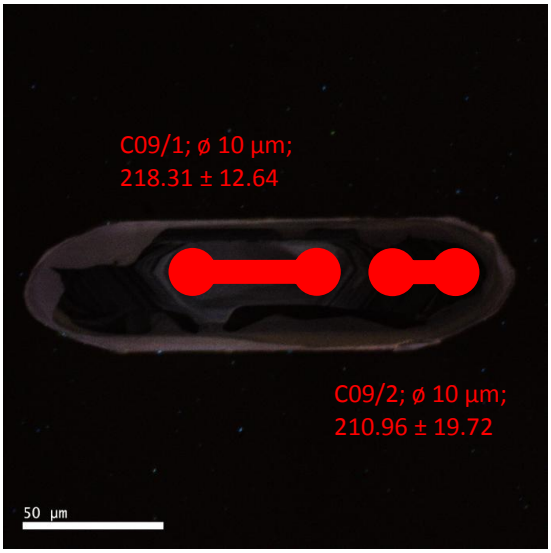
C09/1; ø 10 µm;
218.31 ± 12.64
C09/2; ø 10 µm;
210.96 ± 19.72
50 µm

C09

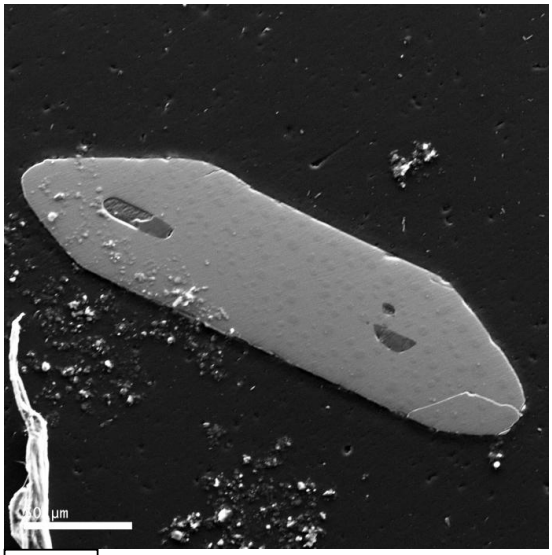
50 µm

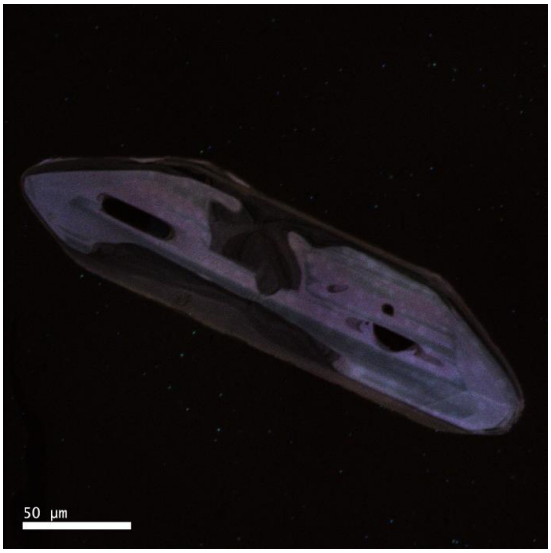
50 µm

C10

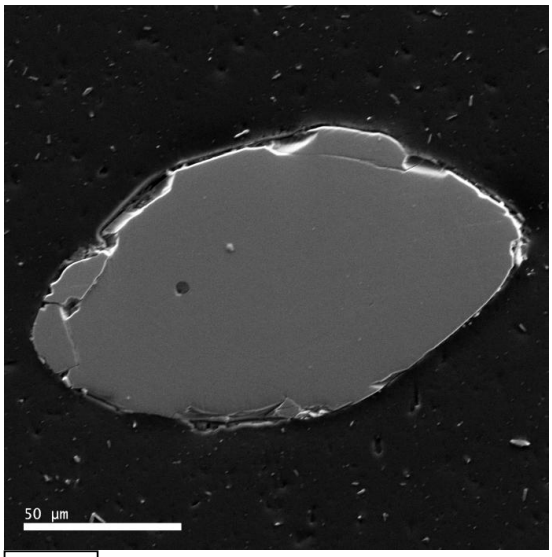
50 µm

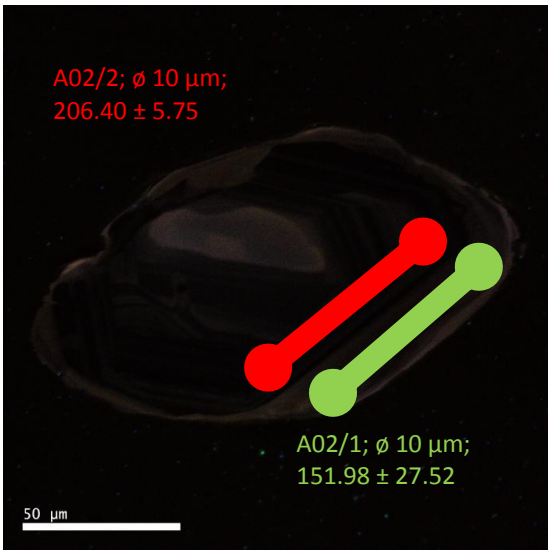
A02/2; ø 10 µm;
206.40 ± 5.75
A02/1; ø 10 µm;
151.98 ± 27.52
50 µm

A02

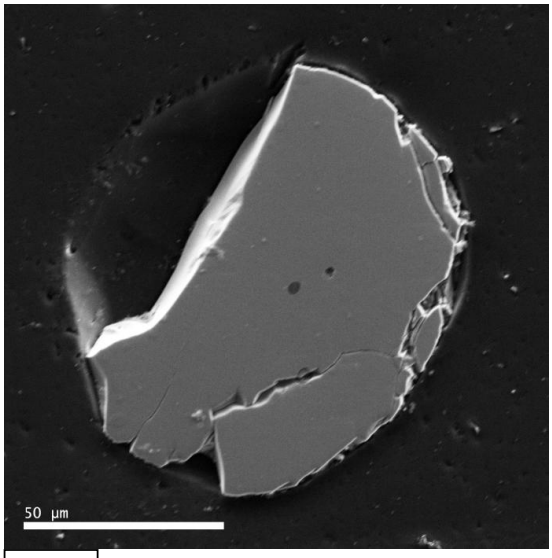
50 µm

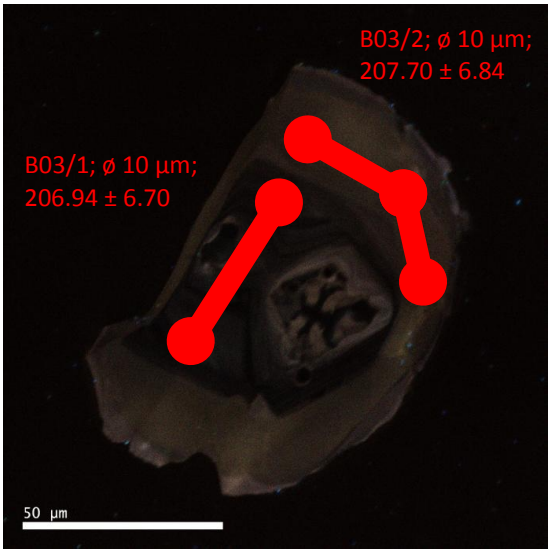
B03/2; ø 10 µm;
207.70 ± 6.84
B03/1; ø 10 µm;
206.94 ± 6.70
50 µm

B03

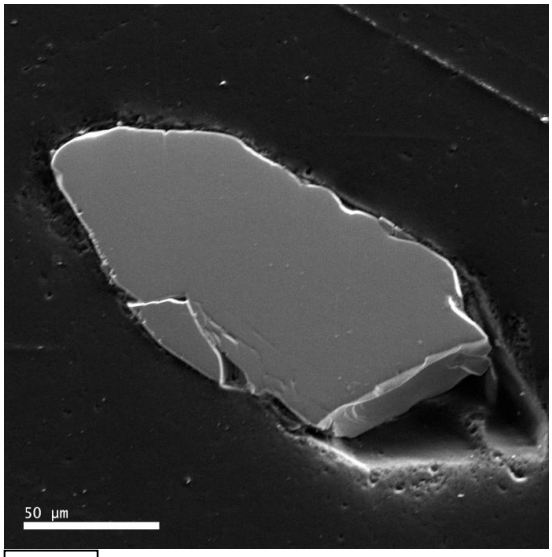
50 µm

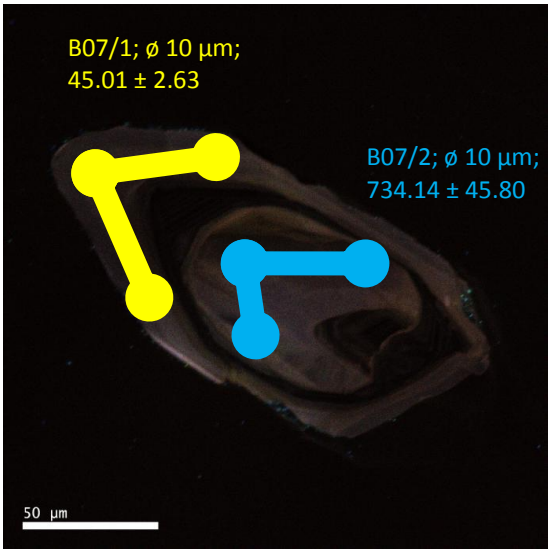
B07/1; ø 10 µm;
45.01 ± 2.63
B07/2; ø 10 µm;
734.14 ± 45.80
50 µm

B07

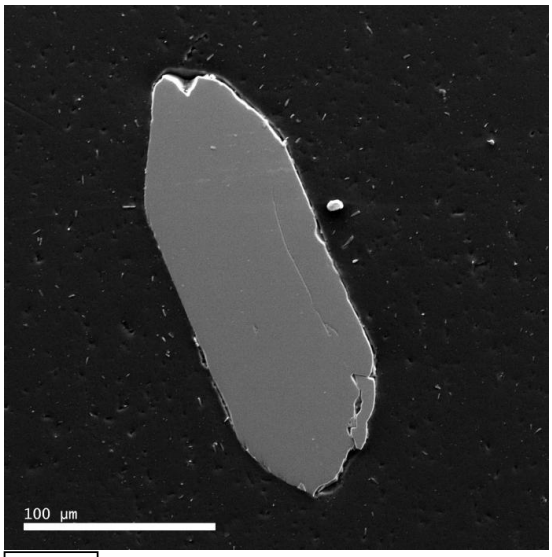
100 µm

C01

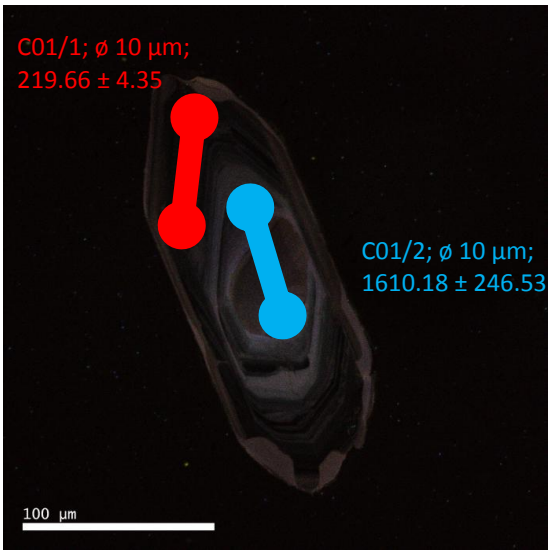
C01/1; ø 10 µm;
219.66 ± 4.35
C01/2; ø 10 µm;
1610.18 ± 246.53
100 µm

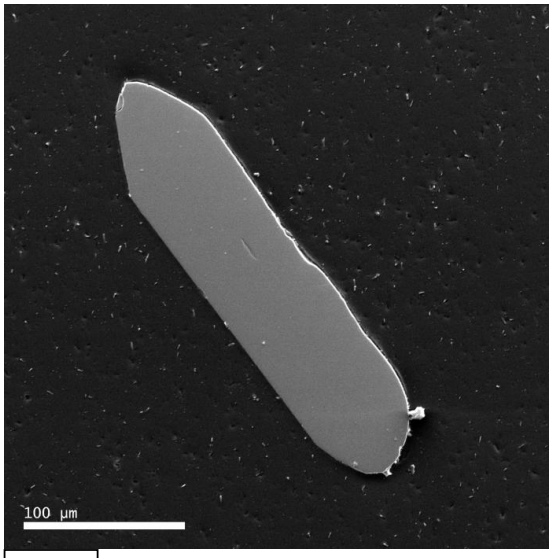
100 µm

C02

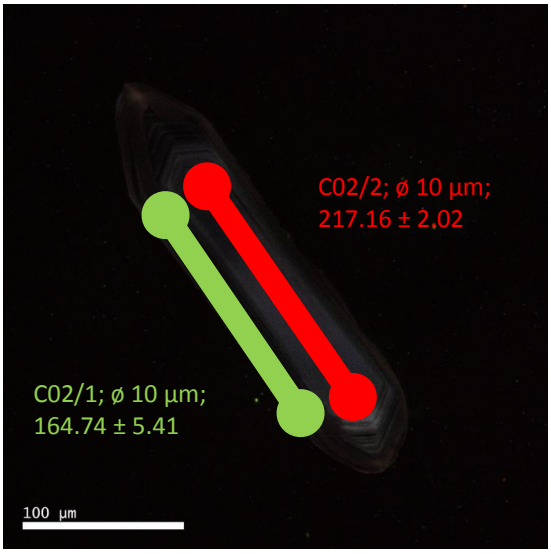
C02/2; ø 10 µm;
217.16 ± 2,02
C02/1; ø 10 µm;
164.74 ± 5.41
100 µm

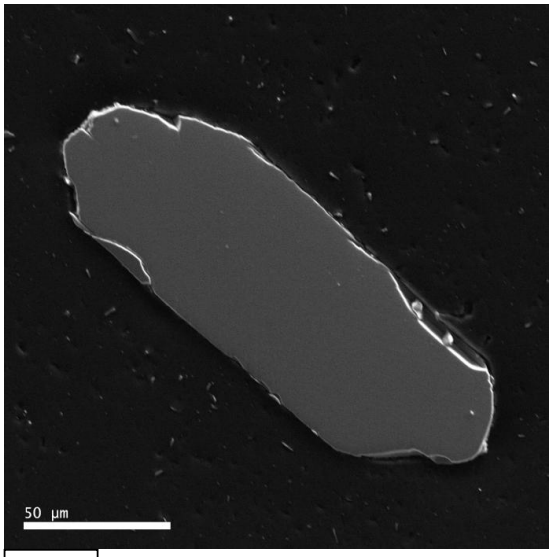
50 µm

D02

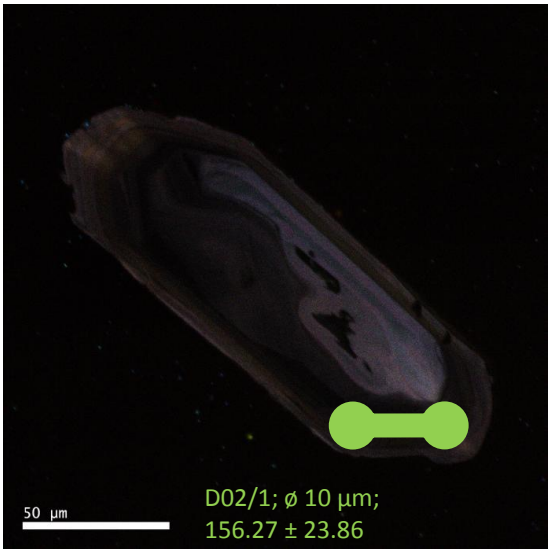
D02/1; ø 10 µm;
156.27 ± 23.86
50 µm

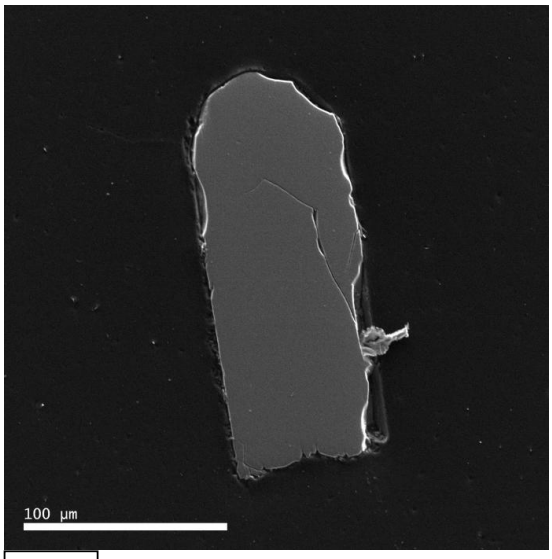
100 µm

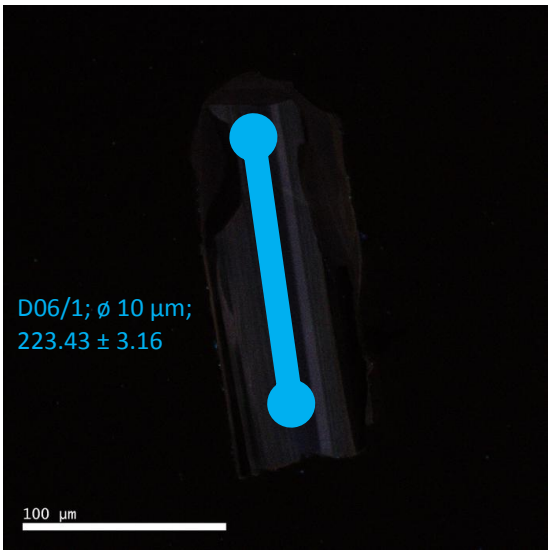
D06/1; ø 10 µm;
223.43 ± 3.16
100 µm

D06

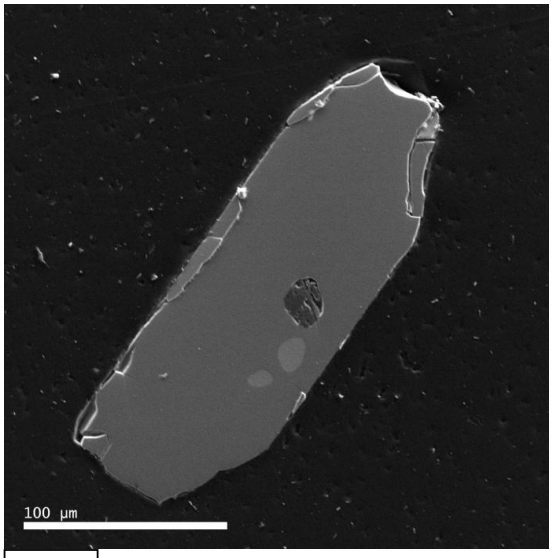
100 µm

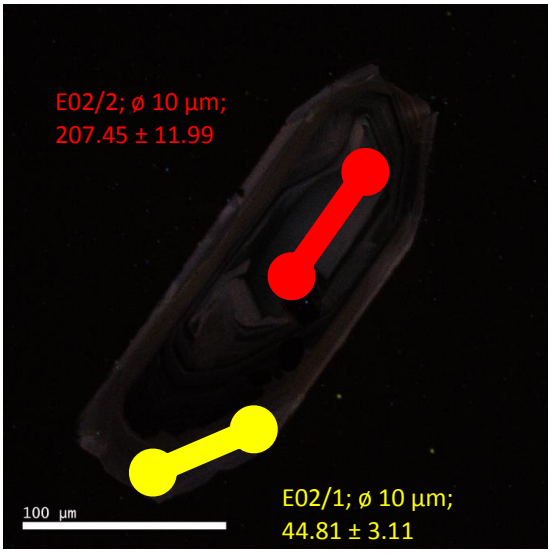
E02/2; ø 10 µm;
207.45 ± 11.99
100 µm
E02/1; ø 10 µm;
44.81 ± 3.11

E02

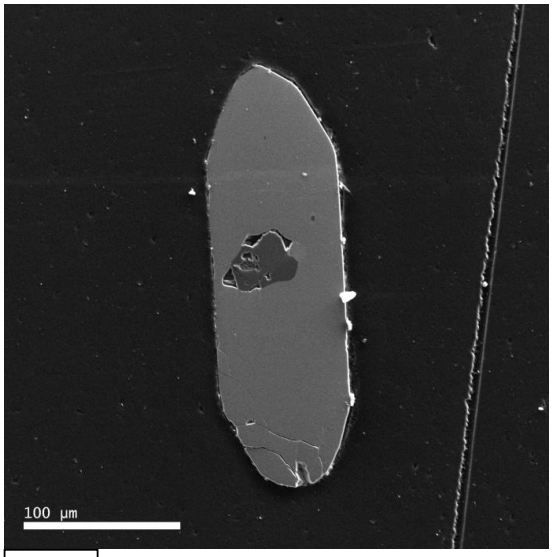
100 µm

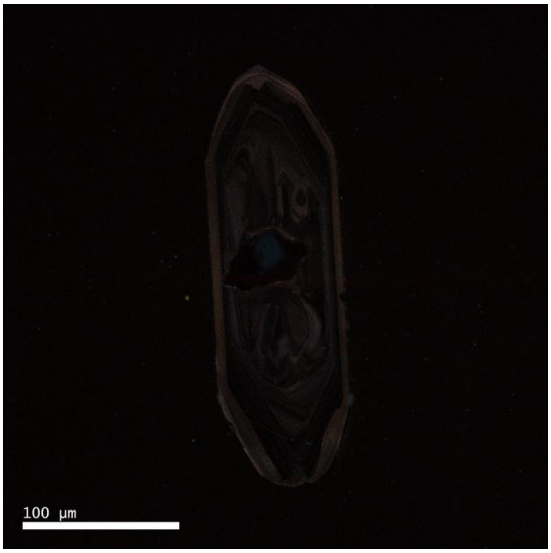
100 µm

E04

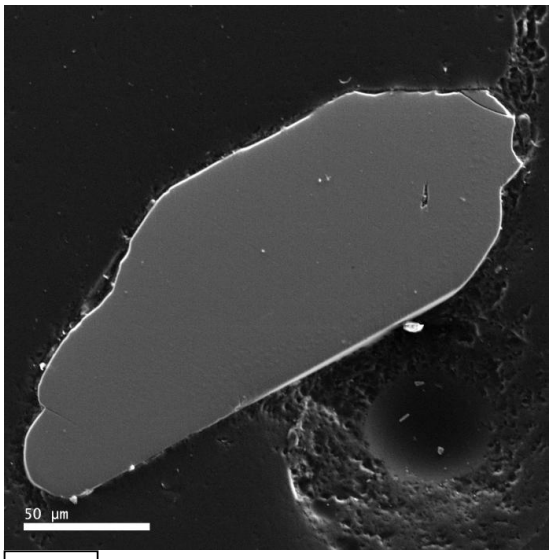
50 µm

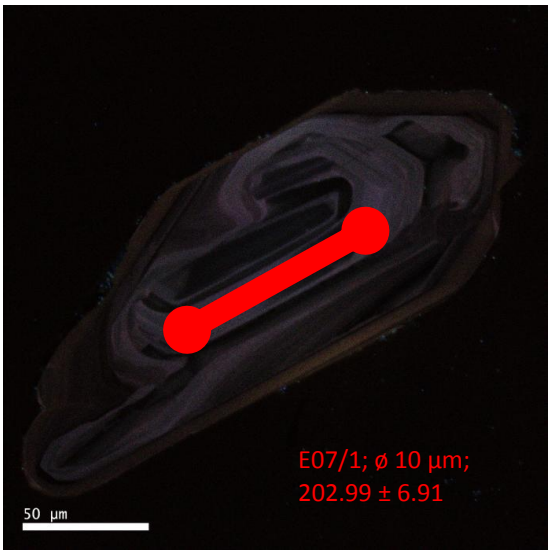
E07/1; ø 10 µm;
202.99 ± 6.91
50 µm

E07

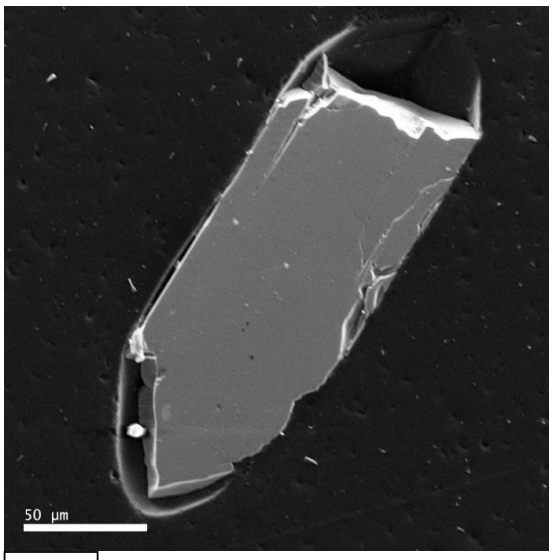
50 µm

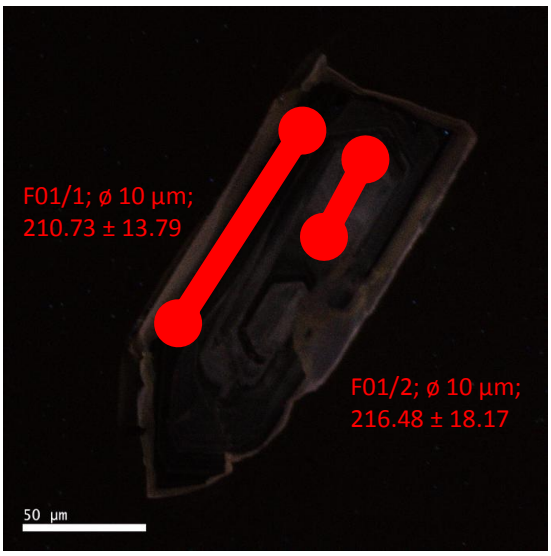
F01/1; ø 10 µm;
210.73 ± 13.79
F01/2; ø 10 µm;
216.48 ± 18.17
50 µm

F01

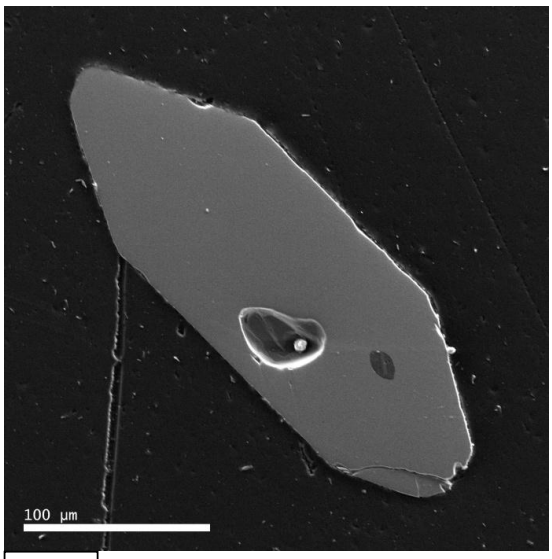
100 µm

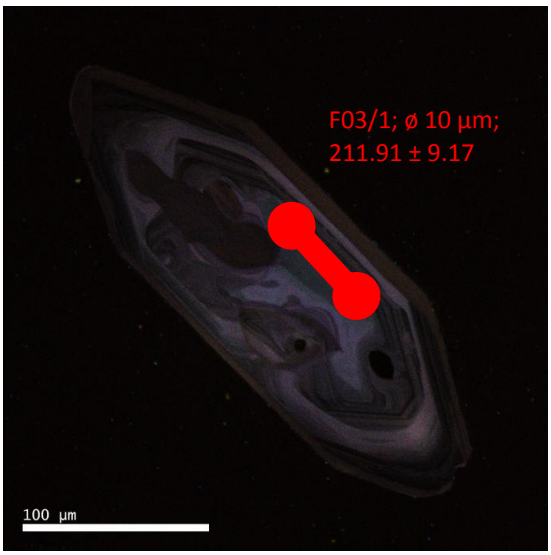
F03/1; ø 10 µm;
211.91 ± 9.17
100 µm

F03

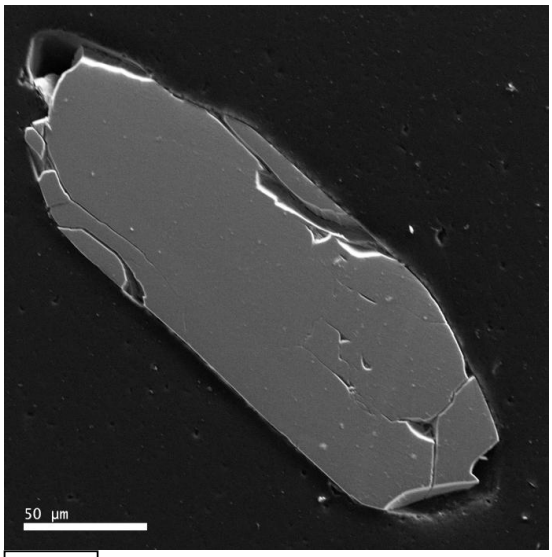
50 µm

F04

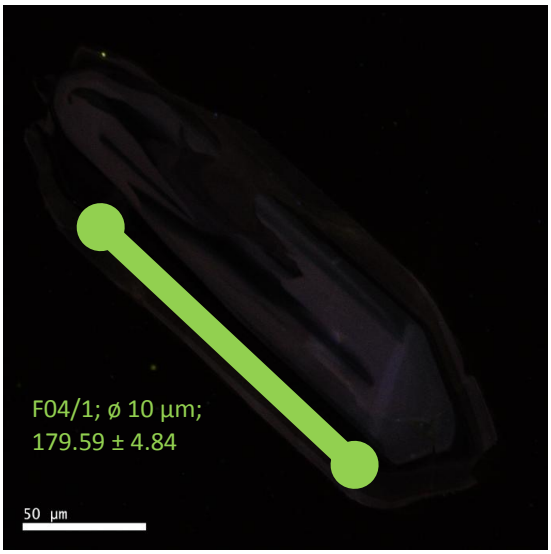
F04/1; ø 10 µm;
179.59 ± 4.84
50 µm

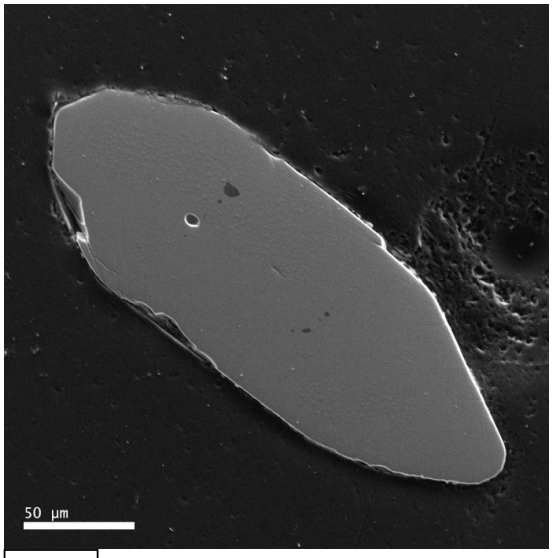
50 µm

F06

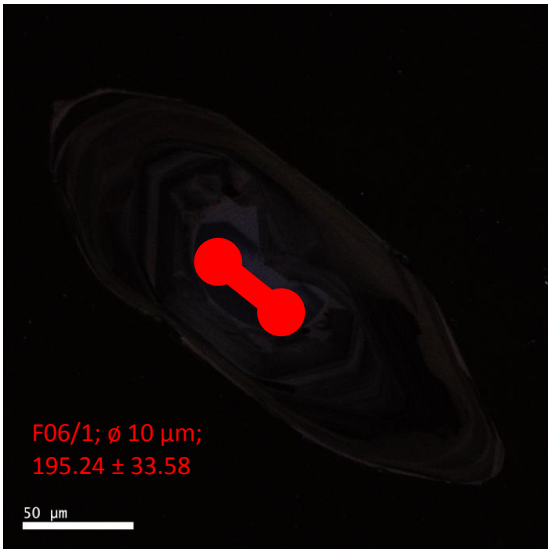
F06/1; ø 10 µm;
195.24 ± 33.58
50 µm

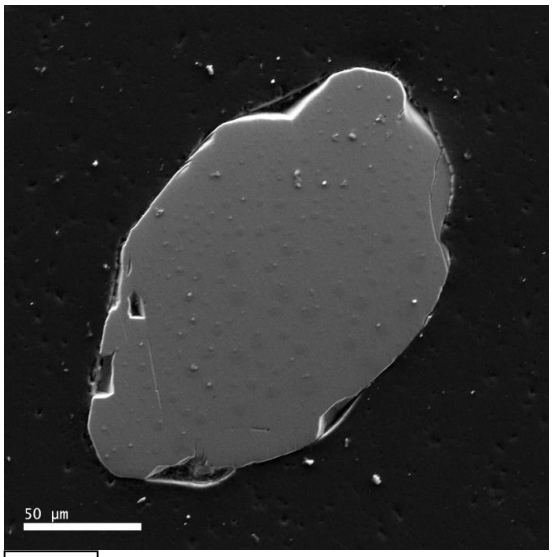
50 µm

A01

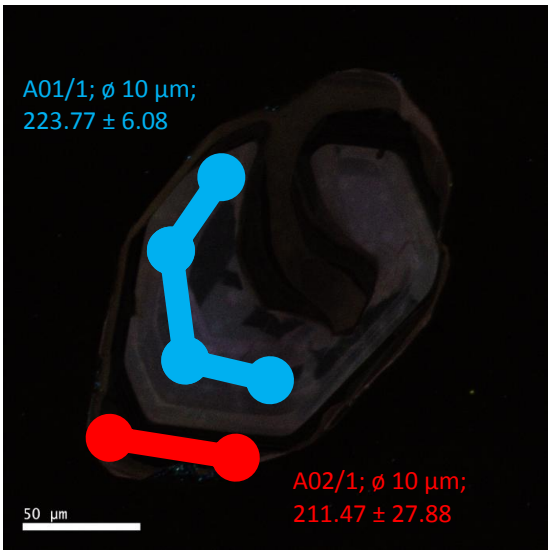
A01/1; ø 10 µm;
223.77 ± 6.08
A02/1; ø 10 µm;
211.47 ± 27.88
50 µm

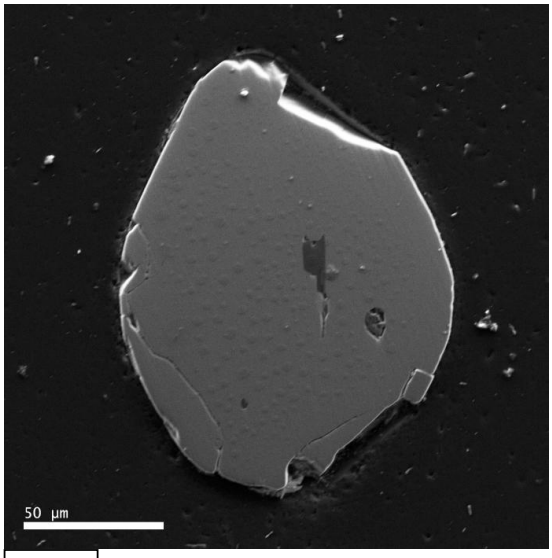
50 µm

A05

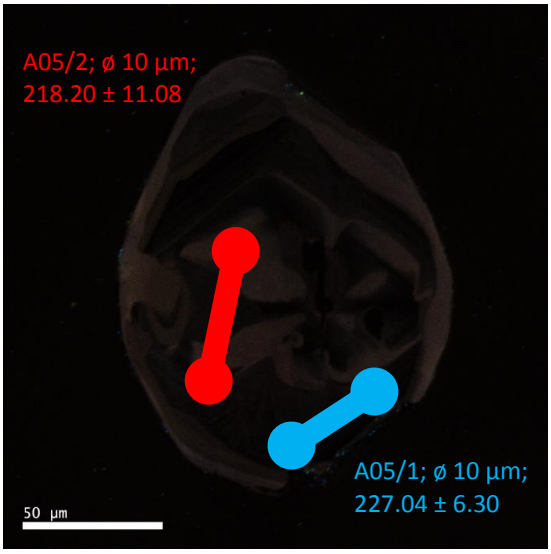
A05/2; ø 10 µm;
218.20 ± 11.08
A05/1; ø 10 µm;
227.04 ± 6.30
50 µm

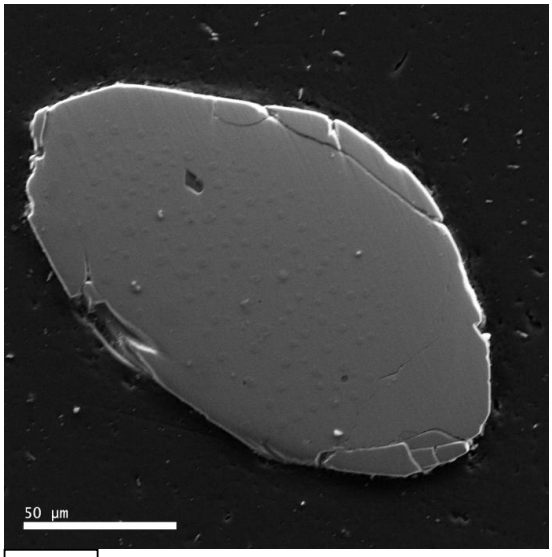
50 µm

A06

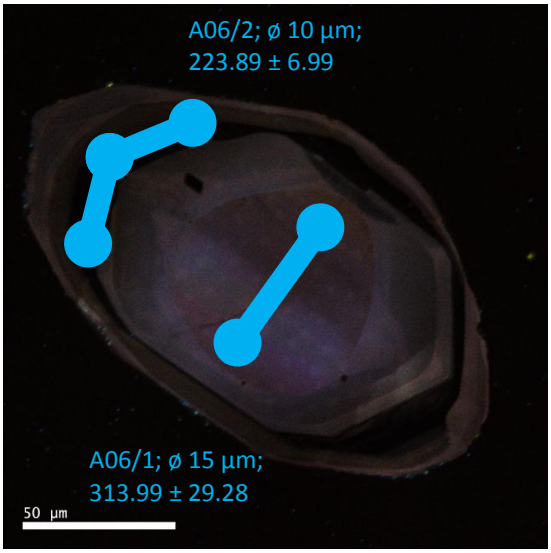
A06/2; ø 10 µm;
223.89 ± 6.99
A06/1; ø 15 µm;
313.99 ± 29.28
50 µm

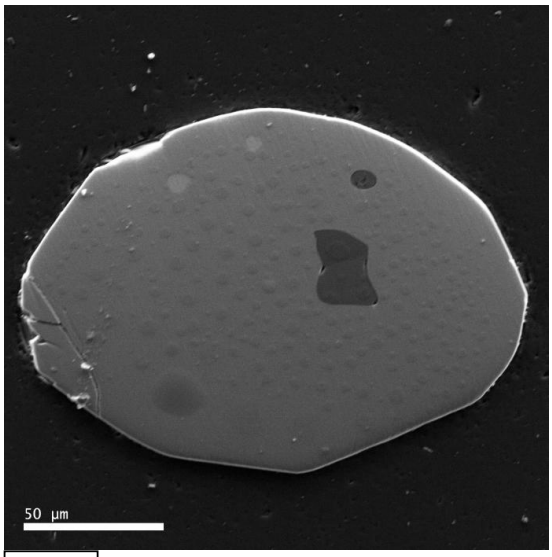
50 µm

A07

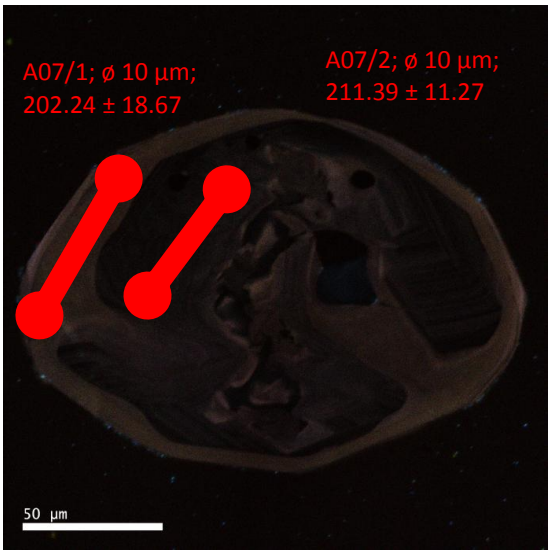
A07/1; ø 10 µm;
202.24 ± 18.67
A07/2; ø 10 µm;
211.39 ± 11.27
50 µm

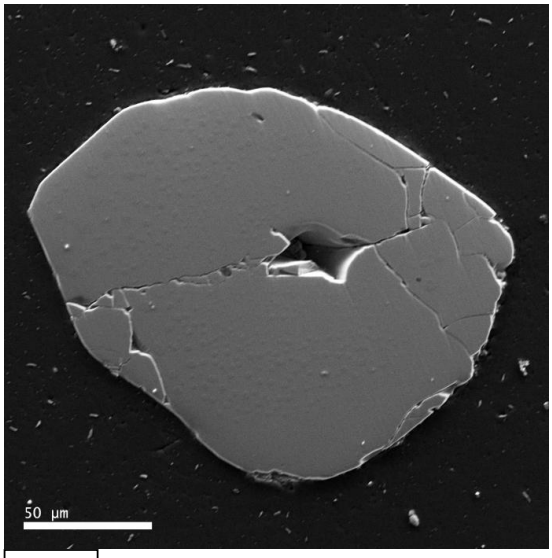
50 µm

A10

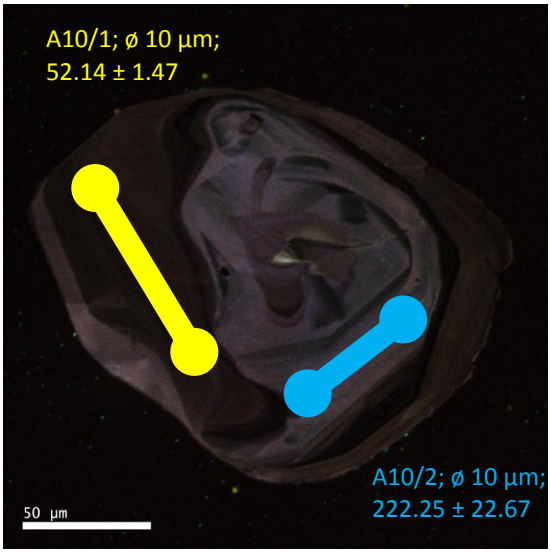
A10/1; ø 10 µm;
52.14 ± 1.47
A10/2; ø 10 µm;
222.25 ± 22.67
50 µm

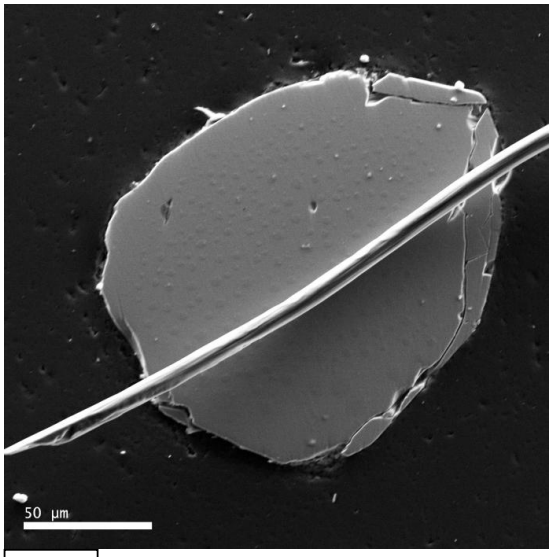
50 µm

B02

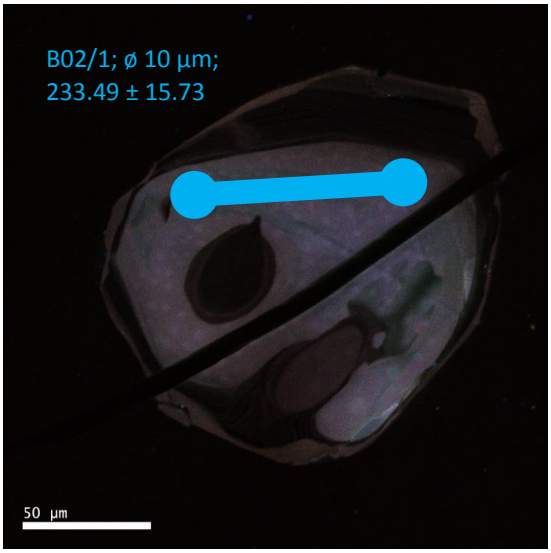
B02/1; ø 10 µm;
233.49 ± 15.73
50 µm

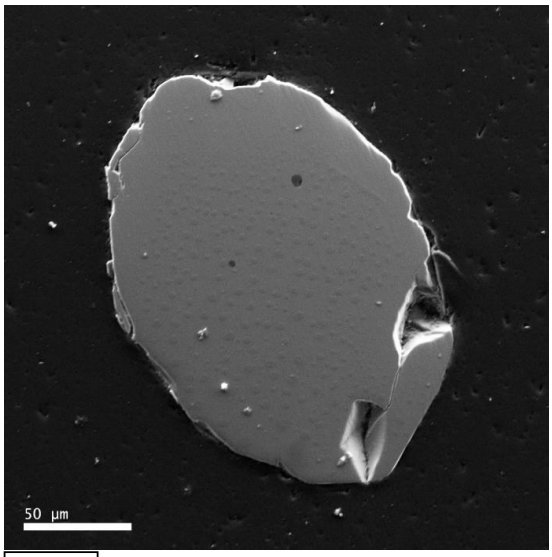
50 µm

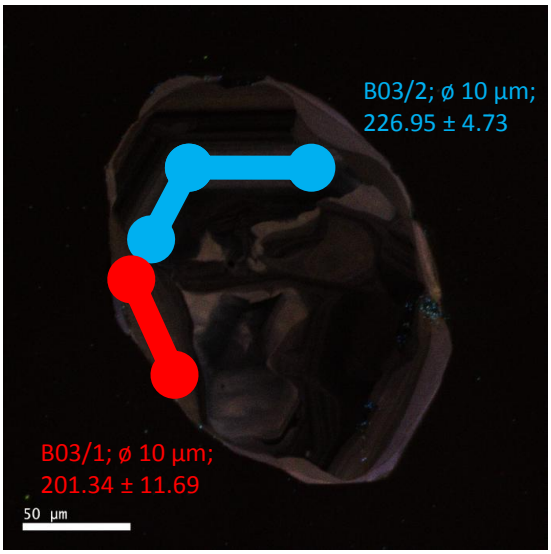
B03/2; ø 10 µm;
226.95 ± 4.73
B03/1; ø 10 µm;
201.34 ± 11.69
50 µm

B03

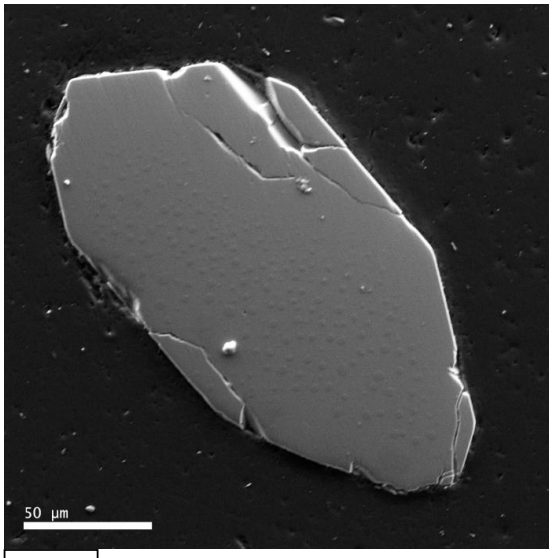
50 µm

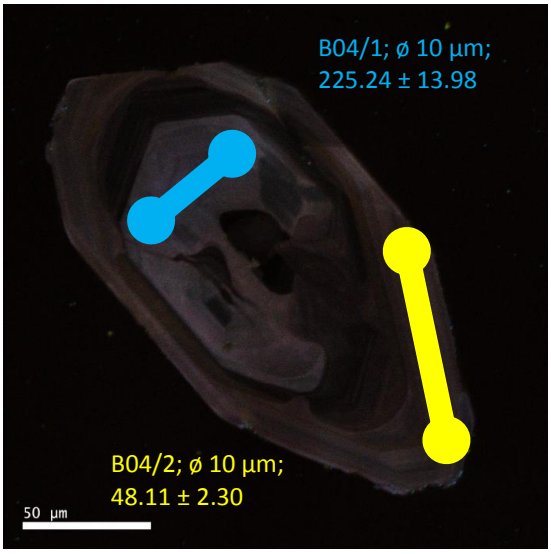
B04/1; ø 10 µm;
225.24 ± 13.98
B04/2; ø 10 µm;
48.11 ± 2.30
50 µm

B04

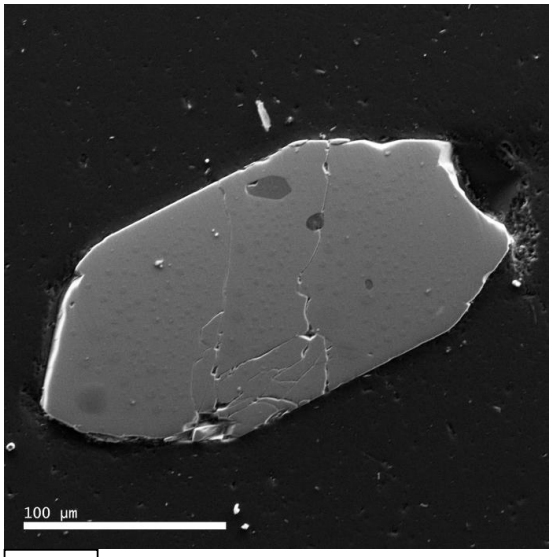
100 µm

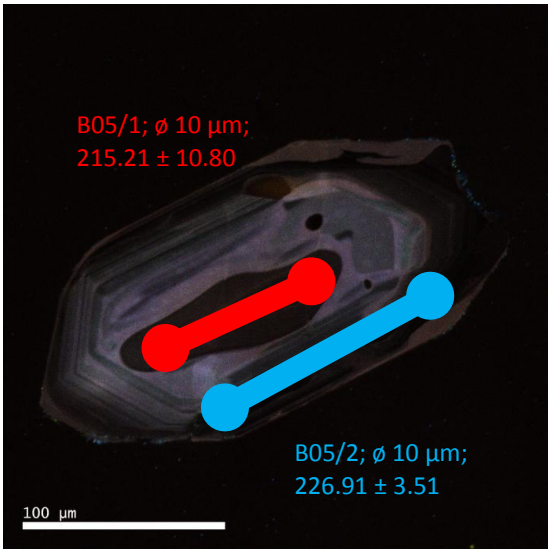
B05/1; ø 10 µm;
215.21 ± 10.80
B05/2; ø 10 µm;
226.91 ± 3.51
100 µm

B05

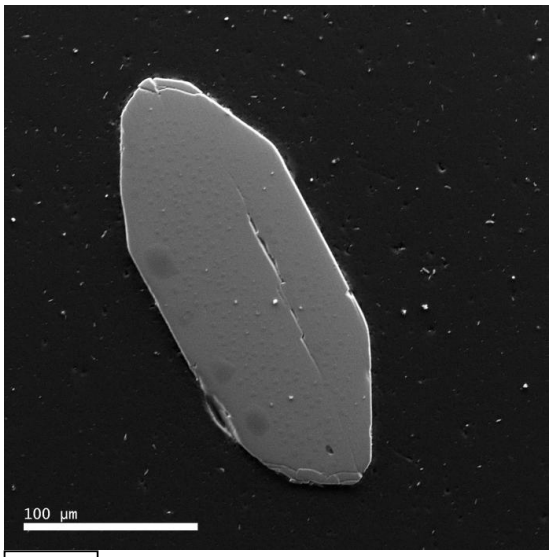
100 µm

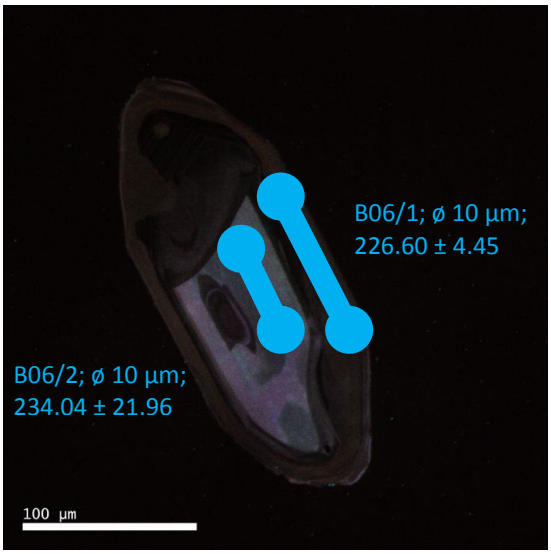
B06/1; ø 10 µm;
226.60 ± 4.45
B06/2; ø 10 µm;
234.04 ± 21.96
100 µm

B06

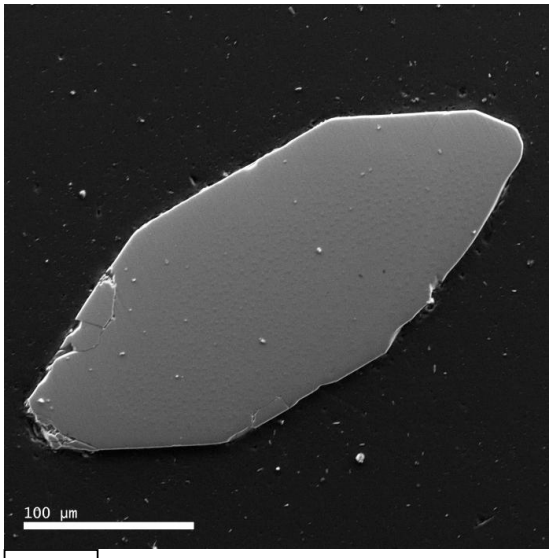
100 µm

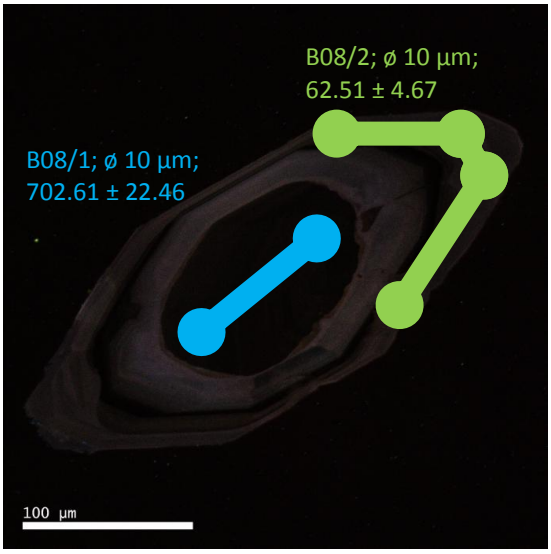
B08/2; ø 10 µm;
62.51 ± 4.67
B08/1; ø 10 µm;
702.61 ± 22.46
100 µm

B08

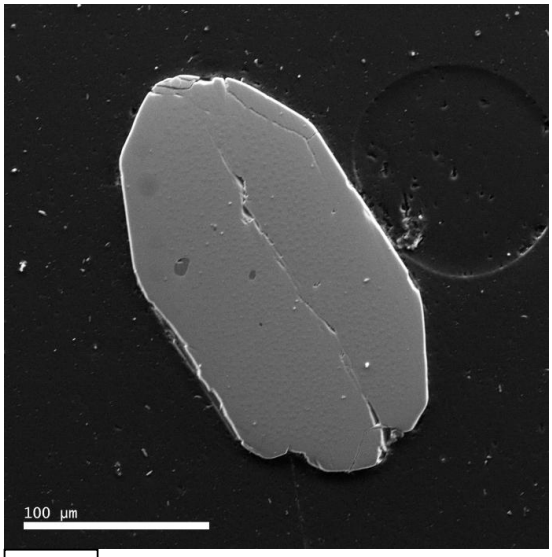
100 µm

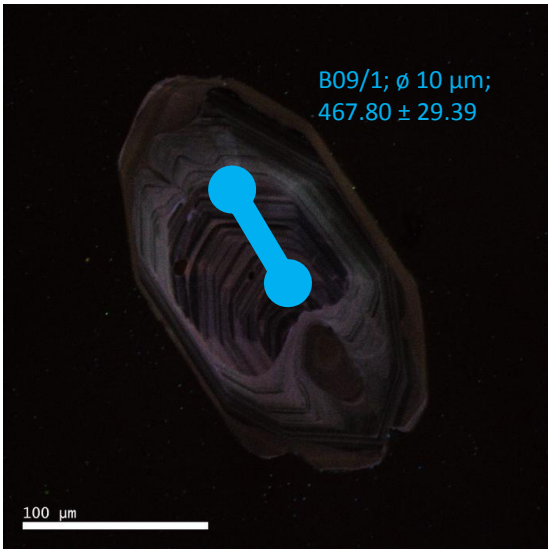
B09/1; ø 10 µm;
467.80 ± 29.39
100 µm

B09

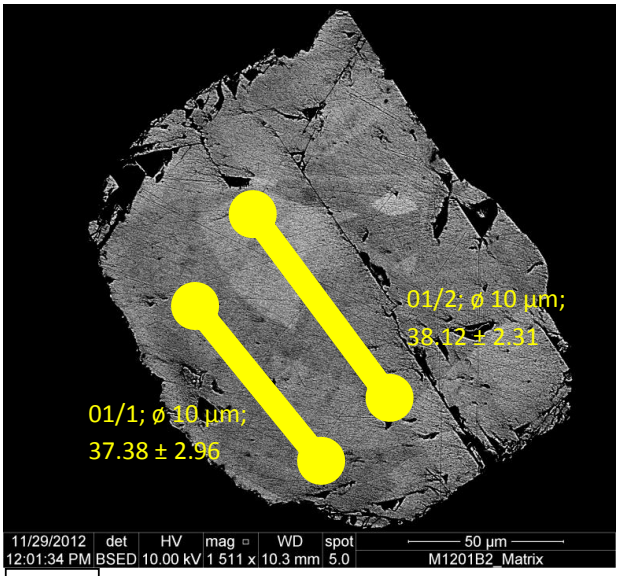
01/2; ø 10 µm;
38.12 ± 2.31
01/1; ø 10 µm;
37.38 ± 2.96
11/29/2012 det HV mag WD spot 50 µm
12:01:34 PM BSED 10.00 kV 1 511 x 10.3 mm 5.0 M1201B2_Matrix

01

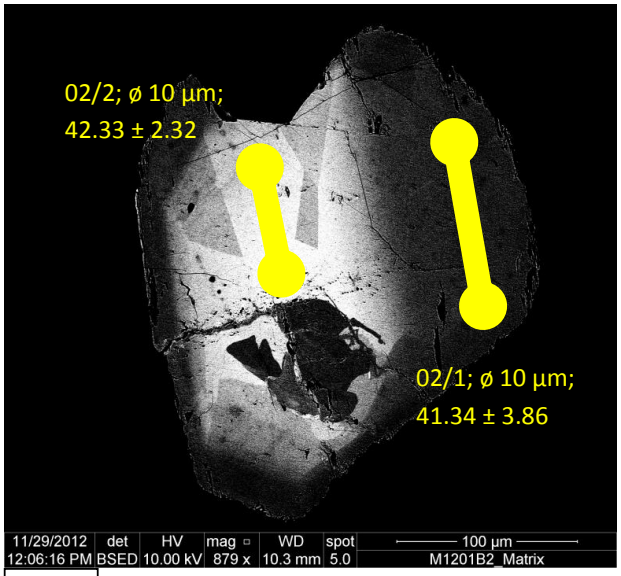
02/2; ø 10 µm;
42.33 ± 2.32
02/1; ø 10 µm;
41.34 ± 3.86
11/29/2012 det HV mag WD spot 100 µm
12:06:16 PM BSED 10.00 kV 879 x 10.3 mm 5.0 M1201B2_Matrix

02

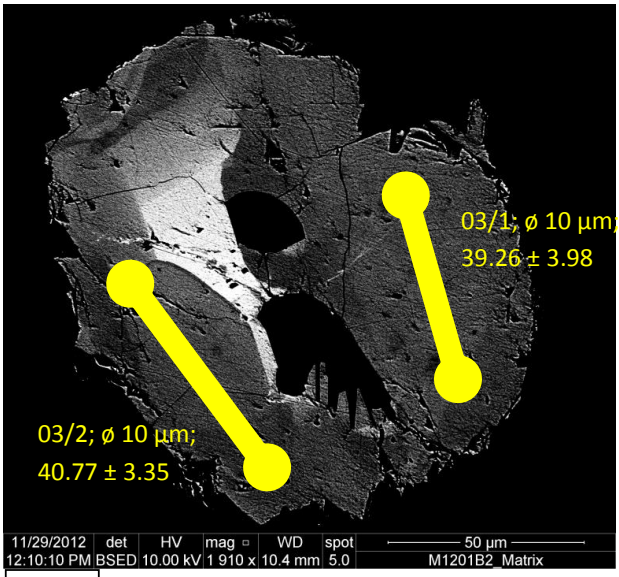
03/1; ø 10 µm;
39.26 ± 3.98
03/2; ø 10 µm;
40.77 ± 3.35
11/29/2012 det HV mag WD spot 50 µm
12:10:10 PM BSED 10.00 kV 1 910 x 10.4 mm 5.0 M1201B2_Matrix

03

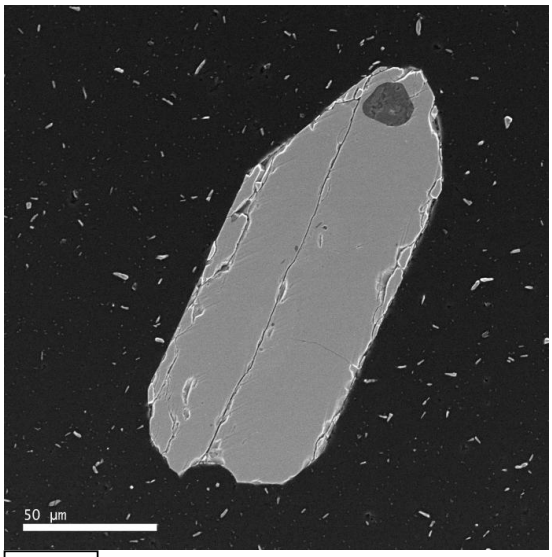
50 µm

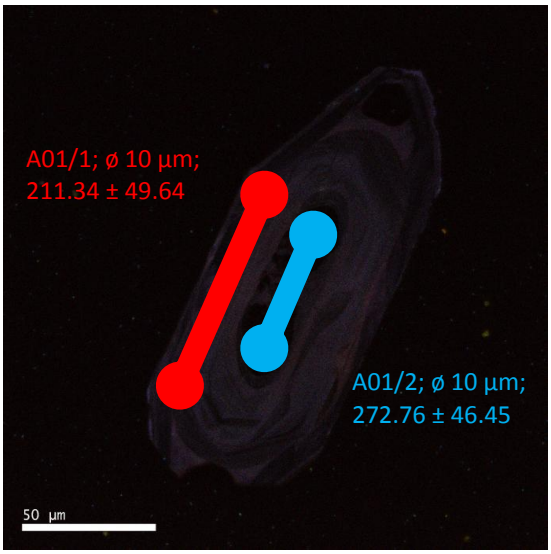
A01/1; ø 10 µm;
211.34 ± 49.64
A01/2; ø 10 µm;
272.76 ± 46.45
50 µm

A01

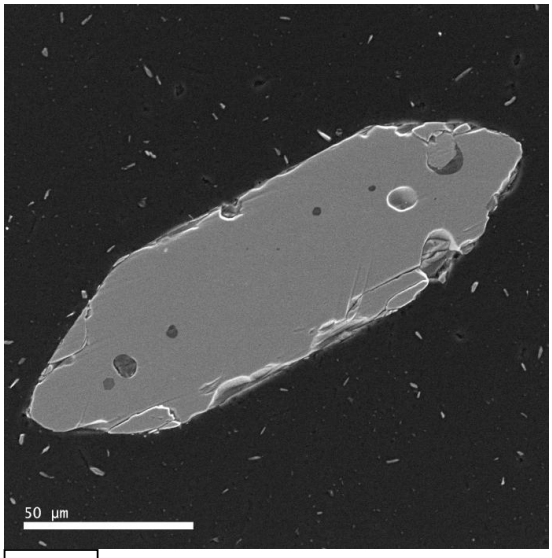
50 µm

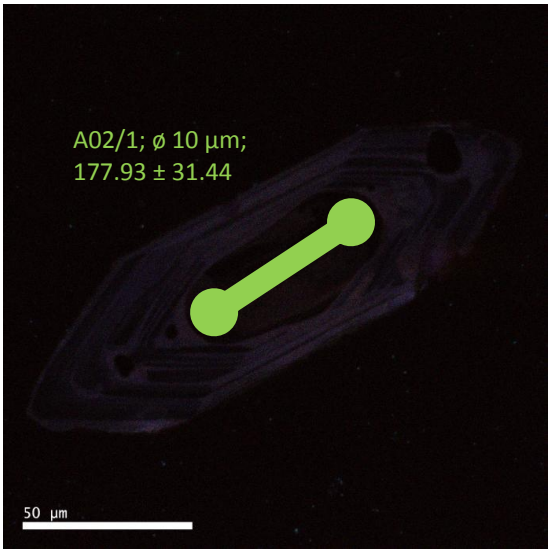
A02/1; ø 10 µm;
177.93 ± 31.44
50 µm

A02

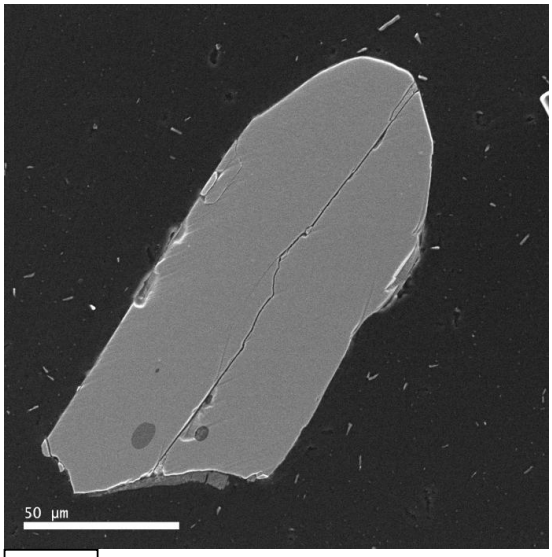
50 µm

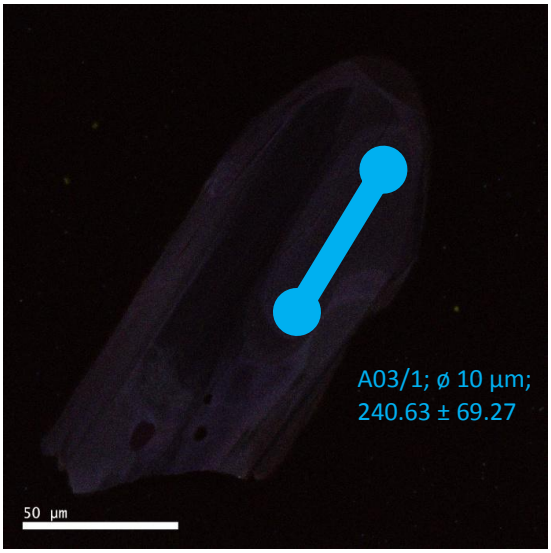
A03/1; ø 10 µm;
240.63 ± 69.27
50 µm

A03

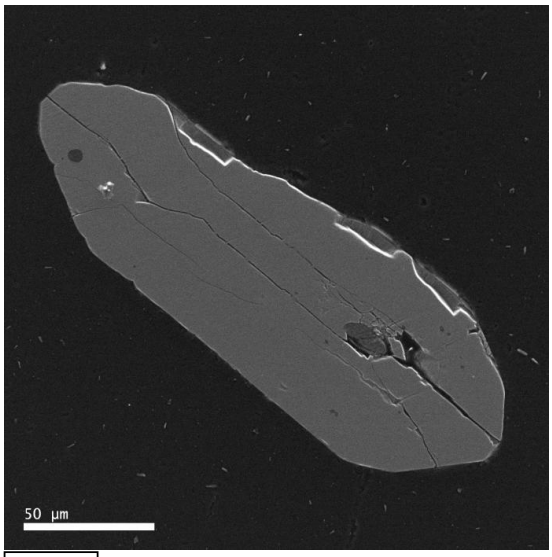
50 µm

A04

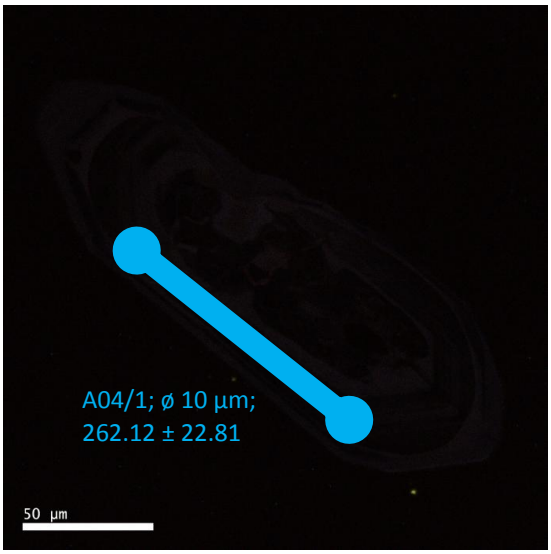
A04/1; ø 10 µm;
262.12 ± 22.81
50 µm

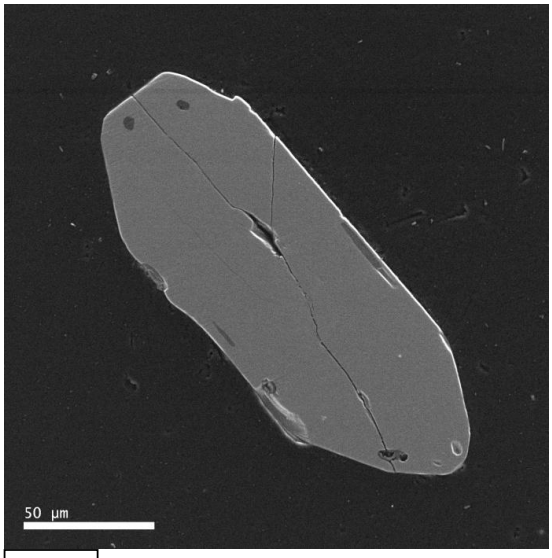
50 µm

A05

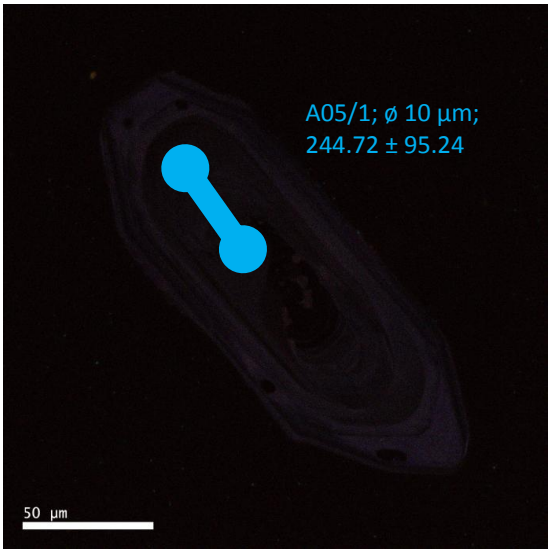
A05/1; ø 10 µm;
244.72 ± 95.24
50 µm

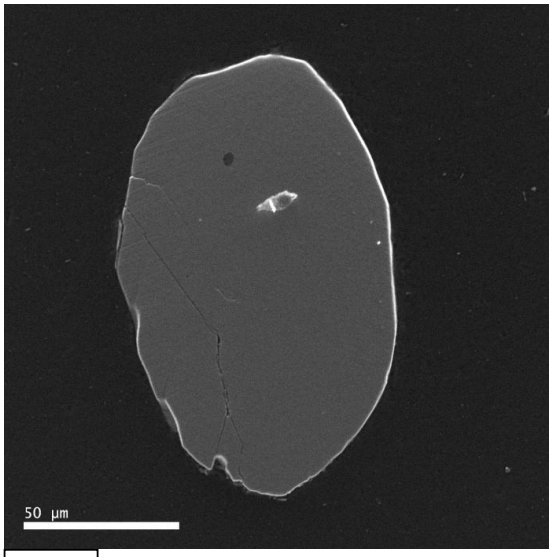
50 µm

A06

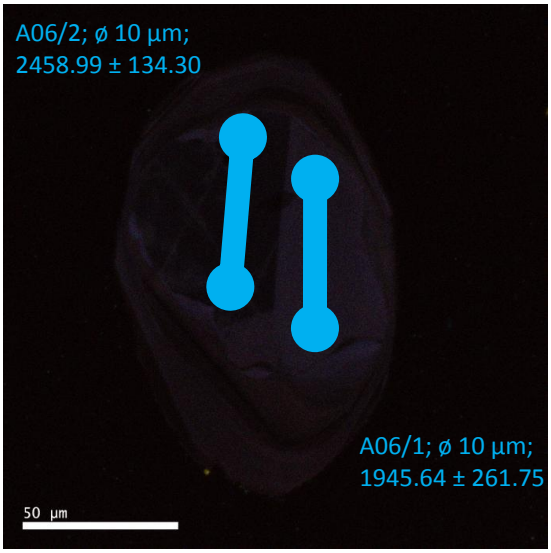
A06/2; ø 10 µm;
2458.99 ± 134.30
A06/1; ø 10 µm;
1945.64 ± 261.75
50 µm

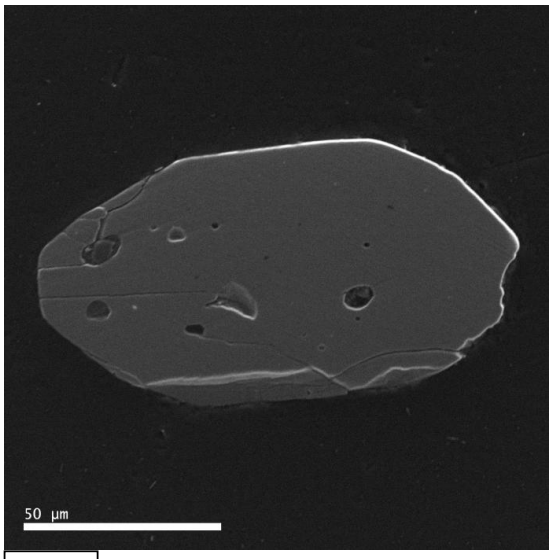
50 µm

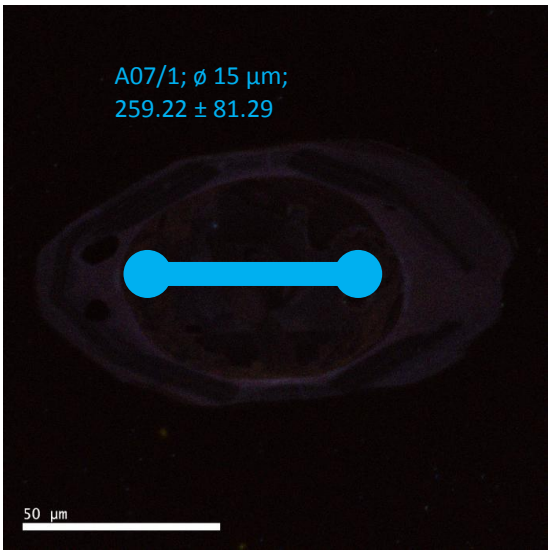
A07/1; ø 15 µm;
259.22 ± 81.29
50 µm

A07

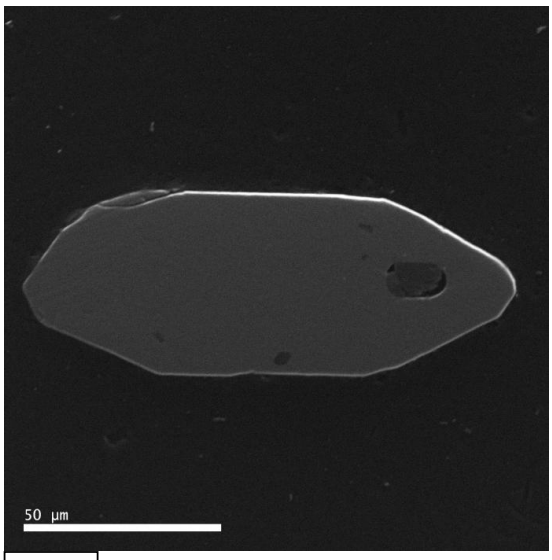
50 µm

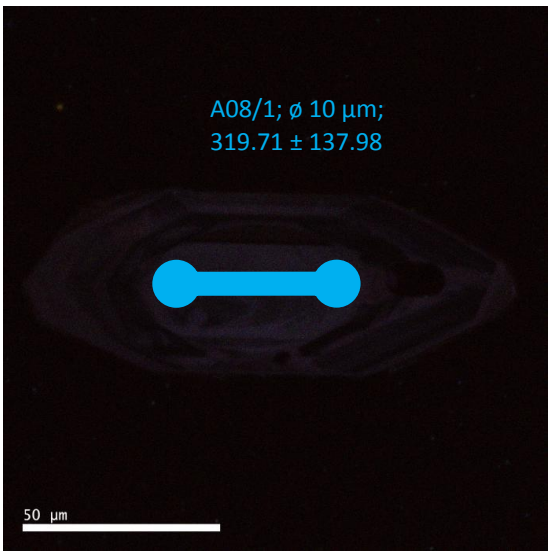
A08/1; ø 10 µm;
319.71 ± 137.98
50 µm

A09

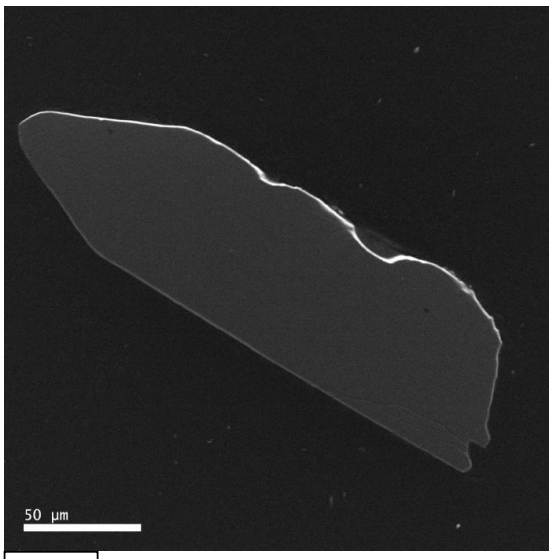
50 µm

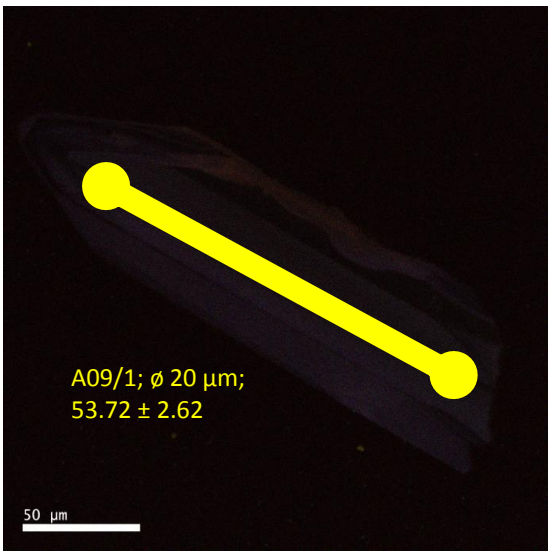
A09/1; ø 20 µm;
53.72 ± 2.62
50 µm

A09

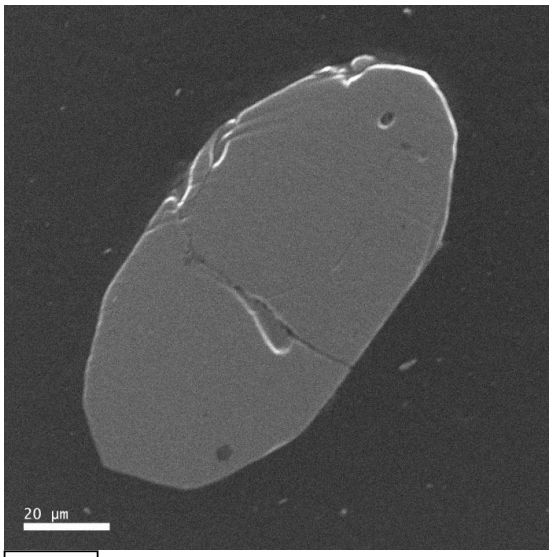
20 µm

A10

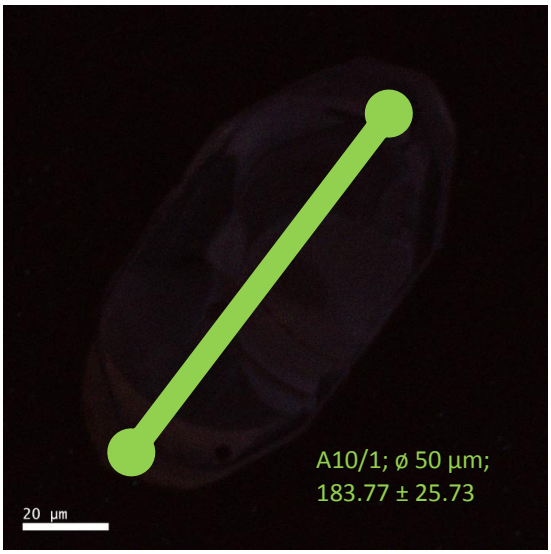
A10/1; ø 50 µm;
183.77 ± 25.73
20 µm

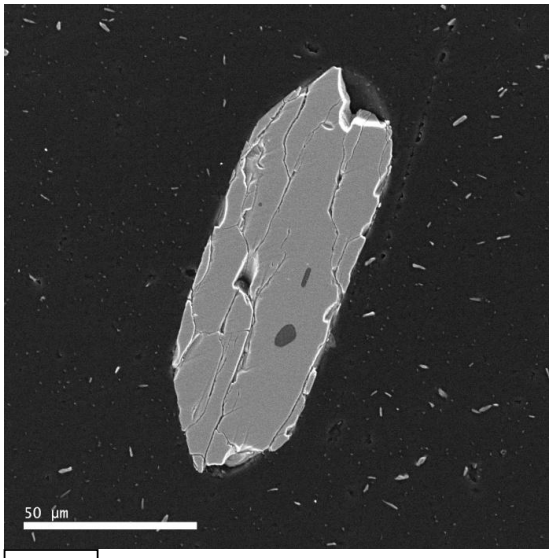
50 µm

B01

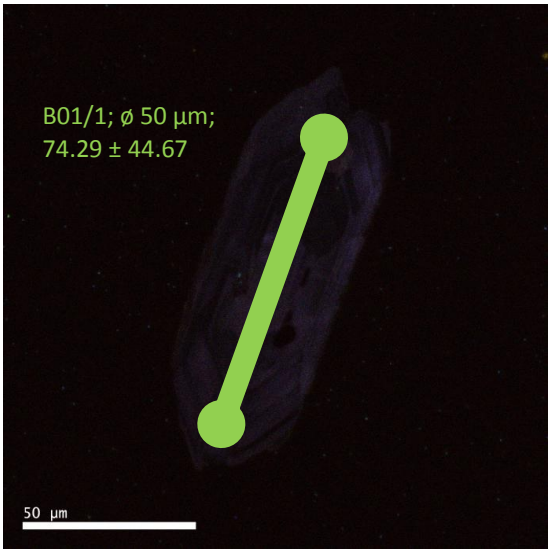
B01/1; ø 50 µm;
74.29 ± 44.67
50 µm

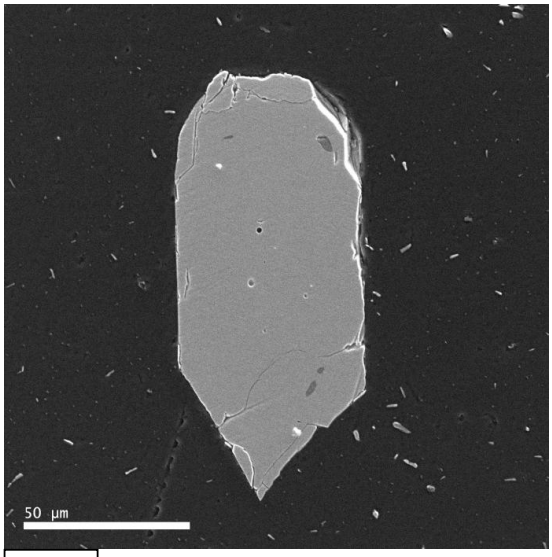
50 µm

B02

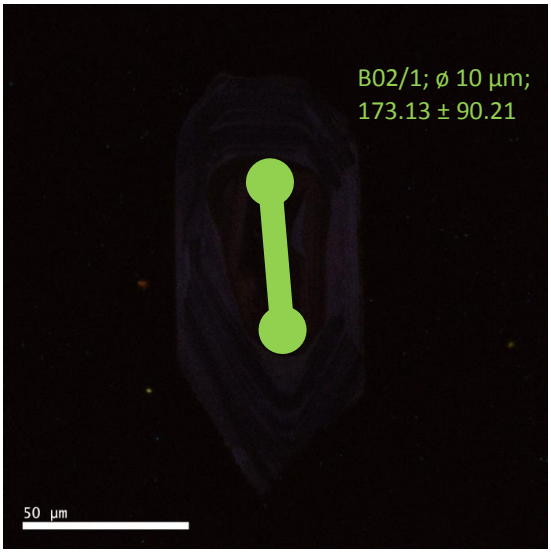
B02/1; ø 10 µm;
173.13 ± 90.21
50 µm

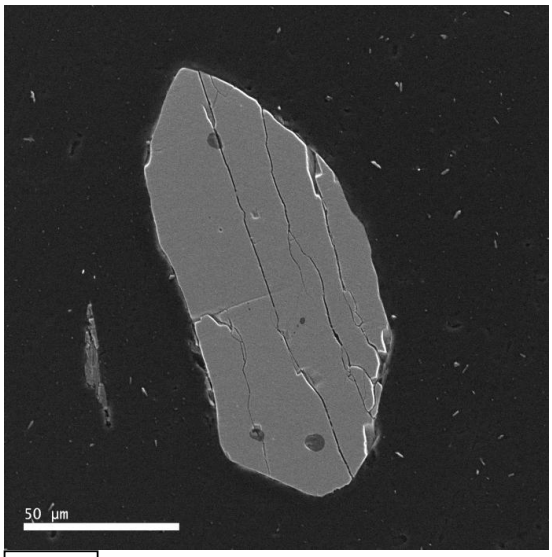
50 µm

B03

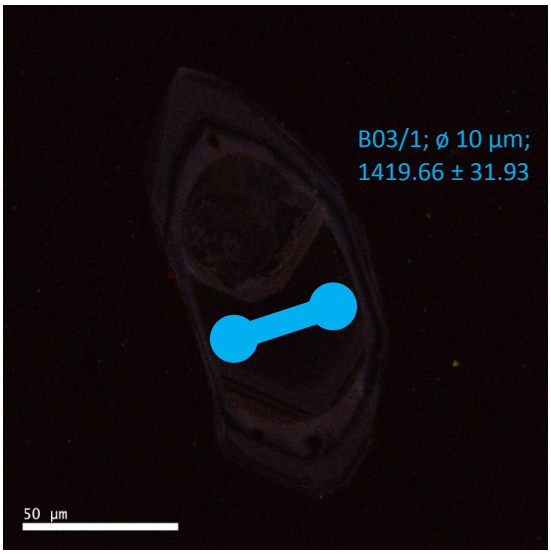
B03/1; ø 10 µm;
1419.66 ± 31.93
50 µm

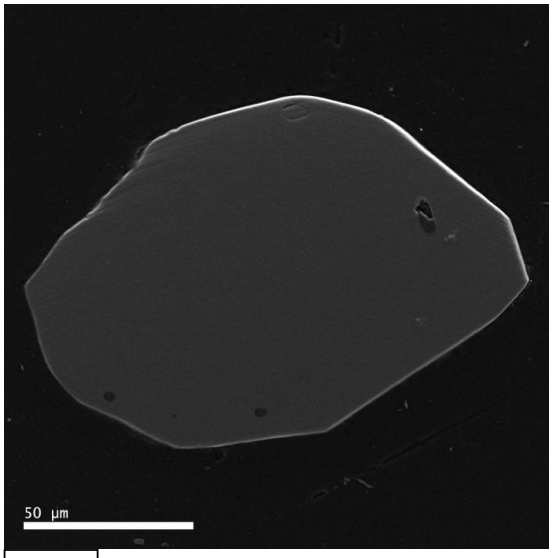
50 µm

B04

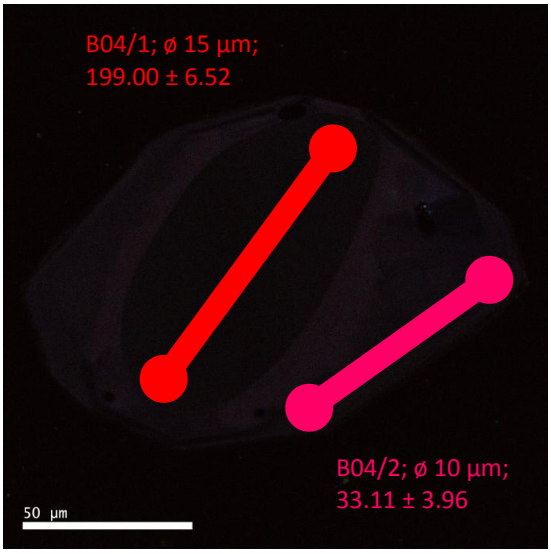
B04/1; ø 15 µm;
199.00 ± 6.52
B04/2; ø 10 µm;
33.11 ± 3.96
50 µm

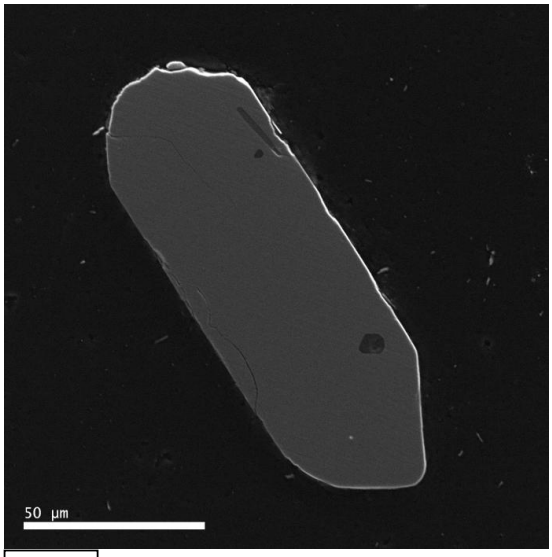
50 µm

C01

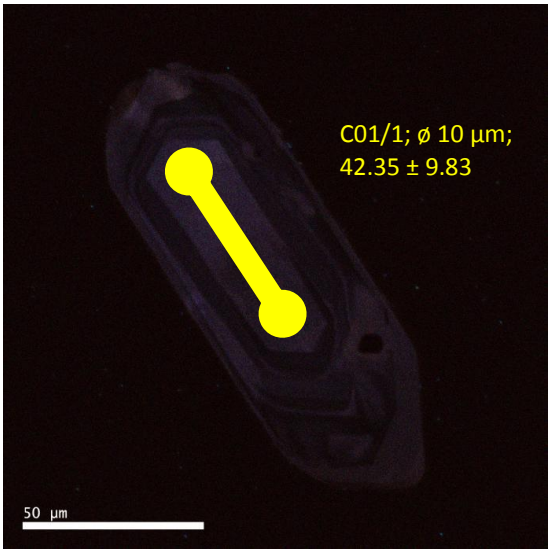
C01/1; ø 10 µm;
42.35 ± 9.83
50 µm

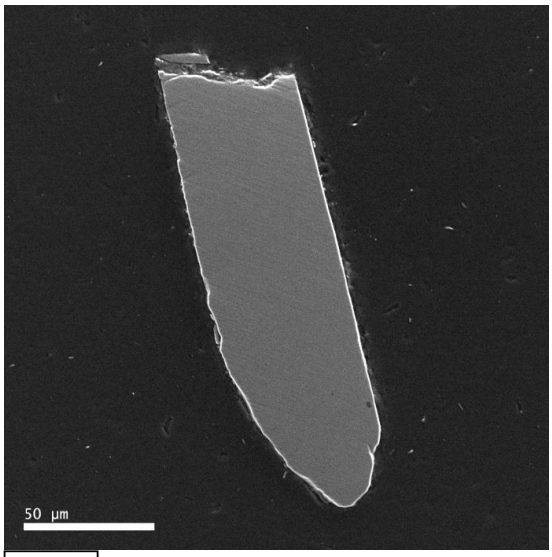
50 µm

C02

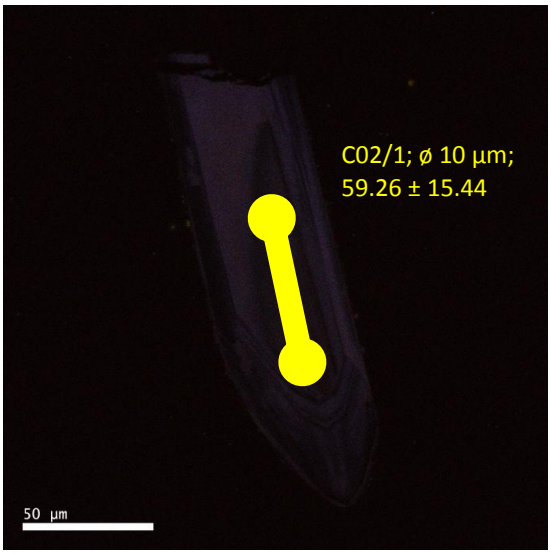
C02/1; ø 10 µm;
59.26 ± 15.44
50 µm

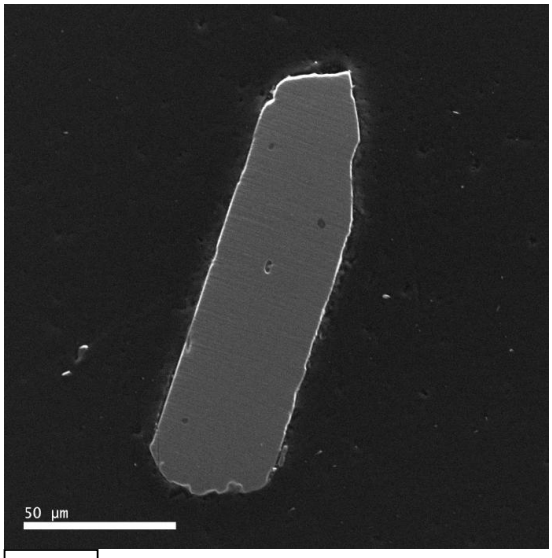
50 µm

C03

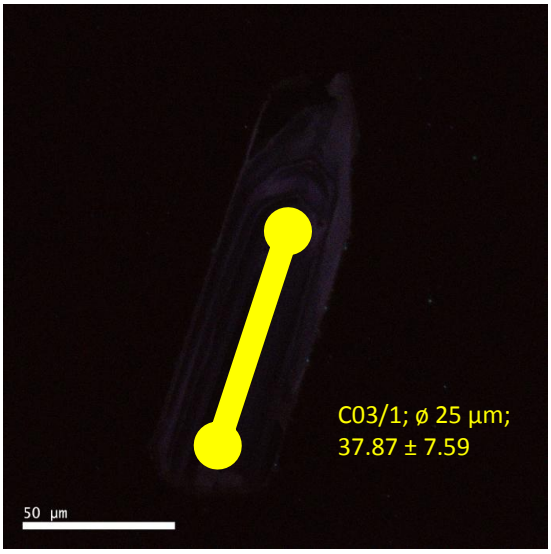
C03/1; ø 25 µm;
37.87 ± 7.59
50 µm

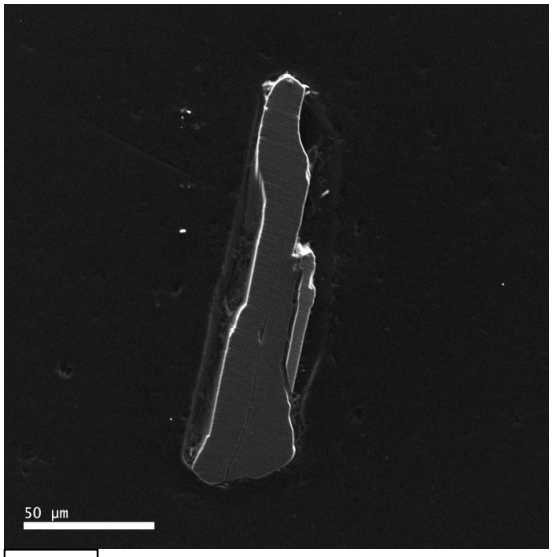
50 µm

C05

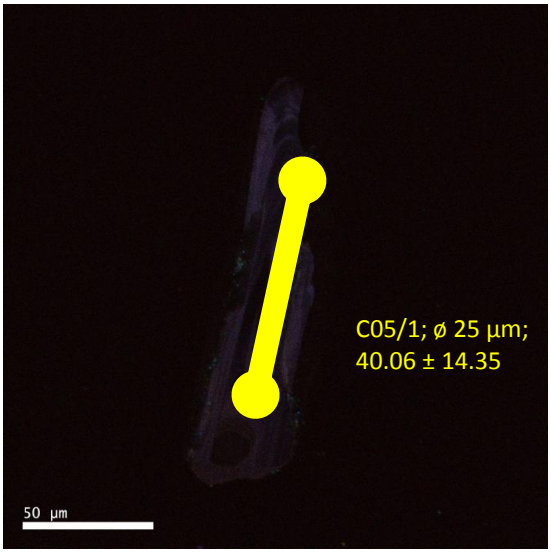
C05/1; ø 25 µm;
40.06 ± 14.35
50 µm

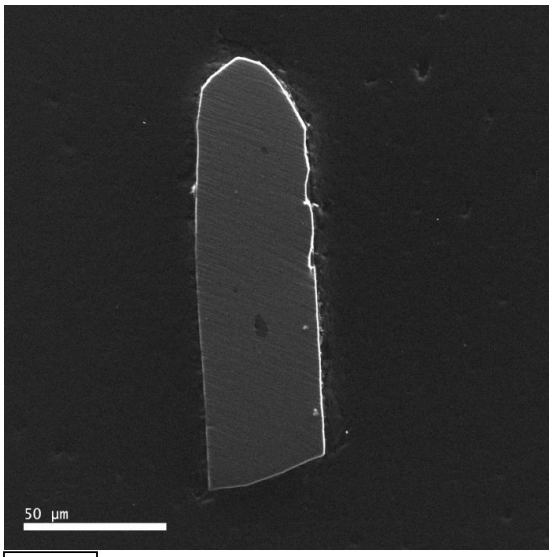

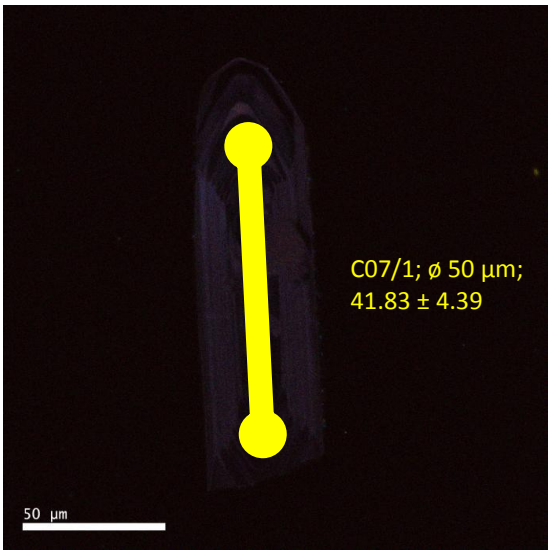

C07

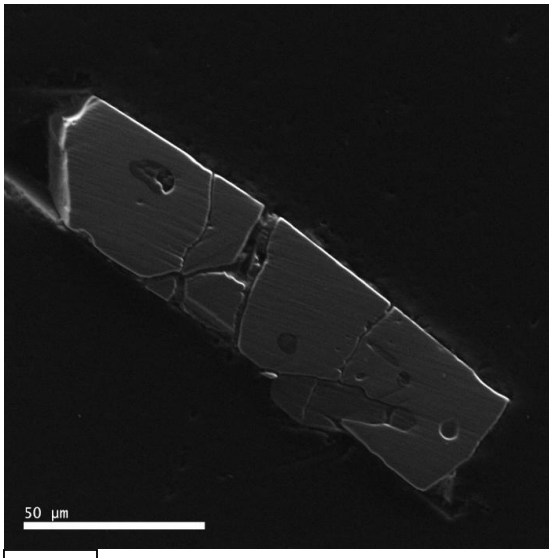

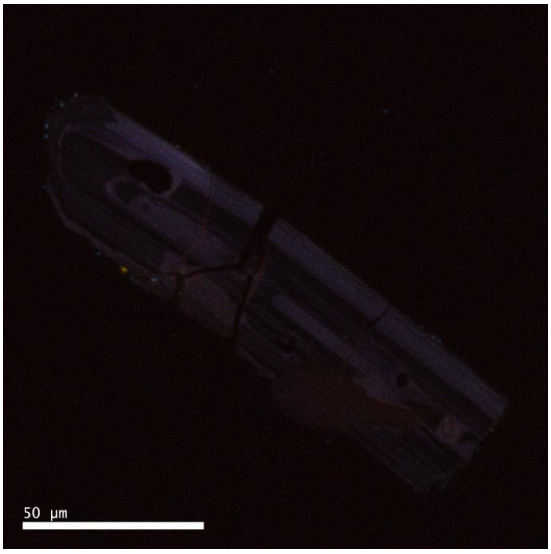

D04

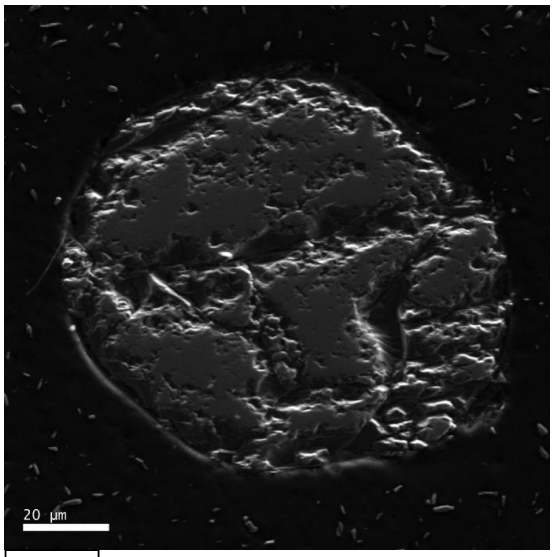

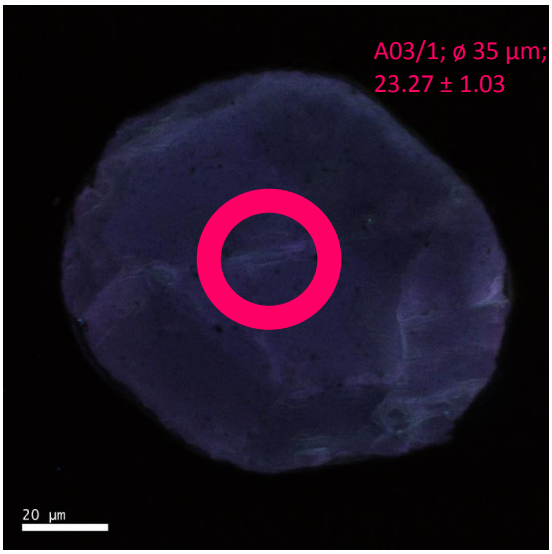

A03

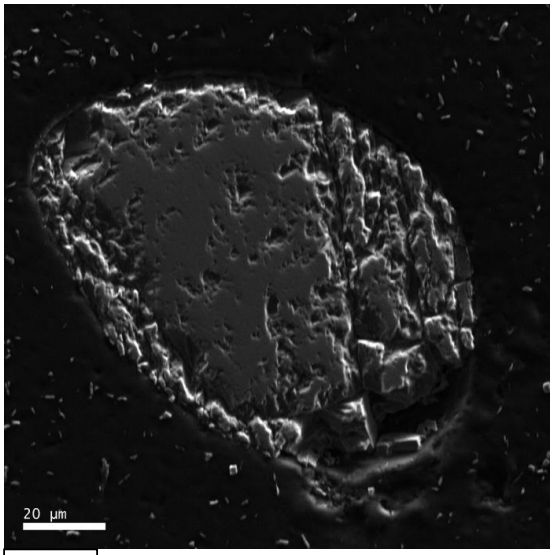

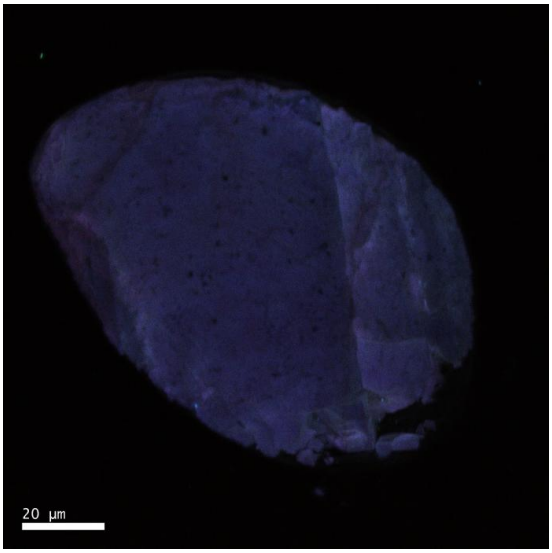

A07

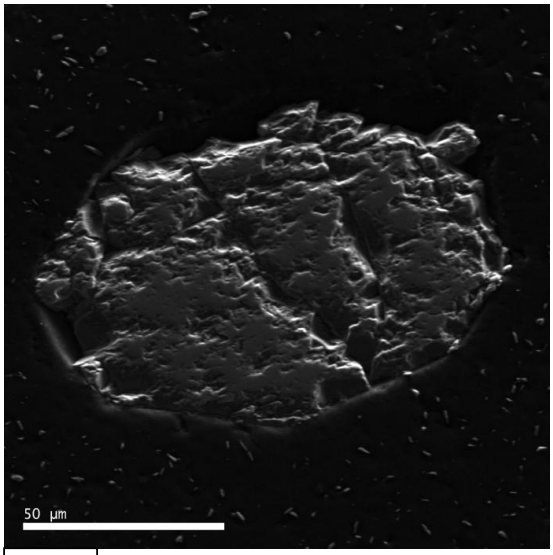

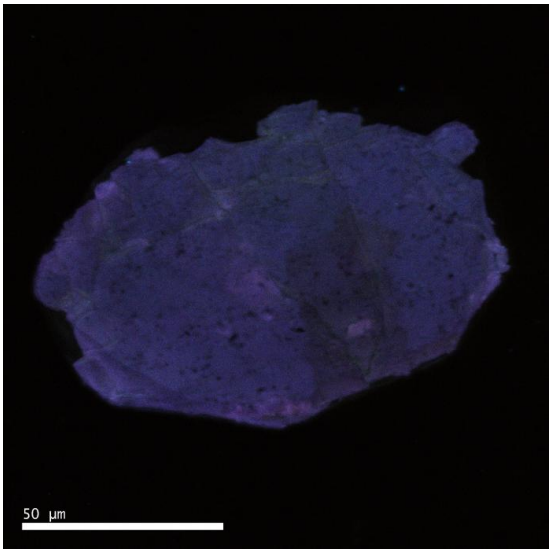

C06

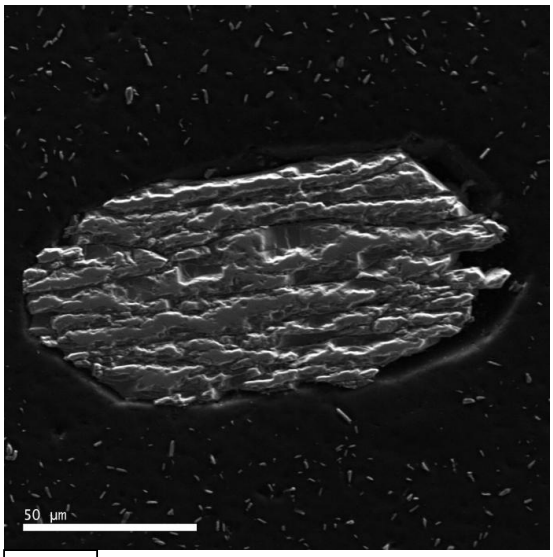
50 µm

D01

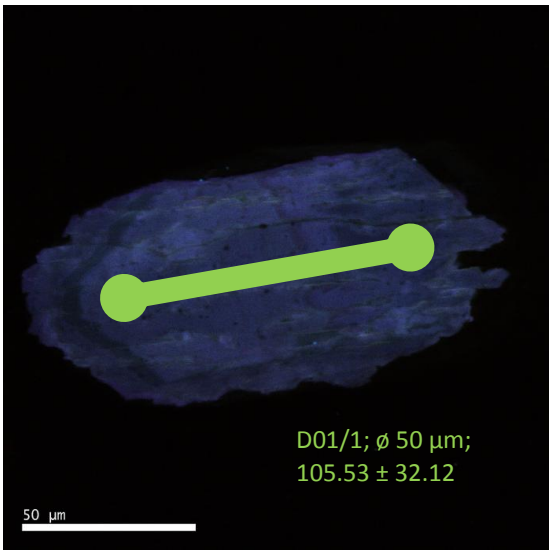
D01/1; ø 50 µm;
105.53 ± 32.12
50 µm

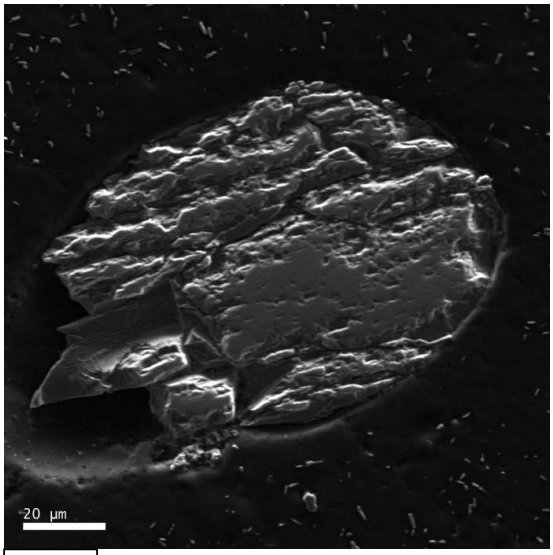
20 µm

D03

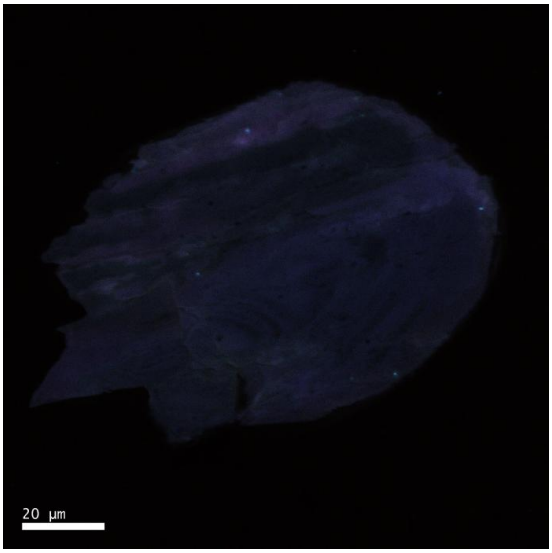
20 µm

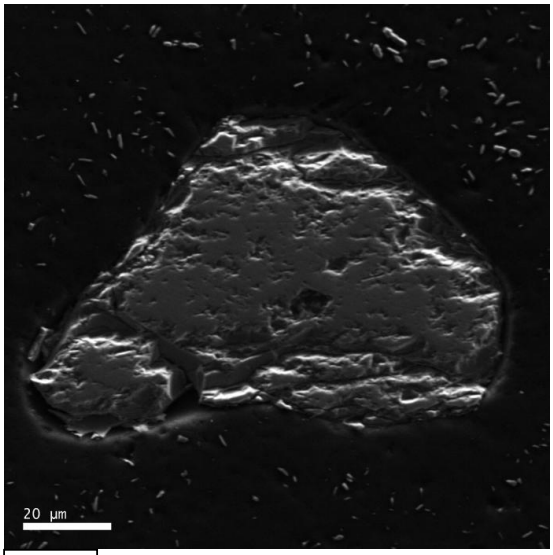
20 µm

D04

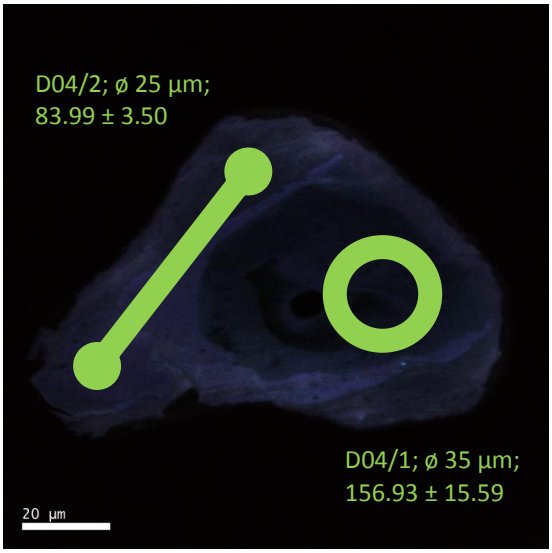
D04/2; ø 25 µm;
83.99 ± 3.50
D04/1; ø 35 µm;
156.93 ± 15.59
20 µm

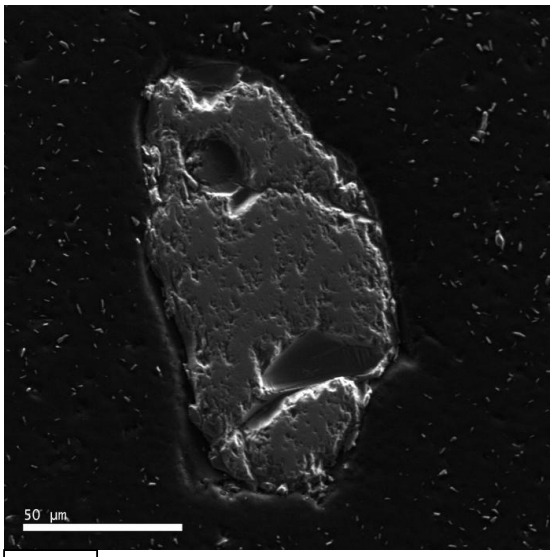
50 µm

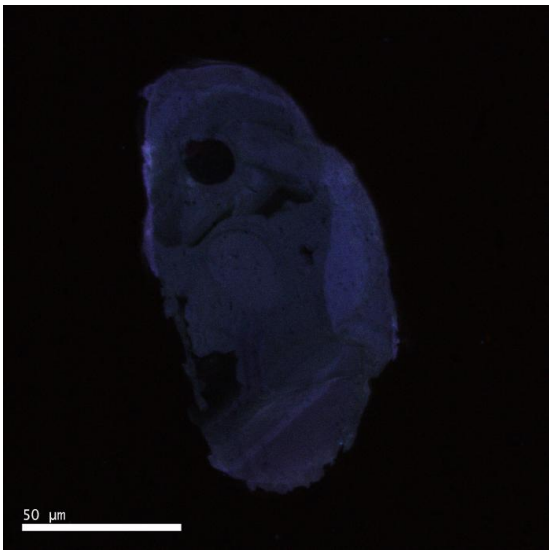
50 µm

D06

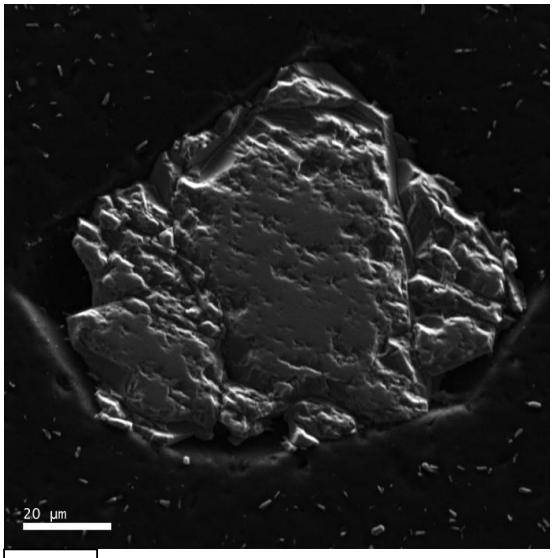
20 µm

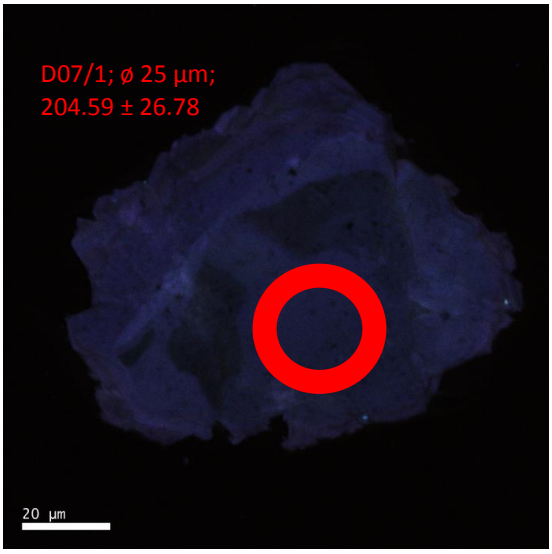
D07/1; ø 25 µm;
204.59 ± 26.78
20 µm

D07

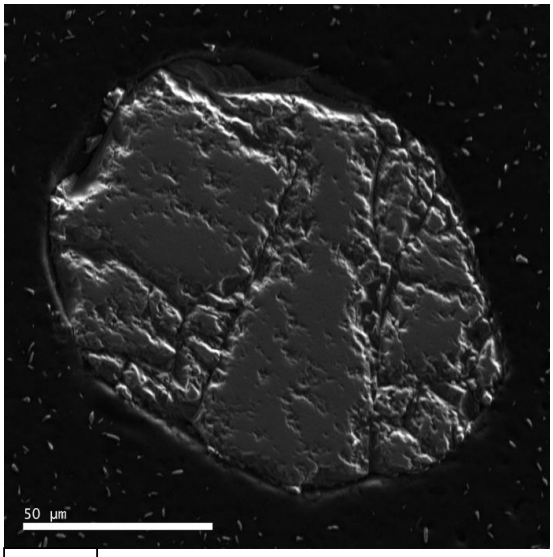
50 µm

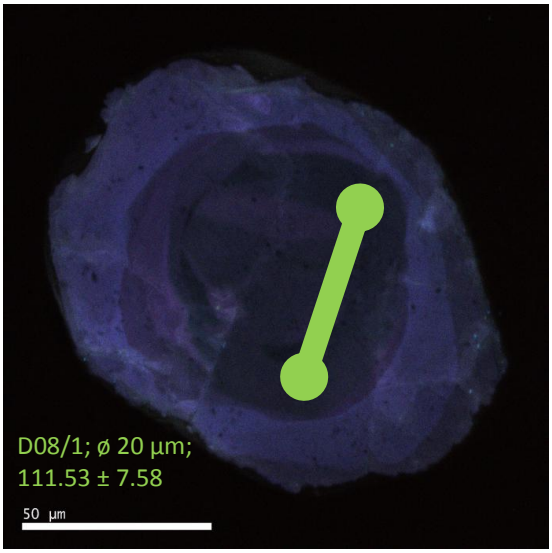
D08/1; ø 20 µm;
111.53 ± 7.58
50 µm

D08

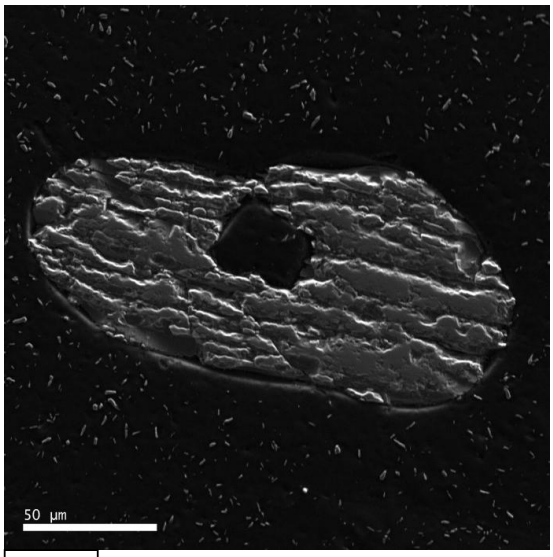
50 µm

D09

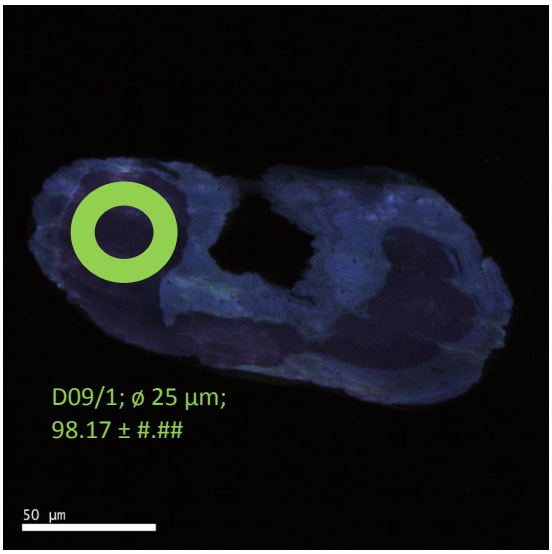
D09/1; ø 25 µm;
98.17 ± #.##
50 µm

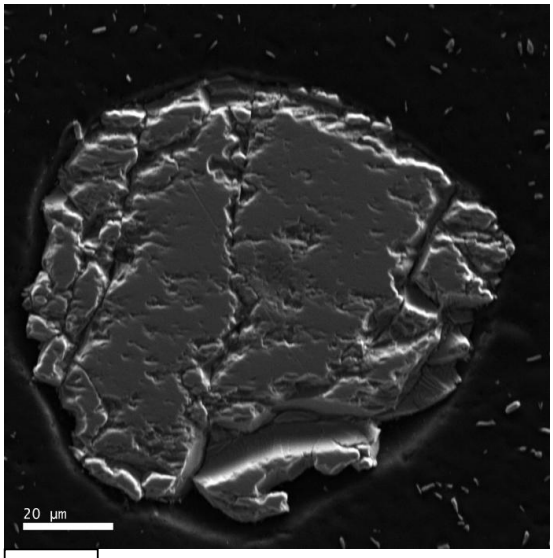
20 µm

D10

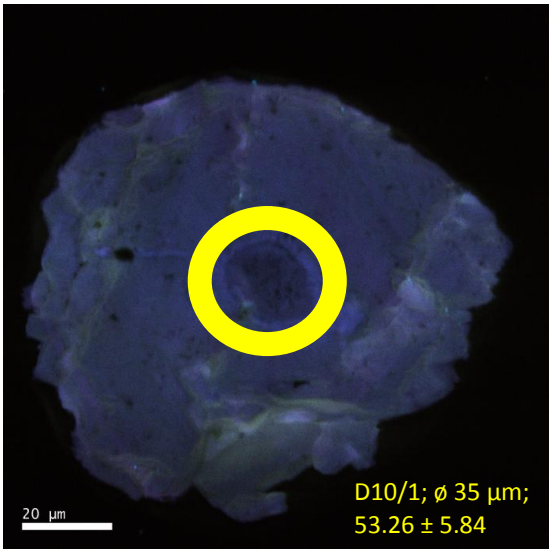
20 µm
D10/1; ø 35 µm;
53.26 ± 5.84

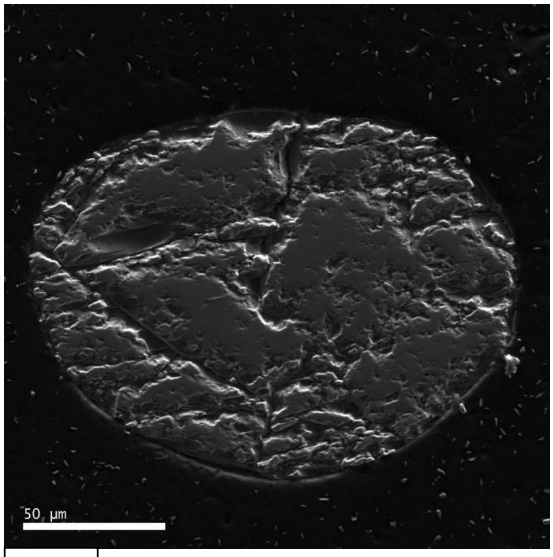
50 µm

E04

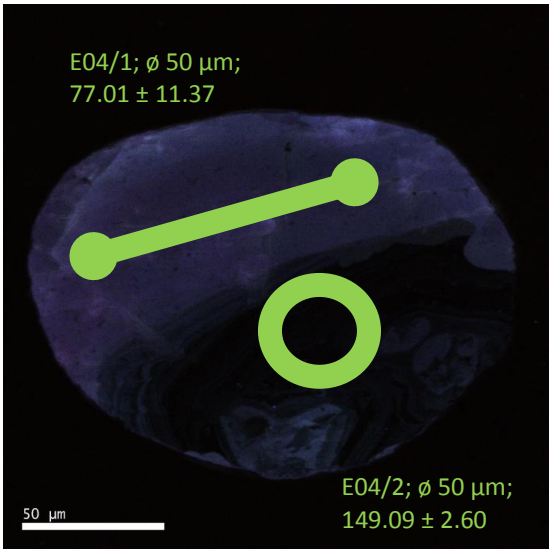
E04/1; ø 50 µm;
77.01 ± 11.37
50 µm
E04/2; ø 50 µm;
149.09 ± 2.60

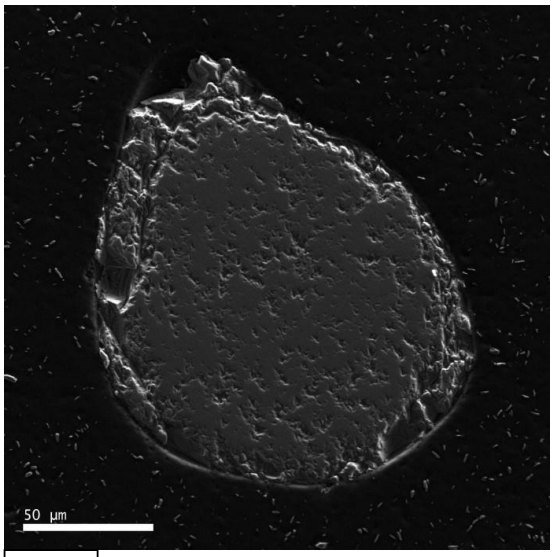
50 µm

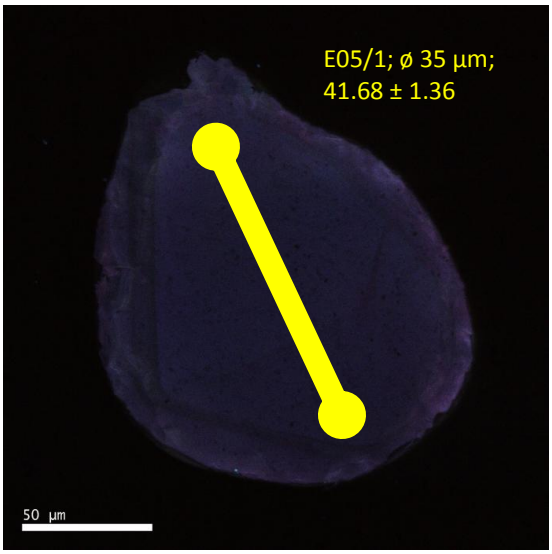
E05/1; ø 35 µm;
41.68 ± 1.36
50 µm

E05

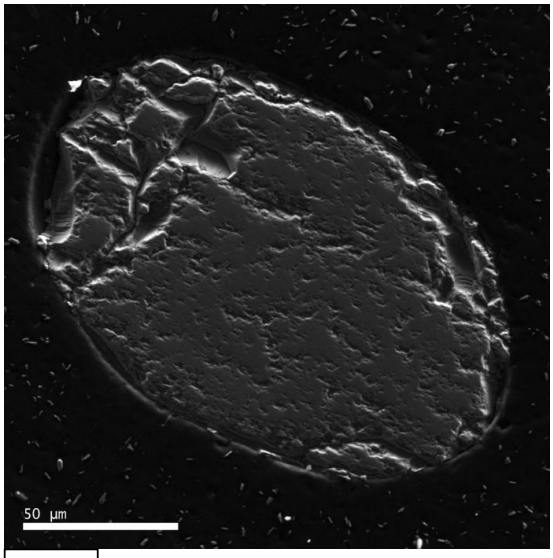
50 µm

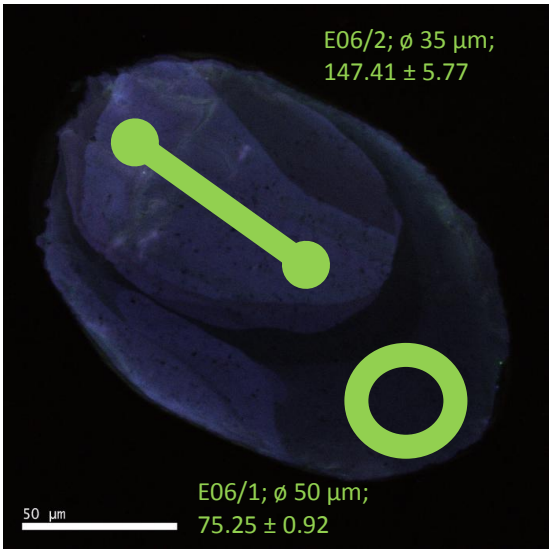
E06/2; ø 35 µm;
147.41 ± 5.77
E06/1; ø 50 µm;
75.25 ± 0.92
50 µm

E06

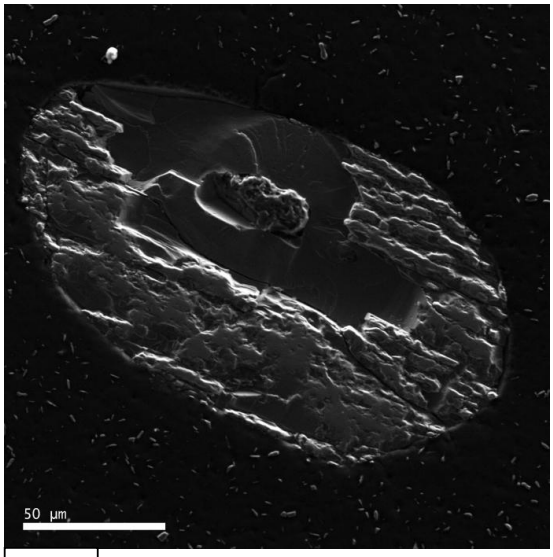
50 µm

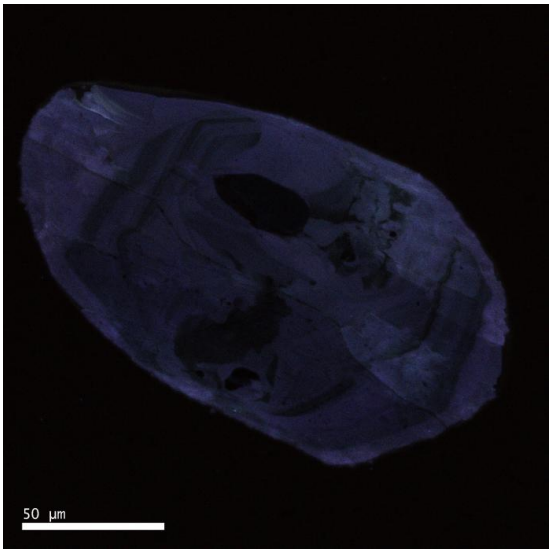
50 µm

E07

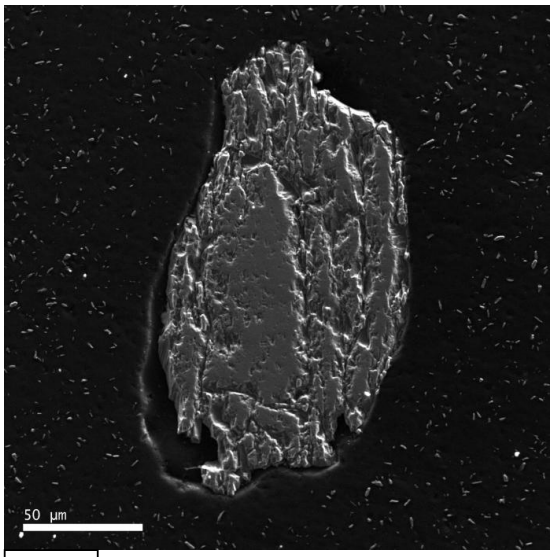

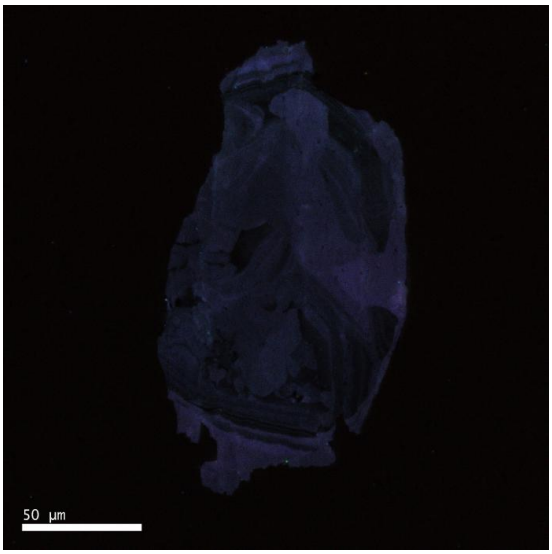

E08

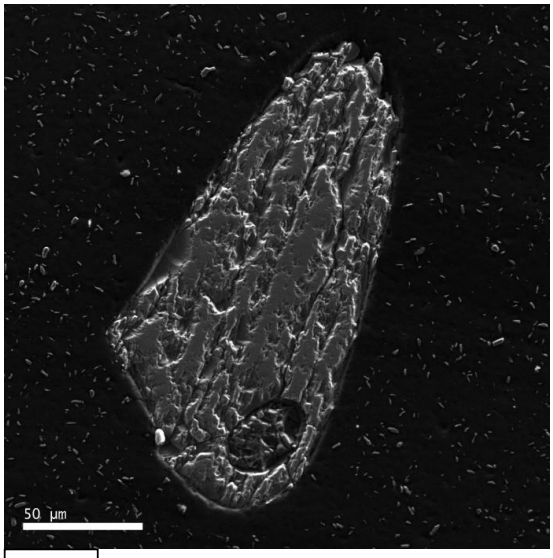

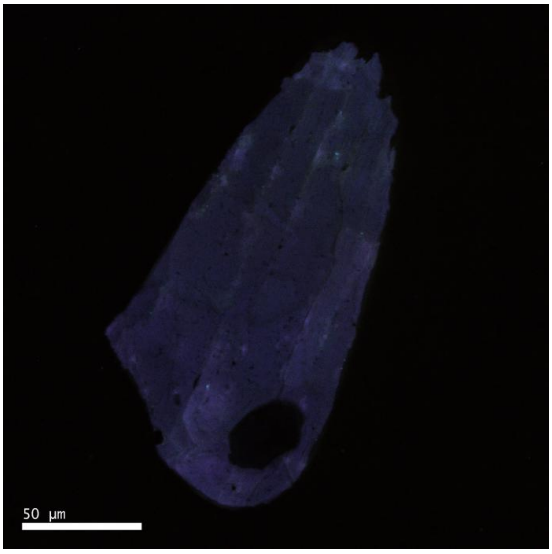

E09

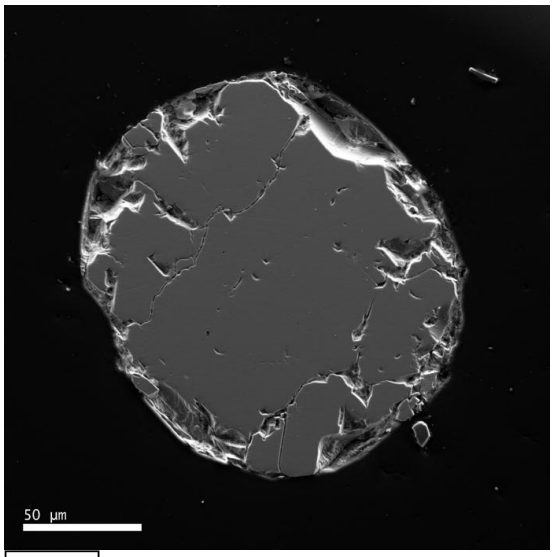
50 µm

A01

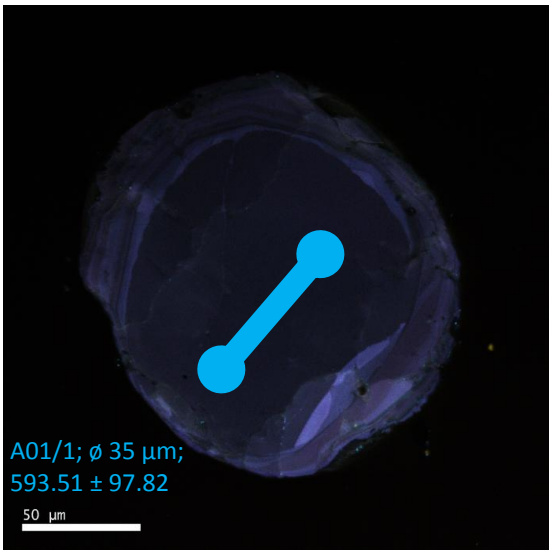
A01/1; ø 35 µm;
593.51 ± 97.82
50 µm

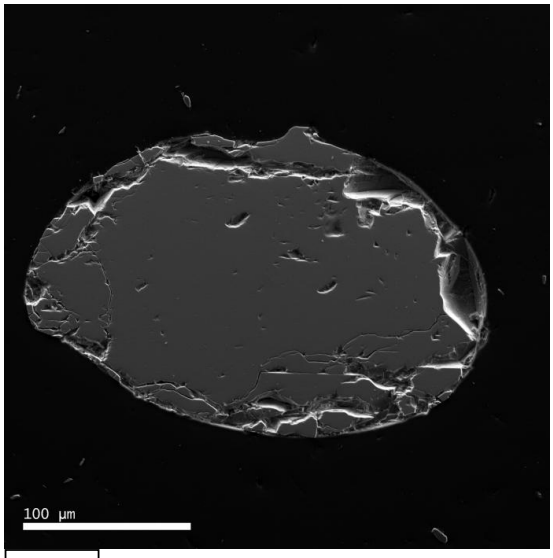
100 µm

A02

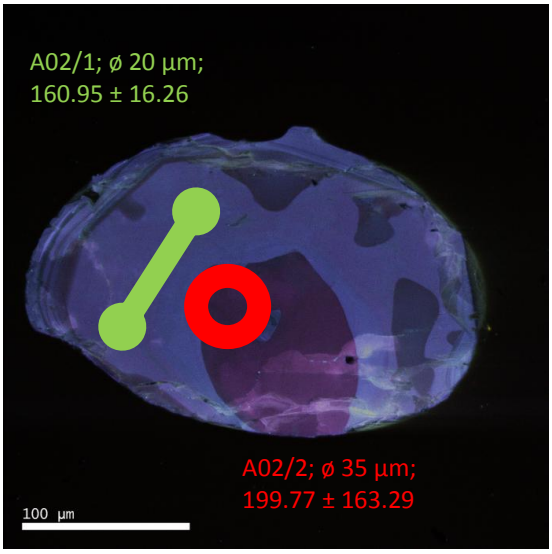
A02/1; ø 20 µm;
160.95 ± 16.26
A02/2; ø 35 µm;
199.77 ± 163.29
100 µm

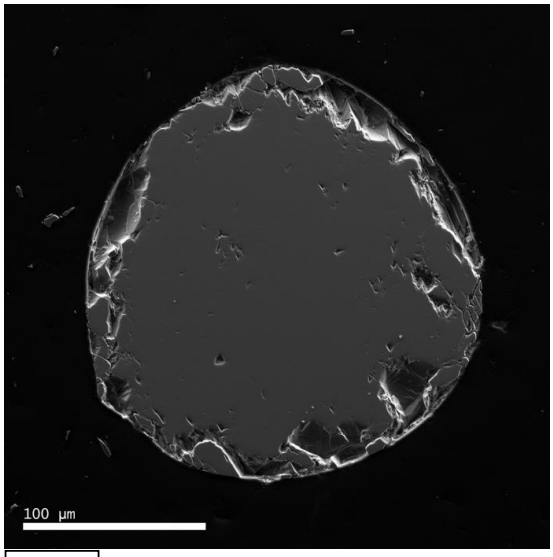
100 µm

A03

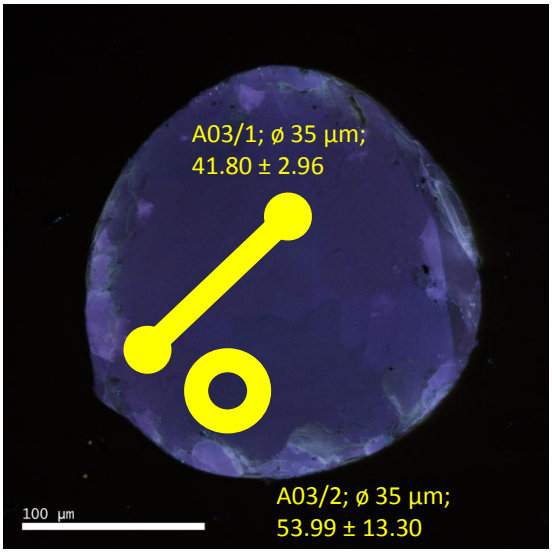
A03/1; ø 35 µm;
41.80 ± 2.96
A03/2; ø 35 µm;
53.99 ± 13.30
100 µm

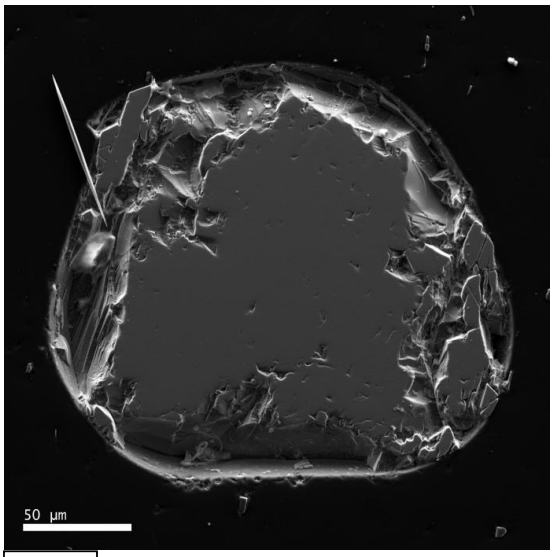
50 µm

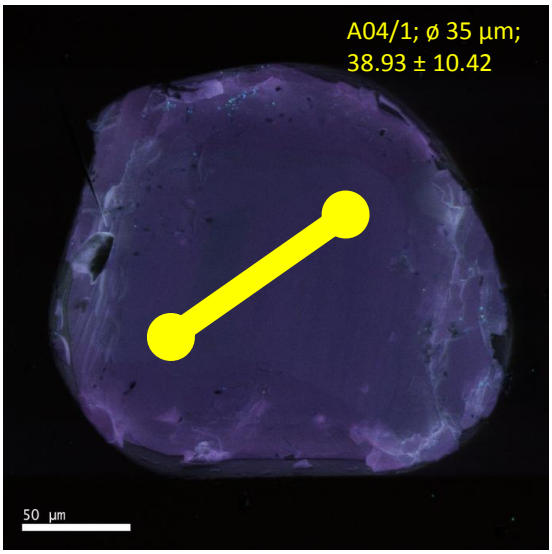
A04/1; ø 35 µm;
38.93 ± 10.42
50 µm

A04

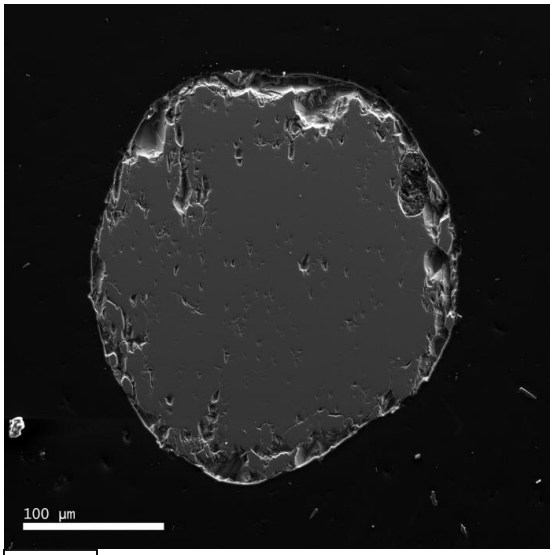
100 µm

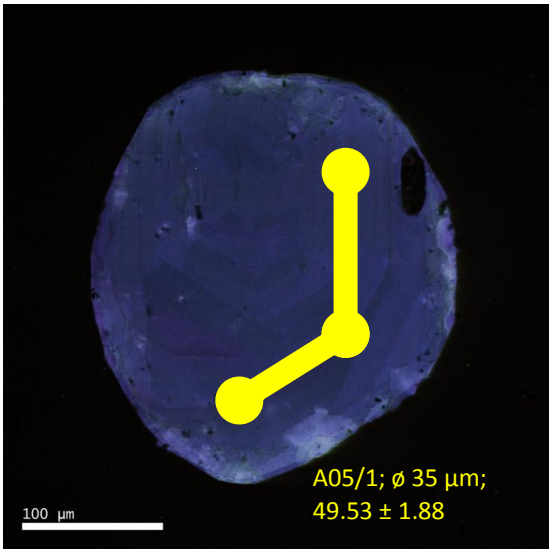
A05/1; ø 35 µm;
49.53 ± 1.88
100 µm

A05

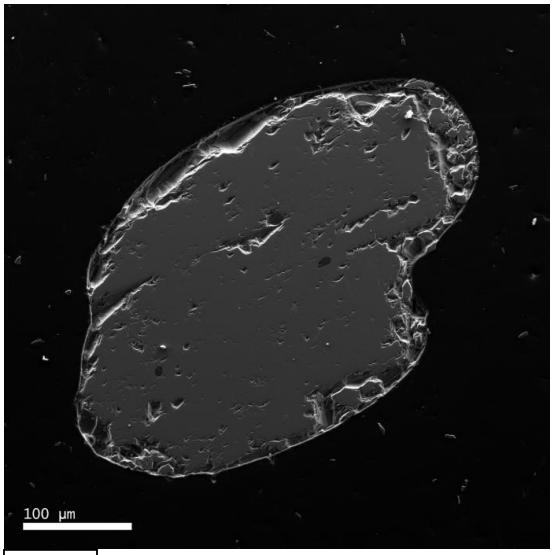
100 µm

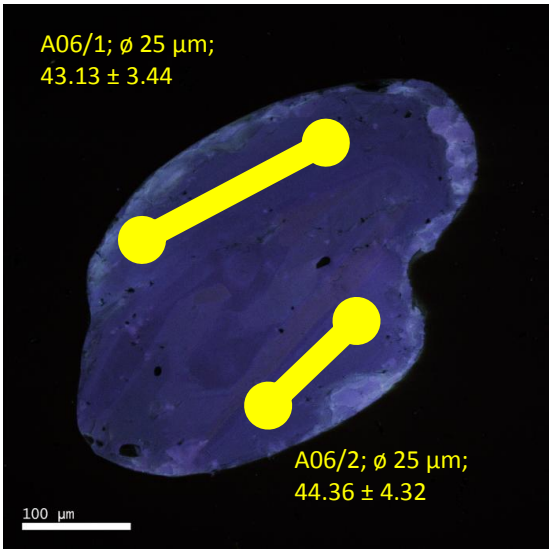
A06/1; ø 25 µm;
43.13 ± 3.44
A06/2; ø 25 µm;
44.36 ± 4.32
100 µm

A06

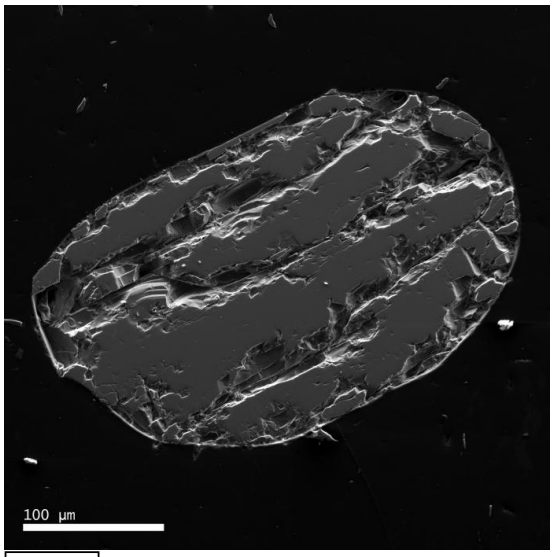
100 µm

A07

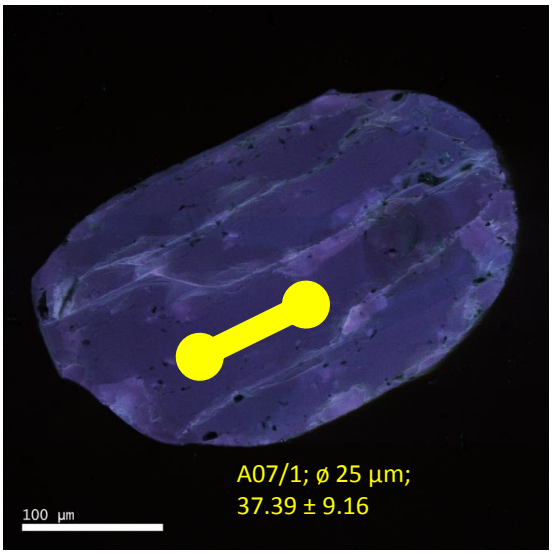
A07/1; ø 25 µm;
37.39 ± 9.16
100 µm

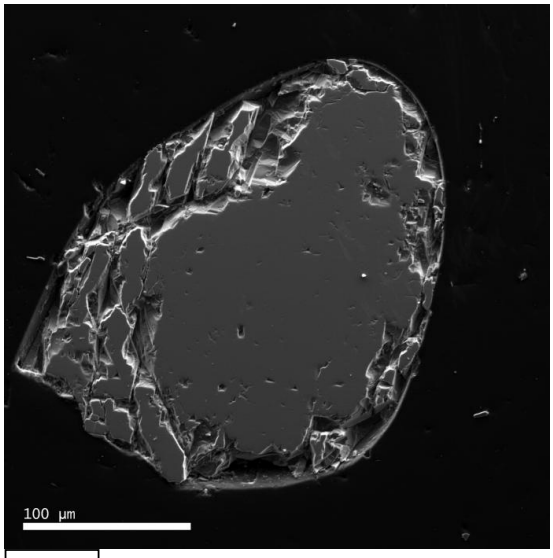
100 µm

A08

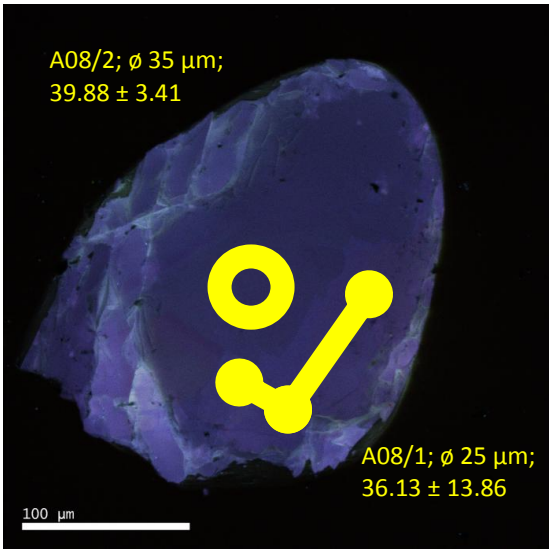
A08/2; ø 35 µm;
39.88 ± 3.41
A08/1; ø 25 µm;
36.13 ± 13.86
100 µm

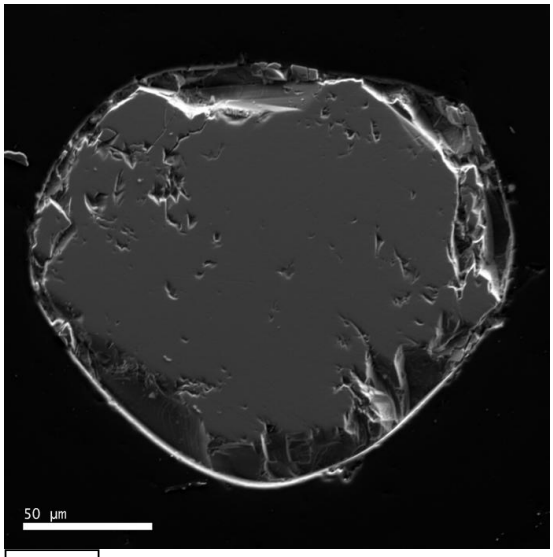
50 µm

A09

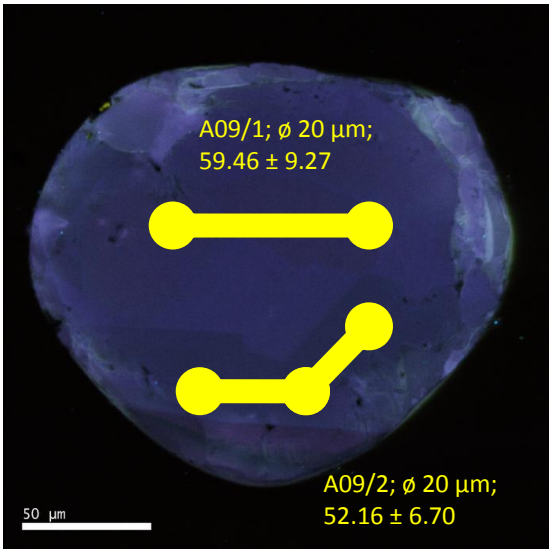
A09/1; ø 20 µm;
59.46 ± 9.27
A09/2; ø 20 µm;
52.16 ± 6.70
50 µm

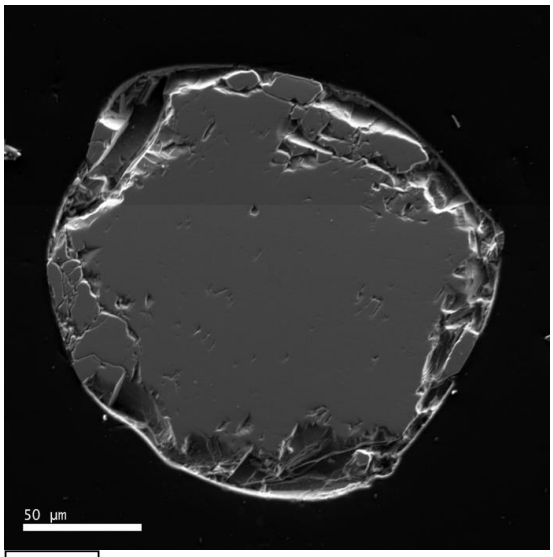

A10

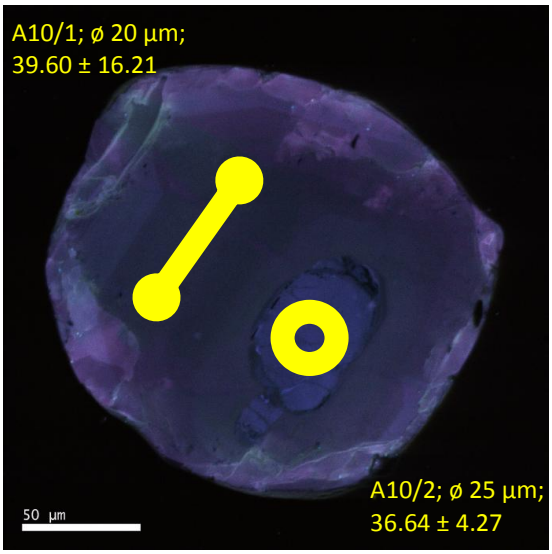

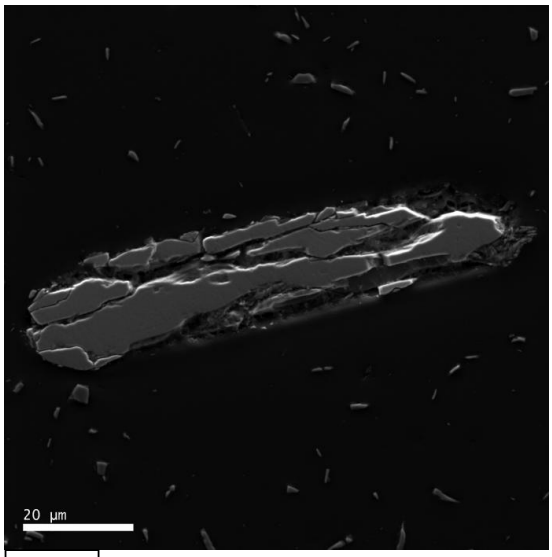
20 µm

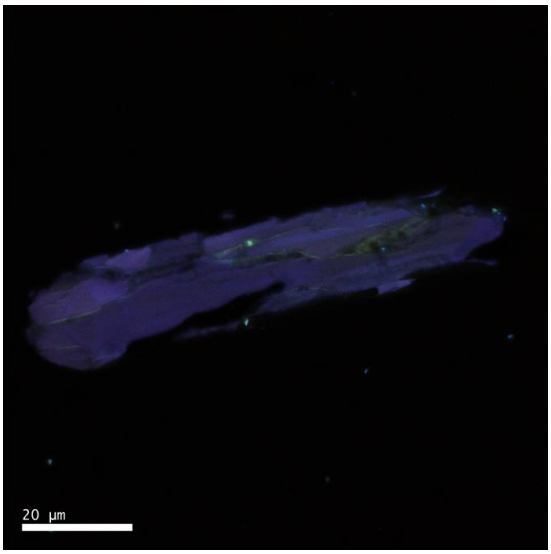
20 µm

A01

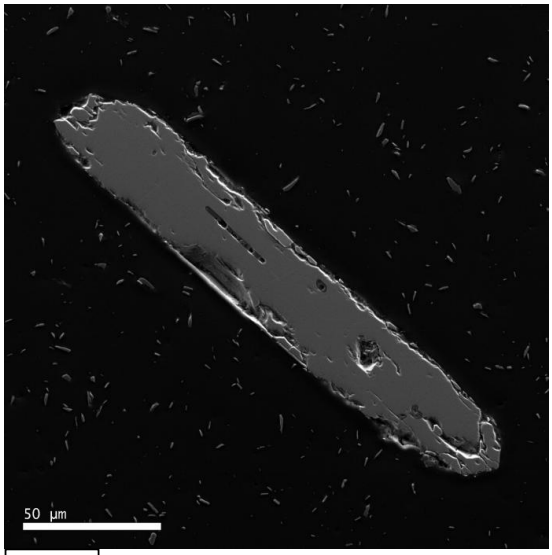
50 µm

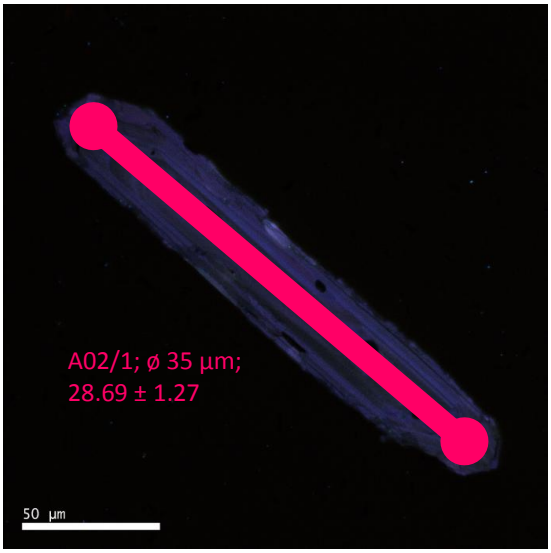
A02/1; ø 35 µm;
28.69 ± 1.27
50 µm

A02

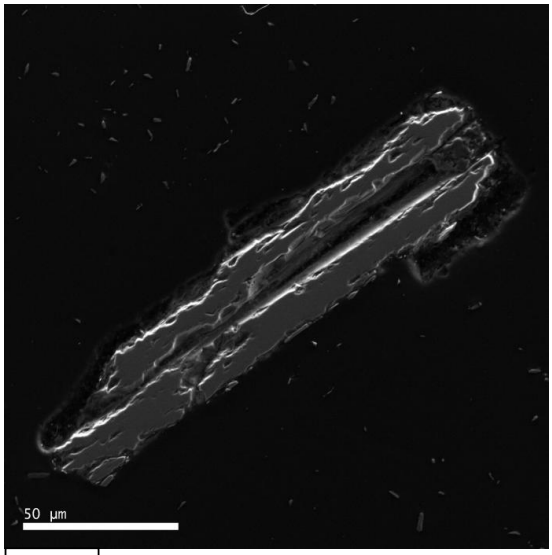
50 µm

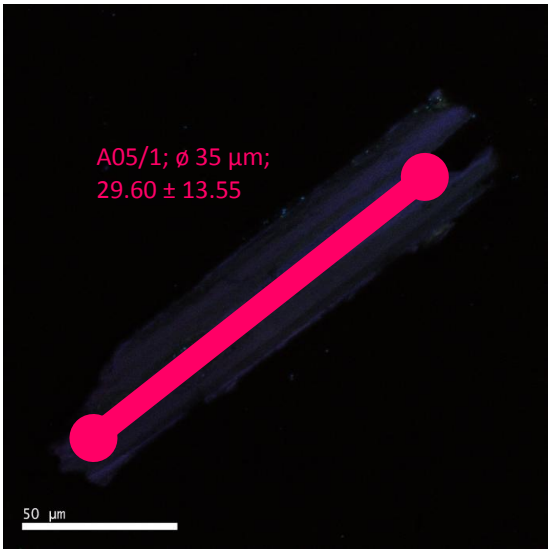
A05/1; ø 35 µm;
29.60 ± 13.55
50 µm

A05

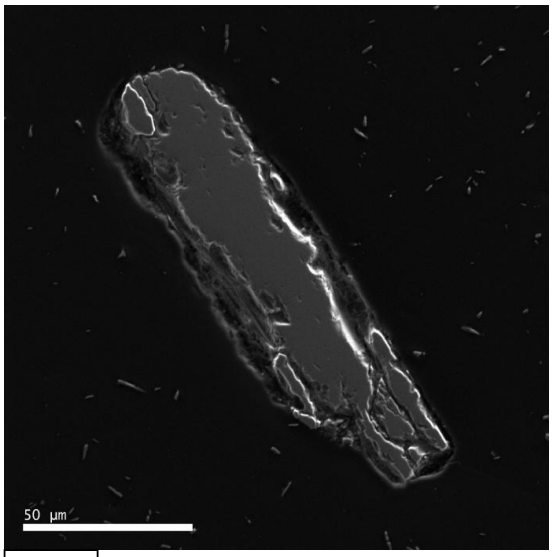
50 µm

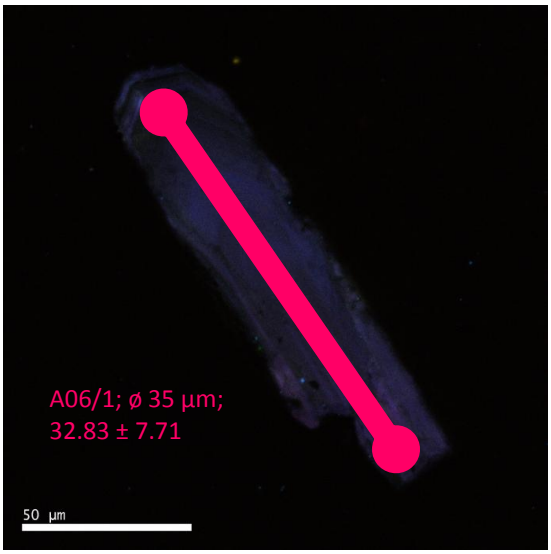
A06/1; ø 35 µm;
32.83 ± 7.71
50 µm

A06

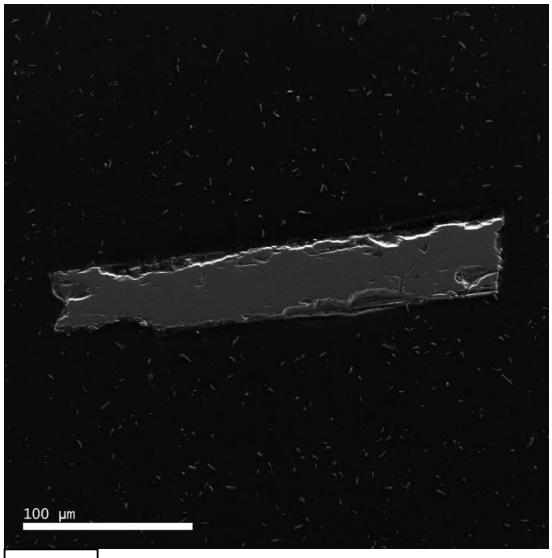
100 µm

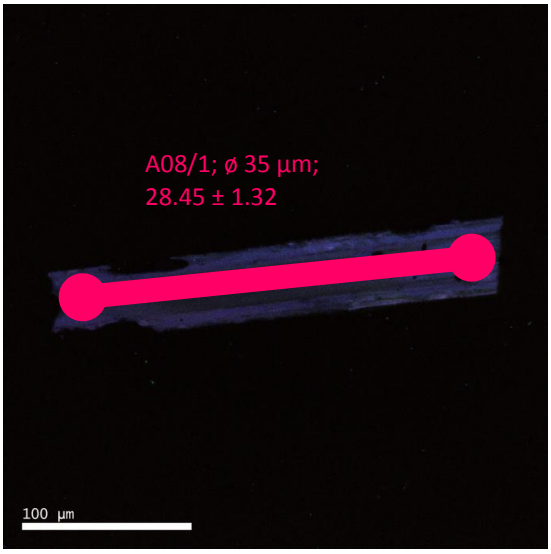
A08/1; ø 35 µm;
28.45 ± 1.32
100 µm

A08

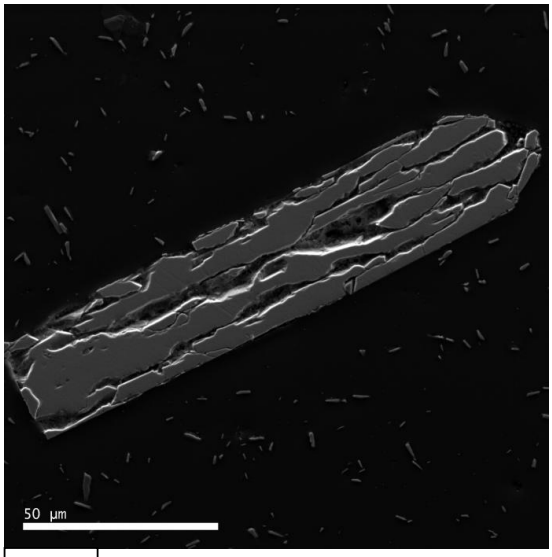
50 µm

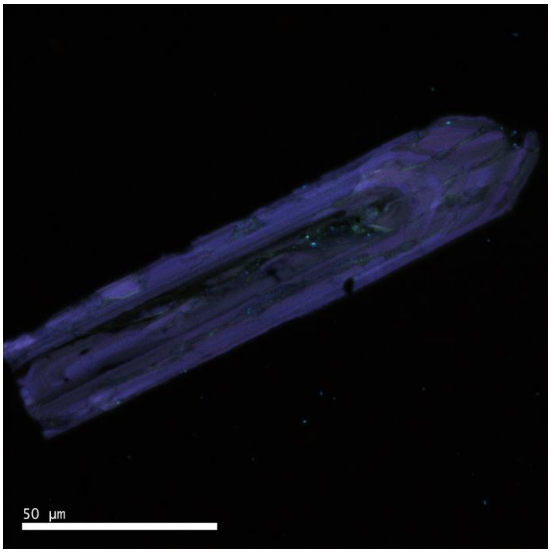
50 µm

B01

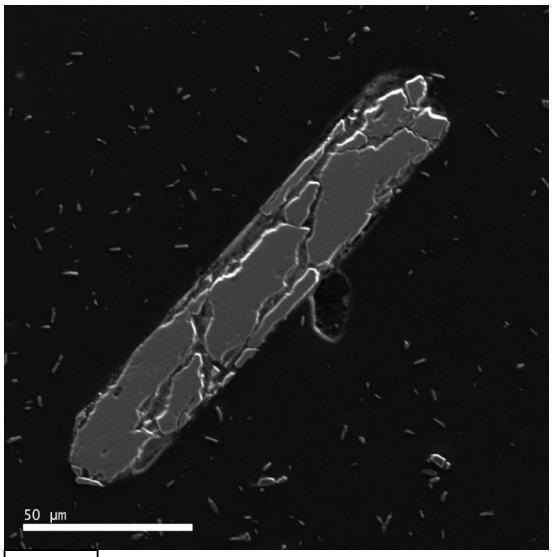
50 µm

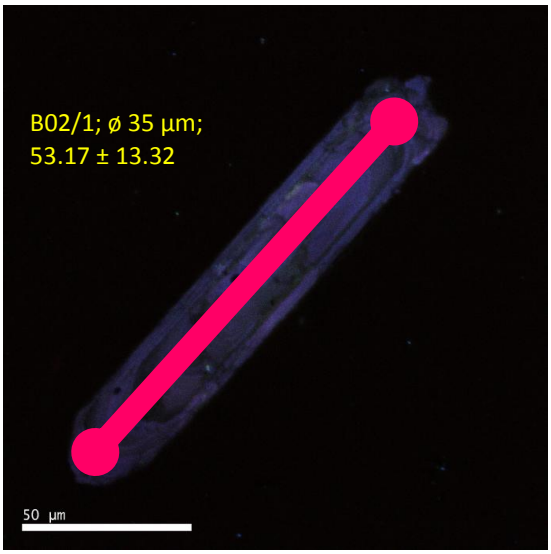
B02/1; ø 35 µm;
53.17 ± 13.32
50 µm

B02

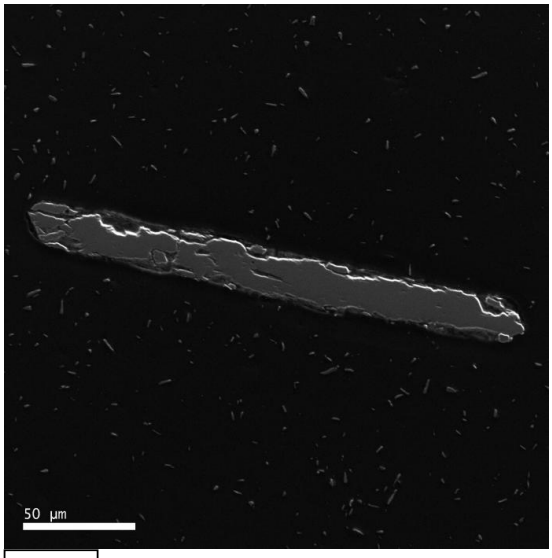
50 µm

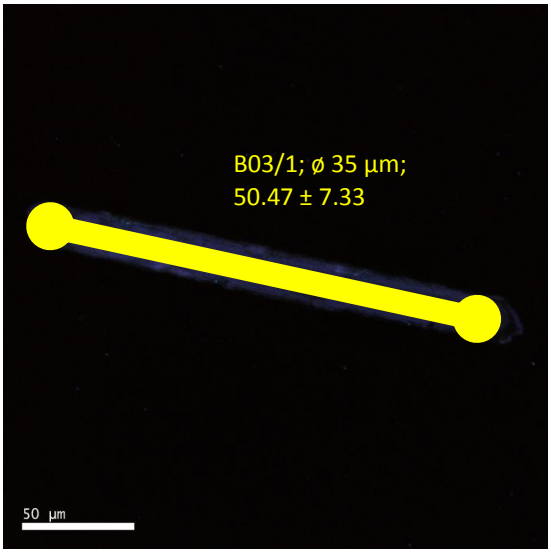
B03/1; ø 35 µm;
50.47 ± 7.33
50 µm

B03

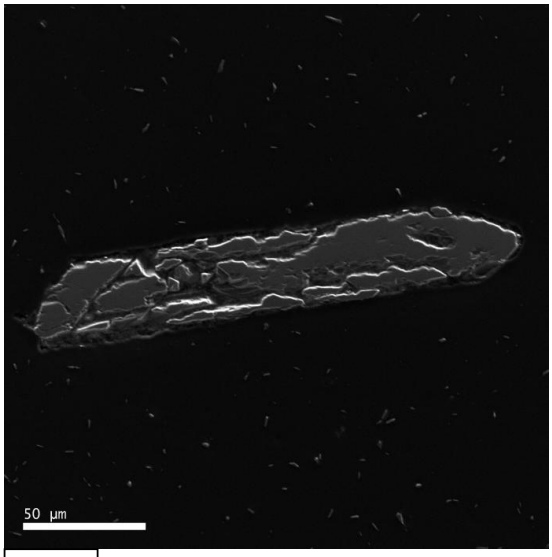
50 µm

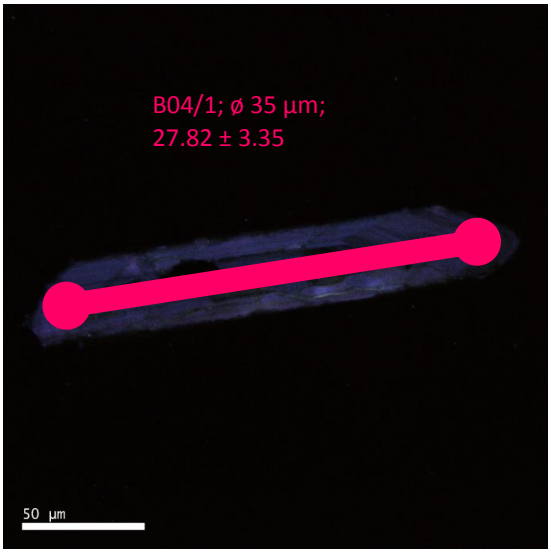
B04/1; ø 35 µm;
27.82 ± 3.35
50 µm

B04

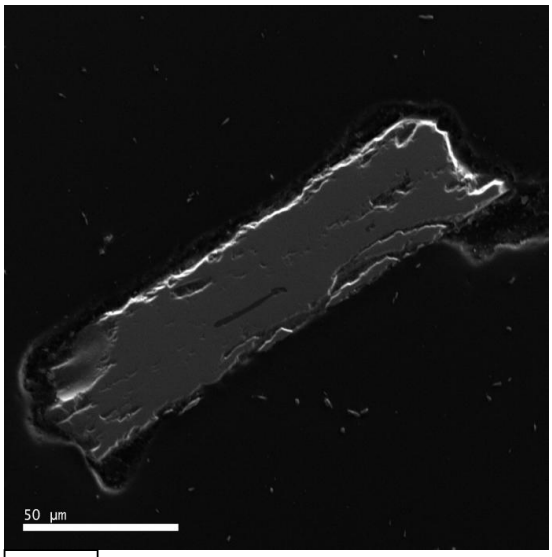
50 µm

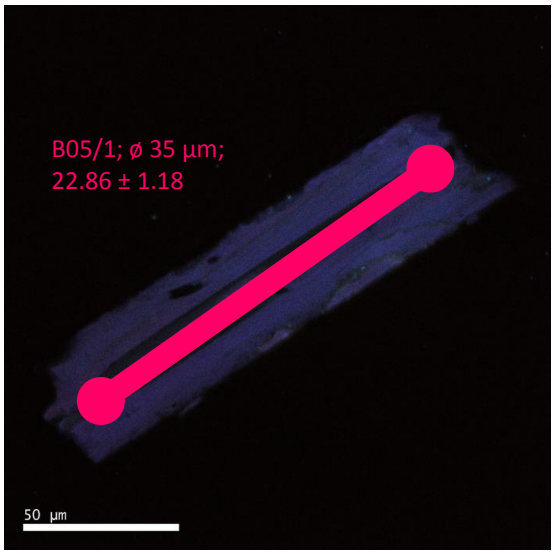
B05/1; ø 35 µm;
22.86 ± 1.18
50 µm

B05

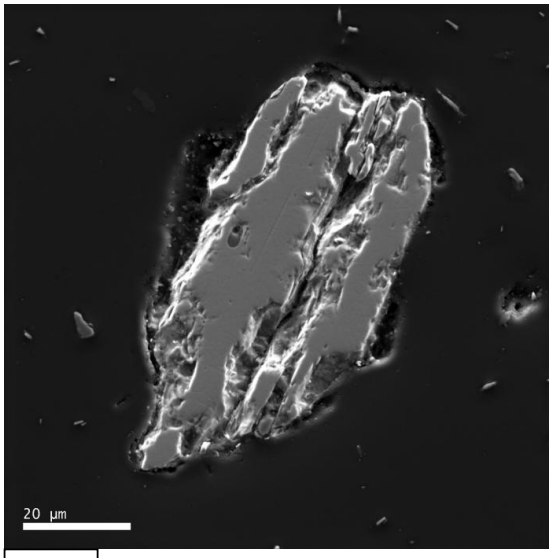
20 µm

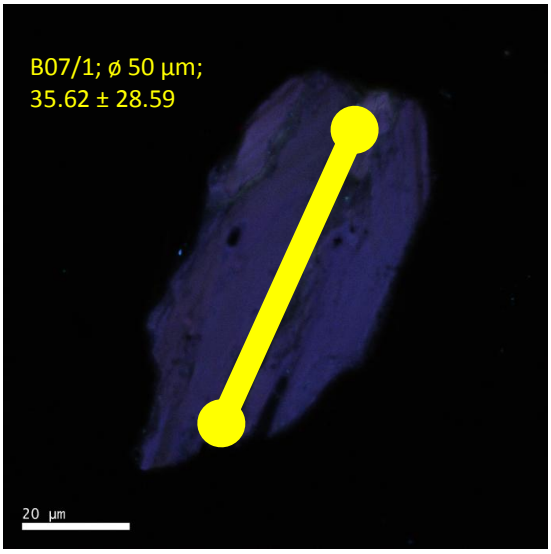
B07/1; ø 50 µm;
35.62 ± 28.59
20 µm

B07

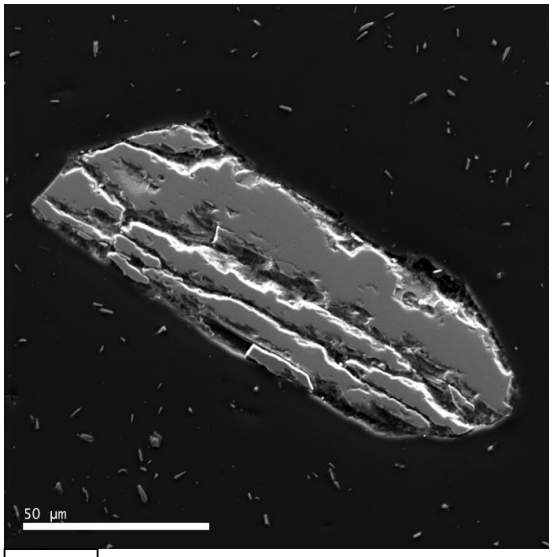
50 µm

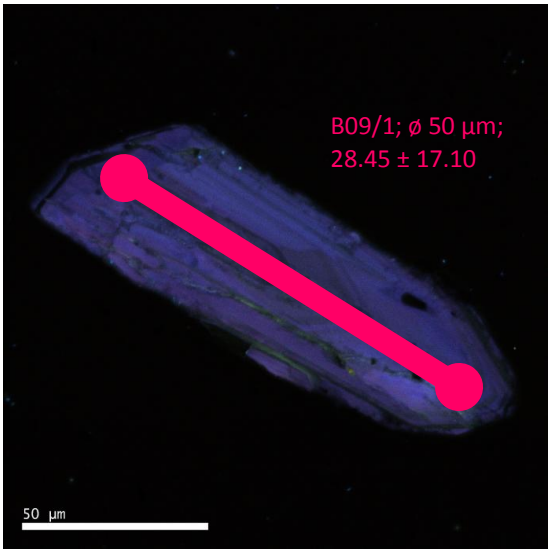
B09/1; ø 50 µm;
28.45 ± 17.10
50 µm

B09

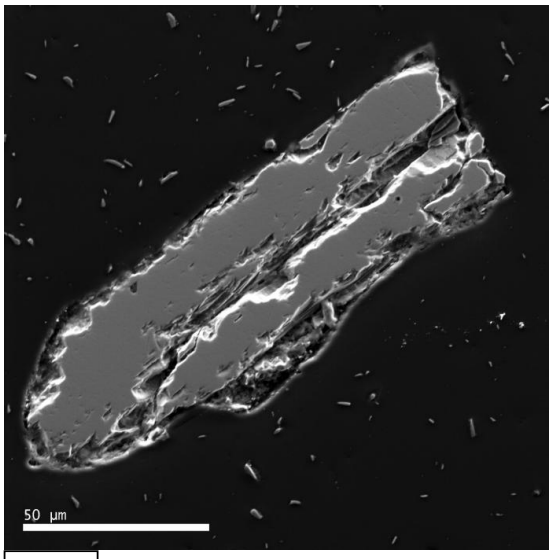
50 µm

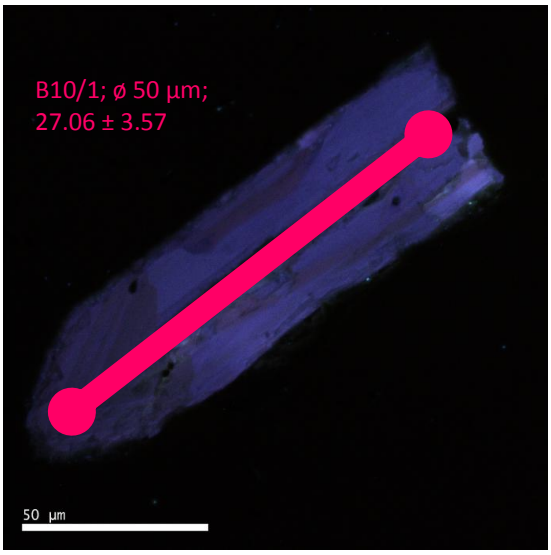
B10/1; ø 50 µm;
27.06 ± 3.57
50 µm

B10

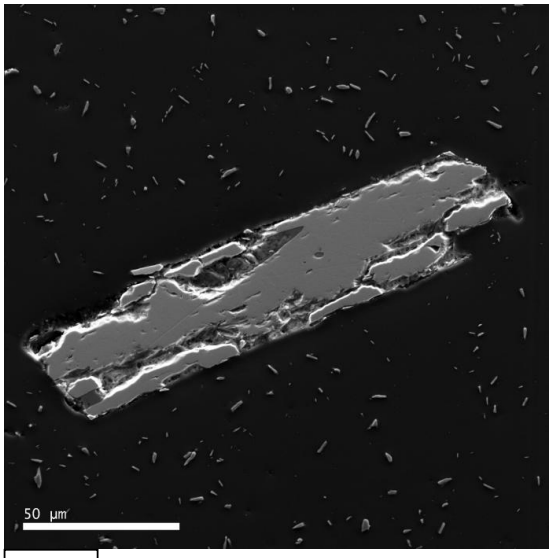
50 µm

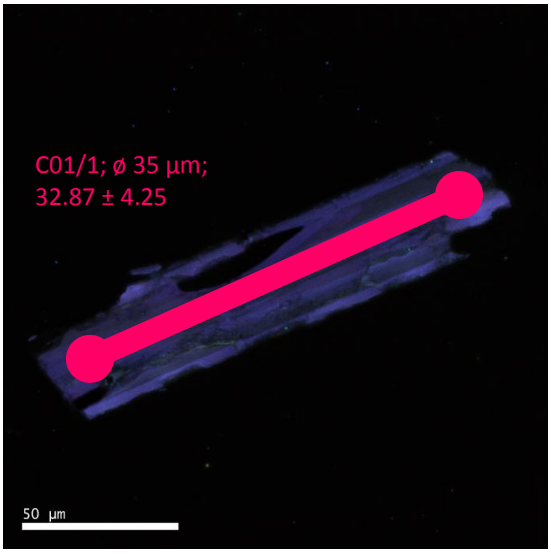
C01/1; ø 35 µm;
32.87 ± 4.25
50 µm

C01

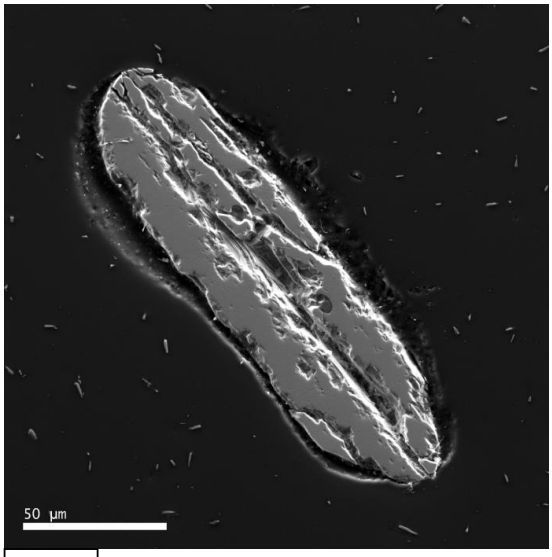
50 µm

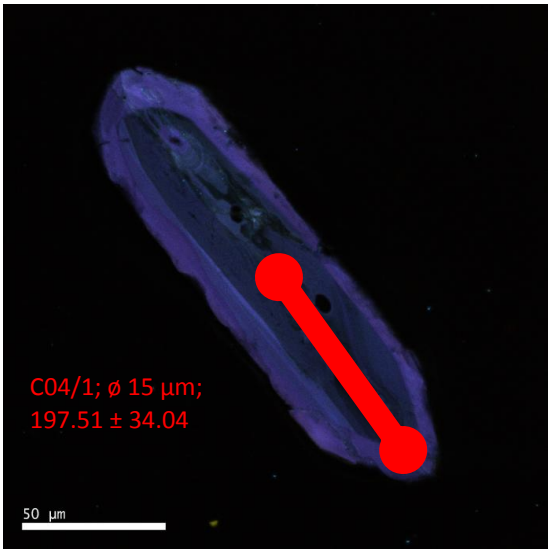
C04/1; ø 15 µm;
197.51 ± 34.04
50 µm

C04

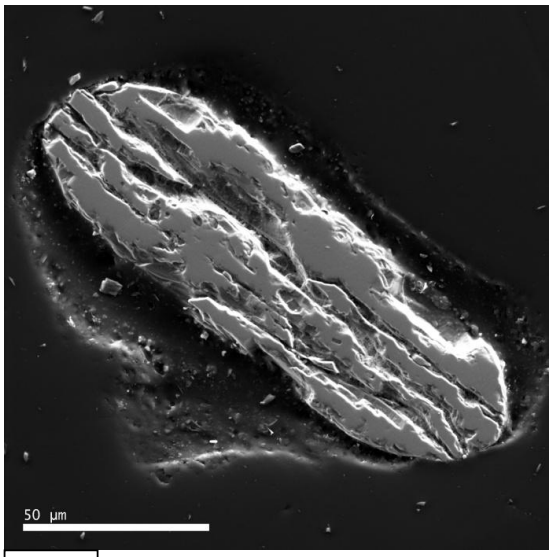
50 µm

C05

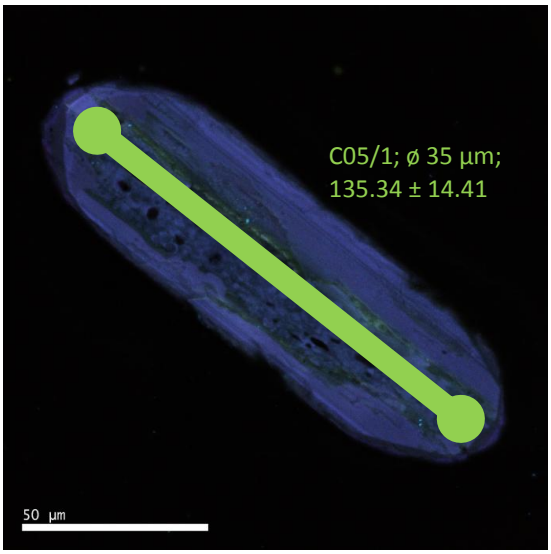
C05/1; ø 35 µm;
135.34 ± 14.41
50 µm

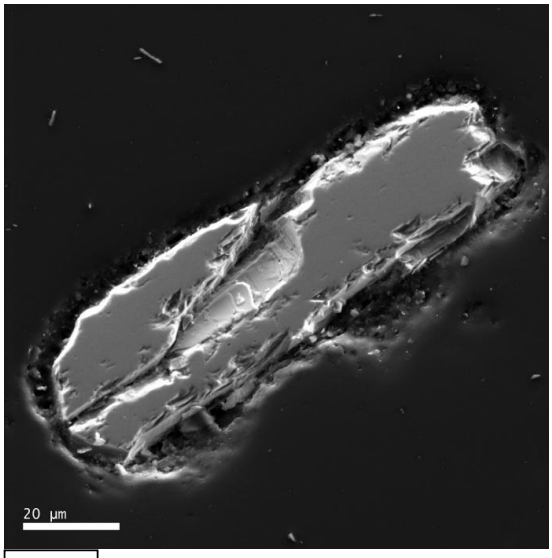
20 µm

C06

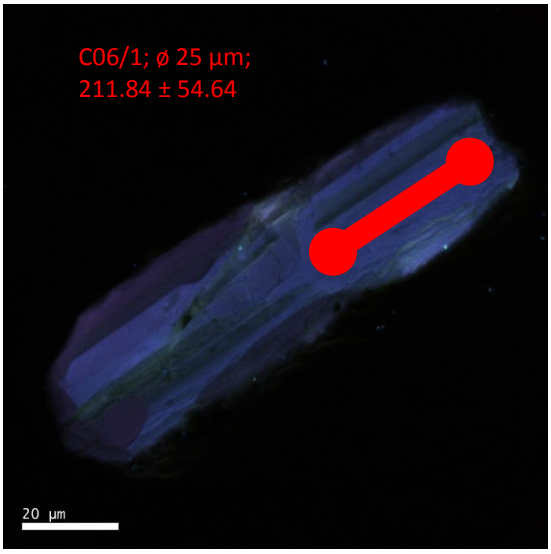
C06/1; ø 25 µm;
211.84 ± 54.64
20 µm

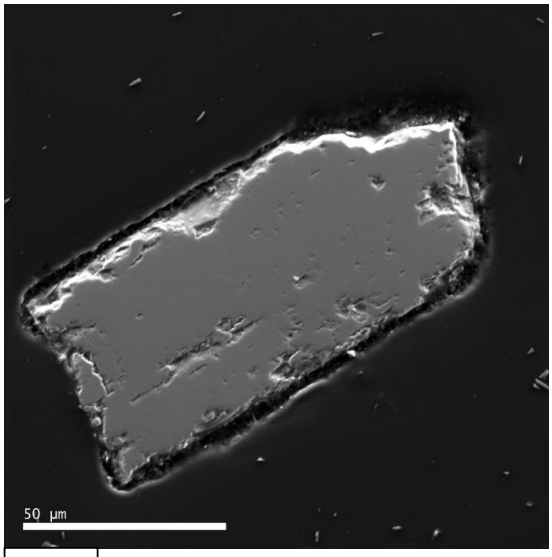
50 µm

C07

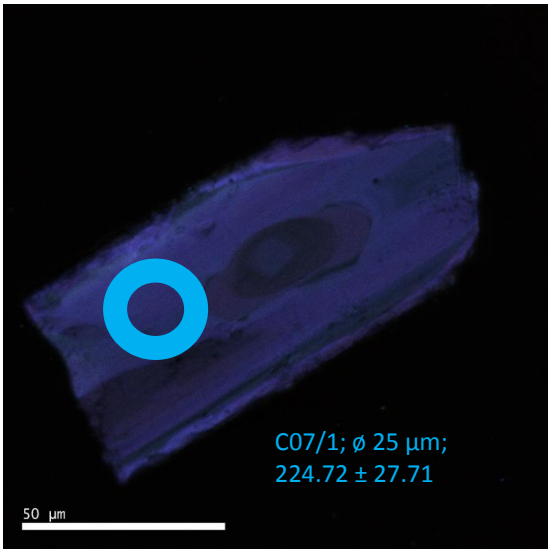
C07/1; ø 25 µm;
224.72 ± 27.71
50 µm

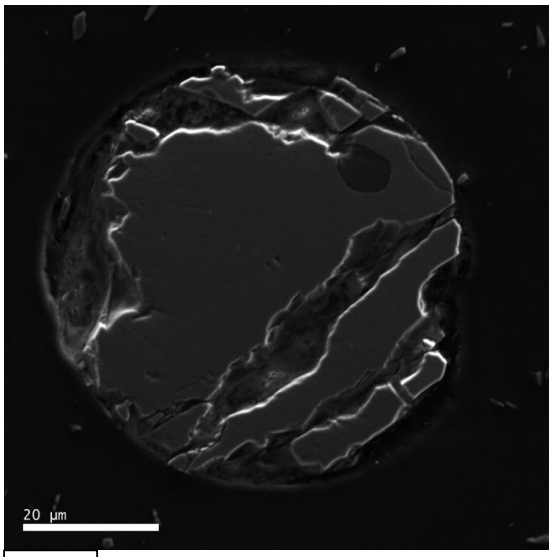
20 µm

01

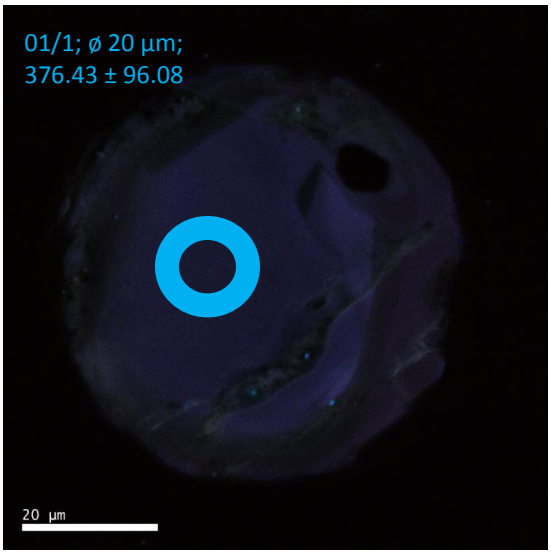
01/1; ø 20 µm;
376.43 ± 96.08
20 µm

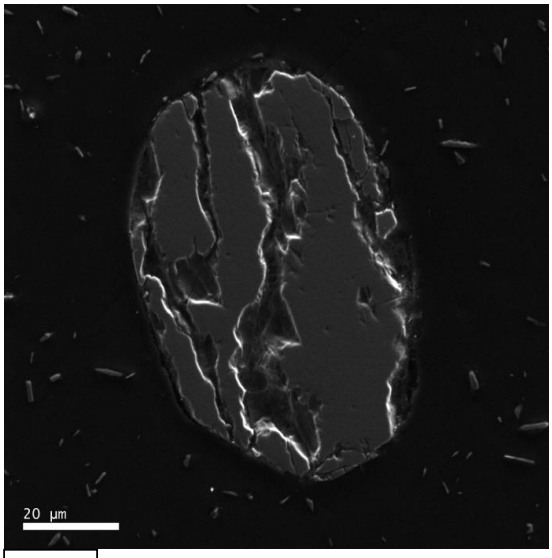
20 µm

02

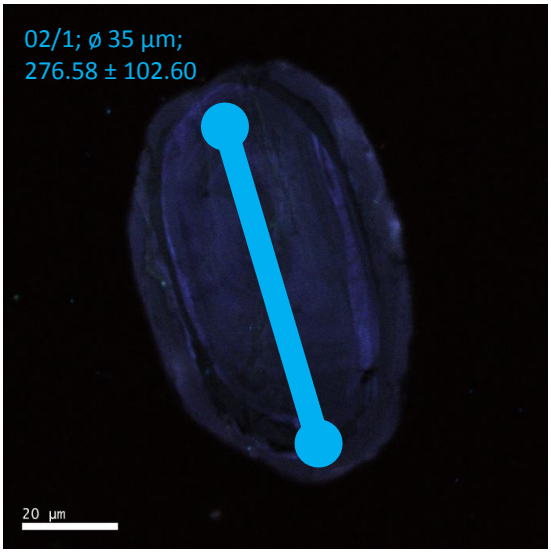
02/1; ø 35 µm;
276.58 ± 102.60
20 µm

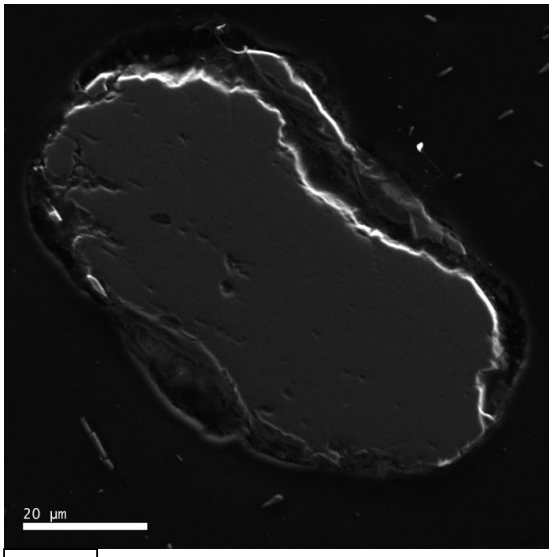
20 µm

03

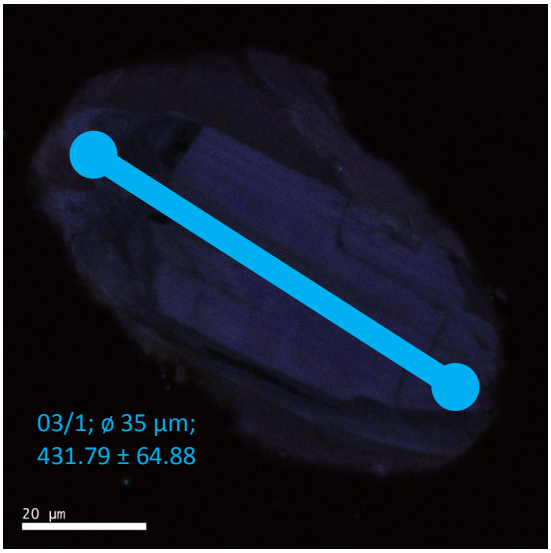
03/1; ø 35 µm;
431.79 ± 64.88
20 µm

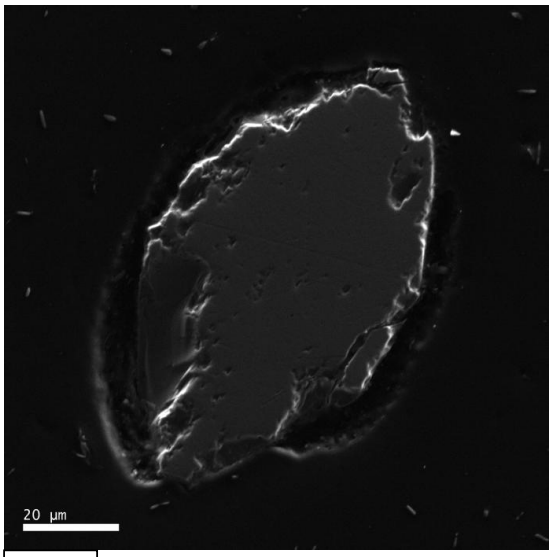

05

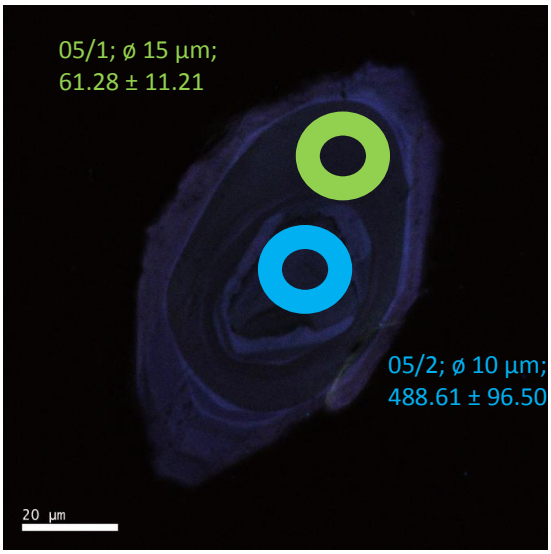

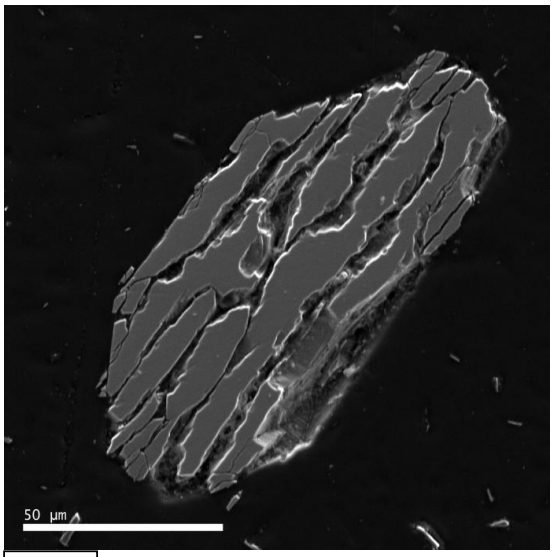

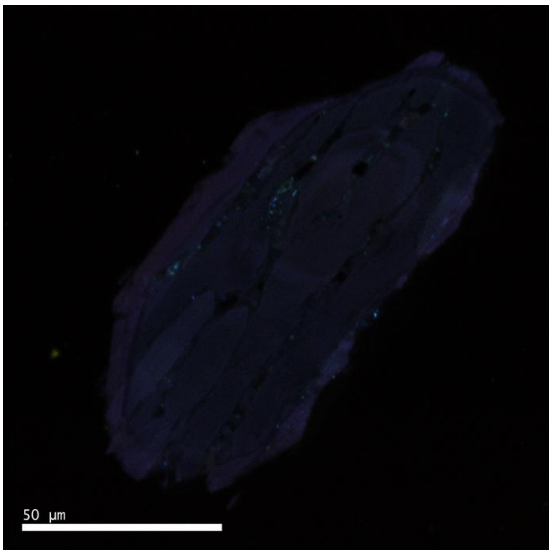

A01

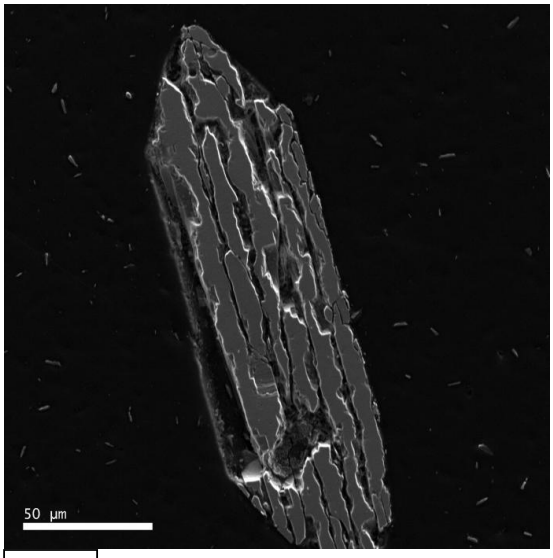

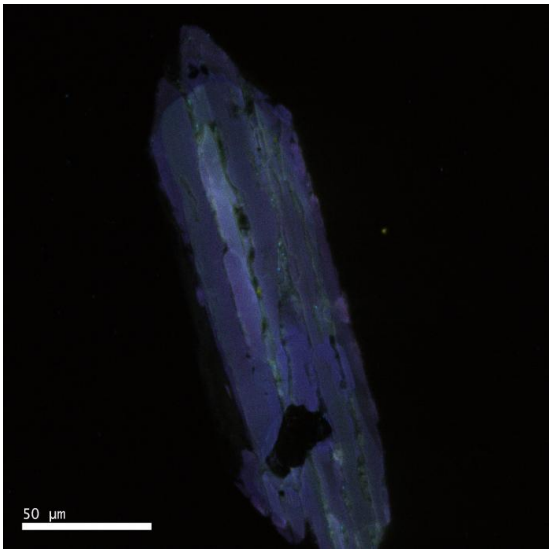

A02

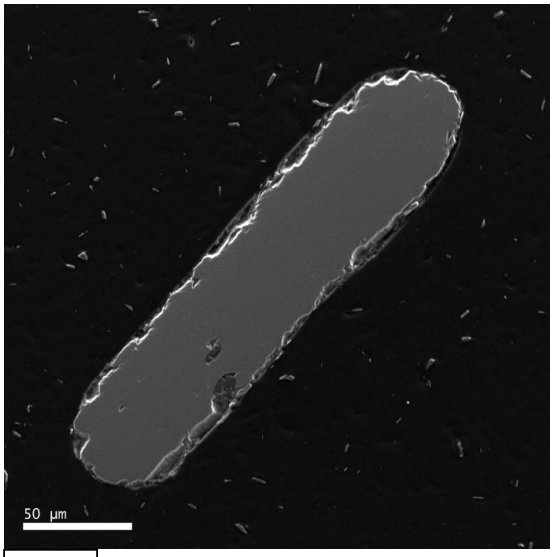

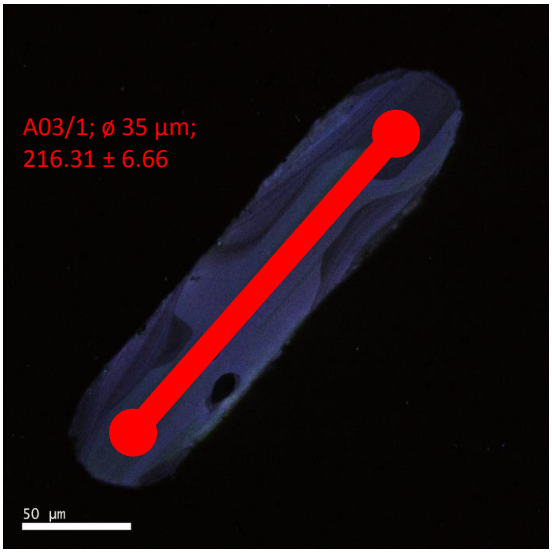

A03

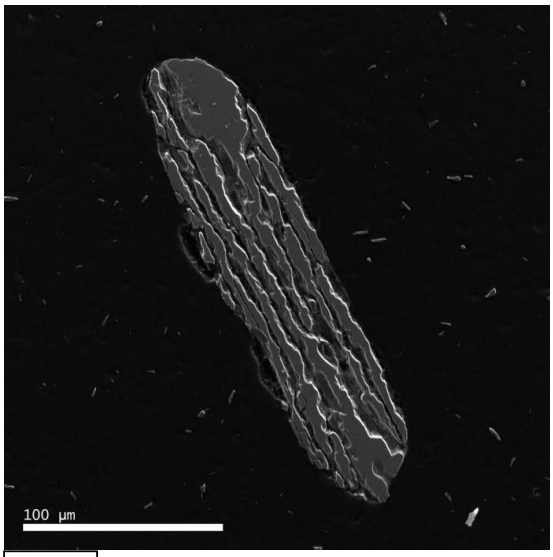

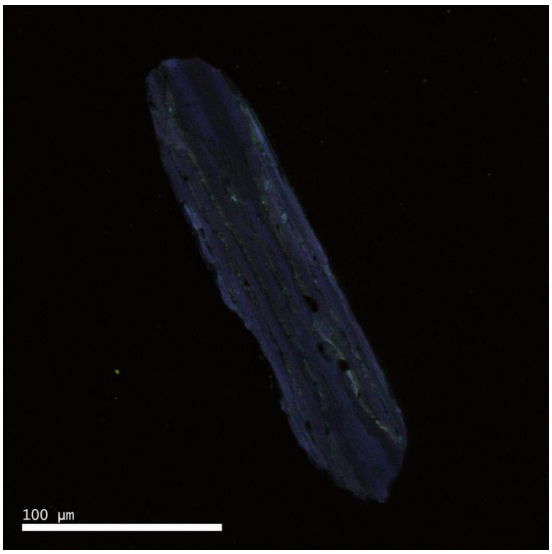

A04

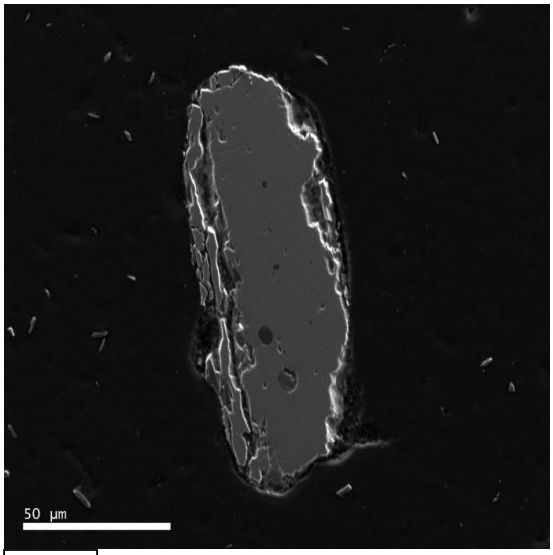

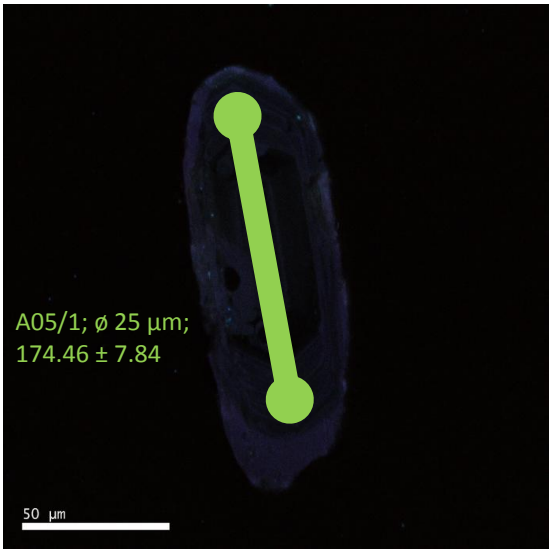

A05

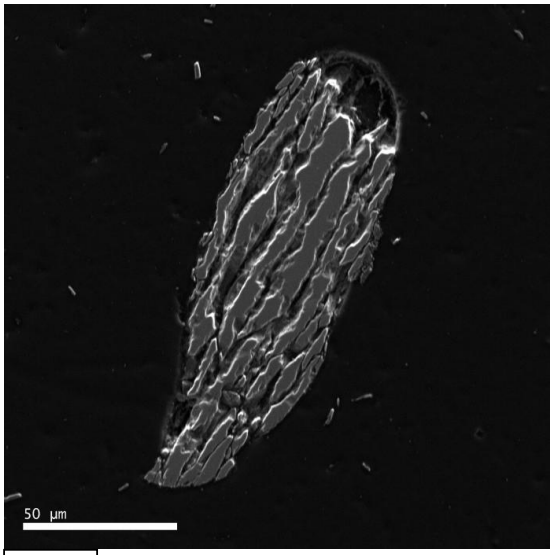

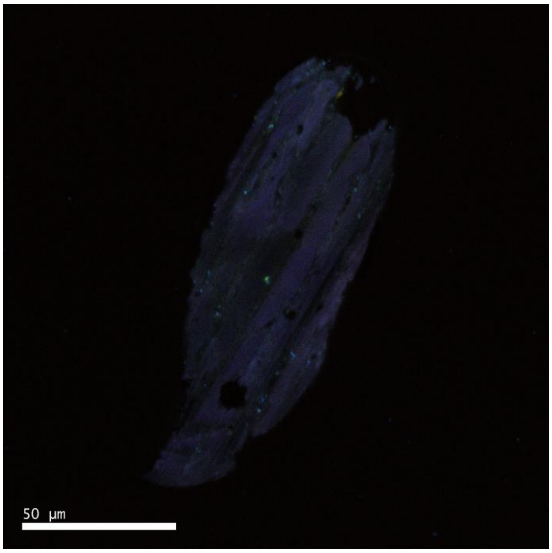

A06

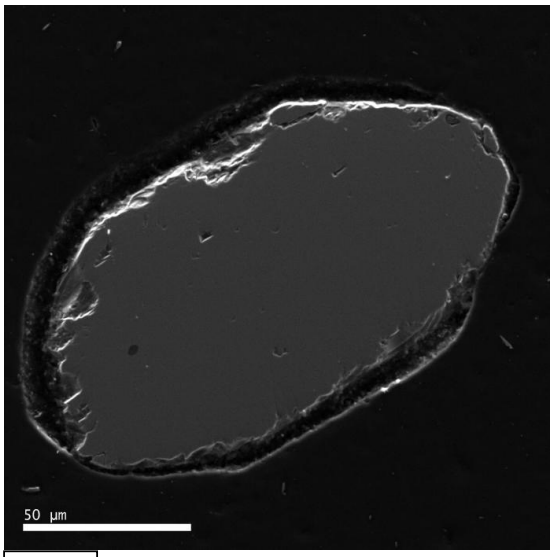
50 µm

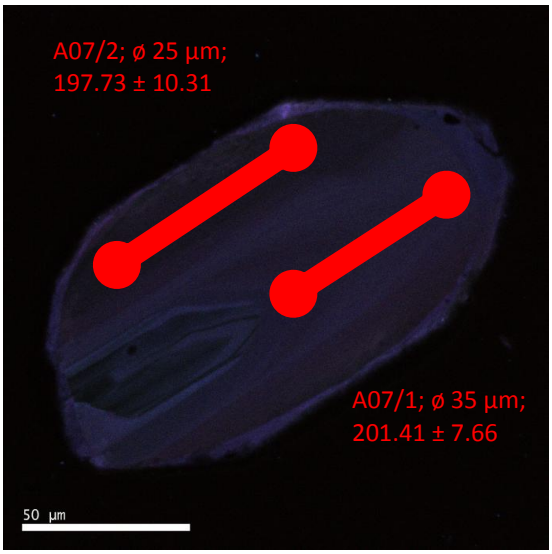
A07/2; ø 25 µm;
197.73 ± 10.31
A07/1; ø 35 µm;
201.41 ± 7.66
50 µm

A07

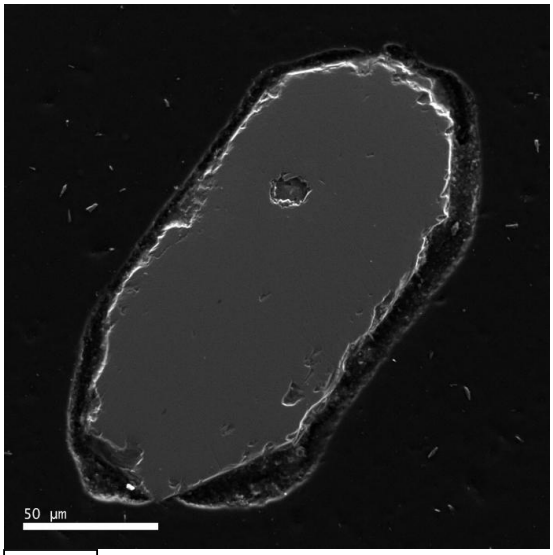
50 µm

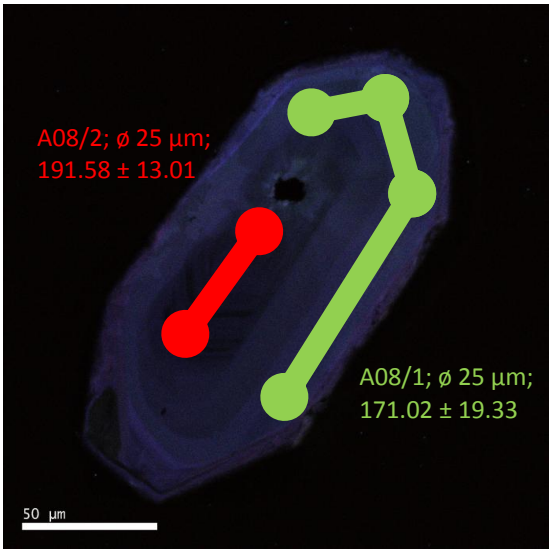
A08/2; ø 25 µm;
191.58 ± 13.01
A08/1; ø 25 µm;
171.02 ± 19.33
50 µm

A08

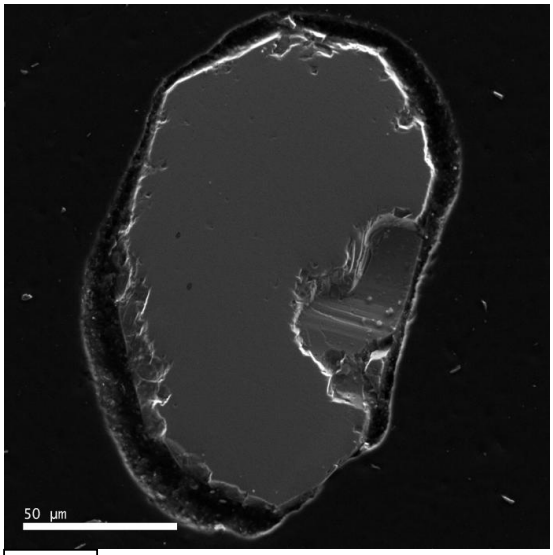
50 µm

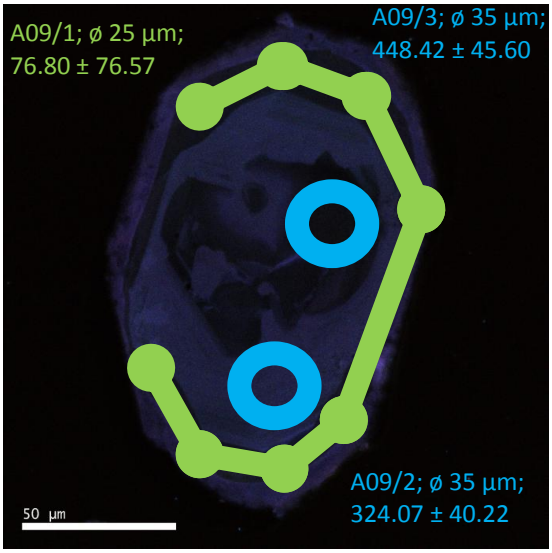
A09/1; ø 25 µm;
76.80 ± 76.57
A09/3; ø 35 µm;
448.42 ± 45.60
A09/2; ø 35 µm;
324.07 ± 40.22
50 µm

A09

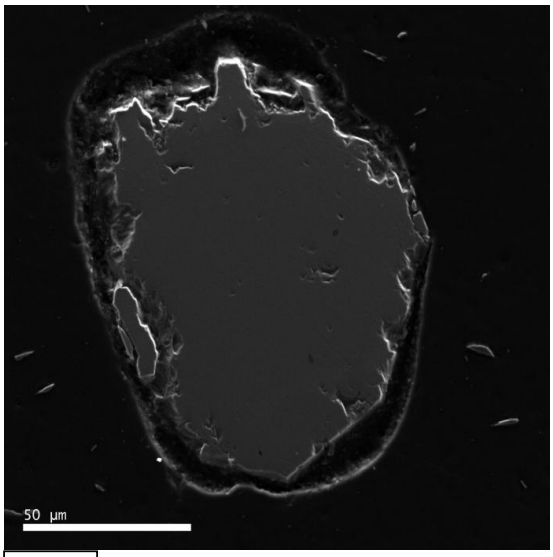

A10

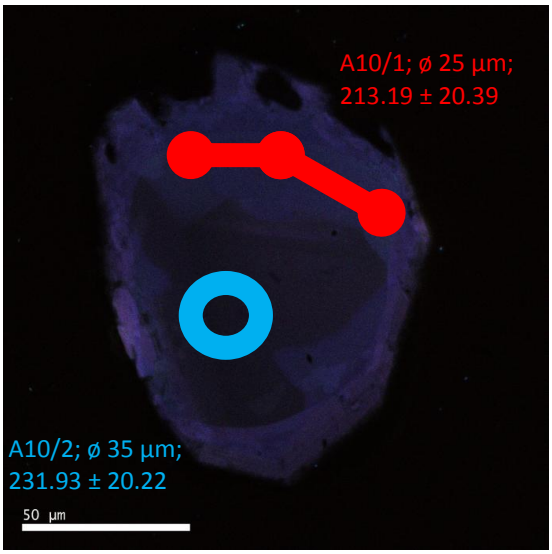

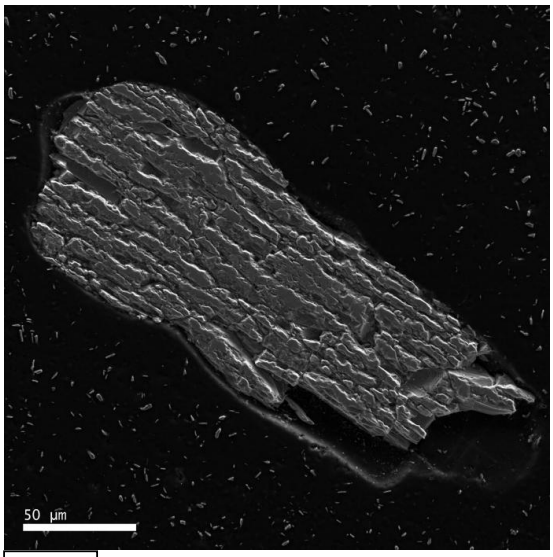
50 µm

A01

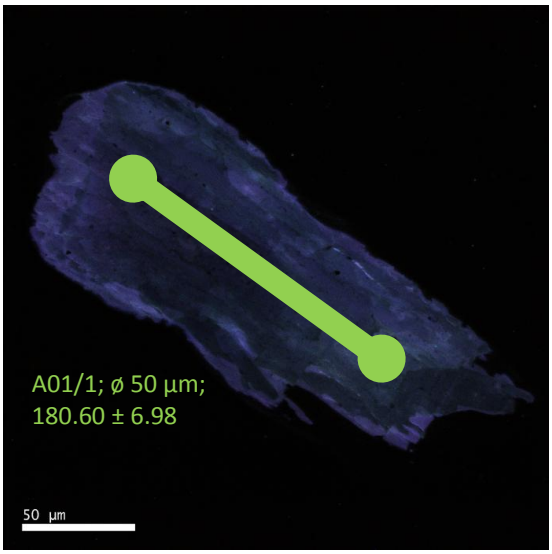
A01/1; ø 50 µm;
180.60 ± 6.98
50 µm

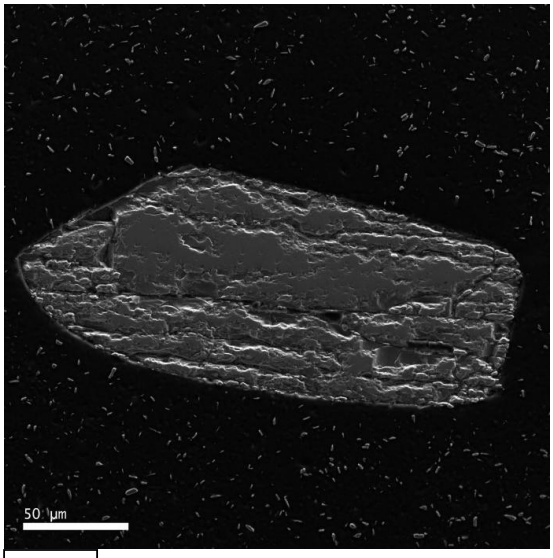
50 µm

A02

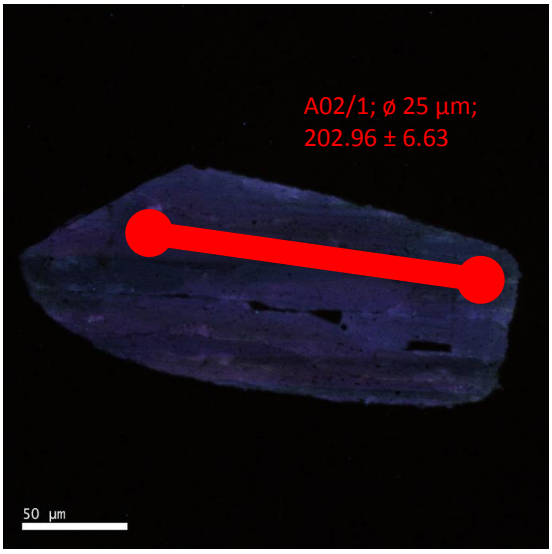
A02/1; ø 25 µm;
202.96 ± 6.63
50 µm

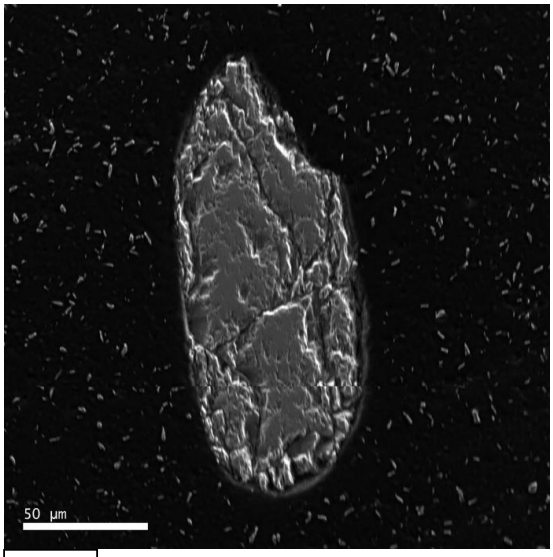
50 µm

A03

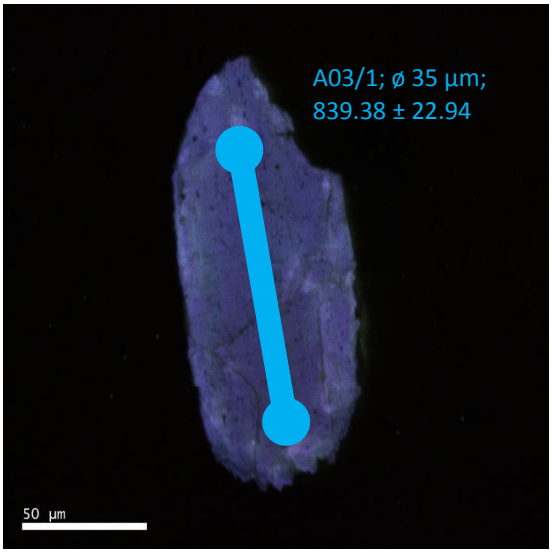
A03/1; ø 35 µm;
839.38 ± 22.94
50 µm

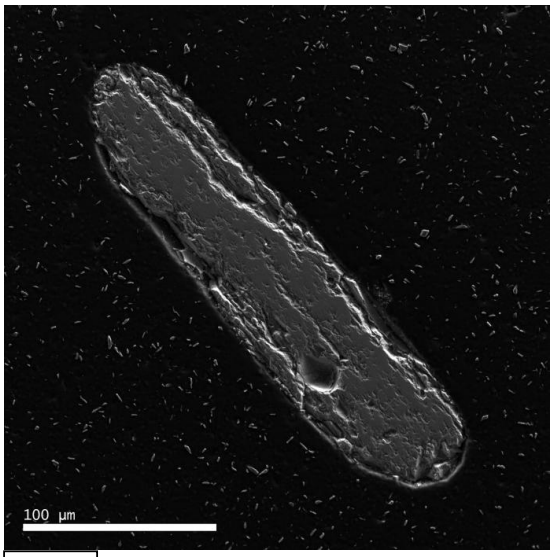
100 µm

A04

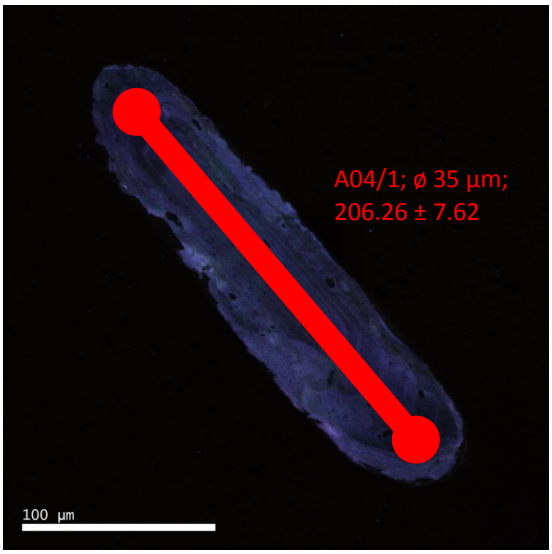
A04/1; ø 35 µm;
206.26 ± 7.62
100 µm

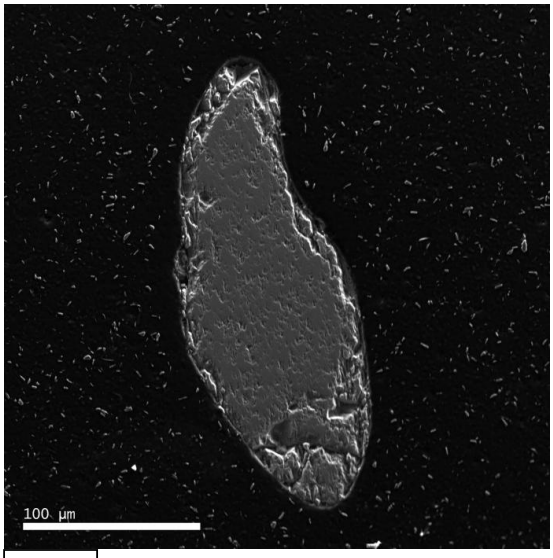
100 µm

A05


A05/1; ø 35 µm;
26.43 ± 0.71
100 µm

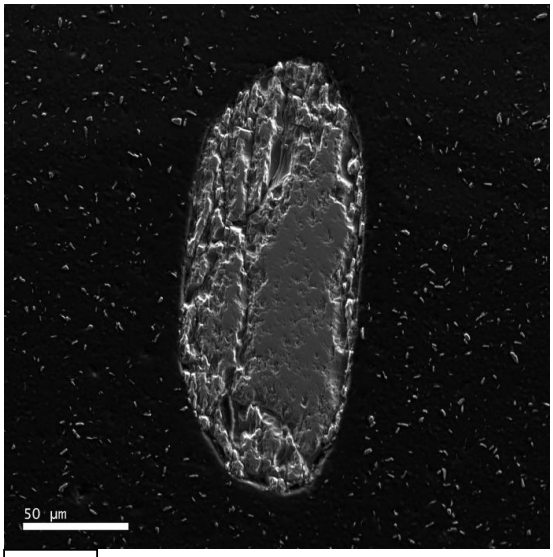
50 µm

A07

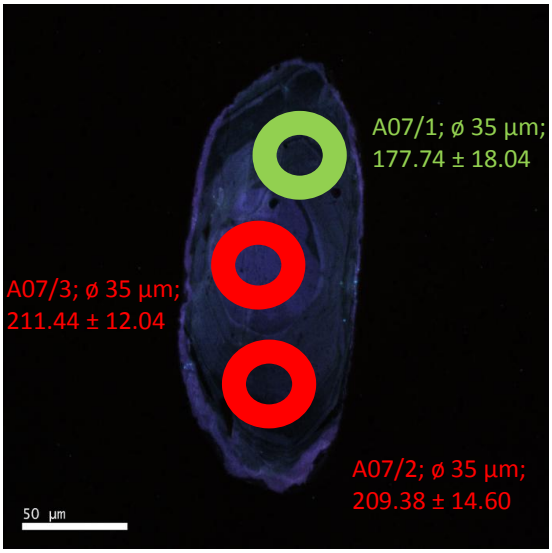
A07/1; ø 35 µm;
177.74 ± 18.04
A07/3; ø 35 µm;
211.44 ± 12.04
A07/2; ø 35 µm;
209.38 ± 14.60
50 µm

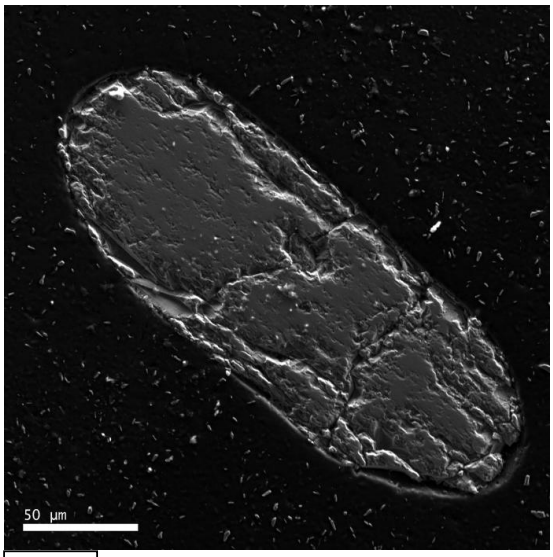
50 µm

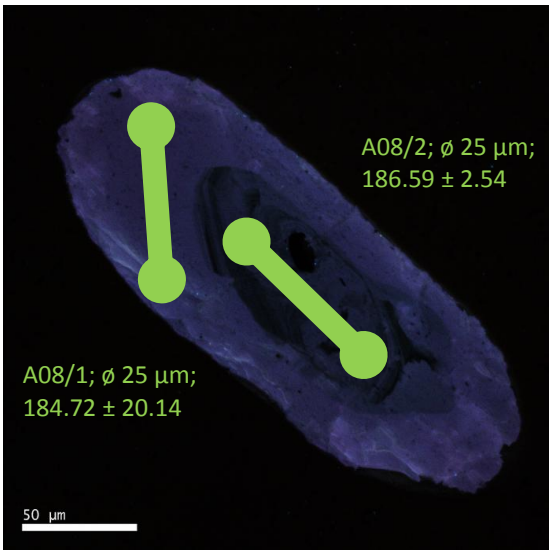
A08/2; ø 25 µm;
186.59 ± 2.54
A08/1; ø 25 µm;
184.72 ± 20.14
50 µm

A08

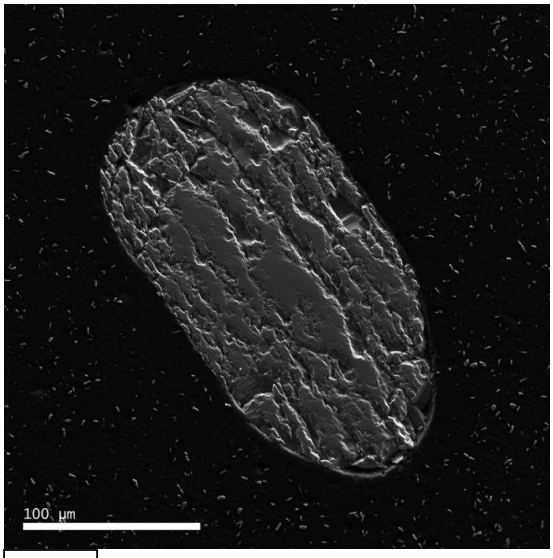
100 µm

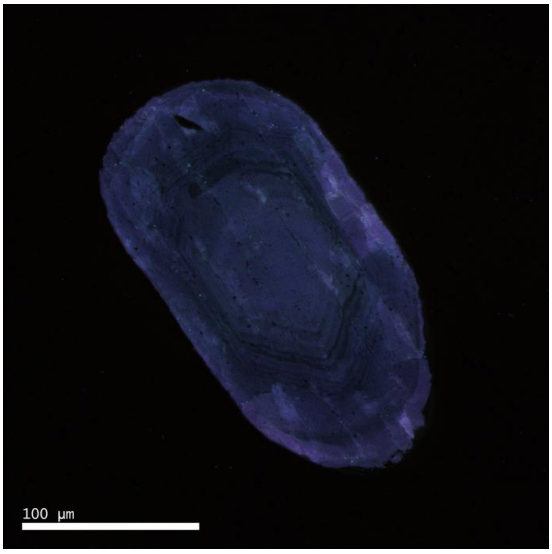
100 µm

A10

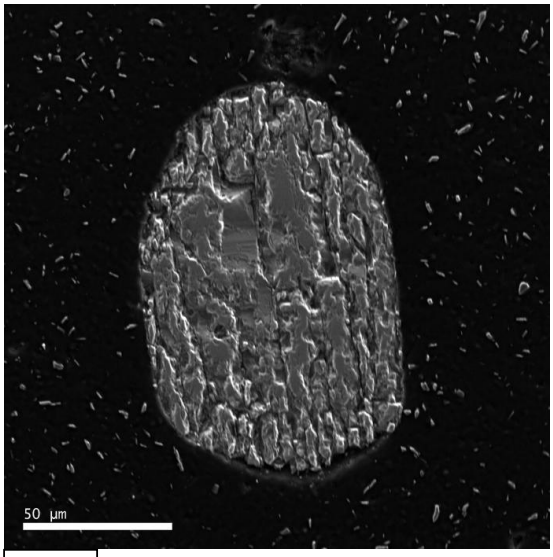
50 µm

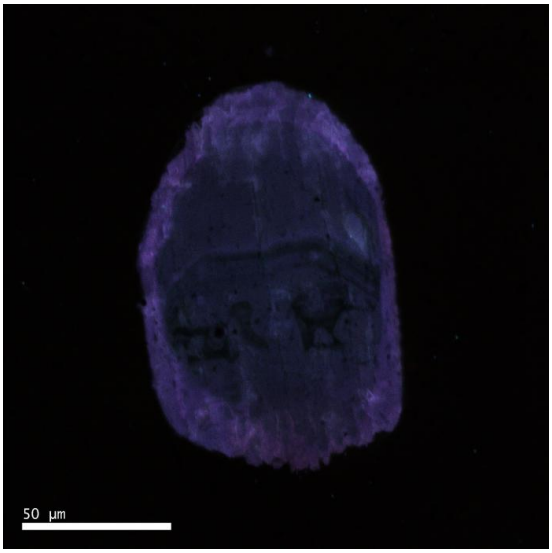
50 µm

B01

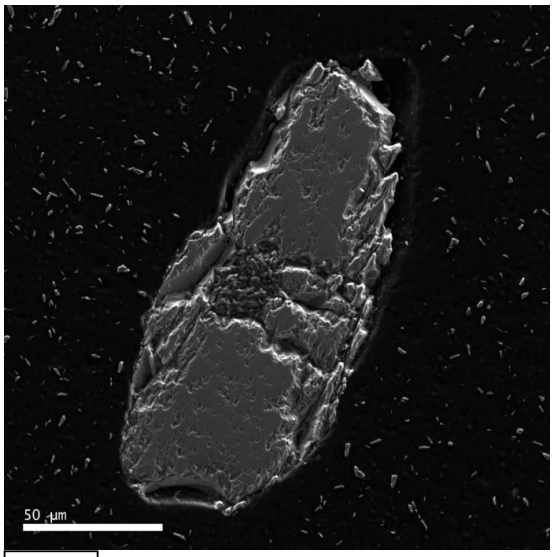
50 µm

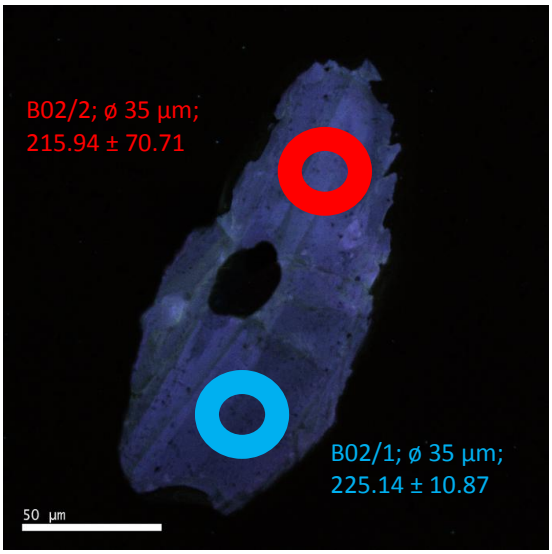
B02/2; ø 35 µm;
215.94 ± 70.71
B02/1; ø 35 µm;
225.14 ± 10.87
50 µm

B02

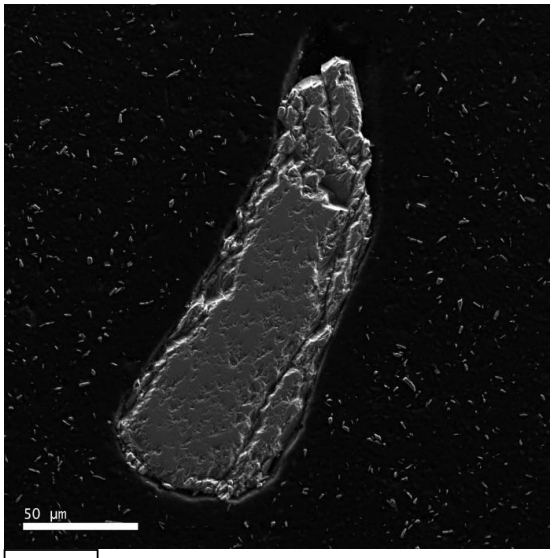
50 µm

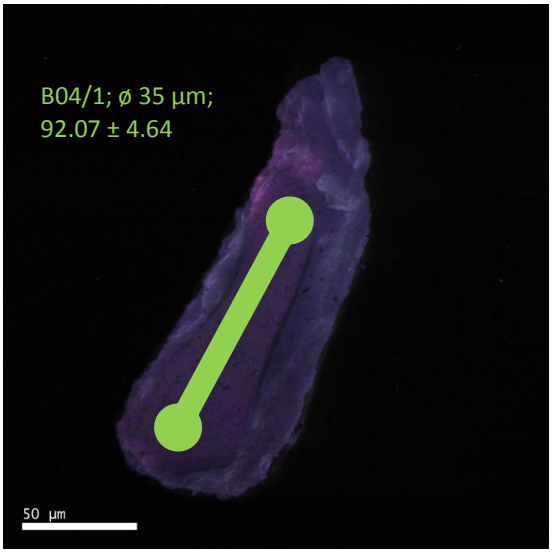
B04/1; ø 35 µm;
92.07 ± 4.64
50 µm

B04

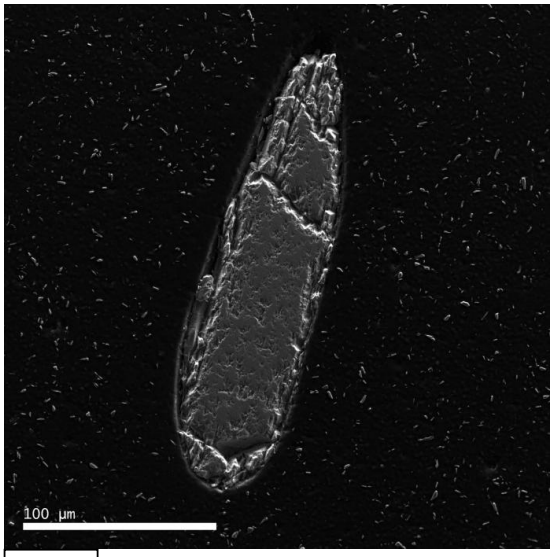
100 µm

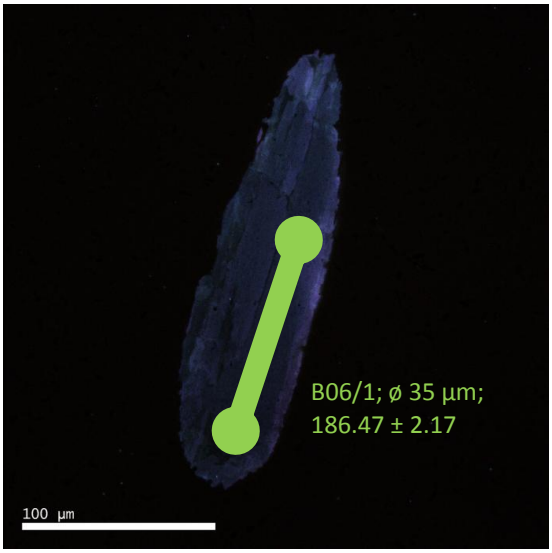
B06/1; ø 35 µm;
186.47 ± 2.17
100 µm

B06

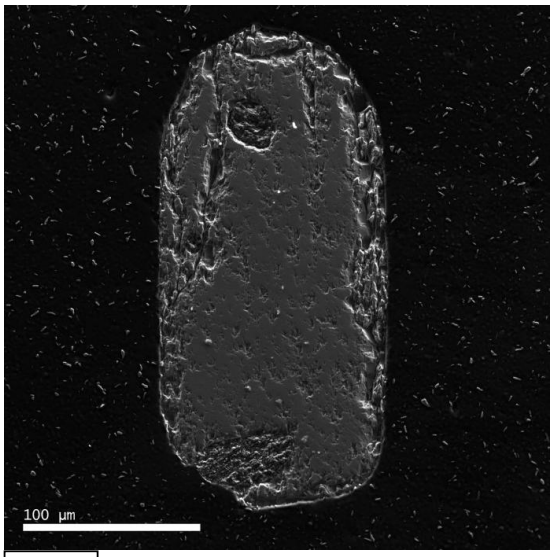
100 µm

B07

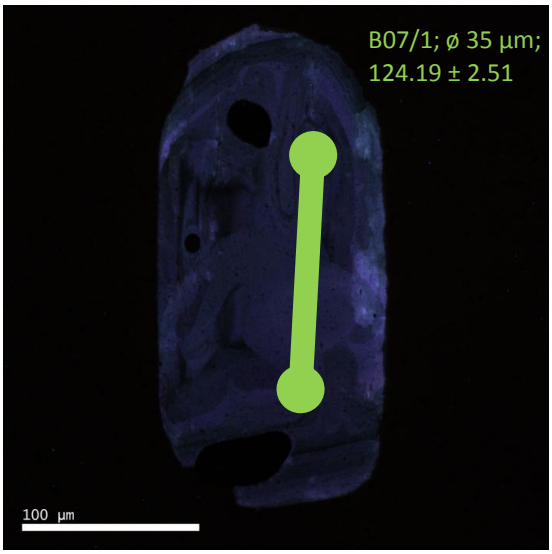
B07/1; ø 35 µm;
124.19 ± 2.51
100 µm

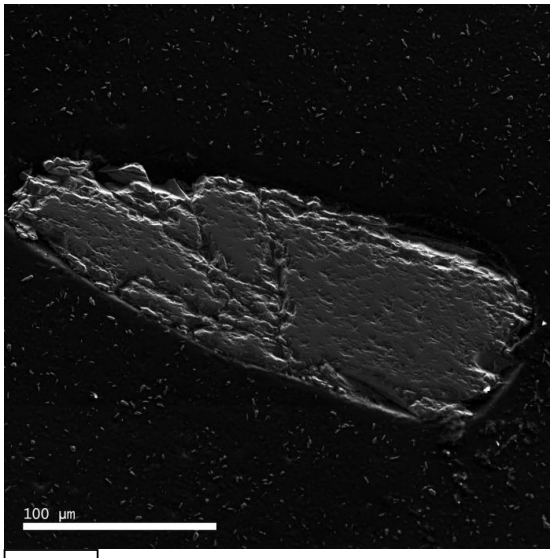
100 µm

B08

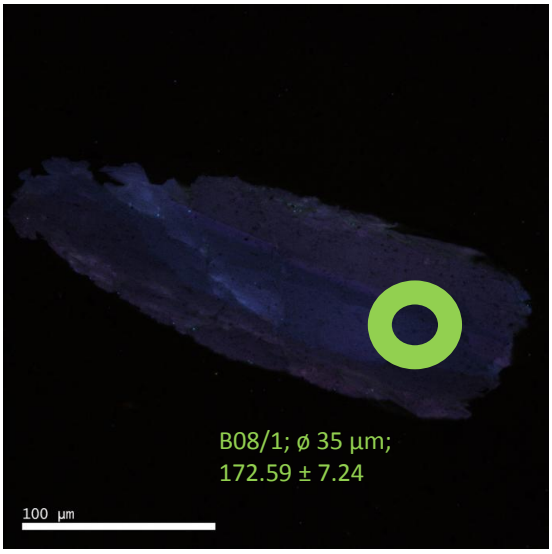
B08/1; ø 35 µm;
172.59 ± 7.24
100 µm

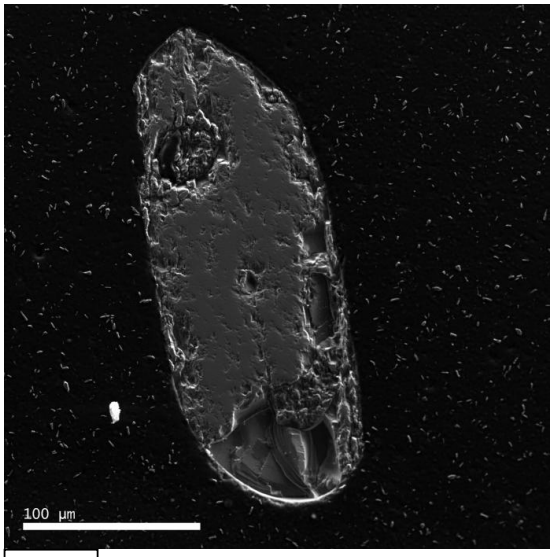
100 µm

B09

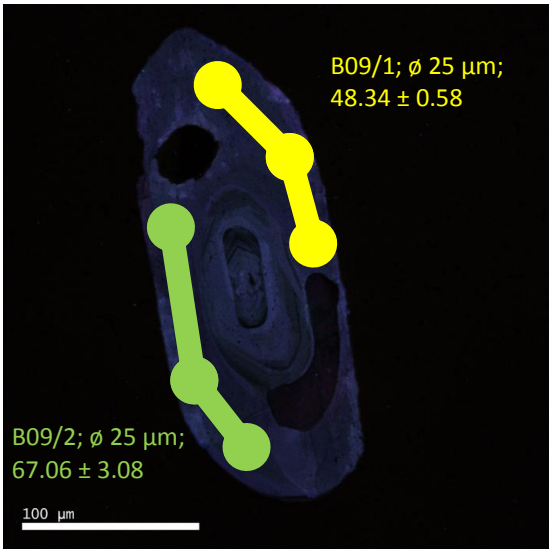
B09/1; ø 25 µm;
48.34 ± 0.58
B09/2; ø 25 µm;
67.06 ± 3.08
100 µm

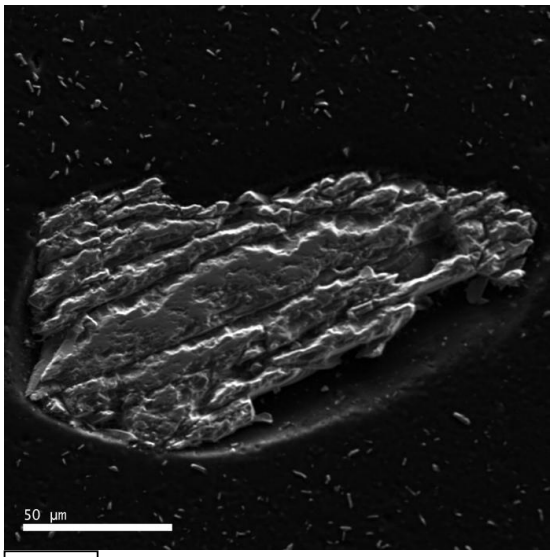

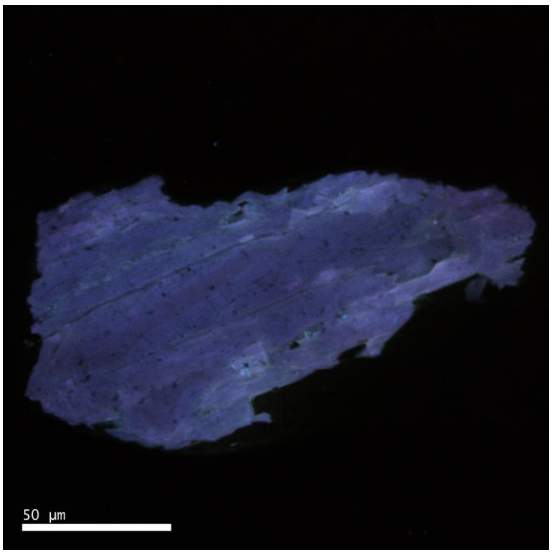

B10

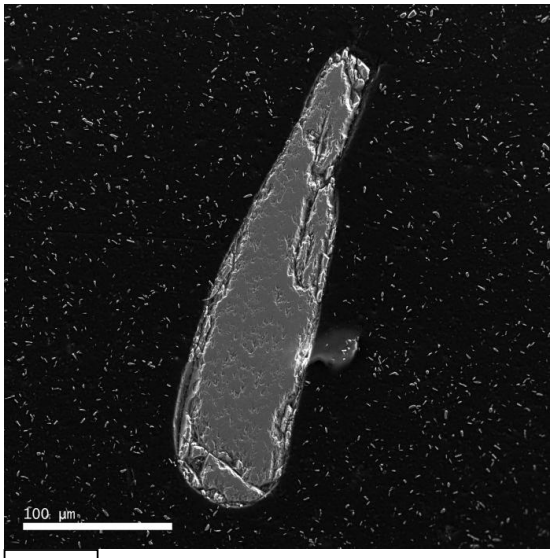

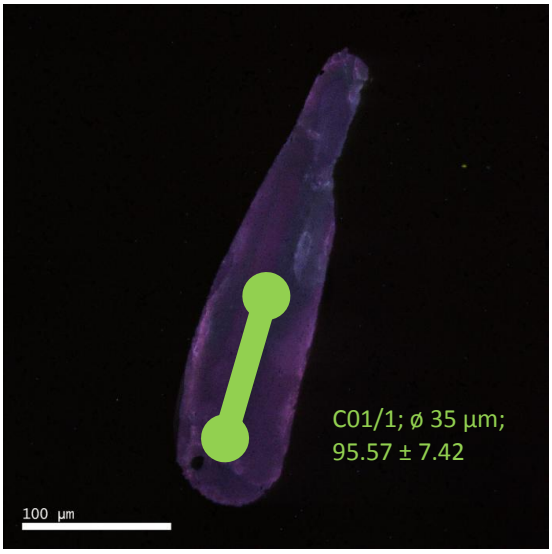

C01

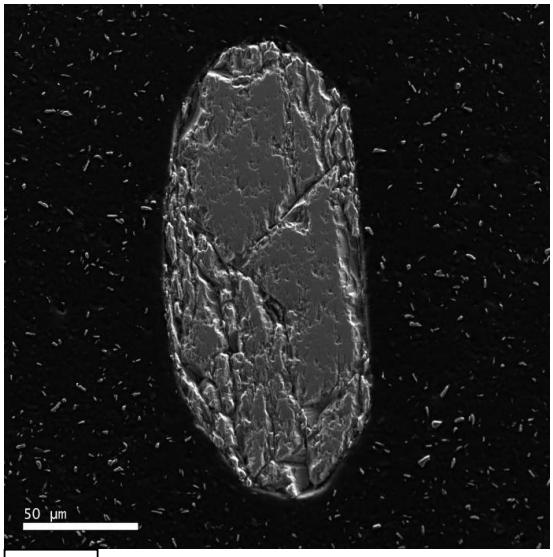

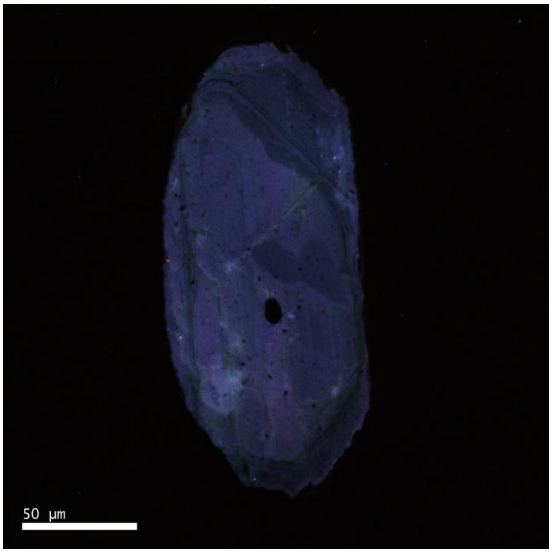

C02

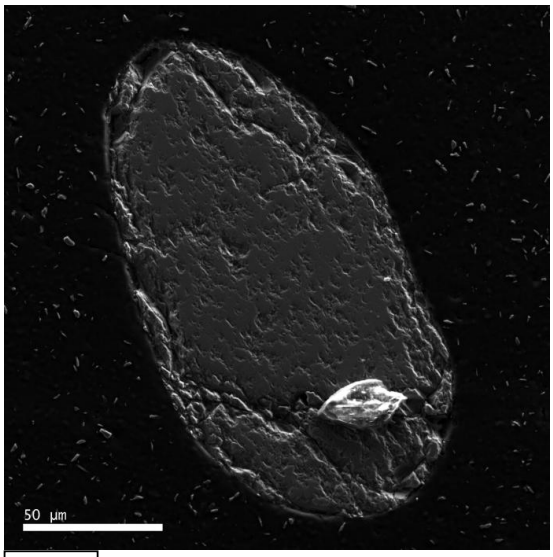
50 µm

C04

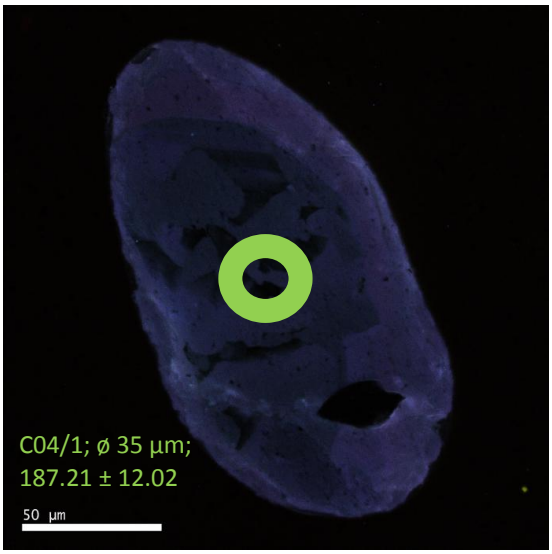
C04/1; ø 35 µm;
187.21 ± 12.02
50 µm

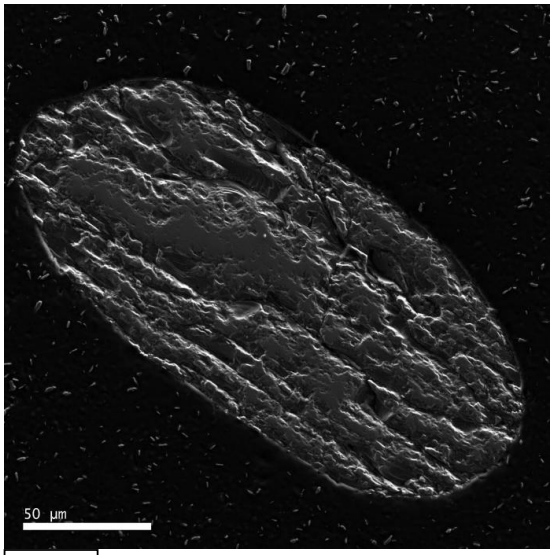
50 µm

C05

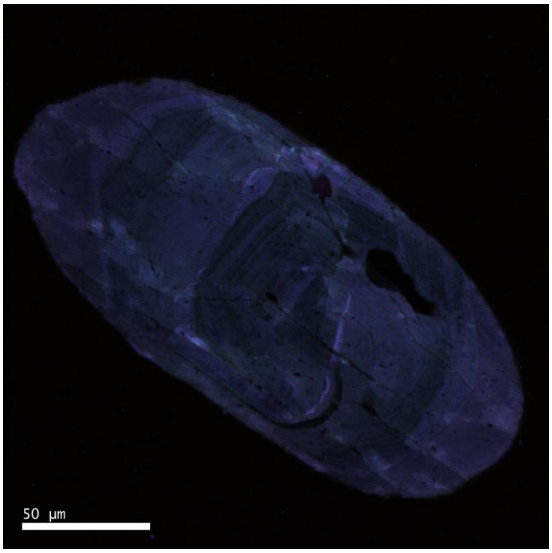
50 µm

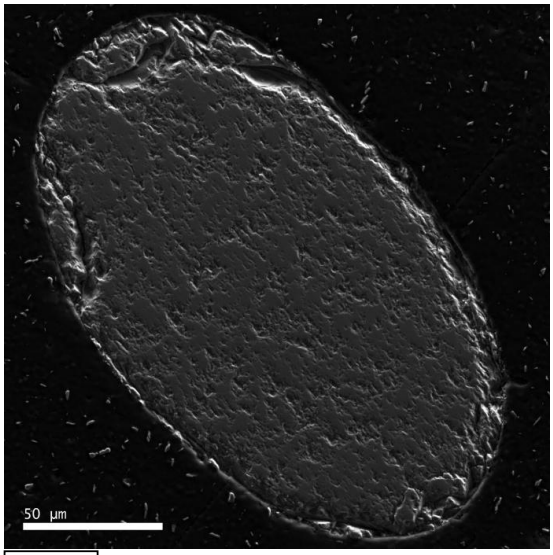
50 µm

C06

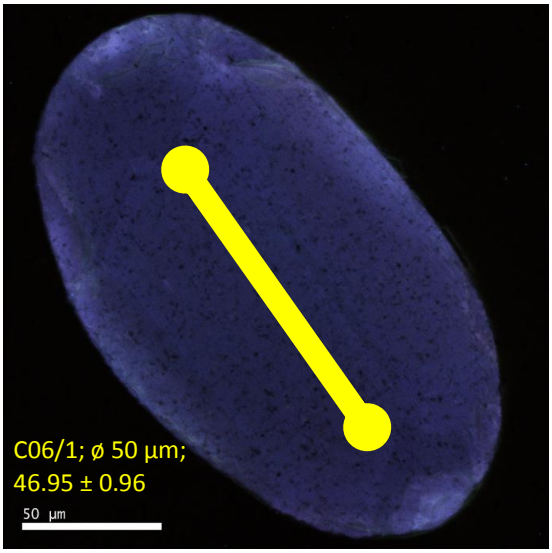
C06/1; ø 50 µm;
46.95 ± 0.96
50 µm

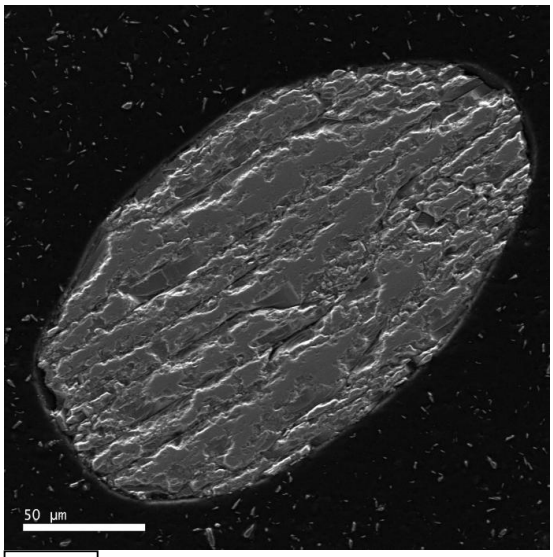

A01

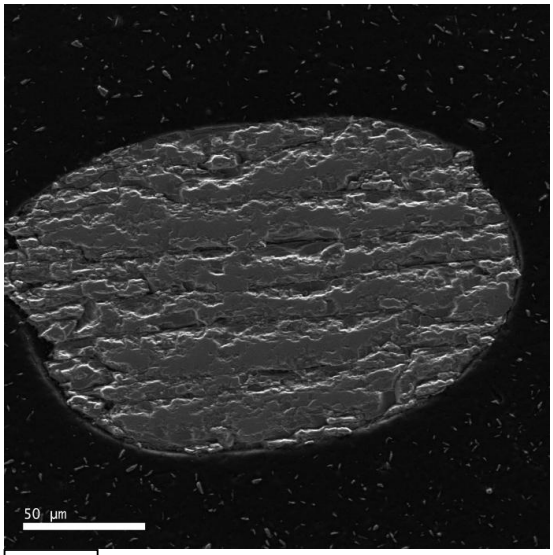

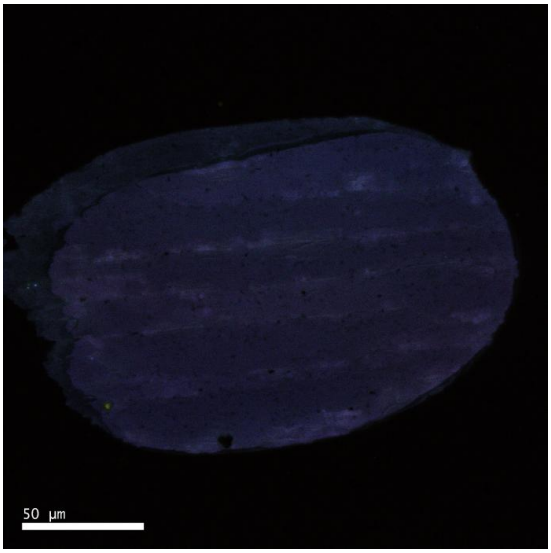

A02

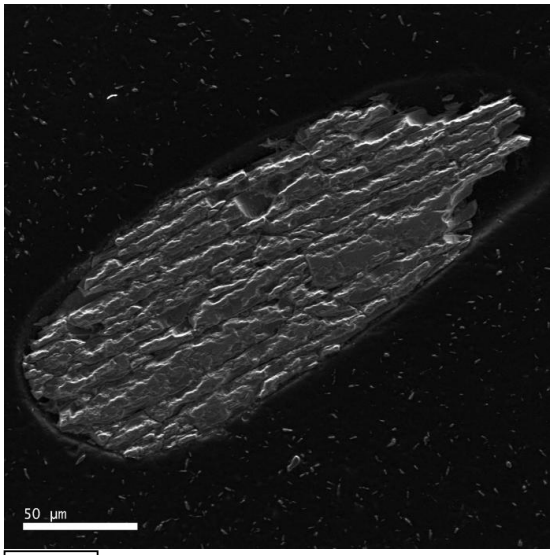

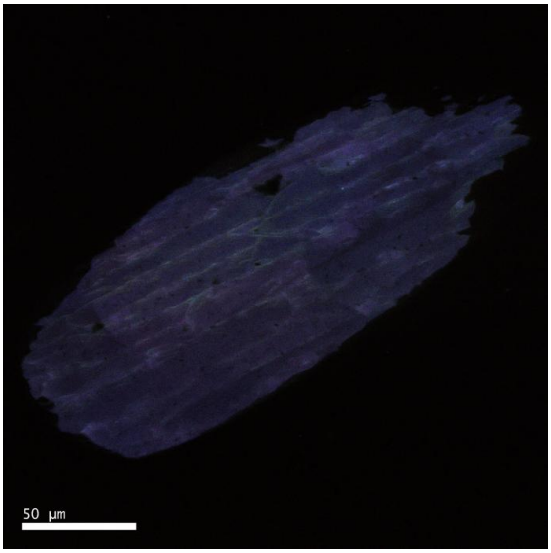

A04

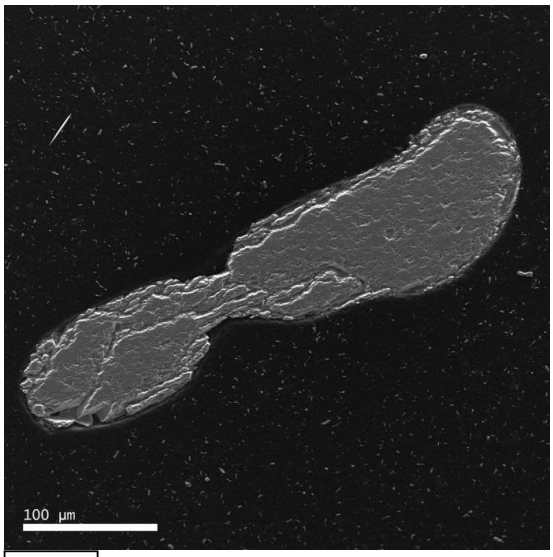
100 µm

A05

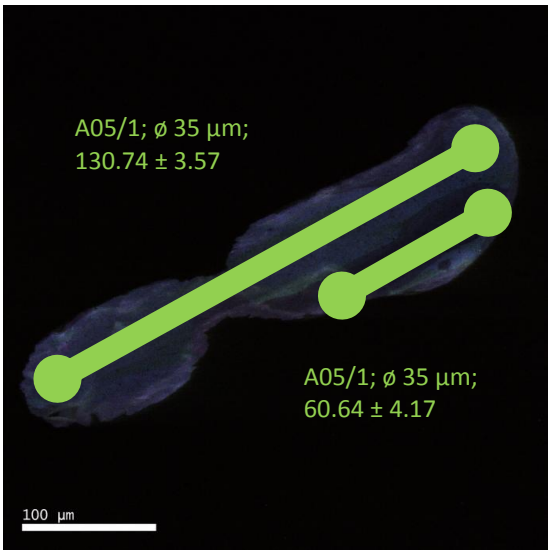
A05/1; ø 35 µm;
130.74 ± 3.57
A05/1; ø 35 µm;
60.64 ± 4.17
100 µm

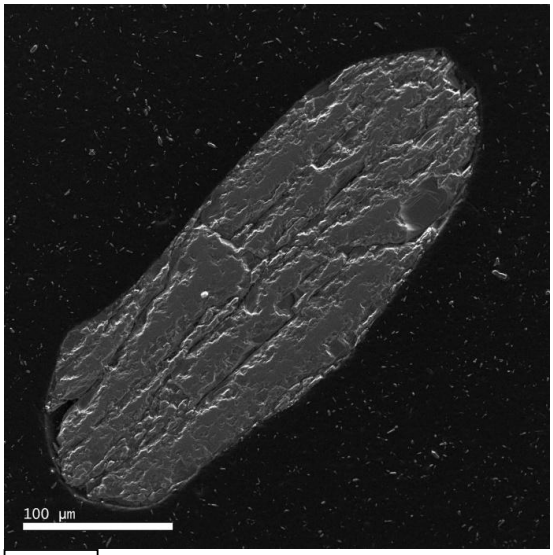
100 µm

A06

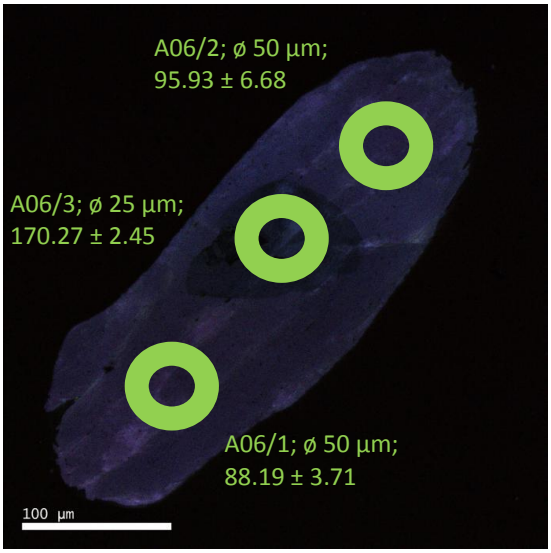
A06/2; ø 50 µm;
95.93 ± 6.68
A06/3; ø 25 µm;
170.27 ± 2.45
A06/1; ø 50 µm;
88.19 ± 3.71
100 µm

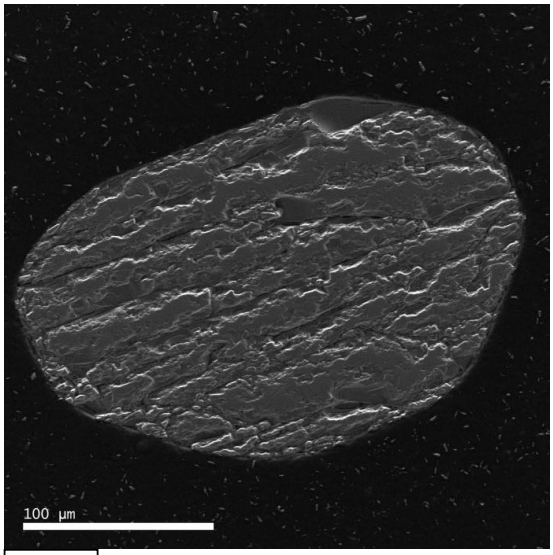
100 µm

A07

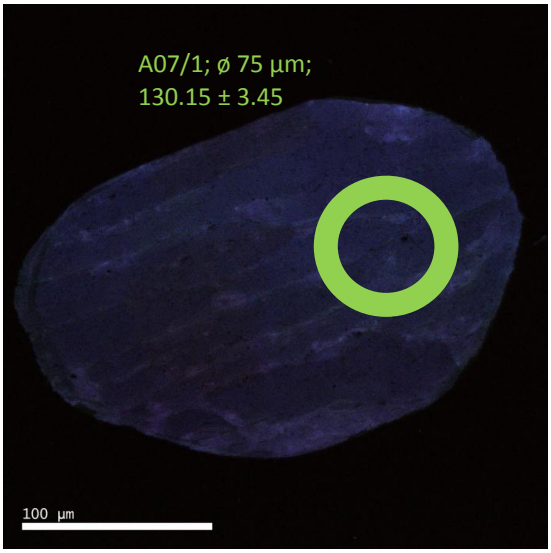
A07/1; ø 75 µm;
130.15 ± 3.45
100 µm

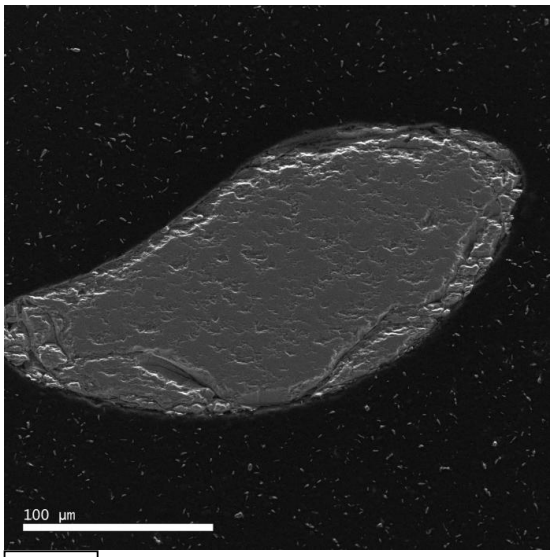
100 µm

A08

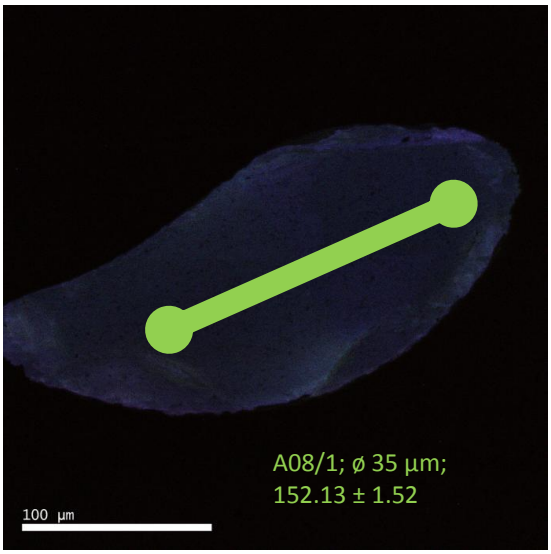
A08/1; ø 35 µm;
152.13 ± 1.52
100 µm

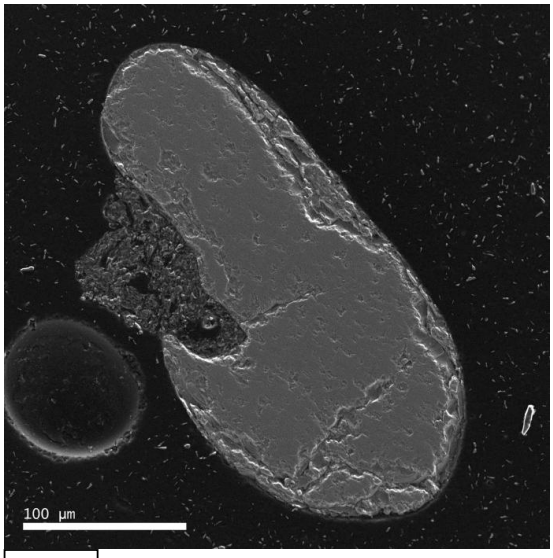
100 µm

A09

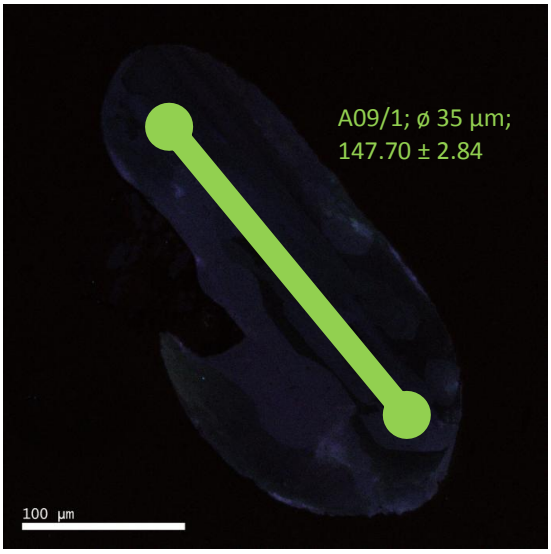
A09/1; ø 35 µm;
147.70 ± 2.84
100 µm

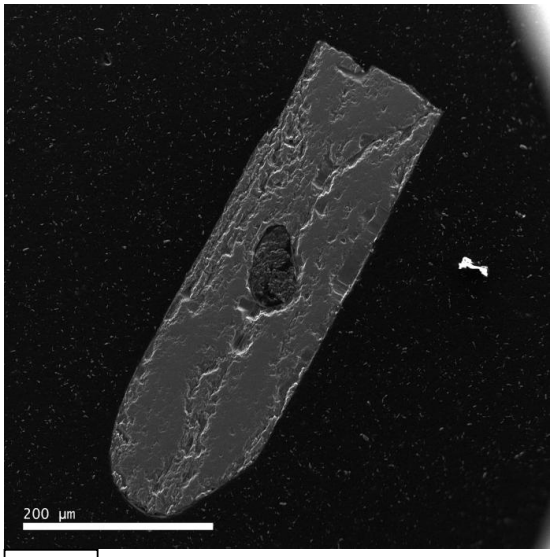
200 µm

B02

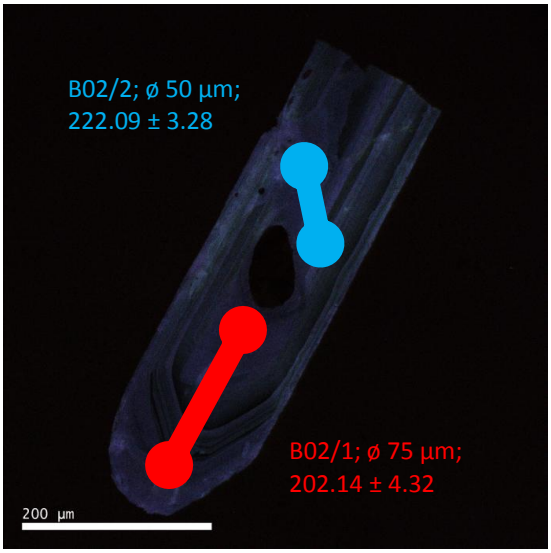
B02/2; ø 50 µm;
222.09 ± 3.28
B02/1; ø 75 µm;
202.14 ± 4.32
200 µm

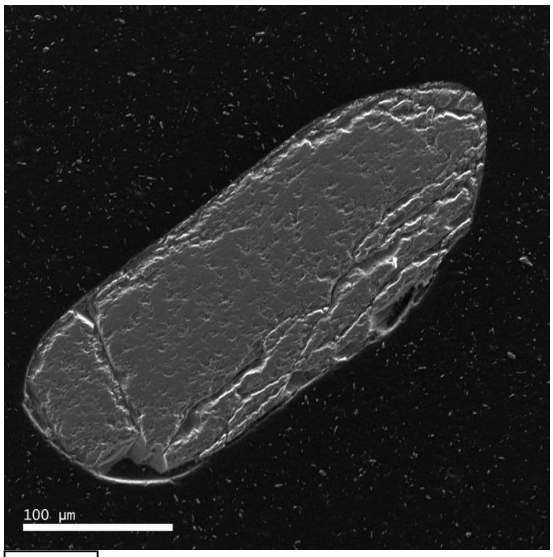
100 µm

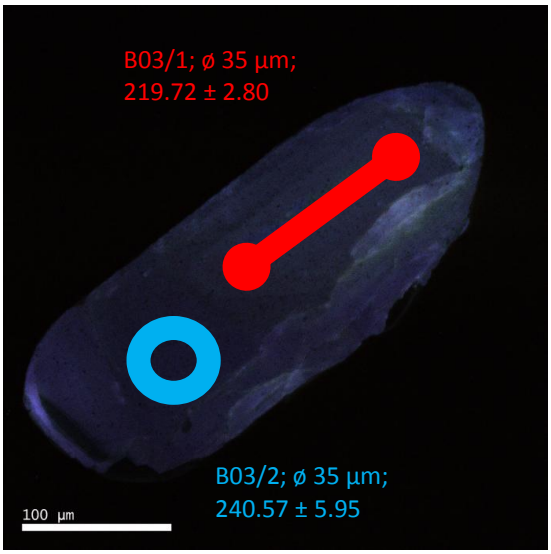
B03/1; ø 35 µm;
219.72 ± 2.80
B03/2; ø 35 µm;
240.57 ± 5.95
100 µm

B03

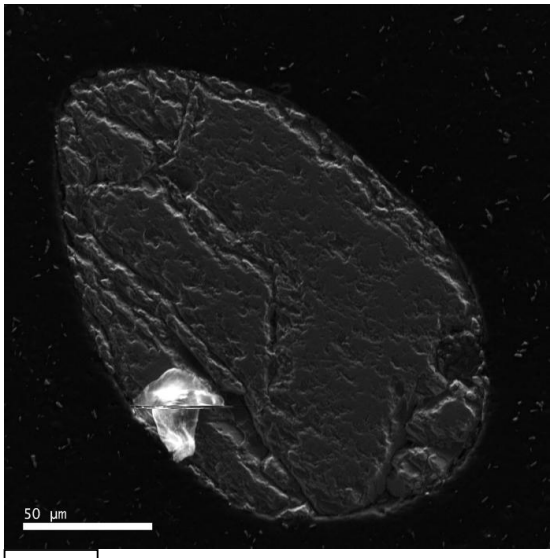
50 µm

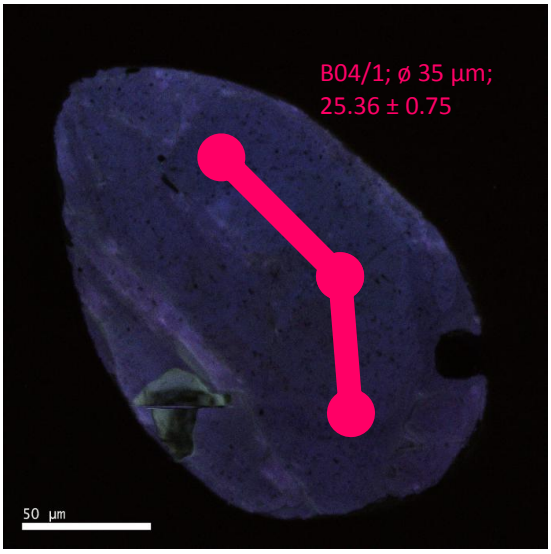
B04/1; ø 35 µm;
25.36 ± 0.75
50 µm

B04

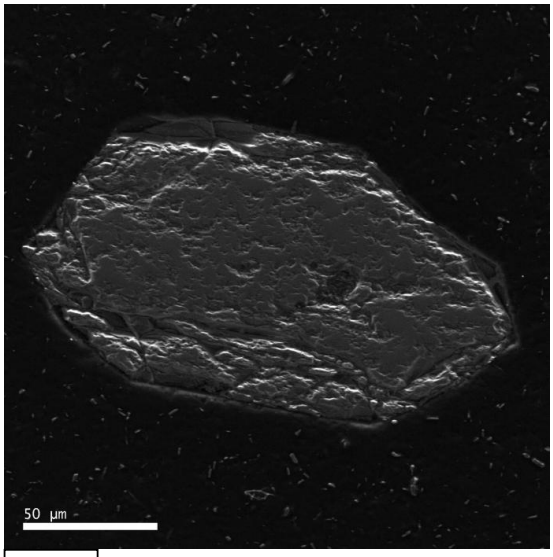
50 µm

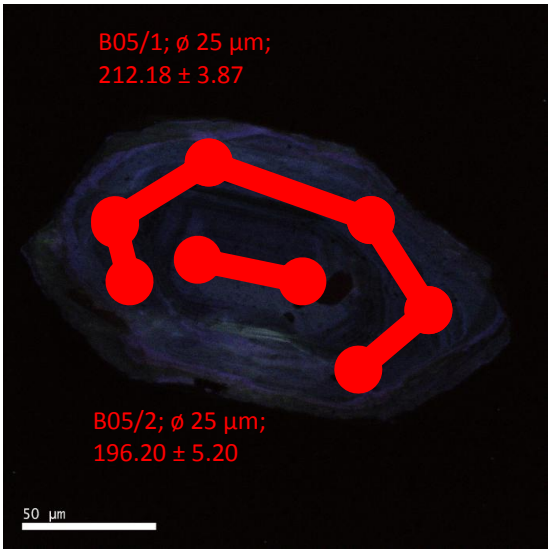
B05/1; ø 25 µm;
212.18 ± 3.87
B05/2; ø 25 µm;
196.20 ± 5.20
50 µm

B05

Input CIPW

Sample	SiO2	TiO2	Al2O3	Fe2O3	FeO	MnO	MgO	CaO	Na2O	K2O	P2O5
p06/01 (2)	71.48	2.05	14.47	0.00	0.00	0.00	0.72	2.56	3.46	2.84	0.09
p01/01 (4)	66.27	3.86	16.36	0.00	0.00	0.00	1.59	3.89	3.87	1.62	0.20
p13/01 (4)	71.35	2.12	14.62	0.00	0.00	0.00	0.74	2.55	3.44	2.81	0.09
p12/02 (5)	68.68	2.70	16.20	0.00	0.00	0.00	1.11	3.40	4.24	1.19	0.14
p12/02 (2)	68.76	2.82	15.89	0.00	0.00	0.00	1.13	3.11	3.46	2.78	0.15
p12/02 (3)	71.23	1.98	14.55	0.00	0.00	0.00	0.72	1.40	2.59	6.09	0.10

Output CIPW

Sample	Quartz	Orthoclase	Albite	Anorthite
p06/01 (2)	34.18	16.78	29.28	12.11
p01/01 (4)	27.42	9.57	32.75	17.99
p13/01 (4)	34.27	16.61	29.11	12.06
p12/02 (5)	31.10	7.03	35.88	15.95
p12/02 (2)	30.07	16.43	29.28	14.45
p12/02 (3)	29.07	35.99	21.92	6.29

not normalized values

Sample	Quartz	Alkali-feldspar	Plagioclase
p06/01 (2)	34.18	16.78	41.39
p01/01 (4)	27.42	9.57	50.74
p13/01 (4)	34.27	16.61	41.17
p12/02 (5)	31.10	7.03	51.83
p12/02 (2)	30.07	16.43	43.73
p12/02 (3)	29.07	35.99	28.21

normalized values

Sample	Quartz	Alkali-feldspar	Plagioclase
p06/01 (2)	37.01	18.17	44.82
p01/01 (4)	31.25	10.91	57.84
p13/01 (4)	37.23	18.04	44.73
p12/02 (5)	34.57	7.81	57.61
p12/02 (2)	33.33	18.21	48.47
p12/02 (3)	31.17	38.59	30.25

Input CIPW

Sample	SiO2	TiO2	Al2O3	Fe2O3	FeO	MnO	MgO	CaO	Na2O	K2O	P2O5
p06/01 (2)	71.48	2.05	14.47	0.00	0.00	0.00	0.72	2.56	3.46	2.84	0.09
p01/01 (4)	66.27	3.86	16.36	0.00	0.00	0.00	1.59	3.89	3.87	1.62	0.20
p13/01 (4)	71.35	2.12	14.62	0.00	0.00	0.00	0.74	2.55	3.44	2.81	0.09
p12/02 (5)	68.68	2.70	16.20	0.00	0.00	0.00	1.11	3.40	4.24	1.19	0.14
p12/02 (2)	68.76	2.82	15.89	0.00	0.00	0.00	1.13	3.11	3.46	2.78	0.15
p12/02 (3)	71.23	1.98	14.55	0.00	0.00	0.00	0.72	1.40	2.59	6.09	0.10

Output CIPW

Sample	Quartz	Orthoclase	Albite	Anorthite
p06/01 (2)	34.18	16.78	29.28	12.11
p01/01 (4)	27.42	9.57	32.75	17.99
p13/01 (4)	34.27	16.61	29.11	12.06
p12/02 (5)	31.10	7.03	35.88	15.95
p12/02 (2)	30.07	16.43	29.28	14.45
p12/02 (3)	29.07	35.99	21.92	6.29

not normalized values

Sample	Quartz	Alkali-feldspar	Plagioclase
p06/01 (2)	34.18	16.78	41.39
p01/01 (4)	27.42	9.57	50.74
p13/01 (4)	34.27	16.61	41.17
p12/02 (5)	31.10	7.03	51.83
p12/02 (2)	30.07	16.43	43.73
p12/02 (3)	29.07	35.99	28.21

normalized values

Sample	Quartz	Alkali-feldspar	Plagioclase
p06/01 (2)	37.01	18.17	44.82
p01/01 (4)	31.25	10.91	57.84
p13/01 (4)	37.23	18.04	44.73
p12/02 (5)	34.57	7.81	57.61
p12/02 (2)	33.33	18.21	48.47
p12/02 (3)	31.17	38.59	30.25

REE	p06/01 (2)	p01/01 (4)	p13/01 (4)	p12/02 (5)	p12/02 (2)	p12/02 (3)
La	33.4	59.8	32.0	53.4	48.3	46.3
Ce	55.1	107.5	54.8	90.4	85.2	94.8
Pr	5.66	11.06	5.44	9.00	8.85	10.89
Nd	19.2	36.0	17.5	28.1	30.4	38.8
Sm	2.85	4.91	2.78	4.05	4.25	7.17
Eu	0.76	1.14	0.73	0.90	1.16	0.93
Gd	2.36	3.28	2.2	3.05	2.95	4.96
Tb	0.30	0.38	0.30	0.32	0.36	0.45
Dy	1.66	1.84	1.6	1.84	1.71	1.83
Ho	0.32	0.32	0.31	0.25	0.3	0.22
Er	0.85	0.82	0.84	0.72	0.82	0.48
Tm	0.11	0.13	0.12	0.11	0.13	0.07
Yb	0.78	0.70	0.91	0.67	0.82	0.46
Lu	0.12	0.12	0.11	0.11	0.12	0.07

Chondrite normalized values

REE	c1 M&S1995	p06/01 (2)	p01/01 (4)	p13/01 (4)	p12/02 (5)	p12/02 (2)	p12/02 (3)
La	0.237	140.93	252.32	135.02	225.32	203.80	195.36
Ce	0.613	89.89	175.37	89.40	147.47	138.99	154.65
Pr	0.0928	60.99	119.18	58.62	96.98	95.37	117.35
Nd	0.457	42.01	78.77	38.29	61.49	66.52	84.90
Sm	0.148	19.26	33.18	18.78	27.36	28.72	48.45
Eu	0.0563	13.50	20.25	12.97	15.99	20.60	16.52
Gd	0.199	11.86	16.48	11.06	15.33	14.82	24.92
Tb	0.0361	8.31	10.53	8.31	8.86	9.97	12.47
Dy	0.246	6.75	7.48	6.50	7.48	6.95	7.44
Ho	0.0546	5.86	5.86	5.68	4.58	5.49	4.03
Er	0.16	5.31	5.13	5.25	4.50	5.13	3.00
Tm	0.0247	4.45	5.26	4.86	4.45	5.26	2.83
Yb	0.161	4.84	4.35	5.65	4.16	5.09	2.86
Lu	0.0246	4.88	4.88	4.47	4.47	4.88	2.85

McDonough W. F. and Sun S.- s. (1995)
"The composition of the Earth"
Chemical Geology 120, 223–253.